Theoretical Study on Quantum Dynamics of Coherent Phonon Generation in the Early-Time Region

Yohei Watanabe

February 2018

Theoretical Study on Quantum Dynamics of Coherent Phonon Generation in the Early-Time Region

Yohei Watanabe

Doctoral Program in Materials Science

Submitted to the Graduate School of
Pure and Applied Sciences
in Partial Fulfillment of the Requirements
for the Degree of Doctoral Philosophy in
Engineering

at the
University of Tsukuba

Abstract

Coherent phonon (CP) generation is one of the representative ultrafast and non-equilibrium phenomena induced by the irradiation of the ultrashort pulse laser. In particular, in the early-stage of the CP generation, the longitudinal optical (LO) phonon and heavily photoexcited carriers interact with each other. Therefore, quantum mechanical effects inherent in the CP generation dynamics and their microscopic mechanisms have been targets of considerable interest for a long time.

In this dissertation, we construct a fully quantum mechanical model for the CP generation dynamics applicable for both nonpolar and polar semiconductors on an equal footing, on the basis of a polaronic-quasiparticle (PQ) picture. In this model, the PQ is constituted of the LO phonon, the plasmon, and the single-particle excitation. Thereby, we tackle the problem of the transient and nonlinear Fano resonance (FR). This quantum mechanical effect manifests itself immediately after the carrier excitation by the ultrashort pulse laser; this was observed exclusively in lightly n-doped Si [M. Hase, *et. al.*, Nature (London) **426**, 51 (2003)], though not observed yet in GaAs. Moreover, we explore still-hidden quantum mechanical effects in the CP generation dynamics.

The PQ model straightforward shows that the LO phonon discrete state is embedded in the electron-hole continuum state of the single-particle excitation, which is a requirement of the transient FR in the present system. We conduct numerical calculations of induced photoemission spectra relevant to the retarded longitudinal susceptibility in the non-equilibrium and transient system of concern. The photoemission spectra show an asymmetric line shape characteristic of FR transiently in undoped Si, although not in GaAs. This result is in agreement with the existing experimental results. It is found that the difference between the obtained results of the spectra is attributed to a phase factor of an effective LO phonon-carrier interaction.

We also investigate the time signal ascribed to an induced charge density of an ionic core under the various pulse laser conditions characterized by the Rabi frequency Ω_{0cv} corresponding to the peak magnitude of the pump pulse, and the detuning Δ defined by the difference between laser frequency and the band gap energy. It is found that in the time signals, irregular oscillatory patterns with anomalously enhanced amplitudes are manifested at specific conditions, where the energy of the plasmon due to the photoexcited carriers coincides with that of the LO phonon leading to the striking anticrossings. The irregular oscillations due to the energetically *resonant* interaction between the LO phonon and the plasmon appear just in the early-stage of the CP generation, and further, result in asymmetric spectral profiles of associated power spectra. Calculated results of Fano's asymmetric q value of the spectra with respect to Δ are in harmony with experimental ones. Moreover, the oscillatory patterns are subject to the Rabi flopping of the excited carriers depending on Ω_{0cv}. These quantum mechanical effects enrich the dynamics in the early-stage of the CP generation.

List of Figures

3

4

List of Published Papers

1. Y. Watanabe, K. Hino, M. Hase and N. Maeshima,

    "Polaronic quasiparticle picture for generation dynamics of coherent phonons in semi-conductors: Transient and nonlinear Fano resonance,"
    Phys. Rev. B **95**, 014301 (2017).

2. Y. Watanabe, K. Hino, M. Hase and N. Maeshima,

    "Irregular oscillatory patterns in the early-time region of coherent phonon generation in silicon,"
    Phys. Rev. B **96**, 125204 (2017).

3. Y. Watanabe, K. Hino, M. Hase and N. Maeshima,

    "Quantum Generation Dynamics of Coherent Phonons: Analysis of Transient Fano Resonance,"
    J. Phys.: Conf. Ser. **864**, 012079 (2017).

4. K. Hino, Y. Watanabe, M. Hase and N. Maeshima,

    "Laser-Induced Fano Resonance in Condensed Matter Physics,"
    in *Resonance*, edited by Jan Awrejcewicz (InTech Open, 2017) Chap. 11. ISBN: 978-953-51-5617-8.

5. Y. Watanabe, K. Hino, M. Hase and N. Maeshima,

    (in preparation).

Contents

Chapter 1

Introduction

1.1   Coherent Phonon Generation

The development of the technology for ultrashort pulse laser with high intensity has enabled us to explore a new research area of ultrafast and non-equilibrium phenomena governed by heavily photoexcited carriers [1]. The irradiation of the ultrashort pulse laser excites a longitudinal optical (LO) phonon mode coherently, namely, with the same frequency [2, 3]. Here, it is required that temporal width of the pulse is much shorter than a period of the LO phonon; since the typical frequency of the LO phonon in materials is in the 10 THz regime, femtosecond laser pulses are suitable for coherent phonon (CP) generation. This is undoubtedly one of the representative ultrafast phenomena unveiled by the irradiation of the ultrashort pulse laser.

The coherent lattice vibration causes the macroscopic temporal change in optical properties such as reflectivity and transmission, and this is distinct from thermal lattice vibrations which does not induce the macroscopic polarization. Thus, the CP signals are measured in the time domain through the changes of the optical properties, typically using the pump-probe experiments [2, 3]; the pump pulse creates photoexcited carriers, followed by the probe pulse, delayed in time, which detects the modulations of the optical properties. For various purposes of exploring underlying new physics, detecting phonon modes with different symmetries in time domain, manipulating collective lattice motions, and other objectives, the CP generation has been investigated in a variety of materials such as semiconductors [4, 5, 6, 7, 8, 9, 10], semimetals/metals [11, 12, 13, 14, 15, 16, 17], high-T_c superconductors [18, 19, 20, 21], and other materials [22, 23, 24, 25, 26].

1.2   Theory of the Coherent Phonon Generation

1.2.1   Phenomenological oscillator models

Thus far, the CP generation mechanism has been discussed by means of classical models based on a damped forced-oscillation, which is expressed as [2, 3]

$$\frac{d^2Q(t)}{dt^2} + 2\gamma\frac{dQ(t)}{dt} + \omega^2 Q(t) = \frac{F(t)}{m}. \tag{1.1}$$

Here, $Q(t)$ is a CP displacement amplitude, ω is the frequency of the phonon, γ is a phenomenological damping parameter, $F(t)$ is an external driving force, and m is a re-

duced lattice mass. Under the conditions that both $Q(t)$ and $dQ(t)/dt$ are zero before $F(t)$ is applied, Eq. (1.1) is solved by use of either the Green function technique or the Laplace-transform method as

$$Q(t) = \int_{-\infty}^{t} \frac{F(t')}{m} \frac{e^{-\gamma(t-t')} \sin\left[\sqrt{\omega^2 - \gamma^2}(t - t')\right]}{\sqrt{\omega^2 - \gamma^2}} dt'. \tag{1.2}$$

There are two well-known models for the CP generation as the limiting cases of $F(t)$. One is the impulsive stimulated Raman scattering (ISRS) model [27, 28], and the other is the displacive excitation of CP (DECP) model [29, 30]. In the ISRS model, $F(t)$ is associated with the Raman polarizability, namely, a derivative of electronic susceptibility with respect to lattice displacement, and the impulsive force induces the oscillation around the current equilibrium position. Supposing that the force is given by $F(t) = I\delta(t)$, the solution of Eq. (1.2) is readily cast into

$$Q(t) = \frac{I\theta(t)}{m\sqrt{\omega^2 - \gamma^2}} e^{-\gamma t} \sin\left(\sqrt{\omega^2 - \gamma^2}\, t\right), \tag{1.3}$$

that is, $Q(t)$ becomes of the sine form. In the transparent region, the ISRS is considered to be the key mechanism for the CP generation.

On the other hand, in the DECP model, the interband excitation of carriers causes an impulsive shift of the equilibrium position of the lattice vibration, and the external force is related to the excited carrier density. Supposing that the force is provided by $F(t) = F\theta(t)/m$, Eq. (1.2) is directly integrated, and thus we obtain $Q(t)$ as

$$Q(t) = \frac{F\theta(t)}{m\omega^2}\left[1 - \left\{\frac{\gamma}{\sqrt{\omega^2 - \gamma^2}} \sin\left(\sqrt{\omega^2 - \gamma^2}\, t\right) + \cos\left(\sqrt{\omega^2 - \gamma^2}\, t\right)\right\} e^{-\gamma t}\right]. \tag{1.4}$$

In fact, $\omega \gg \gamma$, and thus, $Q(t)$ becomes of the cosine form with the center of the oscillation shifted. It is understood that the DECP is the key mechanism in the opaque region. Besides, Kuznetsov *et al.* presented a microscopic explanation of this model by means of the phenomenological Hamiltonian for two-band semiconductors [30]. According to this model, $F(t)$ is given by the diagonal components of the electronic density matrix, that is, the phonon mode with momentum $\boldsymbol{q} = 0$ is coupled with the excited carriers.

In addition to the two models mentioned above, one more mechanism of the transient depletion field screening has been studied in polar semiconductors [31, 32]. A static electric field perpendicular to the surface attributed to the surface depletion layer [33] leads atoms to a new equilibrium position. The pump pulse irradiation gives rise to screening of the surface field due to the photoexcited carriers on a subpicosecond time scale. In other words, the initial band bending at the surface is relaxed toward a flat band due to charge separation by the drift process. Thus, switching off the surface field launches the longitudinal oscillation of the atoms, and its behavior indicates the cosine form. The surface field is strongly dependent on the doping level, and the different types of the oscillation have been observed among intrinsic, *n*-type, and *p*-type GaAs so far [32, 34]. In particular, the phase of the oscillation is deviated by 180° between the *n*- and *p*-type samples [31].

Initial phase

Indeed, these classical models have succeeded in revealing overall character of the CP generation dynamics. Given the results of these models, the phase shift built in an asymptotic damped harmonic vibration, termed as an initial phase θ, is considered to include the information about the CP generation mechanism, and it is typically defined in such a form

$$Q(t) \propto e^{-\gamma t} \cos(\omega t + \theta). \tag{1.5}$$

Therefore, a great number of experimental results have been examined from the viewpoint of the initial phase. However, the experimentally obtained initial phases varied from material to material, and further, they were strongly dependent on the doping level [7], the pulse laser conditions [8], and the symmetry of the phonon modes [12, 15]. Therefore, the relation between the CP generation mechanism and the associated initial phase is still controversial.

Several theoretical studies related with the classical models have been reported so far [35, 36, 37, 38, 39, 40]. In particular, Merlin and co-workers developed an extended stimulated Raman scattering model − termed as transiently stimulated Raman scattering (TSRS) model [35, 36, 38]− in order to describe light-induced lattice motion of both impulsive and displacive character. Here, the equation of motion of the CP amplitude relevant to Eq. (1.1) was derived in an approximate manner starting from the phenomenological Hamiltonian. According to this model, the external force is composed of both impulsive and displacive contribution, and in particular, the displacive character is described by resonant stimulated Raman scattering. Thereby, they compared the theoretical and experimental results of Sb. Further, Riffe *et al.* devised the TSRS model by hybridizing the ISRS and DECP models; the authors gave a finite lifetime to the excited carrier density, so as to be made in agreement with the experimental results of the initial phases for various materials [40].

1.2.2   Microscopic mechanisms

However, it is a matter of course that the ultrafast carrier-lattice dynamics induced by the ultrashort pulse laser is not able to be described by a single equation such a form of Eq. (1.1), and the couped equations composed of both the phonon and the excited carriers are to be solved. Further, the carriers are coupled each other through the Coulomb potential interaction, leading to various considerable effects such as the formation of the plasmon and the exciton [41]. Therefore, the above-mentioned approaches based on the classical models encounter difficulties in not only demonstrating the details of the dynamics of concern embedded in the initial phases, but also revealing unexplored quantum mechanical effects. For the above-mentioned reason, microscopic mechanisms of the CP generation dynamics have been targets of great interest for a long time.

Several theoretical studies apart from the classical models have been reported so far, and the brief summary is provided in the following. Scholz *et al.* applied the density-matrix theory in order to comprehend the external forces and the initial phases in the system of Ge [42]. Lee *et al.* numerically solved the time-dependent Schrödinger equation in an electron-phonon system to demonstrate the quantum effect experimentally observed [43]. Shinohara *et al.* applied the time-dependent density-functional theory to the CP generation of Si [44] and Sb [45], and calculated physical quantities such as the

initial phases and the amplitudes under several pulse laser conditions. Riffe constructed a classical Fano oscillator model based on the Fano-Anderson Hamiltonian [46], and investigated the Fano resonance (FR) [47] effect on the initial phases [48]. Nakamura *et al.* applied a simple two-level model and showed the dependence of the CP generation mechanism on pulse width and detuning [49]. Kayanuma *et al.* proposed a dynamic Jahn-Teller approach to elucidate the generation mechanism of asymmetric modes [50]. Nevertheless, the understanding of microscopic mechanisms focusing on quantum effects has not sufficed yet thus far.

1.3 Quantum Mechanical Effect Concomitant to the Coherent Phonon Generation

Quantum effects are caused in the initial stage of the CP dynamics where heavily photoexcited carriers still stay in the excited states without relaxation and interact with the LO phonon; hereafter, this time region is termed as the early time region (ETR). The non-equilibrium carriers generated by the pump pulse irradiation are relaxed into the quasi-equilibrium state due to the intervalley scattering through the emission of phonons, and carrier-carrier scattering [3], diminishing the contribution from the carriers to the concerned dynamics. This time region after the ETR is termed as the classical region, and in this region, the CP signal overall shows just a damped harmonic oscillation. Incidentally, in fact, additional complicated signals due to coherent artifact attributed to nonlinear optical interference between the pump and probe pulses [51, 52, 53] manifest themselves in the ETR, which result in masking inherent dynamics in the CP generation.

As regards the quantum effect accompanied by the CP generation, FR has been observed transiently in the ETR for lightly n-doped Si [6]. This FR is considered to be caused by interference between a discrete state of the LO phonon and continuum states of the excited carriers. This is discerned just in a moment before the carrier relaxation time. Further, it is speculated that the manifestation of the FR is the vestige of the birth of a polaronic quasiparticle (PQ) due to the strong carrier-LO phonon interaction [54]. Here, it is noted that the transient FR has been observed exclusively in semimetals/metals of Zn [13] and Bi [14, 17] in addition to lightly n-doped Si, not observed in GaAs and p-doped Si so far. Incidentally, recently, a dynamical Fano-like effect was observed in CuCl semiconductor microcavities, which was attributed to the interference between CPs and short-lived Rabi oscillations [10]

Concerning theoretical studies of the transient FR, in Ref. [43], a displacement function of CP was calculated under the far above-gap excitation conditions, and the associated continuous-wavelet transform (CWT) was conducted for the system of GaAs. The CWT spectra showed asymmetric shapes characteristic of FR, although it was not in consistency with the existing experimental results. Further, it was argued that the resulting FR originated from interference between two types of vibrational Raman scattering processes. In Ref. [48], analytical expressions of the Fano absorption line shape and the initial phase were derived by means of the classical Fano oscillator model, and it was shown that the two quantities are relevant to each other. However in Ref. [17], the Fourier transform of the Fano's spectral formula into the time domain was taken in a direct manner, and thus, the different initial-phase dependence of the line shape was shown. Further, it was confirmed that the experimental results of the CP signal for Bi were in agreement with

the obtained initial-phase dependence.

Transient and nonlinear Fano resonance

As is well known, FR is a quantum mechanical resonance effect due to the coupling between discrete states and energetically degenerate continuum states, and this is characterized by asymmetric line shapes composed of both a peak and a dip [47]. FR is one of the fundamental and common concepts in diverse fields of chemistry and physics [55].

As regards FR observed in a Si crystal, a different type of FR from the concerned one has been well studied so far; incoherent Raman scattering driven by the irradiation of a continuous wave (cw) laser generates this FR in heavily doped Si [56, 57, 58, 59, 60, 61, 62]. This FR effect was observed in the system of heavily doped p-type Si in the Γ point [56, 57, 58]. Here, the electron-LO phonon interaction causes an inter-valence-band electronic transition with emission of the LO phonon, resulting in the FR. The similar FR was also observed in the system of heavily doped n-type Si in the X-valley [60]. Interestingly, the manners of doping affect the sign of the resulting Fano's q parameter [47], that is, this parameter inclines to become positive (negative) in $p(n)$-type Si. Besides, this type of FR was also observed in the system of δ-doped GaAs [63, 64, 65].

In particular, as far as the FR process induced by the laser irradiation, the concerned transient FR is categorized into unusual optically *nonlinear* and *transient* processes, which are considerably distinct from most of optically linear and stationary FR processes owing to the cw-laser irradiation. In fact, the concerned FR results from heavily photoexcited carriers created by an ultrashort pulse laser, and manifest itself just in the temporal region where the carriers still in the excited states, that is, immediately after the completion of the pulse irradiation.

As one example which belongs to this type of FR, there is a transient excitonic FR appearing in ultrafast optical processes [66, 67, 68]. However, the number of studies relevant to this type is really limited since theoretical predictions in advance and experimental measurements are quite difficult. Therefore, the studies directed toward this type of FR would provide potentially enriched physics to be explored. Hereafter, we term this type of FR transient FR just for the sake of simplicity unless otherwise stated.

1.4   Aim of the Present Dissertation

The aim of the present dissertation is as follows. First, we construct a fully quantum mechanical model for the CP generation dynamics applicable for both nonpolar and polar semiconductors on an equal footing [69]. Given the supposition of the formation of the PQ in the experiments [6, 54], we introduce PQ operators composed of an LO phonon operator and a set of pairs of electron operators. In the present situation of concern, the photoexcited carriers lead to the plasmon of a collective excitation mode and electron-hole continua of single-particle excitation modes. Here, one more collective excitation mode of exciton is omitted since its bound-state energy locates below the joint-energy band dispersion of concern, and the coupling between the phonon and exciton modes would be negligibly small. Second, on the basis of the PQ model, we examine the origin of the transient FR [69, 70] and other unexplored quantum mechanical effects [71, 72]. In the former, the interference between the LO phonon and the electron-hole continua plays a key role, while in the latter, a coupling between two discrete states of the LO phonon and
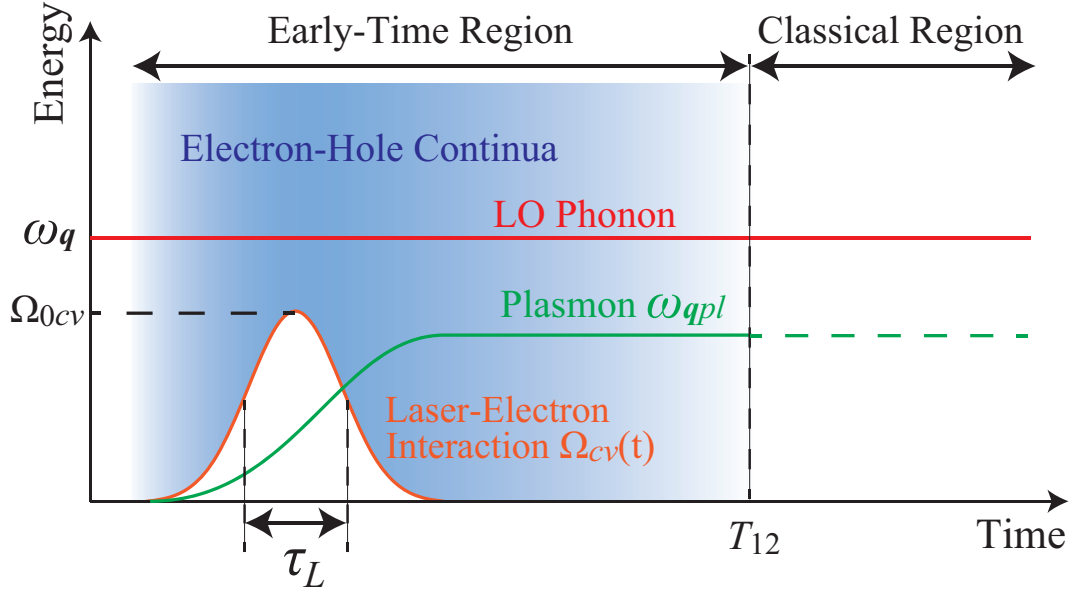
Figure 1.1: The schematic diagram of the time evolution of the CP generation dynamics. The energy of the LO phonon ω_q, the plasmon, and the electron-hole continua are represented by a red line, a green line, and gradation of blue color, respectively. The gradation shows how high the excited carrier density is in a schematic manner. Further, the green dashed line in the classical region represents the plasmon mode which is decoupled with the phonon due to the relaxation. T_{12} is the phenomenological relaxation time of induced carrier density, and represents a rough estimate of the border between the early-time region and the classical region. Further, the orange solid line represents the magnitude of the laser-electron interaction dependent on a peak amplitude Ω_{0cv} and temporal width of the pulse τ_L

the plasmon plays a key role. Third, we investigate the features of the CP generation such as the initial phases and the asymptotic amplitudes under various pulse laser conditions, and compare the results with other experimental and theoretical ones [71, 72].

Figure 1.1 depicts the time evolution of the CP dynamics, where a rough border between the ETR and the classical region is delimited by a phenomenological relaxation time constant T_{12} attributed to the carrier relaxation time and the dephasing time of a subpicosecond time scale [3]. It is seen that the energy of the LO phonon ω_q with momentum q − represented by a red solid line − is embedded in the continuum state of the single-particle excitation − represented by gradation of blue color−; the gradation shows how high the excited carrier density is in a schematic manner. Moreover, the energy of the plasmon ω_{qpl} is shown by a green solid line. When the plasmon mode approaches the phonon mode, ω_q and ω_{qpl} show an anticrossing, which influences the physical quantities. The green dashed line in the classical region represents the plasmon mode which is decoupled with the phonon due to the relaxation, although the carriers still stay in the quasi-equilibrium states; the carriers recombine to reach the true equilibrium state on a nanosecond time scale [3]. Further, the magnitude of the laser-electron interaction $\Omega_{cv}(t)$, which depends on a peak amplitude Ω_{0cv} and temporal width of the pulse τ_L, is shown by an orange solid line. This provides the threshold of the continuum, and determines ω_{qpl}.

The details are shown in Sec. 3.

For the above-mentioned purposes, we examine a retarded longitudinal susceptibility leading to transient induced photoemission spectra from photoexcited states, and a CP displacement function; the associated retarded Green functions are described by means of an adiabatic expansion with respect to the PQ operators with time fixed. First, we examine the photoemission spectra in the system of undoped Si and undoped GaAs, in which an asymmetric spectral profile characteristic of FR manifests itself in Si, though not in GaAs [see Sec. 3.1]. Next, we examine the CP displacement function in the system of undoped Si, and irregular oscillatory patterns appear on the occasion that the phonon and the plasmon resonantly interact with each other [see Sec. 3.2]. It is noted that opaque interband transitions accompanying real excited carriers are exclusively taken into account. Further, the delayed formation of plasmon-LO phonon coupled modes in polar semiconductors are not taken into consideration in this study because these modes do not appear immediately after the pulse laser irradiation of the ETR [34, 62, 73, 74, 75, 76, 77, 78].

This dissertation is organized as follows. In Chap. 2, we describe the theoretical framework. In Chap. 3, we present the results and discussion. Finally in Chap. 4, we present the conclusions. Atomic units (a.u.) are used throughout unless otherwise stated.

Chapter 2

Theory

2.1 Equations of Motion

We take into consideration the total Hamiltonian $\hat{H}$, provided by

$$\hat{H} = \hat{H}_e + \hat{H}'(t) + \hat{H}_p + \hat{H}_{e-p}, \tag{2.1}$$

where

$$\hat{H}_e = \sum_{b\boldsymbol{k}} \varepsilon_{b\boldsymbol{k}} a_{b\boldsymbol{k}}^\dagger a_{b\boldsymbol{k}} + \frac{1}{2} \sum_{\boldsymbol{q} \neq 0} V_{\boldsymbol{q}}^{(C)} \sum_{bb'\boldsymbol{k}\boldsymbol{k}'} a_{b\boldsymbol{k}+\boldsymbol{q}}^\dagger a_{b'\boldsymbol{k}'-\boldsymbol{q}}^\dagger a_{b'\boldsymbol{k}'} a_{b\boldsymbol{k}}, \tag{2.2}$$

$$\hat{H}'(t) = -\sum_{\boldsymbol{k}} \left[\Omega_{cv}(t)\, a_{c\boldsymbol{k}}^\dagger a_{v\boldsymbol{k}} + \Omega_{vc}(t)\, a_{v\boldsymbol{k}}^\dagger a_{c\boldsymbol{k}} \right], \tag{2.3}$$

$$\hat{H}_p = \sum_{\boldsymbol{q}} \omega_{\boldsymbol{q}} c_{\boldsymbol{q}}^\dagger c_{\boldsymbol{q}}, \tag{2.4}$$

and

$$\hat{H}_{e-p} = \sum_{b\boldsymbol{q}\boldsymbol{k}} \left(g_{b\boldsymbol{q}} c_{\boldsymbol{q}} a_{b\boldsymbol{k}+\boldsymbol{q}}^\dagger a_{b\boldsymbol{k}} + g_{b\boldsymbol{q}}^* c_{\boldsymbol{q}}^\dagger a_{b\boldsymbol{k}}^\dagger a_{b\boldsymbol{k}+\boldsymbol{q}} \right). \tag{2.5}$$

$\hat{H}_e$ is a two-band electron Hamiltonian, where we consider the energetically-lowest conduction band ($b = c$) and the energetically-highest valence band ($b = v$). $a_{b\boldsymbol{k}}^\dagger$ and $a_{b\boldsymbol{k}}$ represent creation and annihilation operators of the electron, respectively, with the energy dispersion $\varepsilon_{b\boldsymbol{k}}$ and the Bloch momentum $\boldsymbol{k}$ in band b; $\varepsilon_{b\boldsymbol{k}}$ is given based on the effective-mass approximation with parabolic dispersion in the proximity of Γ point. $V_{\boldsymbol{q}}^{(C)}$ is a Coulomb potential represented as

$$V_{\boldsymbol{q}}^{(C)} = \frac{4\pi}{\epsilon_\infty V} \frac{1}{\boldsymbol{q}^2}, \tag{2.6}$$

where ϵ_∞, V, and $\boldsymbol{q}$ are a dielectric constant in the high-frequency limit, volume of crystal, and momentum, respectively. $\hat{H}'(t)$ is the electron-light interaction at time t, and $\Omega_{b\bar{b}}(t)$ is expressed as

$$\Omega_{b\bar{b}}(t) = \Omega_{0b\bar{b}} f(t) \cos \omega_0 t, \tag{2.7}$$

where the Rabi frequency $\Omega_{0b\bar{b}}$ is provided by the product of a peak amplitude of an irradiated electric field and the electric dipole moment between the c- and v-bands. Here, we assume that the dependence of the dipole moment on $\boldsymbol{k}$ is negligibly small. The

barred index $\bar{b}$ means that the index is unequal to b; $\bar{c} = v$ and $\bar{v} = c$. Further, ω_0 and $f(t)$ are laser frequency and a pulse-envelope function, respectively. $\hat{H}_p$ and $\hat{H}_{e-p}$ are an LO phonon Hamiltonian and the electron-phonon interaction, respectively. $c_{\boldsymbol{q}}^\dagger$ and $c_{\boldsymbol{q}}$ represent creation and annihilation operators of the LO phonon, respectively, with the energy dispersion $\omega_{\boldsymbol{q}}$. We omit the zero-point energy of the phonon just for the sake of simplicity. Further, $g_{b\boldsymbol{q}}$ represents a coupling constant between the b-band electron and the LO phonon.

The non-equilibrium dynamics driven by the pump laser irradiation of concern is described by time-evolution of the phonon operator and a composite operator representing an induced carrier density, defined as

$$A_{\boldsymbol{q}}^\dagger(\boldsymbol{k}bb') = a_{b\boldsymbol{k}+\boldsymbol{q}}^\dagger a_{b'\boldsymbol{k}}. \tag{2.8}$$

It is remarked that the transferred momentum $\boldsymbol{q}$ is finite, even though it is quite small: $\boldsymbol{q} \neq 0$. The equation of motion of $A_{\boldsymbol{q}}^\dagger(\boldsymbol{k}bb')$ is expressed in terms of the Heisenberg equation as

$$-i\left(\frac{d}{dt} + \frac{1}{T_{\boldsymbol{q}\boldsymbol{k}bb'}}\right) A_{\boldsymbol{q}}^\dagger(\boldsymbol{k}bb') = [\hat{H}_e + \hat{H}'(t), A_{\boldsymbol{q}}^\dagger(\boldsymbol{k}bb')] + [\hat{H}_{e-p}, A_{\boldsymbol{q}}^\dagger(\boldsymbol{k}bb')], \tag{2.9}$$

where $T_{\boldsymbol{q}\boldsymbol{k}bb'}$ is a phenomenological relaxation time constant of $A_{\boldsymbol{q}}^\dagger(\boldsymbol{k}bb')$. The expression of the first commutator in the right-hand side of Eq. (2.9) is obtained as

$$[\hat{H}_e + \hat{H}'(t), A_{\boldsymbol{q}}^\dagger(\boldsymbol{k}bb')] \approx \sum_{\tilde{\boldsymbol{k}}\tilde{b}\tilde{b}'} A_{\boldsymbol{q}}^\dagger(\tilde{\boldsymbol{k}}\tilde{b}\tilde{b}') Z_{\boldsymbol{q}}(\tilde{\boldsymbol{k}}\tilde{b}\tilde{b}', \boldsymbol{k}bb'), \tag{2.10}$$

where a c-number non-Hermitian matrix $Z_{\boldsymbol{q}}$ is represented as

$$\begin{aligned} Z_{\boldsymbol{q}}(\boldsymbol{k}_1 b_1 b_1', \boldsymbol{k}_2 b_2 b_2') &= \omega_{b_1 b_1' \boldsymbol{k}_1 \boldsymbol{q}} \delta_{b_1 b_2} \delta_{b_1' b_2'} \delta_{\boldsymbol{k}_1 \boldsymbol{k}_2} + V_{\boldsymbol{q}}^{(C)} \delta_{b_1 b_1'} \Delta\rho_{b_2 b_2' \boldsymbol{k}_2 \boldsymbol{q}} \\ &\quad - \Omega_{b_1 \bar{b}_1 \boldsymbol{k}_1}^{(R)} \delta_{b_1 \bar{b}_2} \delta_{b_1' b_2'} \delta_{\boldsymbol{k}_1 \boldsymbol{k}_2} + \Omega_{\bar{b}_1' b_1' \boldsymbol{k}_1}^{(R)} \delta_{b_1' \bar{b}_2'} \delta_{b_1 b_2} \delta_{\boldsymbol{k}_1 \boldsymbol{k}_2}. \end{aligned} \tag{2.11}$$

Here,

$$\omega_{bb'\boldsymbol{k}\boldsymbol{q}} = \varepsilon_{b\boldsymbol{k}+\boldsymbol{q}}^{(r)} - \varepsilon_{b'\boldsymbol{k}}^{(r)} \tag{2.12}$$

with a renormalized electron energy in band b as

$$\varepsilon_{b\boldsymbol{k}}^{(r)} = \varepsilon_{b\boldsymbol{k}} - \sum_{\boldsymbol{q}} V_{\boldsymbol{q}}^{(C)} \rho_{bb\boldsymbol{k}+\boldsymbol{q}}, \tag{2.13}$$

and

$$\Omega_{b\bar{b}\boldsymbol{k}}^{(R)}(t) = \Omega_{b\bar{b}}(t) + \sum_{\boldsymbol{q}} V_{\boldsymbol{q}}^{(C)} \rho_{\bar{b}b\boldsymbol{k}+\boldsymbol{q}}. \tag{2.14}$$

Besides, a single-particle density matrix $\rho_{bb'\boldsymbol{k}} \equiv \langle a_{b\boldsymbol{k}}^\dagger a_{b'\boldsymbol{k}} \rangle$ and

$$\Delta\rho_{bb'\boldsymbol{k}\boldsymbol{q}} = \rho_{bb'\boldsymbol{k}} - \rho_{bb'\boldsymbol{k}+\boldsymbol{q}}, \tag{2.15}$$

where $\langle \hat{O} \rangle$ represents an expectation value of operator $\hat{O}$ with respect to the ground state. It is noted that we evaluate Eq. (2.9) by employing a factorization approximation, and four operator terms such as $a_{b,\tilde{\boldsymbol{k}}+\tilde{\boldsymbol{q}}}^\dagger a_{\tilde{b}'\tilde{\boldsymbol{k}}} a_{b,\boldsymbol{k}+\boldsymbol{q}}^\dagger a_{b'\boldsymbol{k}}$ is split into a product of the operator $A_{\tilde{\boldsymbol{q}}}^\dagger(\tilde{\boldsymbol{k}}\tilde{b}\tilde{b}')$ and the single-particle density matrix $\rho_{bb'\boldsymbol{k}}$. The detail is shown in Appendix A.

Moreover, we employ the rotating wave approximation [41, 79], and thus high-frequency contributions are removed from Eq. (2.9); $A_{\boldsymbol{q}}^{\dagger}(\boldsymbol{k}bb')$ and $\rho_{bb'\boldsymbol{k}}$ are replaced by $e^{i\bar{\omega}_{bb'}t}\bar{A}_{\boldsymbol{q}}^{\dagger}(\boldsymbol{k}bb')$ and $e^{i\bar{\omega}_{bb'}t}\bar{\rho}_{bb'\boldsymbol{k}}$, respectively, where $\bar{\omega}_{cv} = \omega_0$, $\bar{\omega}_{vc} = -\omega_0$, and $\bar{\omega}_{bb} = 0$. Thus, Eqs. (2.9) and (2.11) are cast into

$$
\begin{aligned}
-i\left(\frac{d}{dt} + \frac{1}{T_{\boldsymbol{q}\boldsymbol{k}bb'}}\right)\bar{A}_{\boldsymbol{q}}^{\dagger}(\boldsymbol{k}bb') &= [\hat{H}_e + \hat{H}'(t), \bar{A}_{\boldsymbol{q}}^{\dagger}(\boldsymbol{k}bb')] - \bar{A}_{\boldsymbol{q}}^{\dagger}(\boldsymbol{k}bb')\bar{\omega}_{bb'} + [\hat{H}_{e-p}, \bar{A}_{\boldsymbol{q}}^{\dagger}(\boldsymbol{k}bb')] \\
&\approx \sum_{\tilde{\boldsymbol{k}}\tilde{b}\tilde{b}'}\bar{A}_{\boldsymbol{q}}^{\dagger}(\tilde{\boldsymbol{k}}\tilde{b}\tilde{b}')\bar{Z}_{\boldsymbol{q}}(\tilde{\boldsymbol{k}}\tilde{b}\tilde{b}', \boldsymbol{k}bb') + [\hat{H}_{e-p}, \bar{A}_{\boldsymbol{q}}^{\dagger}(\boldsymbol{k}bb')] \quad (2.16)
\end{aligned}
$$

and

$$
\begin{aligned}
\bar{Z}_{\boldsymbol{q}}(\boldsymbol{k}_1 b_1 b_1', \boldsymbol{k}_2 b_2 b_2') &= \bar{\omega}_{b_1 b_1' \boldsymbol{k}_1 \boldsymbol{q}}\delta_{b_1 b_2}\delta_{b_1' b_2'}\delta_{\boldsymbol{k}_1 \boldsymbol{k}_2} + V_{\boldsymbol{q}}^{(C)}\delta_{b_1 b_1'}\Delta\bar{\rho}_{b_2 b_2' \boldsymbol{k}_2 \boldsymbol{q}} \\
&\quad -\bar{\Omega}_{b_1 \bar{b}_1 \boldsymbol{k}_1}^{(R)}\delta_{b_1 \bar{b}_2}\delta_{b_1' b_2'}\delta_{\boldsymbol{k}_1 \boldsymbol{k}_2} + \bar{\Omega}_{\bar{b}_1' b_1' \boldsymbol{k}_1}^{(R)}\delta_{b_1' \bar{b}_2'}\delta_{b_1 b_2}\delta_{\boldsymbol{k}_1 \boldsymbol{k}_2}, \quad (2.17)
\end{aligned}
$$

respectively, where

$$
\bar{\omega}_{bb'\boldsymbol{k}\boldsymbol{q}} = \omega_{bb'\boldsymbol{k}\boldsymbol{q}} - \bar{\omega}_{bb'} \quad (2.18)
$$

and

$$
\bar{\Omega}_{b\bar{b}\boldsymbol{k}}^{(R)}(t) = \frac{1}{2}\Omega_{0b\bar{b}}f(t) + \sum_{\boldsymbol{q}}V_{\boldsymbol{q}}^{(C)}\bar{\rho}_{\bar{b}b\boldsymbol{k}+\boldsymbol{q}}. \quad (2.19)
$$

As regards the equation of motion of $c_{\boldsymbol{q}}^{\dagger}$, it is straightforward derived in terms of the Heisenberg equation as

$$
-i\left(\frac{d}{dt} + \frac{1}{T_{\boldsymbol{q}ph}}\right)c_{\boldsymbol{q}}^{\dagger} = \omega_{\boldsymbol{q}}c_{\boldsymbol{q}}^{\dagger} + \sum_{b\boldsymbol{k}}g_{b\boldsymbol{q}}\bar{A}_{\boldsymbol{q}}^{\dagger}(\boldsymbol{k}bb), \quad (2.20)
$$

where $T_{\boldsymbol{q}ph}$ is a phenomenological relaxation time constant of $c_{\boldsymbol{q}}^{\dagger}$ due to phonon anharmonicity.

2.2   Retarded Longitudinal Susceptibility

On the basis of the linear response theory, an induced charge density $n_{\boldsymbol{q}}^{(ind)}(t)$ caused by a weak external optical field $f_{\boldsymbol{q}}(t)$ is given by [79, 80]

$$
n_{\boldsymbol{q}}^{(ind)}(t) = \frac{1}{4\pi V}\int_{-\infty}^{t}dt'\,\chi_{\boldsymbol{q}}^{(t)}(t, t')f_{\boldsymbol{q}}(t'). \quad (2.21)
$$

$\chi_{\boldsymbol{q}}^{(t)}(t, t')$ is a retarded longitudinal susceptibility in the nonequilibrium and transient system of concern, which consists of two contributions as

$$
\chi_{\boldsymbol{q}}^{(t)}(t, t') = \chi_{\boldsymbol{q}}(t, t') + \chi_{\boldsymbol{q}}'(t, t'), \quad (2.22)
$$

where $\chi_{\boldsymbol{q}}(t, t')$ and $\chi_{\boldsymbol{q}}'(t, t')$ are retarded susceptibilities attributed to an electron-induced interaction and an LO phonon-induced interaction, respectively. $\chi_{\boldsymbol{q}}(t, t')$ is expressed as

$$
\chi_{\boldsymbol{q}}(t, t') \equiv 4\pi V D_{\boldsymbol{q}}^{R}(t, t') = \chi_{-\boldsymbol{q}}^{*}(t, t'), \quad (2.23)
$$

where $D_{\boldsymbol{q}}^{R}(t,t')$ represents a retarded density-density correlation function of electrons provided by

$$D_{\boldsymbol{q}}^{R}(t,t') = -i\langle[\hat{n}_{\boldsymbol{q}}(t),\hat{n}_{-\boldsymbol{q}}(t')]\rangle\theta(t-t'). \tag{2.24}$$

Here, a density operator is given by

$$\hat{n}_{\boldsymbol{q}}(t) = \frac{1}{V}\sum_{b\boldsymbol{k}} a_{b\boldsymbol{k}+\boldsymbol{q}}^{\dagger} a_{b\boldsymbol{k}} \tag{2.25}$$

with

$$\hat{n}_{-\boldsymbol{q}}(t) = \hat{n}_{\boldsymbol{q}}^{\dagger}(t), \tag{2.26}$$

and

$$D_{\boldsymbol{q}}^{R\dagger}(t,t') = D_{-\boldsymbol{q}}^{R}(t,t'). \tag{2.27}$$

On the other hand, $\chi'_{\boldsymbol{q}}(t,t')$ in Eq. (2.22) is expressed as

$$\chi'_{\boldsymbol{q}}(t,t') = \frac{4\pi}{V}|g'_{\boldsymbol{q}}|^{2} D_{\boldsymbol{q}}'^{R}(t,t'), \tag{2.28}$$

where

$$|g'_{\boldsymbol{q}}|^{2} = \left|\frac{g_{\boldsymbol{q}}^{0}}{v_{\boldsymbol{q}}^{(C)}}\right|^{2} \tag{2.29}$$

with $g_{\boldsymbol{q}}^{0} = (g_{c\boldsymbol{q}} + g_{v\boldsymbol{q}})/2$ and

$$v_{\boldsymbol{q}}^{(C)} = \epsilon_{\infty}V_{\boldsymbol{q}}^{(C)} = \frac{4\pi}{V}\frac{1}{\boldsymbol{q}^{2}}. \tag{2.30}$$

$D_{\boldsymbol{q}}'^{R}(t,t')$ represents a retarded phonon Green function [79] defined as

$$
\begin{aligned}
D_{\boldsymbol{q}}'^{R}(t,t') &= -i\Big\langle\Big[c_{\boldsymbol{q}}(t)+c_{-\boldsymbol{q}}^{\dagger}(t),c_{-\boldsymbol{q}}(t')+c_{\boldsymbol{q}}^{\dagger}(t')\Big]\Big\rangle\theta(t-t')\\
&= -i\Big\langle\Big[c_{\boldsymbol{q}}(t),c_{\boldsymbol{q}}^{\dagger}(t')\Big]-\Big[c_{-\boldsymbol{q}}(t),c_{-\boldsymbol{q}}^{\dagger}(t')\Big]^{\dagger}\Big\rangle\theta(t-t')\\
&\equiv \bar{D}_{\boldsymbol{q}}'^{R}(t,t')+\Big[\bar{D}_{-\boldsymbol{q}}'^{R}(t,t')\Big]^{*},
\end{aligned} \tag{2.31}
$$

where

$$\bar{D}_{\boldsymbol{q}}'^{R}(t,t') = -i\Big\langle\Big[c_{\boldsymbol{q}}(t),c_{\boldsymbol{q}}^{\dagger}(t')\Big]\Big\rangle\theta(t-t'). \tag{2.32}$$

In the present study, we investigate two physical quantities associated with the retarded susceptibilities. One is a transient induced photoemission spectrum for an analysis of the transient FR, and the other is a CP displacement function. We derive analytic expressions of the two quantities, and the theoretical frameworks are described in Secs. 2.3 and 2.4, respectively. Here, we introduce the PQ operator to the present model, which is composed of $\bar{A}_{\boldsymbol{q}}^{\dagger}(\boldsymbol{k}bb')$ and $c_{\boldsymbol{q}}^{\dagger}$, and two physical quantities are expressed in terms of the PQ operator.

2.3 Analysis of the Transient Fano Resonance

In this section, we derive the analytical expression of the transient induced photoemission spectra so as to examine the transient FR. Here, we employ some approximation in addition to the factrization approximation and the rotating wave approximation, and solve the present problem as a multichannel scattering problem.

2.3.1 Introduction of polaronic quasiparticle operators

Quasiboson operator

First of all, we solve left and right eigenvalue problems [81] of the non-Hermitian matrix $\bar{Z}_{\boldsymbol{q}}$ of Eq. (2.17) with t fixed as an adiabatic parameter, represented by

$$U_{\boldsymbol{q}}^{L\dagger}\bar{Z}_{\boldsymbol{q}} = \mathcal{E}_{\boldsymbol{q}}U_{\boldsymbol{q}}^{L\dagger} \tag{2.33}$$

and

$$\bar{Z}_{\boldsymbol{q}}U_{\boldsymbol{q}}^{R} = U_{\boldsymbol{q}}^{R}\mathcal{E}_{\boldsymbol{q}}, \tag{2.34}$$

respectively. $\mathcal{E}_{\boldsymbol{q}}$ is an adiabatic eigenvalue diagonal matrix, and $\left\{U_{\boldsymbol{q}}^{L}, U_{\boldsymbol{q}}^{R}\right\}$ are the associated biorthogonal set of eigenvectors. The eigenvectors satisfy the orthogonality relation $U_{\boldsymbol{q}}^{L\dagger}U_{\boldsymbol{q}}^{R} = 1$ and the completeness $U_{\boldsymbol{q}}^{R}U_{\boldsymbol{q}}^{L\dagger} = 1$. We employ matrix notations, that is, $\bar{Z}_{\boldsymbol{q}} = \left\{\bar{Z}_{\boldsymbol{q}}(\tilde{\boldsymbol{k}}\tilde{b}\tilde{b}', \boldsymbol{k}bb')\right\}$, $\mathcal{E}_{\boldsymbol{q}} = \{\mathcal{E}_{\boldsymbol{q}\alpha}\}$, and $U_{\boldsymbol{q}}^{L/R} = \left\{U_{\boldsymbol{q}\alpha}^{L/R}(\boldsymbol{k}bb')\right\}$, where $\mathcal{E}_{\boldsymbol{q}\alpha}$ and $U_{\boldsymbol{q}\alpha}^{L/R}(\boldsymbol{k}bb')$ represent the eigenvalue and eigenvector of the αth state, respectively. As shown in Appendix B, we solve Eqs. (2.33) and (2.34) in an analytic manner, and thus, obtain the expressions of the αth left and right eigenvectors as

$$U_{\boldsymbol{q}\alpha}^{L\dagger} = N_{\boldsymbol{q}\alpha}^{L}V_{\boldsymbol{q}}^{(C)}u_{\boldsymbol{q}\alpha}^{L\dagger} \tag{2.35}$$

and

$$U_{\boldsymbol{q}\alpha}^{R} = N_{\boldsymbol{q}\alpha}^{R}V_{\boldsymbol{q}}^{(C)}u_{\boldsymbol{q}\alpha}^{R}, \tag{2.36}$$

respectively. Here, $u_{\boldsymbol{q}}^{L/R} = \left\{u_{\boldsymbol{q}\alpha}^{L/R}(\boldsymbol{k}bb')\right\}$, and $N_{\boldsymbol{q}\alpha}^{L/R}$ represents a normalization constant, which is determined by

$$N_{\boldsymbol{q}\alpha}^{L}N_{\boldsymbol{q}\alpha}^{R}[V_{\boldsymbol{q}}^{(C)}]^{2}\left(u_{\boldsymbol{q}\alpha}^{L\dagger}u_{\boldsymbol{q}\alpha}^{R}\right) = 1. \tag{2.37}$$

The creation operator of the quasiboson of the αth state is defined as

$$B_{\boldsymbol{q}\alpha}^{\dagger} = \sum_{\boldsymbol{k}bb'}\bar{A}_{\boldsymbol{q}}^{\dagger}(\boldsymbol{k}bb')U_{\boldsymbol{q}\alpha}^{R}(\boldsymbol{k}bb') \equiv \bar{A}_{\boldsymbol{q}}^{\dagger}U_{\boldsymbol{q}\alpha}^{R}. \tag{2.38}$$

It is noted that we introduce this operator so as to make sure the commutation relation of $[\hat{H}_{e}^{(\mathrm{eff})}(t), B_{\boldsymbol{q}\alpha}^{\dagger}(t)] = B_{\boldsymbol{q}\alpha}^{\dagger}(t)\mathcal{E}_{\boldsymbol{q}\alpha}(t)$, where $\hat{H}_{e}^{(\mathrm{eff})}(t)$ is an effective electronic Hamiltonian under the rotating wave approximation[1]. We define the adiabatic ground state of $\hat{H}_{e}^{(\mathrm{eff})}(t)$ as $|0\rangle$, and obtain the results of $[\hat{H}_{e}^{(\mathrm{eff})}(t), B_{\boldsymbol{q}\alpha}^{\dagger}(t)]|0\rangle = [\hat{H}_{e}^{(\mathrm{eff})}(t) - \mathcal{E}_{0}]|1; \boldsymbol{q}\alpha\rangle = \mathcal{E}_{\boldsymbol{q}\alpha}|1; \boldsymbol{q}\alpha\rangle$, where $|1; \boldsymbol{q}\alpha\rangle$ represents the single-quasiboson state. The mode $\boldsymbol{q}\alpha$ is defined as $|1; \boldsymbol{q}\alpha\rangle = B_{\boldsymbol{q}\alpha}^{\dagger}(t)|0\rangle$, and $\mathcal{E}_{0}$ is the zero-point energy; we set $\mathcal{E}_{0} = 0$ for the sake of simplicity. Thus, we obtain the expression of $\hat{H}_{e}^{(\mathrm{eff})}(t)|1; \boldsymbol{q}\alpha\rangle = \mathcal{E}_{\boldsymbol{q}\alpha}(t)|1; \boldsymbol{q}\alpha\rangle$. This procedure of the quasibosonization reminds us of Dyson's method of bosonization [82, 83]. It is remarked that this procedure of the quasibosonization is correct just for the single-quasiboson state. It would be questionable in the case that the number of quasibosons increases; for instance, $\hat{H}_{e}^{(\mathrm{eff})}(t)|2; \boldsymbol{q}\alpha\rangle \neq 2\mathcal{E}_{\boldsymbol{q}\alpha}(t)|2; \boldsymbol{q}\alpha\rangle$, where a two-quasiboson state $|2; \boldsymbol{q}\alpha\rangle$ is defined as $|2; \boldsymbol{q}\alpha\rangle = \sqrt{2}^{-1}[B_{\boldsymbol{q}\alpha}^{\dagger}(t)]^{2}|0\rangle$.

---

[1]Consulting the approximations employed in Sec. 2.3.2, the correction to $\hat{H}_{e} + \hat{H}'(t)$ is given by $-\sum_{\alpha\alpha'}B_{\boldsymbol{q}\alpha}^{\dagger}U_{\boldsymbol{q}\alpha}^{L\dagger}\bar{\omega}U_{\boldsymbol{q}\alpha'}^{R}B_{\boldsymbol{q}\alpha'}$.

The annihilation operator corresponding to the above-stated operator is defined as

$$B_{\boldsymbol{q}\alpha} = \sum_{\boldsymbol{k}bb'} U_{\boldsymbol{q}\alpha}^{R\dagger}(\boldsymbol{k}bb') \bar{A}_{\boldsymbol{q}}(\boldsymbol{k}bb') \equiv U_{\boldsymbol{q}\alpha}^{R\dagger} \bar{A}_{\boldsymbol{q}}. \qquad (2.39)$$

Employing the relation $\bar{Z}_{\boldsymbol{q}} = U_{\boldsymbol{q}}^R \mathcal{E}_{\boldsymbol{q}} U_{\boldsymbol{q}}^{L\dagger}$, Eq. (2.16) is recast as follows:

$$-i\frac{dB_{\boldsymbol{q}\alpha}^{\dagger}}{dt} = B_{\boldsymbol{q}\alpha}^{\dagger} \mathcal{E}_{\boldsymbol{q}\alpha} + i\sum_{\alpha'} B_{\boldsymbol{q}\alpha'}^{\dagger} \mathcal{W}_{\boldsymbol{q}\alpha'\alpha} + [\hat{H}_{e-p}, B_{\boldsymbol{q}\alpha}^{\dagger}], \qquad (2.40)$$

where

$$\mathcal{W}_{\boldsymbol{q}\alpha'\alpha} = W_{\boldsymbol{q}\alpha'\alpha} + \frac{\gamma_{\boldsymbol{q}\alpha'\alpha}^{(B)}}{2} \qquad (2.41)$$

with a non-adiabatic coupling between the αth and α'th adiabatic states given by

$$W_{\boldsymbol{q}\alpha'\alpha} = \sum_{\boldsymbol{k}bb'} \frac{dU_{\boldsymbol{q}\alpha'}^{L\dagger}(\boldsymbol{k}bb')}{dt} U_{\boldsymbol{q}\alpha}^R(\boldsymbol{k}bb') \equiv \frac{dU_{\boldsymbol{q}\alpha'}^{L\dagger}}{dt} U_{\boldsymbol{q}\alpha}^R, \qquad (2.42)$$

and

$$\frac{\gamma_{\boldsymbol{q}\alpha'\alpha}^{(B)}}{2} = \sum_{\boldsymbol{k}bb'} U_{\boldsymbol{q}\alpha'}^{L\dagger}(\boldsymbol{k}bb') \frac{1}{T_{\boldsymbol{q}\boldsymbol{k}bb'}} U_{\boldsymbol{q}\alpha}^R(\boldsymbol{k}bb'). \qquad (2.43)$$

Equation (2.40) represents an adiabatic coupled equation, where $\mathcal{E}_{\boldsymbol{q}\alpha}(t)$ is adiabatic energy at t related to the operator $B_{\boldsymbol{q}\alpha}^{\dagger}(t)$. It is remarked that $B_{\boldsymbol{q}\alpha}(t)$ and $B_{\boldsymbol{q}\alpha}^{\dagger}(t)$ do not fulfill the equal-time commutation relations for a real boson: $[B_{\boldsymbol{q}\alpha}(t), B_{\boldsymbol{q}'\alpha'}^{\dagger}(t)] \neq \delta_{\boldsymbol{q}\boldsymbol{q}'}\delta_{\alpha\alpha'}$. Further, $\mathcal{E}_{\boldsymbol{q}\alpha}$ is generally a complex number, although $B_{\boldsymbol{q}\alpha}^{\dagger}$ is Hermitian-conjugate of $B_{\boldsymbol{q}\alpha}$. The set of eigenstates $\{\alpha\}$ consists of a single discrete state signified as α_1 with eigenenergy $\mathcal{E}_{\boldsymbol{q}\alpha_1}$ and continuum states signified as β with eigenenergy $\mathcal{E}_{\boldsymbol{q}\beta}$: $\{\alpha\} = (\alpha_1, \{\beta\})$. The states α_1 and $\{\beta\}$ correspond to a plasmon-like mode and single-particle excitation modes in interbands, respectively. Moreover, on the complex analogy of the Hellman-Feynman theorem, $W_{\boldsymbol{q}\alpha'\alpha}$ is readily rewritten as

$$W_{\boldsymbol{q}\alpha'\alpha} = \frac{U_{\boldsymbol{q}\alpha'}^{L\dagger} \frac{d\bar{Z}_{\boldsymbol{q}}}{dt} U_{\boldsymbol{q}\alpha}^R}{\mathcal{E}_{\boldsymbol{q}\alpha'} - \mathcal{E}_{\boldsymbol{q}\alpha}}, \quad \alpha' \neq \alpha, \qquad (2.44)$$

and $W_{\boldsymbol{q}\alpha\alpha} \neq 0$.

It is noted that we omit the exciton of another collective excitation mode; its energy of the bound-states is below the joint-energy band dispersion, therefore, we assume that the coupling between the phonon and exciton modes are negligibly small compared with other electronic modes, and the effect of the exciton on the dynamics of concern is negligible. This approximation is done by neglecting the terms relevant to the exciton in the calculation of Eq. (2.11).

Quasiboson-LO phonon interaction

Following Eqs. (2.38) and (2.39), $\hat{H}_{e-p}$ of Eq. (2.5) is rewritten as

$$\hat{H}_{e-p} = \sum_{\boldsymbol{q},\alpha} \left(M_{\boldsymbol{q}\alpha} c_{\boldsymbol{q}} B_{\boldsymbol{q}\alpha}^{\dagger} + M_{\boldsymbol{q}\alpha}^* c_{\boldsymbol{q}}^{\dagger} B_{\boldsymbol{q}\alpha} \right), \qquad (2.45)$$

where an effective coupling constant between a quasiboson and the LO phonon is given by

$$M_{\boldsymbol{q}\alpha} = \sum_{\boldsymbol{k}b} g_{b\boldsymbol{q}} U_{\boldsymbol{q}\alpha}^{L\dagger}(\boldsymbol{k}bb). \tag{2.46}$$

Thus, the commutator of $[\hat{H}_{e-p}, c_{\boldsymbol{q}}^{\dagger}]$ is readily evaluated as

$$[\hat{H}_{e-p}, c_{\boldsymbol{q}}^{\dagger}] = \sum_{\alpha} M_{\boldsymbol{q}\alpha} B_{\boldsymbol{q}\alpha}^{\dagger}. \tag{2.47}$$

On the other hand, the commutator of $[\hat{H}_{e-p}, B_{\boldsymbol{q}\alpha}^{\dagger}]$ in Eq. (2.40) leads to

$$[\hat{H}_{e-p}, B_{\boldsymbol{q}\alpha}^{\dagger}] \approx M_{-\boldsymbol{q}\alpha}'' c_{-\boldsymbol{q}} + M_{\boldsymbol{q}\alpha}'^{*} c_{\boldsymbol{q}}^{\dagger}, \tag{2.48}$$

where the factorization approximation is employed; $[B_{\boldsymbol{q}\alpha}, B_{\boldsymbol{q}'\alpha'}^{\dagger}]$ and $[B_{\boldsymbol{q}\alpha}^{\dagger}, B_{\boldsymbol{q}'\alpha'}^{\dagger}]$ are replaced by $\langle[B_{\boldsymbol{q}\alpha}, B_{\boldsymbol{q}'\alpha'}^{\dagger}]\rangle$ and $\langle[B_{\boldsymbol{q}\alpha}^{\dagger}, B_{\boldsymbol{q}'\alpha'}^{\dagger}]\rangle$, respectively, and

$$M_{-\boldsymbol{q}\alpha}'' = \sum_{\alpha'} M_{-\boldsymbol{q}\alpha'} \langle[B_{-\boldsymbol{q}\alpha'}^{\dagger}, B_{\boldsymbol{q}\alpha}^{\dagger}]\rangle = \sum_{\boldsymbol{k}bb'} \left(g_{b-\boldsymbol{q}} \bar{\rho}_{bb'\boldsymbol{k}} - g_{b'-\boldsymbol{q}} \bar{\rho}_{bb'\boldsymbol{k}+\boldsymbol{q}}\right) U_{\boldsymbol{q}\alpha}^{R}(\boldsymbol{k}bb') \tag{2.49}$$

and

$$M_{\boldsymbol{q}\alpha}'^{*} = \sum_{\alpha'} M_{\boldsymbol{q}\alpha'}^{*} \langle[B_{\boldsymbol{q}\alpha'}, B_{\boldsymbol{q}\alpha}^{\dagger}]\rangle = \sum_{\boldsymbol{k}bb'} \left(g_{b\boldsymbol{q}}^{*} \bar{\rho}_{bb'\boldsymbol{k}} - g_{b'\boldsymbol{q}}^{*} \bar{\rho}_{bb'\boldsymbol{k}+\boldsymbol{q}}\right) U_{\boldsymbol{q}\alpha}^{R}(\boldsymbol{k}bb'). \tag{2.50}$$

It is noted that $M_{\boldsymbol{q}\alpha}$, $M_{\boldsymbol{q}\alpha}'$, and $M_{-\boldsymbol{q}\alpha}''$ slowly vary in time because these functions are given by the adiabatic eigenvectors $U_{\boldsymbol{q}}^{L\dagger}$ and $U_{\boldsymbol{q}}^{R}$, and furthermore, the density matrices $\bar{\rho}_{bb'\boldsymbol{k}}$ slowly vary in time, particularly after the pulse irradiation. This fact is an essential point that provides a theoretical basis to the introduction of the PQ picture.

As regards the effective coupling constant $M_{\boldsymbol{q}\alpha}$, it is represented by the sum of $M_{\boldsymbol{q}\alpha}^{F}$ and $M_{\boldsymbol{q}\alpha}^{D}$ which originate from the Fröhlich interaction and the deformation potential interaction, respectively, that is,

$$M_{\boldsymbol{q}\alpha} = M_{\boldsymbol{q}\alpha}^{F} + M_{\boldsymbol{q}\alpha}^{D}. \tag{2.51}$$

The coupling constant $g_{b\boldsymbol{q}}$ for the Fröhlich interaction in polar crystals is approximately independent of the band indices; $g_{b\boldsymbol{q}} \approx g_{\boldsymbol{q}}^{F}$, and $g_{\boldsymbol{q}}^{F}$ is pure imaginary with $|g_{\boldsymbol{q}}^{F}| \propto |\boldsymbol{q}|^{-1}$ [41]. Following Eq. (2.46), $M_{\boldsymbol{q}\alpha}^{F}$ is represented as

$$M_{\boldsymbol{q}\alpha}^{F} \simeq g_{\boldsymbol{q}}^{F} \sum_{\boldsymbol{k}b} U_{\boldsymbol{q}\alpha}^{L\dagger}(\boldsymbol{k}bb) = g_{\boldsymbol{q}}^{F} N_{\boldsymbol{q}\alpha}^{L}, \tag{2.52}$$

and in the small-$\boldsymbol{q}$ limit, the leading term of $M_{\boldsymbol{q}\alpha}^{F}$ is independent of $\boldsymbol{q}$ due to $N_{\boldsymbol{q}\alpha}^{L} \propto |\boldsymbol{q}|$. On the other hand, $g_{b\boldsymbol{q}}$ for the deformation potential interaction represented by $g_{b\boldsymbol{q}}^{D}$ is real and approximately independent of $\boldsymbol{q}$. $M_{\boldsymbol{q}\alpha}^{D}$ is given by

$$M_{\boldsymbol{q}\alpha}^{D} \simeq \sum_{\boldsymbol{k}b} g_{b\boldsymbol{q}}^{D} U_{\boldsymbol{q}\alpha}^{L\dagger}(\boldsymbol{k}bb), \tag{2.53}$$

where the leading term of $M_{\boldsymbol{q}\alpha}^{D}$ is independent of $\boldsymbol{q}$. The similar results hold correctly for both $M_{-\boldsymbol{q}\alpha}''$ and $M_{\boldsymbol{q}\alpha}'^{*}$

Polaronic quasiparticle operators

Following Eq. (2.48), the adiabatic coupled equation of Eq. (2.40) is rewritten as

$$-i\frac{dB_{\boldsymbol{q}\alpha}^{\dagger}}{dt} = B_{\boldsymbol{q}\alpha}^{\dagger}\mathcal{E}_{\boldsymbol{q}\alpha} + c_{\boldsymbol{q}}^{\dagger}M_{\boldsymbol{q}\alpha}'^{*} + i\sum_{\alpha'}B_{\boldsymbol{q}\alpha'}^{\dagger}\mathcal{W}_{\boldsymbol{q}\alpha'\alpha} + M_{-\boldsymbol{q}\alpha}''c_{-\boldsymbol{q}}. \tag{2.54}$$

Further, the equation of motion of the LO phonon of Eq. (2.20) becomes of the form:

$$-i\left(\frac{d}{dt} + \frac{1}{T_{\boldsymbol{qph}}}\right)c_{\boldsymbol{q}}^{\dagger} = c_{\boldsymbol{q}}^{\dagger}\omega_{\boldsymbol{q}} + \sum_{\alpha}B_{\boldsymbol{q}\alpha}^{\dagger}M_{\boldsymbol{q}\alpha}. \tag{2.55}$$

We integrate Eqs. (2.54) and (2.55) into a single equation in a matrix form of

$$-i\frac{d}{dt}[B_{\boldsymbol{q}}^{\dagger}, c_{\boldsymbol{q}}^{\dagger}] = [B_{\boldsymbol{q}}^{\dagger}, c_{\boldsymbol{q}}^{\dagger}]h_{\boldsymbol{q}} + [iB_{\boldsymbol{q}}^{\dagger}\mathcal{W}_{\boldsymbol{q}} + M_{-\boldsymbol{q}}''c_{-\boldsymbol{q}}, 0]. \tag{2.56}$$

Here, $h_{\boldsymbol{q}} \equiv \{h_{\boldsymbol{q}\gamma\gamma'}\}$ is a non-Hermitian matrix provided by

$$h_{\boldsymbol{q}} = \left[\begin{array}{cc} \mathcal{E}_{\boldsymbol{q}} & M_{\boldsymbol{q}} \\ M_{\boldsymbol{q}}'^{\dagger} & \omega_{\boldsymbol{q}} \end{array}\right] \tag{2.57}$$

with $\gamma, \gamma' = 1 \sim N + 2$. N represents the number of electron-hole (discretized) continua of single-particle excitation modes, that is, $\beta = 1 \sim N$ except for two discrete states of the plasmon-like mode and the LO phonon mode signified as α_1 and α_2, respectively: $\{\gamma\} = (\{\beta\}, \alpha_1, \alpha_2)$. It is noted that we will adopt the matrix indices of α', β', γ', and α_i' ($i = 1, 2$) with the same meaning as α, β, γ, and α_i, respectively.

In this section, we are exclusively concerned with the case where the continuum level of $\{\beta\}$ overlaps the two discrete levels of α_1 and α_2. This case is categorized into the Fano problem, in other words, the multichannel scattering problem with one open channel and two closed channels, except for $h_{\boldsymbol{q}}$ being non-Hermitian. We take into account the following coupled equations of

$$\sum_{\gamma'}h_{\boldsymbol{q}\gamma\gamma'}V_{\boldsymbol{q}\gamma'\beta}^{R} = V_{\boldsymbol{q}\gamma\beta}^{R}\mathcal{E}_{\boldsymbol{q}\beta}, \tag{2.58}$$

where $V_{\boldsymbol{q}\beta}^{R} = \{V_{\boldsymbol{q}\gamma\beta}^{R}\}$ represents the right vector of the solution for given energy $\mathcal{E}_{\boldsymbol{q}\beta}$. In terms of $V_{\boldsymbol{q}\beta}^{R}$, we define a set of N operators $F_{\boldsymbol{q}\beta}^{\dagger}$ ($\beta = 1 \sim N$) as

$$F_{\boldsymbol{q}\beta}^{\dagger} = \sum_{\beta'}B_{\boldsymbol{q}\beta'}^{\dagger}V_{\boldsymbol{q}\beta'\beta}^{R} + B_{\boldsymbol{q}\alpha_1}^{\dagger}V_{\boldsymbol{q}\alpha_1\beta}^{R} + c_{\boldsymbol{q}}^{\dagger}V_{\boldsymbol{q}\alpha_2\beta}^{R}. \tag{2.59}$$

Further, we introduce the left vector $V_{\boldsymbol{q}\beta}^{L\dagger} = \{V_{\boldsymbol{q}\beta\gamma}^{L\dagger}\}$ associated with $V_{\boldsymbol{q}\beta}^{R}$ in order to satisfy the inverse relations

$$B_{\boldsymbol{q}\alpha}^{\dagger} = \sum_{\beta}F_{\boldsymbol{q}\beta}^{\dagger}V_{\boldsymbol{q}\beta\alpha}^{L\dagger}, \quad c_{\boldsymbol{q}}^{\dagger} = \sum_{\beta}F_{\boldsymbol{q}\beta}^{\dagger}V_{\boldsymbol{q}\beta\alpha_2}^{L\dagger}, \tag{2.60}$$

where $\sum_{\gamma}V_{\boldsymbol{q}\beta\gamma}^{L\dagger}V_{\boldsymbol{q}\gamma\beta'}^{R} = \delta_{\beta\beta'}$ and $\sum_{\beta}V_{\boldsymbol{q}\gamma\beta}^{R}V_{\boldsymbol{q}\beta\gamma'}^{L\dagger} = \delta_{\gamma\gamma'}$. Here, it is noted that the PQ operator $F_{\boldsymbol{q}\beta}^{\dagger}$ is introduced in a similar manner to that of the quasiboson operator $B_{\boldsymbol{q}\alpha}^{\dagger}$;

the commutation relation $[\hat{H}^{(\mathrm{eff})}(t), F_{\boldsymbol{q}\beta}^{\dagger}(t)] = F_{\boldsymbol{q}\beta}^{\dagger}(t)\mathcal{E}_{\boldsymbol{q}\beta}(t)$ is ensured, where the total effective Hamiltonian $\hat{H}^{(\mathrm{eff})}(t)$ is provided by $\hat{H}^{(\mathrm{eff})}(t) = \hat{H}_{e}^{(\mathrm{eff})}(t) + \hat{H}_{p} + \hat{H}_{e-p}$, and the expression $h_{\boldsymbol{q}}(t) = \sum_{\beta} V_{\boldsymbol{q}\beta}^{R}(t)\mathcal{E}_{\boldsymbol{q}\beta}(t)V_{\boldsymbol{q}\beta}^{L\dagger}(t)$ is employed in terms of Eq. (2.58).

Given Eq. (2.59), we obtain adiabatic coupled equations for $F_{\boldsymbol{q}}^{\dagger}$ from Eq. (2.56):

$$-i\frac{d}{dt}F_{\boldsymbol{q}\beta}^{\dagger} = F_{\boldsymbol{q}\beta}^{\dagger}\mathcal{E}_{\boldsymbol{q}\beta} + i\sum_{\beta'}F_{\boldsymbol{q}\beta'}^{\dagger}\mathcal{I}_{\boldsymbol{q}\beta'\beta} + \sum_{\beta'}\mathcal{M}''_{-\boldsymbol{q}\beta\beta'}F_{-\boldsymbol{q}\beta'}, \tag{2.61}$$

where $F_{\boldsymbol{q}}$ represents Hermitian-conjugate of $F_{\boldsymbol{q}}^{\dagger}$. Further,

$$\mathcal{M}''_{-\boldsymbol{q}\beta\beta'} = \left(\sum_{\alpha}M''_{-\boldsymbol{q}\alpha}V_{\boldsymbol{q}\alpha\beta}^{R}\right)V_{-\boldsymbol{q}\alpha_2\beta'}^{L} \tag{2.62}$$

and

$$\mathcal{I}_{\boldsymbol{q}} = I_{\boldsymbol{q}} + \frac{\gamma_{\boldsymbol{q}}^{(0)}}{2}. \tag{2.63}$$

$I_{\boldsymbol{q}}$ represents a non-adiabatic interaction expressed as

$$\begin{aligned}
I_{\boldsymbol{q}\beta'\beta} &= \sum_{\alpha\alpha'\alpha''}\frac{d\left(V_{\boldsymbol{q}\beta'\alpha'}^{L\dagger}U_{\boldsymbol{q}\alpha'\alpha''}^{L\dagger}\right)}{dt}\left(U_{\boldsymbol{q}\alpha''\alpha}^{R}V_{\boldsymbol{q}\alpha\beta}^{R}\right)\\
&= \sum_{\alpha\alpha'}V_{\boldsymbol{q}\beta'\alpha}^{L\dagger}W_{\boldsymbol{q}\alpha\alpha'}V_{\boldsymbol{q}\alpha'\beta}^{R} + \sum_{\alpha}\frac{dV_{\boldsymbol{q}\beta'\alpha}^{L\dagger}}{dt}V_{\boldsymbol{q}\alpha\beta}^{R}
\end{aligned} \tag{2.64}$$

with $I_{\boldsymbol{q}} \neq -I_{\boldsymbol{q}}^{\dagger}$, and a phenomenological damping factor $\gamma_{\boldsymbol{q}\beta'\beta}^{(0)}$ relevant to $F_{\boldsymbol{q}\beta}^{\dagger}$ is provided by

$$\frac{\gamma_{\boldsymbol{q}\beta'\beta}^{(0)}}{2} = \sum_{\alpha\alpha'}V_{\boldsymbol{q}\beta'\alpha'}^{L\dagger}\frac{\gamma_{\boldsymbol{q}\alpha'\alpha}^{(B)}}{2}V_{\boldsymbol{q}\alpha\beta}^{R}. \tag{2.65}$$

Hereafter, we term the operators $F_{\boldsymbol{q}\beta}^{\dagger}(t)$ and $F_{\boldsymbol{q}\beta}(t)$ a creation operator and an annihilation operator of PQ, respectively. These operators are not bosonic ones, and the ground state of the PQ is provided by the direct product of the ground states of the quasiboson and the LO phonon. Further, $\mathcal{E}_{\boldsymbol{q}\beta}(t)$ represents single-PQ adiabatic energy with mode $\boldsymbol{q}\beta$ at time t.

Retarded Green function associated with the PQ operator

We solve Eq. (2.61) in an approximate manner to obtain the closed analytic forms of $F_{\boldsymbol{q}\beta}^{\dagger}$ and $F_{\boldsymbol{q}\beta}$. The details of the derivation is described in Appendix C. The point of this derivation is to approximate the non-adiabatic interaction $I_{\boldsymbol{q}}(t)$ under the following assumption. $I_{\boldsymbol{q}}(t)$ is affected by the two contributions, namely, $W_{\boldsymbol{q}}(t)$ and a time-derivative of $V_{\boldsymbol{q}}^{L\dagger}(t)$ [see Eq. (2.64)]. We have two pronounced effects on $W_{\boldsymbol{q}}(t)$. One is an effect of a crossing between the adiabatic α'th and αth states. Here, the adiabatic energy curves of $\mathcal{E}_{\boldsymbol{q}\alpha'}(t)$ and $\mathcal{E}_{\boldsymbol{q}\alpha}(t)$ tend to cross at $t = t_j$ —termed as exceptional point— [81], which results in spike-like change of $W_{\boldsymbol{q}\alpha'\alpha}$. It is seen that this effect originates from the energy denominator in Eq. (2.44) reminiscent of a Landau-Zener coupling [84]. The other effect

is attributed to abrupt change of $\Omega_{bb'k}^{(R)}(t)$ of Eq. (2.14), that is, $d\Omega_{bb'k}^{(R)}(t)/dt$. These two effects are also included in the time-derivative of $V_{\boldsymbol{q}}^{L\dagger}(t)$ in Eq. (2.64).

In the present section, we set the pulse-envelop function $f(t)$ in Eq. (2.7) to a squared-shape just for the sake of simplicity, that is,

$$f(t) = \theta(t + \tau_L/2)\theta(t - \tau_L/2), \tag{2.66}$$

where τ_L is temporal width. Thus, spike-like change of $W_{\boldsymbol{q}\alpha'\alpha}(t)$ arises at $t = t_j$ including $t = \pm\tau_L/2$, whereas $\bar{Z}_{\boldsymbol{q}}$, $\mathcal{E}_{\boldsymbol{q}\alpha}$, and $U_{\boldsymbol{q}\alpha}^{L/R}(\boldsymbol{k}bb')$ varies slowly in time owing to the rotating wave approximation except for $t = \pm\tau_L/2$. Accordingly, $I_{\boldsymbol{q}}(t)$ would be well described as

$$I_{\boldsymbol{q}}(t) \approx \sum_j \mathfrak{I}_{\boldsymbol{q}}^{(j)\dagger}\delta(t - t_j), \tag{2.67}$$

where $\mathfrak{I}_{\boldsymbol{q}}^{(j)}$ is a constant matrix with $\mathfrak{I}_{\boldsymbol{q}}^{(j)\dagger} \neq -\mathfrak{I}_{\boldsymbol{q}}^{(j)}$. From among a set of the off-diagonal elements $\{\mathfrak{I}_{\boldsymbol{q}\beta'(\neq\beta)\beta}^{(j)}\}$, we retain just single leading contribution, namely, $\mathfrak{I}_{\boldsymbol{q}\beta'(\neq\beta)\beta}^{(D)}$ at $t = t_D$. In practical calculations, t_D is set to $\tau_L/2$, that is,

$$t_D = \frac{\tau_L}{2}. \tag{2.68}$$

The associated retarded Green function is defined in terms of $F_{\boldsymbol{q}}$ and $F_{\boldsymbol{q}}^{\dagger}$ as [79, 80]

$$G_{\boldsymbol{q}\beta\beta'}^{R}(t,t') = -i\theta(t - t')\left\langle\left[F_{\boldsymbol{q}\beta}(t), F_{\boldsymbol{q}\beta'}^{\dagger}(t')\right]\right\rangle. \tag{2.69}$$

As shown in Appendix C.2, it ends up with

$$G_{\boldsymbol{q}\beta\beta'}^{R}(t,t') = -i\theta(t - t')e^{-i\Theta_{\boldsymbol{q}\beta}(t,t_D)}\sum_{\gamma\gamma'}V_{\boldsymbol{q}\beta\gamma}^{R\dagger}(t_D)T_{\boldsymbol{q}\gamma\gamma'}(t,t')V_{\boldsymbol{q}\gamma'\beta'}^{R}(t_D)e^{i\Theta_{\boldsymbol{q}\beta'}^{*}(t',t_D)}, \tag{2.70}$$

where the matrix $T_{\boldsymbol{q}}$ is given by Eq. (C.38), where all effects of the off-diagonal components $\{\mathfrak{I}_{\boldsymbol{q}\beta'(\neq\beta)\beta}^{(D)}\}$ at $t = t_D$ are incorporated. $\Theta_{\boldsymbol{q}\beta}(t,t')$ represents an adiabatic energy phase provided by

$$\Theta_{\boldsymbol{q}\beta}(t,t') = \int_{t'}^{t}dt''\left\{\mathcal{E}_{\boldsymbol{q}\beta}^{*}(t'') - i\left[\frac{\gamma_{\boldsymbol{q}\beta}^{(0)}(t'')}{2} + I_{\boldsymbol{q}\beta\beta}^{*}(t'')\right]\right\}, \tag{2.71}$$

and the effect of the phenomenological damping is included in it. Further, in $\Theta_{\boldsymbol{q}\beta}(t,t')$, the effect of the non-adiabatic correction due to diagonal components $\{\mathfrak{I}_{\boldsymbol{q}\beta\beta}^{(j)}\}$ is also incorporated. We discuss this additional effect in more detail in Sec. 3.1.2.

2.3.2 Approximations employed

In the present subsection, first, we summarize the approximations employed for the transient FR problem. The major approximation is the factorization approximation employed in Eqs. (2.10) and (2.48) in addition to the rotating wave approximation implemented in Eq. (2.16). Next, we introduce the further approximations for actual calculations as follows. (i) Time integration for solving Eq. (2.61) starts at $t = t_D = \tau_L/2$, where

the temporal width τ_L of the squared pulse is defined by Eq. (2.66). Thus, we neglect contributions from the temporal region $t \leq t_D$. (ii) We assume the relation of $\langle [B_{\bm{q}\alpha}, B^\dagger_{\bm{q}'\alpha'}] \rangle = \delta_{\bm{q}\bm{q}'}\delta_{\alpha\alpha'}$, so that Eq. (2.50) is provided by $M'_{\bm{q}\alpha} = M_{\bm{q}\alpha}$. (iii) We neglect effects of $M''_{-\bm{q}\alpha}$ of Eq. (2.49) on Eqs. (2.54) and (2.61). (iv) We assume that Eq. (2.65) is provided by $\gamma^{(0)}_{\bm{q}\beta\beta'}(t) = \delta_{\beta\beta'}\gamma_{\bm{q}}\theta(t + t_D)$, where $\gamma_{\bm{q}}$ is a real and positive constant.

The approximation (i) is valid in the present system because τ_L is much shorter than the relaxation time of the carrier-density of the order of 100 fs. Therefore, in the temporal region of $t > t_D$, owing to the rotating wave approximation, the adiabatic picture is justified, which is the basis of the PQ picture. Further, we take into account just the leading contribution of the non-adiabatic interaction $\mathfrak{I}^{(D)}_{\bm{q}\beta'(\neq\beta)\beta}$ at $t = t_D$ in Eq. (2.67).

Concerning the approximation (ii), we discuss the criterion of the validity of it in Appendix C.3. This criterion is made sure in the temporal region $t > t_D$ as well as the approximation (i), where the Coulomb correction to the Rabi frequency $\sum_{\bm{q}} V^{(C)}_{\bm{q}} \bar{\rho}_{\bar{b}b\bm{k}+\bm{q}}$ in Eq. (2.19) is much smaller than $\omega_{\bm{q}}$. Besides, this approximation demands that the limited set of $\{\alpha\}$ with $\mathcal{E}_{\bm{q}\alpha}$ of real and positive numbers is employed for all the solutions of Eqs. (2.33) and (2.34). As a result, the matrix $h_{\bm{q}}$ of Eq. (2.57) becomes Hermitian, and $V^L_{\bm{q}\beta}$ and $V^R_{\bm{q}\beta}$ become equivalent, which enables us to employ the solutions of the ordinary Fano problem as a set of the vectors [46].

The approximation (iii) is attributed to the present quasibosonization scheme where the effects of two-quasiboson states are removed as described below Eq. (2.38). Actually, $M''_{-\bm{q}\alpha}$ is pertinent to non-vanishing commutator between different quasi-boson operators [see Eq. (2.49)]. This couples the PQ of the β'th state with that of the βth state accompanying momentum transfer from $-\bm{q}$ to $\bm{q}$. The approximation (iv) is derived from the assumption that $T_{\bm{q}\bm{k}bb'}$ provided in Eq. (2.9) is independent of $\bm{k}$, b, and b', and is generally labeled as $T_{\bm{q}12} : \gamma_{\bm{q}} = 2/T_{\bm{q}12}$

2.3.3 Analytic expression of transient photoemission spectra

In the case that $f_{\bm{q}}(t')$ is provided by a delta pulse as $f_{\bm{q}}(t') = f_{\bm{q}0}\delta(t' - t_p)$, where $f_{\bm{q}0}$ is independent of t', the induced charge density of Eq. (2.21) becomes

$$n^{(ind)}_{\bm{q}}(t_p + \tau) = \frac{1}{4\pi V} f_{\bm{q}0} \chi^{(t)}_{\bm{q}}(t_p + \tau, t_p). \tag{2.72}$$

Here, t_p is the time where $f_{\bm{q}}(t')$ probes dynamics of concern, and $n^{(ind)}_{\bm{q}}(t_p + \tau)$ depends on both t_p and the relative time $\tau = t - t'$, which is different from equilibrium systems; they depend solely on τ, not on t_p since temporal translational invariance is conserved. Therefore, $\chi^{(t)}_{\bm{q}}(t_p + \tau, t_p)$ reveals the way of change in the induced charge density after t_p.

The inverse dielectric function $\epsilon^{-1}_{\bm{q}}(t_p + \tau, t_p)$ is provided as

$$\epsilon^{-1}_{\bm{q}}(t_p + \tau, t_p) = \epsilon^{-1}_{\infty} \left[\delta(\tau) + \frac{V}{4\pi} v^{(C)}_{\bm{q}} \chi^{(t)}_{\bm{q}}(t_p + \tau, t_p)\theta(\tau) \right], \tag{2.73}$$

where $v^{(C)}_{\bm{q}}$ is given by Eq. (2.30), and ϵ_{∞} is a background dielectric constant provided in Eq. (2.6). The Fourier transform of $\epsilon_{\bm{q}}(t_p + \tau, t_p)$ is readily obtained as follows:

$$\tilde{\epsilon}_{\bm{q}}(t_p; \omega) = \int_0^\infty d\tau \, e^{-i\omega\tau} \epsilon_{\bm{q}}(t_p + \tau, t_p), \tag{2.74}$$

where the relation $\int_{-\infty}^{\infty} dt'' \epsilon_{\boldsymbol{q}}^{-1}(t_p + \tau, t'') \epsilon_{\boldsymbol{q}}(t'', t_p) = \delta(\tau)$ is employed. Therefore, we obtain a transient absorption coefficient $\alpha_{\boldsymbol{q}}(t_p; \omega)$ at time t_p represented as

$$\alpha_{\boldsymbol{q}}(t_p; \omega) = \frac{\omega}{n(t_p; \omega)C} I_{\boldsymbol{q}}(t_p; \omega), \tag{2.75}$$

where

$$I_{\boldsymbol{q}}(t_p; \omega) = \mathrm{Im}\tilde{\epsilon}_{\boldsymbol{q}}(t_p; \omega). \tag{2.76}$$

Here, $n(t_p; \omega)$ is the index of refraction, which is approximately provided by $n(t_p; \omega) \approx \sqrt{\epsilon_\infty}$, and C is the speed of light. As regards $I_{\boldsymbol{q}}(t_p; \omega)$, it is remarked that this is nonlinear in the pump field of Eq. (2.7). Further, the sign of ω in Eq. (2.74) is defined such that transient photoemission spectra $I_{\boldsymbol{q}}(t_p; \omega) < 0$ peak at positive ω, while transient photoabsorption spectra $I_{\boldsymbol{q}}(t_p; \omega) > 0$ peak at negative ω. We define the transient induced photoemission spectra as

$$\bar{I}_{\boldsymbol{q}}(t_p; \omega) = -I_{\boldsymbol{q}}(t_p; \omega). \tag{2.77}$$

Next, we derive explicit expressions of the retarded density-density correlation function $D_{\boldsymbol{q}}^R(t, t')$ of Eq. (2.24) and the retarded phonon Green function $\bar{D}_{\boldsymbol{q}}'^R(t, t')$ of Eq. (2.32) within the present scheme. The details of the derivation and the analytical expressions of $\chi_{\boldsymbol{q}}(t, t')$ and $\chi_{\boldsymbol{q}}'(t, t')$ are described in Appendix D. As regards $D_{\boldsymbol{q}}^R(t, t')$, the density operator of Eq. (2.25) becomes of the form

$$\hat{n}_{\boldsymbol{q}}(t) = \frac{1}{V} \sum_\alpha B_{\boldsymbol{q}\alpha}^\dagger N_{\boldsymbol{q}\alpha}^L, \tag{2.78}$$

where Eq. (2.38), $N_{\boldsymbol{q}\alpha}^L = \sum_{\boldsymbol{k}b} U_{\boldsymbol{q}\alpha}^{L\dagger}(\boldsymbol{k}bb)$ of Eq. (B.18), and the orthogonality relation of the quasiboson operator are employed. According to this expression, it is seen that $B_{\boldsymbol{q}\alpha}^\dagger$ represents a fraction of electron density at the αth state weighted with $N_{\boldsymbol{q}\alpha}^L/V$. Using Eq. (2.60), Eq. (2.78) is rewritten as

$$\hat{n}_{\boldsymbol{q}}(t) = \frac{1}{V} \sum_{\beta\alpha} F_{\boldsymbol{q}\beta}^\dagger V_{\boldsymbol{q}\beta\alpha}^{L\dagger} N_{\boldsymbol{q}\alpha}^L. \tag{2.79}$$

Eventually, with Eqs. (2.24), (2.69), and (2.79), we obtain

$$D_{\boldsymbol{q}}^{R*}(t, t') = \frac{1}{V^2} \sum_{\alpha\alpha'\beta\beta'} N_{\boldsymbol{q}\alpha}^{L*}(t) V_{\boldsymbol{q}\alpha\beta}^L(t) G_{\boldsymbol{q}\beta\beta'}^R(t, t') V_{\boldsymbol{q}\beta'\alpha'}^{L\dagger}(t') N_{\boldsymbol{q}\alpha'}^L(t'). \tag{2.80}$$

On the other hand, employing Eqs. (2.60) and (2.69), $\bar{D}_{\boldsymbol{q}}'^R(t, t')$ becomes

$$\bar{D}_{\boldsymbol{q}}'^R(t, t') = \sum_{\beta\beta'} V_{\boldsymbol{q}\alpha_2\beta}^L(t) G_{\boldsymbol{q}\beta\beta'}^R(t, t') V_{\boldsymbol{q}\beta'\alpha_2}^{L\dagger}(t'). \tag{2.81}$$

Lastly, it is noted that an overall phase factor $e^{i\eta_{\boldsymbol{q}\alpha}(t)}$ of the normalization constant $N_{\boldsymbol{q}\alpha}^R(t)$ of the αth solution $U_{\boldsymbol{q}\alpha}^R(t)$ is not determined, where $\eta_{\boldsymbol{q}\alpha}(t)$ represents an arbitrary real function of t. This arbitrariness leads the quasiboson operators $B_{\boldsymbol{q}\alpha}^\dagger(t)$ and $B_{\boldsymbol{q}\alpha}(t)$ to be transformed as $B_{\boldsymbol{q}\alpha}^\dagger(t) \to B_{\boldsymbol{q}\alpha}^\dagger(t) e^{i\eta_{\boldsymbol{q}\alpha}(t)}$ and $B_{\boldsymbol{q}\alpha}(t) \to B_{\boldsymbol{q}\alpha}(t) e^{-i\eta_{\boldsymbol{q}\alpha}(t)}$, respectively. As shown in Appendix E, $\chi_{\boldsymbol{q}}^{(t)}(t, t')$ of Eq. (2.22) is independent of any choice of $\eta_{\boldsymbol{q}\alpha}(t)$, and invariant with respect to these phase transformations.

2.3.4 Allocation of time constants

Here, we summarize time constants employed in the present section. Single-particle density matrices $\rho_{bb'k}$ defined below Eq. (2.14) follow the carrier-density relaxation time constants T_1 and T_2. Here, T_1 describes the relaxation of the carrier distribution function ρ_{bbk} formed by the pump pulse irradiation to a quasi-equilibrium distribution function, and T_2 describes the dephasing of the transition amplitude $\rho_{b\bar{b}k}$ [41, 79]. We assume that the two relaxation time constants of the induced carrier density with isotropic momentum distribution are identical; $T_{12} = T_1 = T_2$. T_{q12} is defined in Sec. 2.3.2, and represents the phenomenological relaxation time constant of the induced carrier density with anisotropic momentum distribution. The temporal region $t < T_{12}$, where strongly photoexcited carriers still stay in the excited states and interact with the phonon, corresponds to the ETR, while the temporal region $t \gtrsim T_{12}$ corresponds to the classical region.

Figure 2.1 represents schematic allocation of the time constants stated in the present section, that is, t_D, T_{q12}, and T_{12} in addition to T_{qph} attributed to phonon anharmonicity. We show the time constants employed in the actual calculations in Table 2.1. Reference [3] summarizes time scales for different stages of relaxation phenomena in photoexcited experiments. For the analysis of the transient FR, we set t_D, T_{q12}, T_{12}, and T_{qph} to 7.5, 20, 90, and 5000 fs, respectively. This allocation of the time constants given by Fig. 2.1 is a requirement for the manifestation of the transient FR of concern, and the detail is discussed in Sec. 3.1.2.
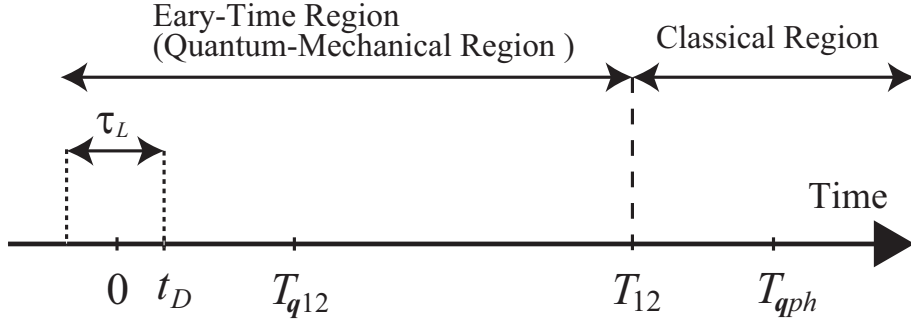
Figure 2.1: Schematic diagram of various time constants employed in the analysis of the transient FR. (From Ref. [69] with partial modification.)

Table 2.1: Time constants employed in the analysis of the transient FR.

Time constants	
t_D	7.5fs
T_{q12}	20fs
T_{12}	90fs
T_{qph}	5ps

Concerning experimental estimates of the time constants, t_D, T_{q12}, T_{12}, and T_{qph} are evaluated as 5, 16, 100, and 1300 fs, respectively by the CP measurements for Si at average excited carrier density $\bar{N}_{ex} = 4 \times 10^{19} \mathrm{cm}^{-3}$ in Ref. [6]. T_{q12} for Si is also estimated in the

pump-probe reflectivity study in Ref. [85] as 32 ± 5 fs at $\bar{N}_{ex} = (5.5 \pm 0.3) \times 10^{18} \mathrm{cm}^{-3}$. T_{12} for GaAs is evaluated by the numerical calculations as 50 fs at $\bar{N}_{ex} = 3 \times 10^{18} \mathrm{cm}^{-3}$ in Ref. [86]. $T_{\boldsymbol{q}ph}$ is estimated from Raman scattering in Si; $T_{\boldsymbol{q}ph} \approx 2500$ fs at low temperature [87], and $T_{\boldsymbol{q}ph} \approx 1500$ fs [87] and 2000 fs [88] at 300 K.

2.4 Analysis of Coherent Phonon Oscillatory Pattens

In the previous section, we solved the multichannel scattering problem. The scheme is based on the approximation that the effects of the interband density matrices $\bar{\rho}_{b\bar{b}\boldsymbol{k}}$ are partly neglected so as to solve the Hermitian problem substituted for the non-Hermitian problem $h_{\boldsymbol{q}}$ of Eq. (2.57). This approximation scheme is justified for the case of the relatively weak excitation conditions. Actually, in the calculations of the induced photoemission spectra $\bar{I}_{\boldsymbol{q}}(t_p; \omega)$ based on the previous scheme, we set the pulse area to 0.12π and 0.20π for undoped Si and undoped GaAs, respectively, as shown in Sec. 3.1.

In the present scheme, we incorporate these neglected effects into calculations, and investigate physical quantities even under the strong excitation conditions such as π- and 2π-pulse laser conditions. However as the price to be paid, the scattering problem to be solved is replaced by the more tractable eigenvalue problem just for the sake of simplicity. We solve the associated non-Hermitian problem, and derive an analytical expression of a CP oscillatory pattern.

2.4.1 Introduction of polaronic quasiparticle operators

First, Eq. (2.16) is recast into the form:

$$-i\left(\frac{d}{dt} + \frac{1}{T_{\boldsymbol{q}\boldsymbol{k}bb}}\right)\bar{A}_{\boldsymbol{q}}^{\dagger}(\boldsymbol{k}bb) = \sum_{\boldsymbol{k}'b'}\bar{A}_{\boldsymbol{q}}^{\dagger}(\boldsymbol{k}'b'b')\mathcal{Z}_{\boldsymbol{q}}(\boldsymbol{k}'b'b', \boldsymbol{k}bb)$$
$$+\bar{\Omega}_{b\bar{b}}^{(R)}(t)\bar{A}_{\boldsymbol{q}}^{\dagger}(\boldsymbol{k}b\bar{b}) - \bar{\Omega}_{\bar{b}b}^{(R)}(t)\bar{A}_{\boldsymbol{q}}^{\dagger}(\boldsymbol{k}\bar{b}b) \qquad (2.82)$$

and

$$-i\left(\frac{d}{dt} + \frac{1}{T_{\boldsymbol{q}\boldsymbol{k}b\bar{b}}}\right)\bar{A}_{\boldsymbol{q}}^{\dagger}(\boldsymbol{k}b\bar{b}) = \bar{\omega}_{b\bar{b}\boldsymbol{k}\boldsymbol{q}}\bar{A}_{\boldsymbol{q}}^{\dagger}(\boldsymbol{k}b\bar{b}) + \bar{\Omega}_{\bar{b}b\boldsymbol{k}}^{(R)}(t)\left\{\bar{A}_{\boldsymbol{q}}^{\dagger}(\boldsymbol{k}bb) - \bar{A}_{\boldsymbol{q}}^{\dagger}(\boldsymbol{k}\bar{b}\bar{b})\right\}$$
$$+V_{\boldsymbol{q}}^{(C)}(\rho_{b\bar{b}\boldsymbol{k}} - \rho_{b\bar{b}\boldsymbol{k}+\boldsymbol{q}})\sum_{\boldsymbol{k}'b'}\bar{A}_{\boldsymbol{q}}^{\dagger}(\boldsymbol{k}'b'b'), \qquad (2.83)$$

where the c-number non-Hermitian matrix $\mathcal{Z}_{\boldsymbol{q}}$ is provided by

$$\mathcal{Z}_{\boldsymbol{q}}(\boldsymbol{k}'b'b', \boldsymbol{k}bb) = \delta_{\boldsymbol{k}\boldsymbol{k}'}\delta_{bb'}\bar{\omega}_{b'b'\boldsymbol{k}'\boldsymbol{q}} + V_{\boldsymbol{q}}^{(C)}(\bar{\rho}_{bb\boldsymbol{k}} - \bar{\rho}_{bb\boldsymbol{k}+\boldsymbol{q}}). \qquad (2.84)$$

Next, we solve left and right eigenvalue problems of $\mathcal{Z}_{\boldsymbol{q}}$ as $\mathcal{U}_{\boldsymbol{q}}^{L\dagger}\mathcal{Z}_{\boldsymbol{q}} = E_{\boldsymbol{q}}\mathcal{U}_{\boldsymbol{q}}^{L\dagger}$ and $\mathcal{Z}_{\boldsymbol{q}}\mathcal{U}_{\boldsymbol{q}}^{R} = \mathcal{U}_{\boldsymbol{q}}^{R}E_{\boldsymbol{q}}$ with t fixed as an adiabatic parameter. Here, $E_{\boldsymbol{q}}$ is the eigenvalue, and $\mathcal{U}_{\boldsymbol{q}}^{L}$ and $\mathcal{U}_{\boldsymbol{q}}^{R}$ represent the associated biorthogonal eigenvectors. In the long wave-length limit of $|\boldsymbol{q}| \to 0$, the non-vanishing solution arises just from the collective excitation mode, whereas intraband single-particle excitation modes vanish [41]. This procedure of introducing the plasmon mode is somewhat different from that developed in the previous section in that here we incorporate just the contribution from intraband excitation. The eigenvalue and the eigenvectors are obtained by a similar manner described in Appendix B that interband

density matrices $\bar{\rho}_{b\bar{b}\boldsymbol{k}}$ are removed from Eqs. (B.56) and (B.62). The adiabatic plasma frequency $\omega_{\boldsymbol{q}pl}$ is provided by

$$\omega_{\boldsymbol{q}pl} = \left[V_{\boldsymbol{q}}^{(C)} \boldsymbol{q}^2 \sum_{\boldsymbol{k}b} \bar{\rho}_{bb\boldsymbol{k}} \nabla_{\boldsymbol{k}}^2 \varepsilon_{b\boldsymbol{k}}^{(r)} \right]^{\frac{1}{2}}, \tag{2.85}$$

and the associated $\mathcal{U}_{\boldsymbol{q}}^{L\dagger}(\boldsymbol{k}bb)$ and $\mathcal{U}_{\boldsymbol{q}}^{R}(\boldsymbol{k}bb)$ are given by

$$\mathcal{U}_{\boldsymbol{q}}^{L\dagger}(\boldsymbol{k}bb) = \mathcal{N}_{\boldsymbol{q}}^{L} V_{\boldsymbol{q}}^{(C)} \mathcal{G}_{bb\boldsymbol{k}\boldsymbol{q}} (\bar{\rho}_{bb\boldsymbol{k}} - \bar{\rho}_{bb\boldsymbol{k}+\boldsymbol{q}}) \tag{2.86}$$

and

$$\mathcal{U}_{\boldsymbol{q}}^{R}(\boldsymbol{k}bb) = \mathcal{N}_{\boldsymbol{q}}^{R} V_{\boldsymbol{q}}^{(C)} \mathcal{G}_{bb\boldsymbol{k}\boldsymbol{q}}, \tag{2.87}$$

respectively, where $\mathcal{G}_{bb\boldsymbol{k}\boldsymbol{q}} = [\omega_{\boldsymbol{q}pl} - \bar{\omega}_{bb\boldsymbol{k}\boldsymbol{q}}]^{-1}$. We determine the normalization constants $\mathcal{N}_{\boldsymbol{q}}^{L}$ and $\mathcal{N}_{\boldsymbol{q}}^{R}$ with the condition of $\mathcal{U}_{\boldsymbol{q}}^{L\dagger}\mathcal{U}_{\boldsymbol{q}}^{R} = 1$. Thus, the plasmon is represented as the following operator:

$$\mathcal{B}_{\boldsymbol{q}}^{\dagger} = \sum_{\boldsymbol{k}b} \bar{A}_{\boldsymbol{q}}^{\dagger}(\boldsymbol{k}bb) \mathcal{U}_{\boldsymbol{q}}^{R}(\boldsymbol{k}bb). \tag{2.88}$$

The equations of motion of $\mathcal{B}_{\boldsymbol{q}}^{\dagger}$, $c_{\boldsymbol{q}}^{\dagger}$, and $\bar{A}_{\boldsymbol{q}}^{\dagger}(\boldsymbol{k}b\bar{b})$ of the interband single-particle excitation mode are expressed in terms of the Heisenberg equations as

$$-i\frac{d\mathcal{B}_{\boldsymbol{q}}^{\dagger}}{dt} = (\omega_{\boldsymbol{q}pl} - iW_{\boldsymbol{q}pl} + i\gamma_{\boldsymbol{q}pl})\mathcal{B}_{\boldsymbol{q}}^{\dagger} + M_{\boldsymbol{q}ph}^{*} c_{\boldsymbol{q}}^{\dagger} + \sum_{\boldsymbol{k}b} M_{\boldsymbol{q}}'(\boldsymbol{k}b\bar{b})\bar{A}_{\boldsymbol{q}}^{\dagger}(\boldsymbol{k}b\bar{b}), \tag{2.89}$$

$$-i\frac{dc_{\boldsymbol{q}}^{\dagger}}{dt} = (\omega_{\boldsymbol{q}ph} + i\gamma_{\boldsymbol{q}ph})c_{\boldsymbol{q}}^{\dagger} + M_{\boldsymbol{q}ph}\mathcal{B}_{\boldsymbol{q}}^{\dagger}, \tag{2.90}$$

and

$$-i\frac{d\bar{A}_{\boldsymbol{q}}^{\dagger}(\boldsymbol{k}b\bar{b})}{dt} = (\bar{\omega}_{b\bar{b}\boldsymbol{k}\boldsymbol{q}} + i\gamma_{b\bar{b}\boldsymbol{k}\boldsymbol{q}})\bar{A}_{\boldsymbol{q}}^{\dagger}(\boldsymbol{k}b\bar{b}) + M_{\boldsymbol{q}}(\boldsymbol{k}b\bar{b})\mathcal{B}_{\boldsymbol{q}}^{\dagger}, \tag{2.91}$$

where effective couplings between the plasmon and single-particle excitation modes are expressed as

$$M_{\boldsymbol{q}}(\boldsymbol{k}b\bar{b}) = \bar{\Omega}_{b\bar{b}\boldsymbol{k}}^{(R)}(t) \left\{ \mathcal{U}_{\boldsymbol{q}}^{L\dagger}(\boldsymbol{k}bb) - \mathcal{U}_{\boldsymbol{q}}^{L\dagger}(\boldsymbol{k}\bar{b}\bar{b}) \right\} + V_{\boldsymbol{q}}^{(C)} \mathcal{N}_{\boldsymbol{q}}^{L} (\bar{\rho}_{b\bar{b}\boldsymbol{k}} - \bar{\rho}_{b\bar{b}\boldsymbol{k}+\boldsymbol{q}}) \tag{2.92}$$

and

$$M_{\boldsymbol{q}}'(\boldsymbol{k}b\bar{b}) = \bar{\Omega}_{b\bar{b}\boldsymbol{k}}^{(R)}(t) \left\{ \mathcal{U}_{\boldsymbol{q}}^{R}(\boldsymbol{k}bb) - \mathcal{U}_{\boldsymbol{q}}^{R}(\boldsymbol{k}\bar{b}\bar{b}) \right\}. \tag{2.93}$$

Further, the non-adiabatic term is given by

$$W_{\boldsymbol{q}pl} = \sum_{\boldsymbol{k}b} \mathcal{U}_{\boldsymbol{q}}^{L\dagger}(\boldsymbol{k}bb) \frac{d\mathcal{U}_{\boldsymbol{q}}^{R}(\boldsymbol{k}bb)}{dt} \tag{2.94}$$

and an effective coupling constant between the LO phonon and the plasmon is given by

$$M_{\boldsymbol{q}ph} = \sum_{\boldsymbol{k}b} g_{b\boldsymbol{q}} \mathcal{U}_{\boldsymbol{q}}^{L\dagger}(\boldsymbol{k}bb). \tag{2.95}$$

Besides, in the derivation of Eqs. (2.89)-(2.91), $\mathcal{U}_{\boldsymbol{q}}^{L\dagger}\mathcal{U}_{\boldsymbol{q}}^{R} = 1$ and $\mathcal{N}_{\boldsymbol{q}}^{L} = \sum_{\boldsymbol{k}b} \mathcal{U}_{\boldsymbol{q}}^{L\dagger}(\boldsymbol{k}bb)$ are used. Moreover,

$$\frac{\gamma_{\boldsymbol{q}ph}}{2} = \frac{1}{T_{\boldsymbol{q}ph}}, \tag{2.96}$$

$$\frac{\gamma_{qpl}}{2} = \sum_{kb} \mathcal{U}_q^{L\dagger}(\boldsymbol{k}bb) \frac{1}{T_{\boldsymbol{q}\boldsymbol{k}bb}} \mathcal{U}_q^R(\boldsymbol{k}bb), \tag{2.97}$$

and

$$\frac{\gamma_{b\bar{b}\boldsymbol{k}\boldsymbol{q}}}{2} = \frac{1}{T_{\boldsymbol{q}\boldsymbol{k}b\bar{b}}}, \tag{2.98}$$

where $T_{\boldsymbol{q}ph}$ is attributed to phonon anharmonicity, and $T_{\boldsymbol{q}\boldsymbol{k}bb'}$ is given in Eq. (2.9).

We integrate Eqs. (2.89)-(2.91) into a single equation, expressed as

$$-i\frac{d}{dt} \left[c_{\boldsymbol{q}}^\dagger, \bar{A}_{\boldsymbol{q}}^\dagger(\boldsymbol{k}b\bar{b}) \cdots, \mathcal{B}_{\boldsymbol{q}}^\dagger \right] = \left[c_{\boldsymbol{q}}^\dagger, \bar{A}_{\boldsymbol{q}}^\dagger(\boldsymbol{k}b\bar{b}) \cdots, \mathcal{B}_{\boldsymbol{q}}^\dagger \right] \bar{\bar{\mathcal{Z}}}_{\boldsymbol{q}}, \tag{2.99}$$

where the non-Hermitian matrix $\bar{\bar{\mathcal{Z}}}_{\boldsymbol{q}}$ is provided by

$$\bar{\bar{\mathcal{Z}}}_{\boldsymbol{q}} = \begin{bmatrix} \omega_{\boldsymbol{q}ph} + i\gamma_{\boldsymbol{q}ph} & 0 & 0 & M_{\boldsymbol{q}ph_-}^* \\ 0 & \bar{\omega}_{b\bar{b}\boldsymbol{k}\boldsymbol{q}} + i\gamma_{b\bar{b}\boldsymbol{k}\boldsymbol{q}} & 0 & M_{\boldsymbol{q}}'(\boldsymbol{k}b\bar{b}) \\ 0 & 0 & \ddots & \vdots \\ M_{\boldsymbol{q}ph} & M_{\boldsymbol{q}}(\boldsymbol{k}b\bar{b}) & \cdots & \omega_{\boldsymbol{q}pl} - iW_{\boldsymbol{q}pl} + i\gamma_{\boldsymbol{q}pl} \end{bmatrix}. \tag{2.100}$$

Here, the indices of ph, pl, and $(\boldsymbol{k}b\bar{b})$ represent the phonon, the plasmon, and the single-particle excitation in interbands, respectively. As shown in Appendix F, we solve the left and right eigenvalue problems [81] of $\bar{\bar{\mathcal{Z}}}_{\boldsymbol{q}}$ as $\mathcal{V}_{\boldsymbol{q}j}^{L\dagger} \bar{\bar{\mathcal{Z}}}_{\boldsymbol{q}} = E_{\boldsymbol{q}j} \mathcal{V}_{\boldsymbol{q}j}^{L\dagger}$ and $\bar{\bar{\mathcal{Z}}}_{\boldsymbol{q}} \mathcal{V}_{\boldsymbol{q}j}^R = \mathcal{V}_{\boldsymbol{q}j}^R E_{\boldsymbol{q}j}$, respectively, with t fixed, and $\{j, j', j''\} = (ph, \{\boldsymbol{k}b\bar{b}\}, pl)$. $E_{\boldsymbol{q}j}$ is the eigenvalue of the jth mode, and $\mathcal{V}_{\boldsymbol{q}j}^L$ and $\mathcal{V}_{\boldsymbol{q}j}^R$ are the associated biorthogonal eigenvectors.

Now, we introduce the PQ operator as

$$P_{\boldsymbol{q}j}^\dagger = c_{\boldsymbol{q}}^\dagger \mathcal{V}_{\boldsymbol{q}ph,j}^R + \mathcal{B}_{\boldsymbol{q}}^\dagger \mathcal{V}_{\boldsymbol{q}pl,j}^R + \sum_{kb} \bar{A}_{\boldsymbol{q}}^\dagger(\boldsymbol{k}b\bar{b}) \mathcal{V}_{\boldsymbol{q}(\boldsymbol{k}b\bar{b}),j}^R, \tag{2.101}$$

and the equation of motion of $P_{\boldsymbol{q}j}^\dagger$ is provided by

$$-i\frac{dP_{\boldsymbol{q}j}^\dagger}{dt} = E_{\boldsymbol{q}j} P_{\boldsymbol{q}j}^\dagger - i\sum_{j'} P_{\boldsymbol{q}j'}^\dagger X_{\boldsymbol{q}j'j}, \tag{2.102}$$

where $X_{\boldsymbol{q}jj'}$ represents a non-adiabatic coupling between the jth and j'th modes expressed as

$$X_{\boldsymbol{q}jj'} = \sum_{j''} \mathcal{V}_{\boldsymbol{q}jj''}^{L\dagger} \frac{d\mathcal{V}_{\boldsymbol{q}j''j'}^R}{dt} \equiv \mathcal{V}_{\boldsymbol{q}j}^{L\dagger} \frac{d\mathcal{V}_{\boldsymbol{q}j'}^R}{dt}. \tag{2.103}$$

By analogy with the Hellman-Feynman theorem, this is cast into

$$X_{\boldsymbol{q}jj'} = \frac{\mathcal{V}_{\boldsymbol{q}j}^{L\dagger} \frac{d\bar{\bar{\mathcal{Z}}}_{\boldsymbol{q}}}{dt} \mathcal{V}_{\boldsymbol{q}j'}^R}{E_{\boldsymbol{q}j'} - E_{\boldsymbol{q}j}}, \quad j \neq j', \tag{2.104}$$

and $X_{\boldsymbol{q}jj} \neq 0$.

We solve Eq. (2.102) in an approximate manner by neglecting the effects of the non-adiabatic coupling. In the temporal region of $t \gtrsim \tau_L$ with the pulse width τ_L, it is assumed that the non-adiabatic coupling term in the right-hand side of Eq. (2.102) is negligibly small. In the present analysis, $f(t)$ in Eq. (2.7) is set to the Gaussian-shaped function:

$$f(t) = \exp(-t^2/2\sigma^2) \tag{2.105}$$

with $\tau_L = 2\sqrt{2\ln 2}\sigma$.

31

2.4.2 Analytic expression of a coherent phonon oscillatory pattern

The retarded phonon Green function given by Eq. (2.32) is rewritten as

$$
\begin{aligned}
\bar{D}_{\boldsymbol{q}}^R(t,t') &= -i\left\langle\left[c_{\boldsymbol{q}}(t),c_{\boldsymbol{q}}^\dagger(t')\right]\right\rangle\theta(t-t') \\
&= -i\sum_{jj'}\mathcal{V}_{\boldsymbol{q}ph,j}^L(t)\left\langle\left[P_{\boldsymbol{q}j}(t),P_{\boldsymbol{q}j'}^\dagger(t')\right]\right\rangle\mathcal{V}_{\boldsymbol{q}j',ph}^{L\dagger}(t')\theta(t-t'),
\end{aligned}
\tag{2.106}
$$

where a relation $c_{\boldsymbol{q}}^\dagger = \sum_j P_{\boldsymbol{q}j}^\dagger \mathcal{V}_{\boldsymbol{q}iph}^{L\dagger}$ is used. According to the linear response theory, $D_{\boldsymbol{q}}^R(t,t')$ indicates an induced charge density of ionic-core resulting from a delta-shaped weak external-potential at t'. The induced charge density ascribed to the CP generation is provided by

$$
Q_{\boldsymbol{q}}(\tau) \equiv D_{\boldsymbol{q}}^R(\tau+t',t') - D_{\boldsymbol{q}}^{R(0)}(\tau+t',t')
\tag{2.107}
$$

except for an unimportant proportional constant with $\tau = t - t' \geq 0$. Here, we subtract the contribution of the free phonon Green function without the pump laser, represented as

$$
D_{\boldsymbol{q}}^{R(0)}(t,t') = -2\sin[\omega_{\boldsymbol{q}}(t-t')]\theta(t-t'),
\tag{2.108}
$$

since this leads to the incoherent phonon signal. Hereafter, we are concerned exclusively with the time of $t' = 0$. Finally, $Q_{\boldsymbol{q}}(\tau)$ is rewritten as

$$
Q_{\boldsymbol{q}}(\tau) = C_{\boldsymbol{q}}(\tau)\cos\left[\omega_{\boldsymbol{q}}\tau + \Theta_{\boldsymbol{q}}(\tau)\right].
\tag{2.109}
$$

$C_{\boldsymbol{q}}(\tau)$ and $\Theta_{\boldsymbol{q}}(\tau)$ are a transitory amplitude and a renormalized phase modulus π at τ, respectively. The Fourier transform of $Q_{\boldsymbol{q}}(\tau)$ and a power spectrum $S_{\boldsymbol{q}}(\omega)$ are given by

$$
\tilde{Q}_{\boldsymbol{q}}(\omega) = \int_0^\infty e^{-i\omega\tau}Q_{\boldsymbol{q}}(\tau)d\tau
\tag{2.110}
$$

and

$$
S_{\boldsymbol{q}}(\omega) \propto |\tilde{Q}_{\boldsymbol{q}}(\omega)|^2,
\tag{2.111}
$$

respectively.

In particular, for the long-time limit of $\tau \gg 2\pi/\omega_{\boldsymbol{q}}$, a non-vanishing value of $\mathcal{V}_{\boldsymbol{q}ph,j}^L(t)$ in Eq. (2.106) and $\mathrm{Re}\left\{E_{\boldsymbol{q}j}(t)\right\} \simeq \omega_{\boldsymbol{q}}$ are exclusively concerned. For an undoped semiconductor, Eq. (2.106) becomes

$$
\bar{D}_{\boldsymbol{q}}^R(t,t') = -ie^{-i\omega_{\boldsymbol{q}}(t-t')}\xi_{\boldsymbol{q}}(t,t')\mathcal{V}_{\boldsymbol{q}ph,ph}^L(t)\mathcal{V}_{\boldsymbol{q}ph,ph}^{L\dagger}(t')\theta(t-t'),
\tag{2.112}
$$

where $\mathcal{V}_{\boldsymbol{q}ph,j}^{R\dagger}(-\infty) = \delta_{ph,j}$, $\left[c_{\boldsymbol{q}}(-\infty),c_{\boldsymbol{q}}^\dagger(-\infty)\right] = 1$, and $\left[c_{\boldsymbol{q}},\mathcal{B}_{\boldsymbol{q}}^\dagger\right] = \left[c_{\boldsymbol{q}},A_{\boldsymbol{q}}^\dagger(\boldsymbol{k}b\bar{b})\right] = 0$ are used. Further,

$$
\begin{aligned}
\xi_{\boldsymbol{q}}(t,t') &= \exp\left[-\int_{-\infty}^t dt''\mathrm{Im}E_{\boldsymbol{q}ph}(t'') - \int_{-\infty}^{t'} dt''\mathrm{Im}E_{\boldsymbol{q}ph}(t'')\right] \\
&\quad \times \exp\left[-i\int_{t'}^t dt''\left\{\mathrm{Re}E_{\boldsymbol{q}ph}(t'') - \omega_{\boldsymbol{q}}\right\}\right].
\end{aligned}
\tag{2.113}
$$

In the present dissertation, undopoed semiconductors are considered for the sake of simplicity. In a doped semiconductor, we have additional contributions from $\mathcal{V}_{\boldsymbol{q}ph,pl}^{R\dagger}(-\infty) \neq$

0 and $\mathcal{V}^R_{\boldsymbol{q}pl,ph}(-\infty) \neq 0$, nevertheless they would be negligibly small compared with $\mathcal{V}^{R\dagger}_{\boldsymbol{q}ph,ph}(-\infty)$ and $\mathcal{V}^R_{\boldsymbol{q}ph,ph}(-\infty)$. The initial phase $\theta_{\boldsymbol{q}}$ and the asymptotic amplitude $C^0_{\boldsymbol{q}}e^{-\gamma_{\boldsymbol{q}ph}\tau}$ are expressed as

$$\theta_{\boldsymbol{q}} = \frac{\pi}{2} - \arg\left[\xi_{\boldsymbol{q}}(\tau,0)\mathcal{V}^{L\dagger}_{\boldsymbol{q}ph,ph}(0) - 1\right] \tag{2.114}$$

modulus π, and

$$C^0_{\boldsymbol{q}} = \left|\xi_{\boldsymbol{q}}(\tau,0)\mathcal{V}^{L\dagger}_{\boldsymbol{q}ph,ph}(0) - 1\right|, \tag{2.115}$$

respectively, where $\mathcal{V}^L_{\boldsymbol{q}ph,ph}(\tau) = 1$ is employed.

Lastly it is noted that the normalization constant $\mathcal{N}^R_{\boldsymbol{q}}(t)$ in $\mathcal{U}^R_{\boldsymbol{q}}(t)$, and the associated operator $\mathcal{B}^\dagger_{\boldsymbol{q}\alpha}(t)$ are not determined up to an overall phase factor in the same way as $N^R_{\boldsymbol{q}\alpha}(t)$ in $U^R_{\boldsymbol{q}\alpha}(t)$ and $B^\dagger_{\boldsymbol{q}\alpha}(t)$ in Sec 2.3. However, physical quantities are unchanged for these phase transformations, and not dependent on any choice of the phase factor for the same reason as that shown in Appendix E.

Chapter 3

Results and Discussion

In Fig. 3.1, we show the scheme of the CP generation dynamics. We take into account exclusively opaque interband transitions accompanying real excited carriers. In the joint-band energy dispersion, the carriers form the energy distribution depending on the Rabi frequency Ω_{0cv} in Eq. (2.7), the pulse width τ_L, and the detuning Δ defined as

$$\Delta = \omega_0 - E_g, \tag{3.1}$$

with the laser frequency ω_0 and the band gap energy at Γ point E_g. Further, the energy distribution partially overlaps with the energy of the LO phonon $\omega_{\boldsymbol{q}}$. The pulse width of concern is of an order of 10 fs, and corresponding spectral width of the laser is approximately 300 meV to 400 meV.
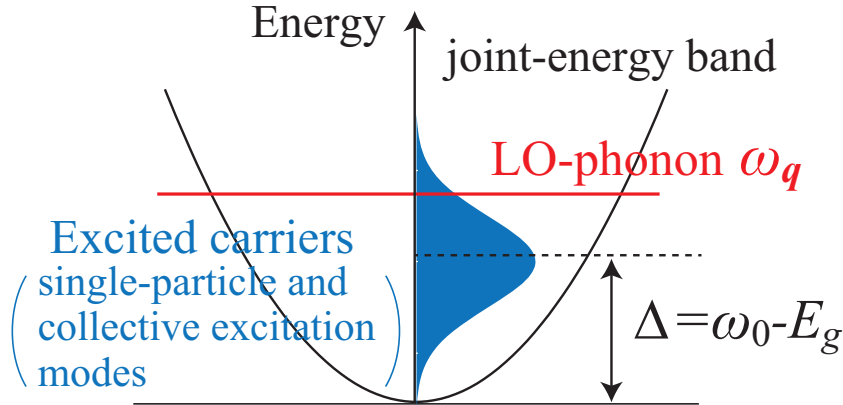
Figure 3.1: The schematic diagram of the CP generation dynamics. Detuning Δ is defined by $\Delta = \omega_0 - E_g$ with the laser frequency ω_0 and the direct band gap E_g. (From Ref. [71] with partial modification.)

Material parameters employed in the actual calculations are provided in Table 3.1. Further, in order to evaluate the single-particle density matrices $\bar{\rho}_{bb'\boldsymbol{k}}(t)$, we solve optical Bloch equations in advance within the two-band model constituted of c- and v-bands. Hereafter, we refer the concerned materials of undoped Si and undoped GaAs just as Si and GaAs, respectively, unless otherwise stated. Further, we assume the crystals to be cubic.

Table 3.1: Materials parameters of undoped Si and undoped GaAs used in the dissertation. m_c and m_v are effective masses of conduction- and valence-electrons at Γ point, respectively. ϵ_0 and ϵ_∞ are a static dielectric constant and a dielectric constant in the high-frequency limit, respectively. $g_{c\boldsymbol{q}}^D$ and $g_{v\boldsymbol{q}}^D$ are coupling constants between the conduction- and valence-band electron and the LO phonon due to deformation-potential interaction, respectively, where more accurate values are given by Ref. [89]. $\omega_{\boldsymbol{q}}$ is LO phonon frequency at Γ point. N_s is the total number of sites considered in calculations, and d is a lattice constant. Atomic units are used, unless otherwise stated.

Parameters	undoped Si	undoped GaAs
m_c	0.158	0.067
m_v	-0.523	-0.45
ϵ_0	11.9	11.53
ϵ_∞	11.9	10.10
$g_{c\boldsymbol{q}}^D$	0	0
$g_{v\boldsymbol{q}}^D$	0.147	0.0676
$\omega_{\boldsymbol{q}}$	63 meV	35 meV
N_s	$70^3 (= 3.43 \times 10^5)$	$64^3 (= 2.62 \times 10^5)$
d	10.5	10.5

3.1 Transient Fano Resonance

In this section, we show the results of the numerical calculations of adiabatic energy in Eqs. (2.33) and (2.34), and the transient induced photoemission spectra of Eq. (2.77) for Si and GaAs. The pulse-envelop function $f(t)$ in Eq. (2.7) is set to a squared-shape with $\tau_L = 15$ fs. Further, the magnitude of momentum $\boldsymbol{q}$ is assumed to be quite small, and set to $|\boldsymbol{q}| = 0.015$ (a.u.). Other parameters of the pulse laser employed in the calculations are provided in Table 3.2.

Table 3.2: Parameters of a square-shaped pulse laser used in Sec. 3.1, where Ω_{0cv} is the Rabi frequency in Eq. (2.7), A_L is the pulse area defined by $A_L = \int_{-\infty}^{\infty} \Omega_{0cv} f(t) dt$ with the pulse-envelop function $f(t)$, Δ is the detuning defined by Eq. (3.1), and N_{el} is the maximum excited-electron density.

Parameters	Si	GaAs
Ω_{0cv}	16.5 meV	27.2 meV
A_L	0.12π	0.20π
Δ	82 meV	73 meV
N_{el}	$6.31 \times 10^{17}/\text{cm}^3$	$5.30 \times 10^{17}/\text{cm}^3$
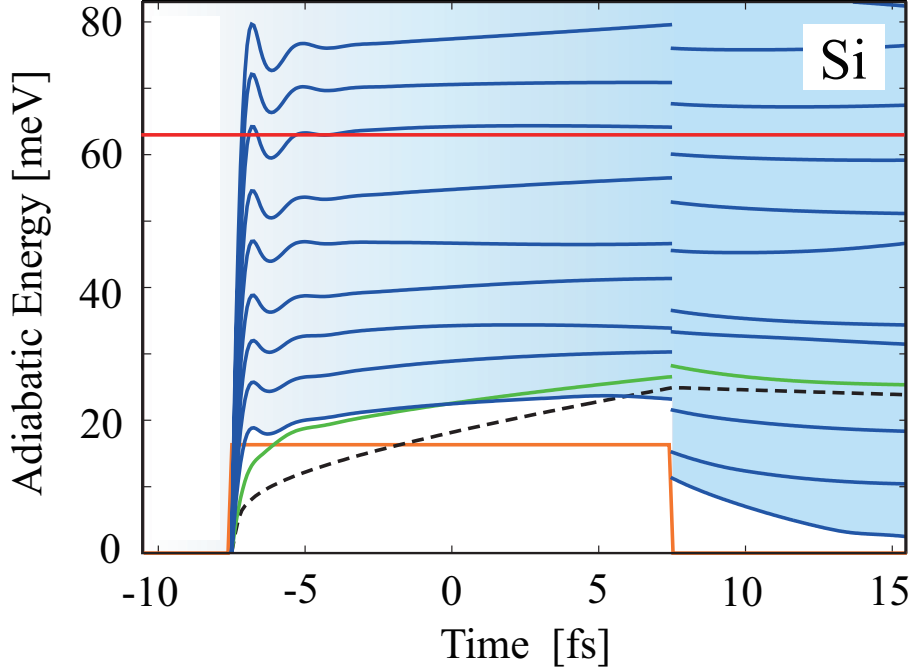
Figure 3.2: Adiabatic energy curves of Si (in the unit of meV) as a function of time (in the unit of fs). A red solid line, blue solid lines, a green solid line, a broken line, and an orange solid line show $\omega_{\bm{q}}$, $\{\mathcal{E}_{\bm{q}\beta}\}$, $\mathcal{E}_{\bm{q}\alpha_1}$, $\omega_{\bm{q}pl}$, and $\Omega_{0cv}f(t)$, respectively. Schematic change of the excited electron density in time is depicted by the gradation of blue color, where the threshold energy of $\{\mathcal{E}_{\bm{q}\beta}\}$ is represented by the lowest limit of this gradation. (From Ref. [69].)

3.1.1 Adiabatic energy configuration

Figure 3.2 shows the calculated result of adiabatic energy curves $\mathcal{E}_{\bm{q}\alpha}(t)$ of quasiboson in Si as a function of time in the small-$\bm{q}$ limit. A green solid line indicates $\mathcal{E}_{\bm{q}\alpha_1}(t)$ ascribed to a plasmon-like mode, and it is seen that the the green line is almost proportional to the plasma frequency $\omega_{\bm{q}pl}(t)$ indicated by a broken line. Here, the maximum of the excited electron density is $6.31 \times 10^{17}\text{cm}^3$. In fact, $\mathcal{E}_{\bm{q}\alpha_1}(t)$ is dependent on Rabi frequencies of $\bar{\Omega}_{cv\bm{k}}^{(R)}(t)$ and $\bar{\Omega}_{vc\bm{k}}^{(R)}(t)$ of Eq. (2.19), and interband density matrices $\bar{\rho}_{cv\bm{k}}(t)$ and $\bar{\rho}_{vc\bm{k}}(t)$ in an intricate manner as shown in Appendix B. The difference of the functional shapes between $\omega_{\bm{q}pl}(t)$ and $\mathcal{E}_{\bm{q}\alpha_1}(t)$ are due to the transient effect of the Rabi frequencies and the interband density matrices. After such effects are suppressed, namely, in the time region of $t > t_L/2 = t_D$, $\mathcal{E}_{\bm{q}\alpha_1}(t)$ becomes equivalent to $\omega_{\bm{q}pl}(t)$, apart from a renormalization effect attributed to $V_{\bm{q}}^{(C)}$ on the Rabi frequencies.

Blue solid lines show discretized adiabatic-energy levels of a bundle of electron-hole continua $\{\mathcal{E}_{\bm{q}\beta}(t)\}$, where the lowest energy of them represents a threshold of these contributions. As described in Appendix C.1, this threshold is provided by $|2\bar{\Omega}_{cv\bm{k}}^{(R)}(t)|$ in an approximate manner, which roughly corresponds to $\Omega_{0cv}f(t)$ [see Eqs. (2.7) and (2.19)] represented by an orange solid line. The energy discretization for $\{\mathcal{E}_{\bm{q}\beta}(t)\}$ originates from the incorporation of the *finite* number of sites in the calculations: $V = N_s d^3$ and $N_s = 70^3$ with lattice constant d. It is remarked that the formation of the continua $\{\mathcal{E}_{\bm{q}\beta}(t)\}$ is attributed exclusively to single-particle excitation modes in interbands, and the effect of

36

intrabands vanishes in the small-$\boldsymbol{q}$ limit. Further, schematic change of the excited carrier density in time is shown by the gradation of blue color. The red line represents the LO phonon energy $\omega_{\boldsymbol{q}} = 63$ meV. Adiabatic energy curves of GaAs as a function of time represent the similar behavior to those of Si, though not shown here.

As is seen in Fig. 3.2, the LO phonon mode α_2 is embedded in the continuum state $\{\beta\}$ of the single-particle excitation modes right after the onset of the laser irradiation. This effect continues even after the completion of the irradiation: $t > t_D$. It is likely that $M_{\boldsymbol{q}\beta}$ of Eq. (2.46) causes a coupling between the LO phonon and the quasiboson continuum state in a resonant manner, that is, at $\mathcal{E}_{\boldsymbol{q}\beta} \approx \omega_{\boldsymbol{q}}$. As a result, FR is generated in the case that the excited carrier density is high enough: $M_{\boldsymbol{q}\beta}$ is dependent on the excited carrier density. Such an energy configuration is one of the essential requirements to be satisfied for the occurrence of the FR in addition to the allocation of the time constants mentioned in Sec. 2.3.4. The plasmon-like mode α_1 inclines to dive into the continua in $t > t_D$. However, FR ascribed to this mode is not expected to manifest itself since the coupling between the α_1th and βth modes is provided by the second-order interaction of the form $M_{\boldsymbol{q}\beta}M_{\boldsymbol{q}\alpha_1}^*$ mediated by the LO phonon, and this would be negligible, as shown later in Sec. 3.1.2.

Moreover, in Fig. 3.2, it is seen that the adiabatic energy curves in $t > t_D$ vary so slowly in time that the PQ model based on the adiabatic picture is verified. The discontinuity at $t = \pm\tau_L/2$ is attributed to the square-shaped pulse of Eq. (2.66).

3.1.2 Transient induced photoemission spectra

Transient induced photoemission spectra $\bar{I}_{\boldsymbol{q}}(t_p; \omega)$ of Eq. (2.77) represent the change of the electronic structure at probe time t_p formed by a nonlinear optical process attributed to the pump pulse irradiation . This is a decisive observable to comprehend the occurrence of transient and nonlinear FR. Here, we take into account $\bar{I}_{\boldsymbol{q}}(t_p; \omega)$ of Si and GaAs as a function of frequency ω. As seen from Eq. (2.22), the two interactions−the dynamically screened Coulomb interaction induced by electron and the LO phonon-induced interaction− play a part to the total retarded longitudinal susceptibility, represented by

$$\tilde{\chi}_{\boldsymbol{q}}^{(t)}(t_p; \omega) = \tilde{\chi}_{\boldsymbol{q}}(t_p; \omega) + \tilde{\chi}_{\boldsymbol{q}}'(t_p; \omega). \tag{3.2}$$

Here, $\tilde{\chi}_{\boldsymbol{q}}^{(t)}(t_p; \omega)$, $\tilde{\chi}_{\boldsymbol{q}}(t_p; \omega)$, and $\tilde{\chi}_{\boldsymbol{q}}'(t_p; \omega)$ show the Fourier transforms of $\chi_{\boldsymbol{q}}^{(t)}(t_p + \tau, t_p)$, $\chi_{\boldsymbol{q}}(t_p + \tau, t_p)$, and $\chi_{\boldsymbol{q}}'(t_p + \tau, t_p)$ with respect to time τ into the frequency ω-domain, respectively. $\tilde{\chi}_{\boldsymbol{q}}(t_p; \omega)$ is proportional to $|\boldsymbol{q}|^2$ in the small-$\boldsymbol{q}$ limit. On the other hand, owing to Eq. (2.29), $\tilde{\chi}_{\boldsymbol{q}}'(t_p; \omega)$ is proportional to $|\boldsymbol{q}|^2$ for the Frölich interaction of long range, and $|\boldsymbol{q}|^4$ for the deformation potential interaction of short range. This fact reflects on $\bar{I}_{\boldsymbol{q}}(t_p; \omega)$ through Eq. (2.73), as it should be; in nonpolar crystals such as Si, since spatial inversion symmetry exists, lattice absorption vanishes in the limit of a dipole transition accompanying no momentum transfer, namely, $\boldsymbol{q} = 0$.

Figure 3.3 shows $\bar{I}_{\boldsymbol{q}}(t_p; \omega)$ of Si and GaAs at probe time $t_p = 15, 65$, and 100 fs. Blue and green lines represent the separate contributions from $\tilde{\chi}_{\boldsymbol{q}}(t_p; \omega)$ and $\tilde{\chi}_{\boldsymbol{q}}'(t_p; \omega)$, respectively, and red lines represent the total one. The contribution of $\tilde{\chi}_{\boldsymbol{q}}(t_p; \omega)$ is mostly dominated by the plasmon-like mode α_1, while that of $\tilde{\chi}_{\boldsymbol{q}}'(t_p; \omega)$ is dominated by the LO phonon mode α_2. $\tilde{\chi}_{\boldsymbol{q}}(t_p; \omega)$ is attributed to electronic excitation through optical interband transitions. $\bar{I}_{\boldsymbol{q}}(t_p; \omega)$ includes structureless background spectra due to electron-hole continuum modes $\{\beta\}$, which are almost constant in ω of concern. In both $\bar{I}_{\boldsymbol{q}}(t_p; \omega)$'s
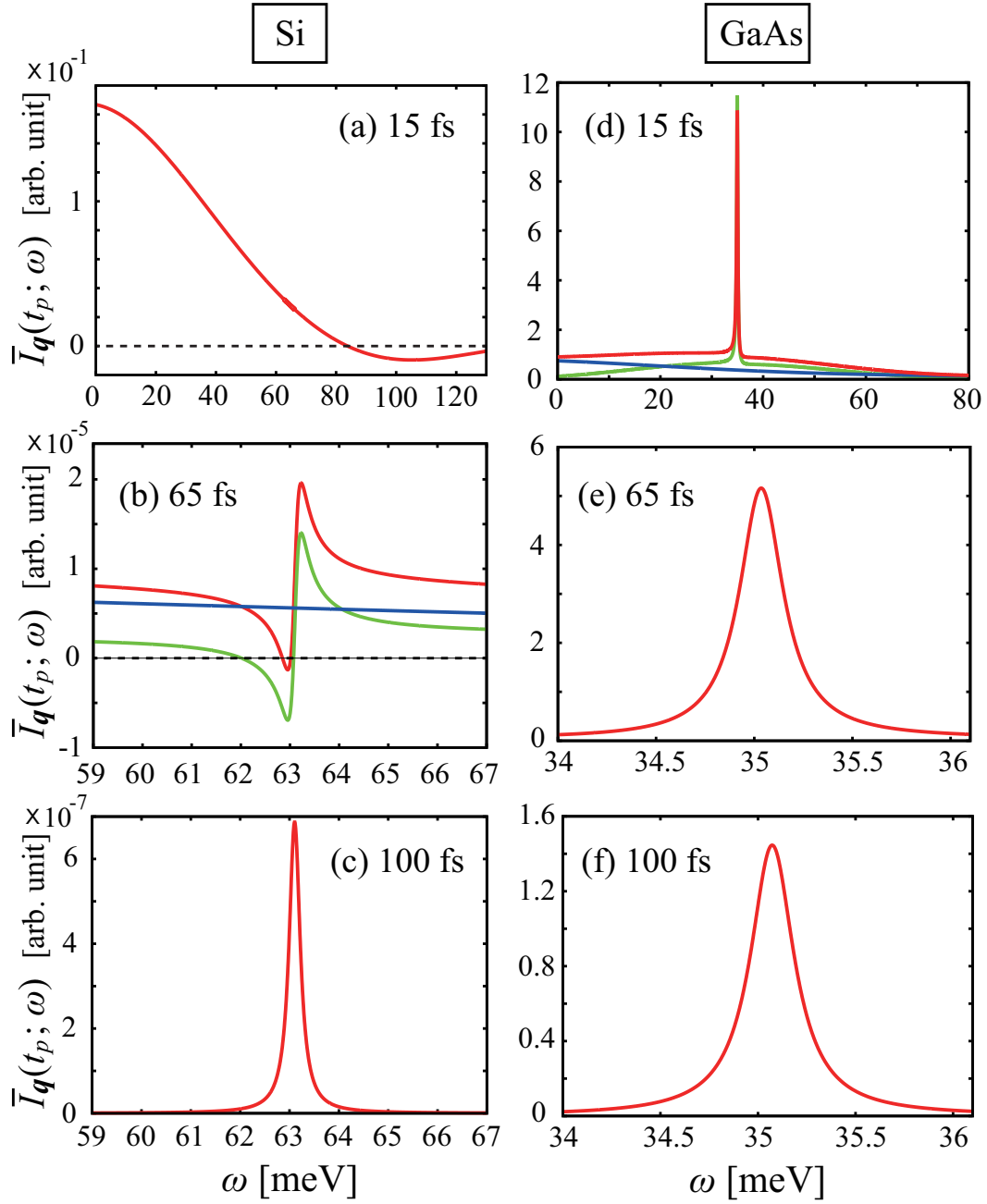
Figure 3.3: Transient induced photoemission spectra $\bar{I}_{\boldsymbol{q}}(t_p; \omega)$ (red line) as a function of frequency ω (in the unit of meV) for Si at probe time t_p of (a) 15 fs, (b) 65 fs, and (c) 100 fs, and those for GaAs at probe time t_p of (d) 15 fs, (e) 65 fs, and (f) 100fs. Blue and green lines represent separate contributions to the spectra from $\tilde{\chi}_{\boldsymbol{q}}(t_p; \omega)$ and $\tilde{\chi}'_{\boldsymbol{q}}(t_p; \omega)$, respectively. (From Ref. [69] with partial modification.)

of Si and GaAs, the formation of spectral peaks is due only to $\tilde{\chi}'_{\boldsymbol{q}}(t_p;\omega)$. The width of the spectral peaks follows $2/T_{\boldsymbol{q}ph} = 0.27$ meV rather than natural spectral width. Further, it is noted that the back ground spectra in Fig 3.3 is attributed just to the α_1th mode. The choice of the baseline, that is, the line of $\bar{I}_{\boldsymbol{q}}(t_p;\omega) = 0$ corresponds to removal of the contributions from the continuum modes $\{\beta\}$, which would be structureless, just for the sake of simplicity of the calculation.

Figure 3.3(a) represents $\bar{I}_{\boldsymbol{q}}(t_p;\omega)$ of Si at $t_p = 15$ fs. The spectrum is governed by the contribution from $\tilde{\chi}_{\boldsymbol{q}}(t_p;\omega)$ attributed to the α_1th mode, that is, $\tilde{\chi}^{(t)}_{\boldsymbol{q}}(t_p;\omega) \approx \tilde{\chi}_{\boldsymbol{q}}(t_p;\omega)$, and the spectrum shows monotonous decrease in ω. On the other hand, the contribution from $\tilde{\chi}'_{\boldsymbol{q}}(t_p;\omega)$ is negligible since it is proportional to $|\boldsymbol{q}|^4$. In Fig. 3.3(b), the contribution from $\tilde{\chi}_{\boldsymbol{q}}(t_p;\omega)$ becomes small due to $T_{\boldsymbol{q}12}$, and therefore comparable with that from $\tilde{\chi}'_{\boldsymbol{q}}(t_p;\omega)$. It is remarked that asymmetric spectrum with a dip followed by a peak appears, which is characteristic of FR . This spectral profile contrasts with that of the Lorentzian profile shown in Fig. 3.3(c) at $t_p = 100$ fs, where the spectrum is governed by $\tilde{\chi}'_{\boldsymbol{q}}(t_p;\omega)$ and $\tilde{\chi}^{(t)}_{\boldsymbol{q}}(t_p;\omega) \approx \tilde{\chi}'_{\boldsymbol{q}}(t_p;\omega)$.

As regards $\bar{I}_{\boldsymbol{q}}(t_p;\omega)$ of GaAs, Fig. 3.3(d) shows spectra at $t_p = 15$ fs with a discernible peak attributed to the α_2th mode. The contributions from $\tilde{\chi}_{\boldsymbol{q}}(t_p;\omega)$ of the background continuum and $\tilde{\chi}'_{\boldsymbol{q}}(t_p;\omega)$ of the peak are comparable order because both are proportional to $|\boldsymbol{q}|^2$. Figure 3.3(e) shows the spectrum at $t_p = 65$ fs governed by $\tilde{\chi}'_{\boldsymbol{q}}(t_p;\omega)$. The spectral profile is symmetric and different a lot from that of Si shown in Fig. 3.3(b). Figure 3.3(f) shows the spectrum at $t_p = 100$ fs representing the similar profile to that in Fig. 3.3(c).

Discussion on the spectral profile of $\bar{I}_{\boldsymbol{q}}(t_p;\omega)$ based on the PQ picture

The origin of the manifestation of the transient FR shown in Fig. 3.3(b) can be elucidated by inspection of the details of the numerical calculation, namely, analytic expression of the retarded longitudinal susceptibility $\chi'_{\boldsymbol{q}}(t,t')$ given by Eq. (2.28) and associated expressions of Eqs. (D.15) and (D.31)-(D.33). According to the procedures, major difference between the results of Si and GaAs originates just from the phase factor of the effective coupling between the LO phonon and the quasiboson, that is,

$$M_{\boldsymbol{q}\beta} = |M_{\boldsymbol{q}\beta}|e^{i\phi_{\boldsymbol{q}\beta}} \tag{3.3}$$

apart from trivial difference of material parameters. As shown in Eqs. (2.51)-(2.53), $M_{\boldsymbol{q}\beta}$ is attributed to a phenomenological LO-phonon-induced deformation-potential interaction $g_{b\boldsymbol{q}} = g^D_{b\boldsymbol{q}}$ that is real in non-polar crystals, and the Fröhlich interaction $g_{b\boldsymbol{q}} = g^F_{b\boldsymbol{q}}$ that is pure imaginary in polar crystals. It is remarked that in GaAs, the contribution of the deformation potential interaction in $M_{\boldsymbol{q}\beta}$ is approximately an order of one thousand times smaller than that of the Fröhlich interaction in our calculations, that is, $g_{b\boldsymbol{q}} \approx g^F_{b\boldsymbol{q}}$. Owing to the approximation (ii) described in Sec. 2.3.2, $U^{L\dagger}_{\boldsymbol{q}\alpha}(\boldsymbol{k}bb)$ in Eq. (2.46) is considered to be real, and therefore $\phi_{\boldsymbol{q}\beta}$ is determined by the phases of $g^D_{b\boldsymbol{q}}$ and $g^F_{b\boldsymbol{q}}$; $\phi_{\boldsymbol{q}\beta} = 0, \pi$ for Si, whereas $\phi_{\boldsymbol{q}\beta} = \pm\pi/2$ for GaAs.

Now, we examine how the difference of $M_{\boldsymbol{q}\beta}$ influences the spectral profile of $\bar{I}_{\boldsymbol{q}}(t_p;\omega)$ with the PQ picture. As shown in Fig. 3.2, the LO phonon discrete state α_2 is embedded in the quasiboson continuum state β. They can be resonantly coupled, leading to the formation of the FR state of the PQ. Given this situation, Fig. 3.4 schematically diagrams the present FR dynamics, and we have the two transition processes. One is a direct process through an optical transition matrix $D^{(c)}_{\boldsymbol{q}\beta}$ from the quasiboson state to the PQ ground
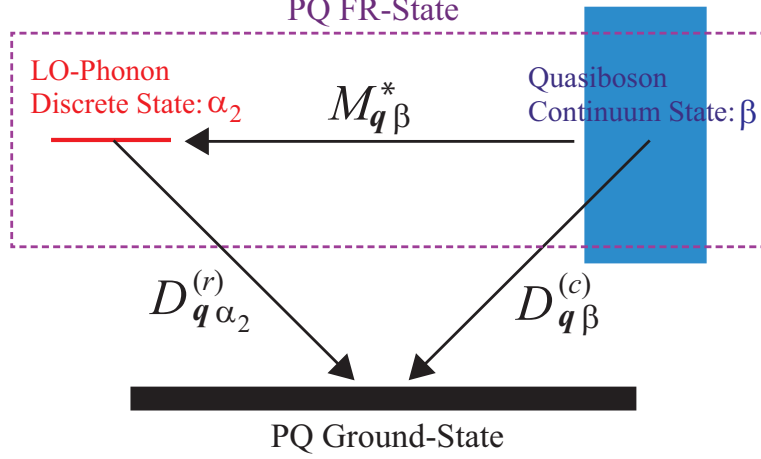
Figure 3.4: Schematic diagram of FR dynamics on the basis of the PQ picture, where the LO phonon discrete state α_2 is embedded in the quasiboson continuum state β . The PQ FR state constituted of α_2 and β is deexcited by an induced photoemission process. Transition matrices of photoemission from α_2 and β to the PQ ground state are represented as $D_{\boldsymbol{q}\alpha_2}^{(r)}$ and $D_{\boldsymbol{q}\beta}^{(c)}$, respectively. Further, a coupling matrix between α_2 and β is represented as $M_{\boldsymbol{q}\beta}^*$. (From Ref. [69] with partial modification.)

state. The other is a two-step resonant process which is mediated by $M_{\boldsymbol{q}\beta}^*$ from β to α_2, followed by a deexcitation process through an optical transition matrix $D_{\boldsymbol{q}\alpha_2}^{(r)}$ from α_2 to the PQ ground state. Here, we omit dependence of $D_{\boldsymbol{q}\beta}^{(c)}$, $D_{\boldsymbol{q}\alpha_2}^{(r)}$, and $M_{\boldsymbol{q}\beta}^*$ on t_p just for the sake of simplicity. Consulting Shore's model [90], the whole transition matrix $D_{\boldsymbol{q}\beta}(t_p;\omega)$ is represented as

$$D_{\boldsymbol{q}\beta}(t_p;\omega) = D_{\boldsymbol{q}\beta}^{(c)} + \frac{D_{\boldsymbol{q}\alpha_2}^{(r)} M_{\boldsymbol{q}\beta}^*}{\omega - \omega_{\boldsymbol{q}} + i\Gamma_{\boldsymbol{q}\alpha_2}/2}, \tag{3.4}$$

where the natural spectral width is provided by $\Gamma_{\boldsymbol{q}\alpha_2} = 2\pi\rho_{\boldsymbol{q}\alpha_2}|M_{\boldsymbol{q}\alpha_2}|^2$. $\rho_{\boldsymbol{q}\alpha_2}$ is the density of state of the quasiboson, and $M_{\boldsymbol{q}\alpha_2}$ is the coupling matrix at $\mathcal{E}_{\boldsymbol{q}\beta} = \omega_{\boldsymbol{q}}$. The induced photoemission spectrum is provided by $\bar{I}_{\boldsymbol{q}}(t_p;\omega) = |D_{\boldsymbol{q}\beta}(t_p;\omega)|^2$, and this shows Shore's spectral profile in the vicinity of $\omega \approx \omega_{\boldsymbol{q}}$, corresponding to well-known Fano's formula [90]. That is,

$$\bar{I}_{\boldsymbol{q}}(t_p;\omega) \approx \mathcal{C}_{\boldsymbol{q}\beta} + \frac{\mathcal{A}_{\boldsymbol{q}\alpha_2}\left(\omega - \omega_{\boldsymbol{q}}\right) + \mathcal{B}_{\boldsymbol{q}\alpha_2}\Gamma_{\boldsymbol{q}\alpha_2}/2}{\left(\omega - \omega_{\boldsymbol{q}}\right)^2 + \left(\Gamma_{\boldsymbol{q}\alpha_2}/2\right)^2}, \tag{3.5}$$

where we obtain Shore's spectral parameters represented by $\mathcal{A}_{\boldsymbol{q}\alpha_2}$, $\mathcal{B}_{\boldsymbol{q}\alpha_2}$, and $\mathcal{C}_{\boldsymbol{q}\beta}$ as

$$\mathcal{A}_{\boldsymbol{q}\alpha_2} = 2|D_{\boldsymbol{q}\beta}^{(c)}||D_{\boldsymbol{q}\alpha_2}^{(r)}||M_{\boldsymbol{q}\beta}|\cos\tilde{\phi}_{\boldsymbol{q}\beta}, \tag{3.6}$$

$$\mathcal{B}_{\boldsymbol{q}\alpha_2} = -2|D_{\boldsymbol{q}\beta}^{(c)}||D_{\boldsymbol{q}\alpha_2}^{(r)}||M_{\boldsymbol{q}\beta}|\sin\tilde{\phi}_{\boldsymbol{q}\beta} + \frac{|D_{\boldsymbol{q}\alpha_2}^{(r)}|^2|M_{\boldsymbol{q}\beta}|^2}{\Gamma_{\boldsymbol{q}\alpha_2}/2}, \tag{3.7}$$

and

$$\mathcal{C}_{\boldsymbol{q}\beta} = |D_{\boldsymbol{q}\beta}^{(c)}|^2, \tag{3.8}$$

respectively. Here, the phase $\tilde{\phi}_{\boldsymbol{q}\beta}$ is provided by $\tilde{\phi}_{\boldsymbol{q}\beta} = \phi_{\boldsymbol{q}\beta} + \Delta\phi_{\boldsymbol{q}\beta}$ with $\Delta\phi_{\boldsymbol{q}\beta} = \arg[D_{\boldsymbol{q}\beta}^{(c)} - D_{\boldsymbol{q}\alpha_2}^{(r)}]$. We obtain the associated Fano's asymmetric q parameter by means of Shore's
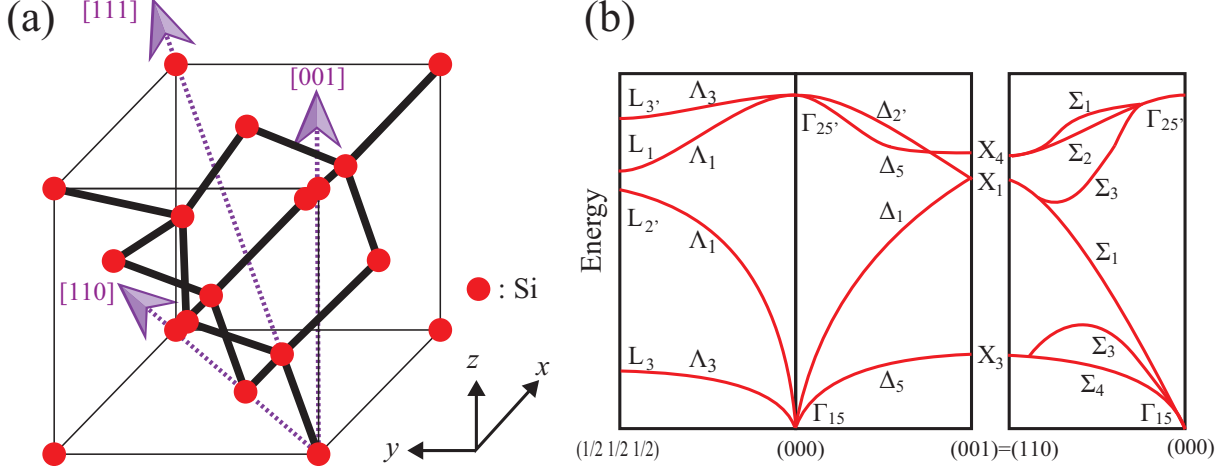
Figure 3.5: (a) The crystal structure of Si (the diamond structure). A red filled circle depicts each Si atom, and an arrow with a purple dotted line represents the direction of electric field of a pump laser; the representative three directions of [001], [111], and [110] are selected. (b) Schematic phonon energy-dispersion curve in Si along high symmetry axes. The number in the abscissa shows Bloch momentum in the unit of $2\pi/d$ with a lattice constant d.

parameters as

$$q_{\boldsymbol{q}\alpha_2}(t_p) = r_{\boldsymbol{q}\alpha_2}(t_p) + \sigma_{\boldsymbol{q}\alpha_2}(t_p)\sqrt{[r_{\boldsymbol{q}\alpha_2}(t_p)]^2 + 1} \qquad (3.9)$$

with $r_{\boldsymbol{q}\alpha_2}(t_p) = \mathcal{B}_{\boldsymbol{q}\alpha_2}/\mathcal{A}_{\boldsymbol{q}\alpha_2}$ and $\sigma_{\boldsymbol{q}\alpha_2}(t_p) = \mathcal{A}_{\boldsymbol{q}\alpha_2}/|\mathcal{A}_{\boldsymbol{q}\alpha_2}|$, and $\mathcal{C}_{\boldsymbol{q}\beta}$ represents a continuum background.

The spectral profile depends on $\mathcal{A}_{\boldsymbol{q}\alpha_2}$. On the occasion of $\phi_{\boldsymbol{q}\beta} = \pm\pi/2$, $\mathcal{A}_{\boldsymbol{q}\alpha_2} = 0$ and the spectral profile of $\bar{I}_{\boldsymbol{q}}(t_p;\omega)$ becomes symmetric with $|q_{\boldsymbol{q}\alpha_2}(t_p)|$ infinite. This situation corresponds to the profile of GaAs in Fig. 3.3(e), where $\Delta\phi_{\boldsymbol{q}\beta} \approx 0$ is assumed so as to match it to experiments. When $\tilde{\phi}_{\boldsymbol{q}\beta} \neq \pm\pi/2$, both $\mathcal{A}_{\boldsymbol{q}\alpha_2}$ and $\mathcal{B}_{\boldsymbol{q}\alpha_2}$ are finite, and the spectral profile becomes asymmetric with $|q_{\boldsymbol{q}\alpha_2}(t_p)|$ finite. The profile of Si in Fig. 3.3(b) with $\phi_{\boldsymbol{q}\beta} = 0, \pi$ is categorized into this case, where $\Delta\phi_{\boldsymbol{q}\beta} \approx 0$ is assumed as well as the case of GaAs. For Figs. 3.3(c) and 3.3(f), because $D_{\boldsymbol{q}\beta}^{(c)}$ and $|M_{\boldsymbol{q}\beta}|$ are negligible, $\bar{I}_{\boldsymbol{q}}(t_p;\omega)$ is dominated by the second term in the right-hand side of Eq. (3.7). As a result, the spectral profile becomes symmetric. In conclusion, the effective coupling constant $M_{\boldsymbol{q}\beta}$ around $\mathcal{E}_{\boldsymbol{q}\beta} \approx \omega_{\boldsymbol{q}}$ plays a key part in the occurrence of the transient FR, and the spectral profile is determined by $\phi_{\boldsymbol{q}\beta}$ as far as $|M_{\boldsymbol{q}\beta}|$ is finite.

Next, we examine the optical transition matrix $D_{\boldsymbol{q}\alpha_2}^{(r)}$ for the LO phonon. A Γ_4 optical phonon of GaAs is categorized into the space group $T_d^2(F\bar{4}3m)$, whereas a $\Gamma_{25'}$ optical phonon of Si is categorized into the space group $O_h^7(Fd3m)$. An infrared photon excites the Γ_4 optical phonon directly through an electric dipole transition, namely, $D_{\boldsymbol{q}\alpha_2}^{(r)} \neq 0$, while the $\Gamma_{25'}$ optical phonon is not infrared active owing to the existence of inversion symmetry. This is the reason why in $\bar{I}_{\boldsymbol{q}}(t_p;\omega)$ of GaAs, the contributions of $\tilde{\chi}'_{\boldsymbol{q}}(t_p;\omega)$ and $\tilde{\chi}_{\boldsymbol{q}}(t_p;\omega)$ are comparable orders even at $t_p = 15$ as shown in Fig. 3.3(d). On the other hand, in the time region for Si, the contribution of $\tilde{\chi}'_{\boldsymbol{q}}(t_p;\omega)$ is much smaller than that of $\tilde{\chi}_{\boldsymbol{q}}(t_p;\omega)$. However, the former contribution for Si does not necessarily vanish, in other words, $D_{\boldsymbol{q}\alpha_2}^{(r)} \neq 0$ in the present optically nonlinear and transient process. With

the increase of t_p, this contribution becomes more dominant as shown in Figs. 3.3(b) and 3.3(c).

We are concerned with a crystal where a pump laser is irradiated in a certain direction, rather than a free crystal, as schematically shown in Fig 3.5(a). Hereafter, we term the former crystal a *dressed* crystal. On the occasion that an electric field of the laser is applied in the representative directions of [001], [111], and [110], the symmetry of the *dressed* crystal is reduced from that of the free crystal of the point group O_h into point groups of C_{4v}, C_{3v}, and C_{2v}, respectively. Thus, we obtain irreducible representations subduced from the irreducible representation $\Gamma_{25'}$ of O_h as follows [91]:

$$\Gamma_{25'} \downarrow C_{4v} = \Delta_{2'} + \Delta_5, \tag{3.10}$$

$$\Gamma_{25'} \downarrow C_{3v} = \Lambda_1 + \Lambda_3, \tag{3.11}$$

and

$$\Gamma_{25'} \downarrow C_{2v} = \Sigma_1 + \Sigma_2 + \Sigma_3. \tag{3.12}$$

Among the subduced representations obtained above, the irreducible representations of Λ_1, Λ_3, and Σ_3 are in agreement with the symmetry of an ionic momentum operator, namely, $\Lambda_1 : \{z\}$, $\Lambda_3 : \{x \pm iy\}$, and $\Sigma_3 : \{z\}$, where Λ_1 and Σ_3 are single-valued representations and Λ_3 is a double-valued one. This result implies that the *dressed* crystal can be infrared-active, and an optical deexcitation arises via an emission process induced by an infrared laser, which differs from the free crystal.

We can interpret Eqs. (3.10)-(3.12) by consulting a phonon energy-dispersion diagram of Si shown schematically in Fig. 3.5(b) [33]. The subduced representations obtained here are in agreement with the compatibility relations with respect to $\Gamma_{25'}$ point [91]. Concretely, for instance, the $\boldsymbol{k}$ group $\mathcal{G}_\Lambda$ related to Λ point ($\boldsymbol{k}_\Lambda$) along the (111) axis of Bloch momentum, that is, the direction of L point is a subgroup of the $\boldsymbol{k}$ group $\mathcal{G}_\Gamma$ related to the Γ point ($\boldsymbol{k}_\Gamma = \boldsymbol{0}$). Here, the symmetry of the *dressed* crystal in Si is lowered from $\boldsymbol{k}_\Gamma$ to $\boldsymbol{k}_\Lambda$ along the (111) axis, and a threefold-degenerate level $\Gamma_{25'}$ is lifted into a twofold-degenerate level Λ_3 and nondegenerate level Λ_1. The similar fact also holds for the subgroups of $\mathcal{G}_\Delta$ and $\mathcal{G}_\Sigma$. According to this discussion, the degree of magnitude of the symmetry lowering is associated with the momentum change of $\boldsymbol{q} \equiv \boldsymbol{k}_\Lambda - \boldsymbol{k}_\Gamma$, which results from spatial inhomogeneity induced by the formation of polarized charge by the pump laser. In other words, spatial inversion symmetry is broken by the generated polarization. This is the reason why in $\bar{I}_{\boldsymbol{q}}(t_p; \omega)$ of Si, the contribution from $\tilde{\chi}'_{\boldsymbol{q}}(t_p; \omega)$ is reduced by the order of $|\boldsymbol{q}|^2$ in comparison with that of GaAs, as seen from Fig. 3.3.

Therefore, a transition process governing $\tilde{\chi}'_{\boldsymbol{q}}(t_p; \omega)$ is regarded as an electric-dipole transition in the *dressed* crystal with absorption of, for example, a Λ_1 optical phonon. Further, this is also considered to be an electric quadrupole transition in the original crystal with absorption of a $\Gamma_{25'}$ optical phonon, as far as $\boldsymbol{q} \approx 0$; actually, the irreducible representation is in harmony with the symmetry $\{xy, yz, zx\}$ [33, 91]. Significant roles of the electric quadrupole transition are also investigated in optical second harmonic generation from Si [92]. Further, it is reported that heavily excited carriers by the strong femtosecond pulse induce lattice instability of Si and GaAs due to LO phonon distortions [93]. It is remarked that the results obtained from a viewpoint of the group theory remain unchanged for the present spectra calculated in a cubic model.
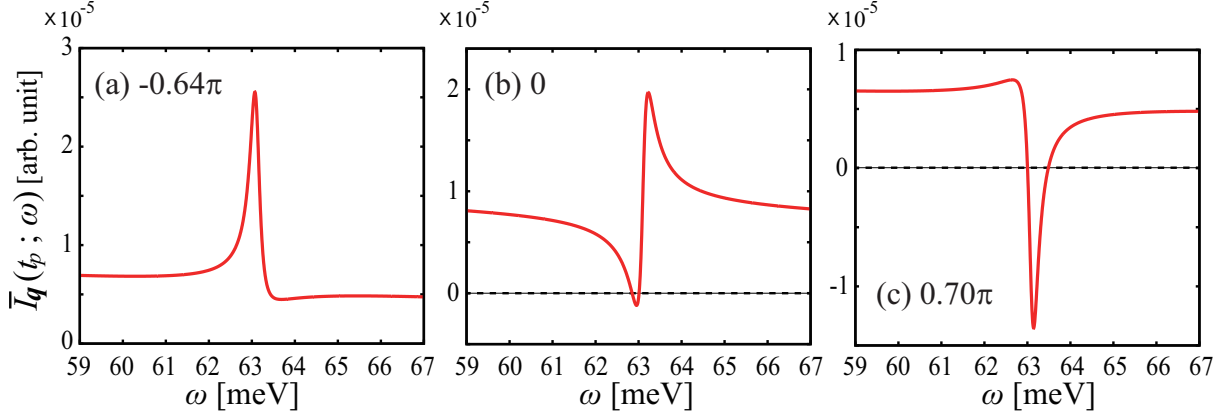
Figure 3.6: Transient induced photoemission spectra $\bar{I}_{\boldsymbol{q}}(t_p; \omega)$ as a function of frequency ω (in the unit of meV) for Si at probe time $t_p = 65$ fs with $\mathrm{Im}\mathfrak{J}^{(C)}_{\boldsymbol{q}\beta_2\beta_2}$ of (a) -0.64π, (b) 0, and 0.70π.
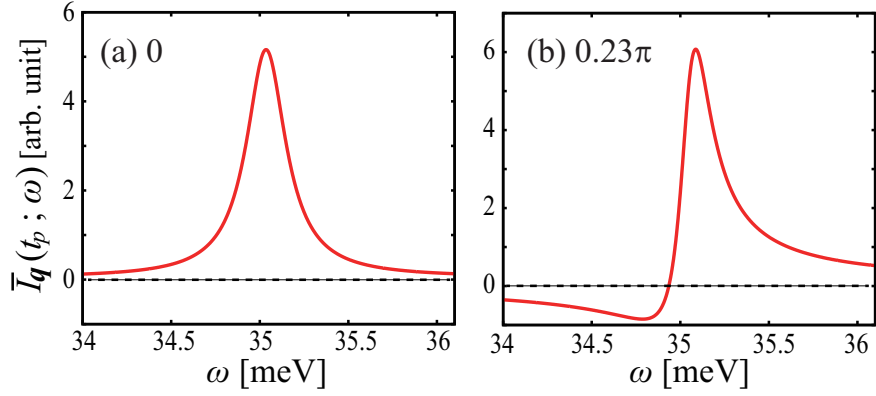
Figure 3.7: The same as Fig.3.6 but for GaAs with $\mathrm{Im}\mathfrak{J}^{(C)}_{\boldsymbol{q}\beta_2\beta_2}$ of (a) 0 and (b) 0.23π.

Effect of the non-adiabatic correction

Next, we examine the effect of the non-adiabatic correction due to $\mathfrak{J}^{(C)}_{\boldsymbol{q}\beta\beta}$ on $\bar{I}_{\boldsymbol{q}}(t_p; \omega)$ [see Eqs. (2.67) and (2.71)]. This effect is fully neglected in the calculations of the spectra shown in Fig. 3.3 as mentioned in Sec. 2.3.2. Here, we conduct the calculation of $\bar{I}_{\boldsymbol{q}}(t_p; \omega)$ at $t_p = 65$ fs with given numerical values of $\mathrm{Im}\mathfrak{J}^{(C)}_{\boldsymbol{q}\beta_2\beta_2}$ at $t = t_C = 72.5$ fs; $\mathfrak{J}^{(C)}_{\boldsymbol{q}\beta_2\beta_2}$ is a diagonal component of the non-adiabatic coupling in the vicinity of $\mathcal{E}_{\boldsymbol{q}\beta} \approx \omega_{\boldsymbol{q}}$, and it is supposed that associated off-diagonal components are much smaller than it. Figures 3.6 and 3.7 show $\bar{I}_{\boldsymbol{q}}(t_p; \omega)$ of Si and GaAs, respectively at $t_p = 65$ fs. It is remarked that spectral profiles of $\bar{I}_{\boldsymbol{q}}(t_p; \omega)$ are influenced by $\mathfrak{J}^{(C)}_{\boldsymbol{q}\beta\beta}$ in the limited region of $t_p < t_C$, and after the time region, the effect is canceled. Therefore, both spectra of Figs. 3.3(c) and 3.3(f) are independent of this effect. Further, the profile depends just on $\mathrm{Im}\mathfrak{J}^{(C)}_{\boldsymbol{q}\beta\beta}$, and $\mathrm{Re}\mathfrak{J}^{(C)}_{\boldsymbol{q}\beta\beta}$ leads to the damping effect, as readily seen from Eqs. (2.70) and (2.71). First, as regards Si shown in Fig. 3.6, the spectral profiles of $\bar{I}_{\boldsymbol{q}}(t_p; \omega)$ are definitely dependent on the value of $\mathrm{Im}\mathfrak{J}^{(C)}_{\boldsymbol{q}\beta_2\beta_2}$. The profile of Fig. 3.6(b), which is the same as that of Fig. 3.3(b), changes to the profile with a peak followed by a dip of Fig. 3.6(a) for $\mathrm{Im}\mathfrak{J}^{(C)}_{\boldsymbol{q}\beta_2\beta_2} = -0.64\pi$. This profile

43

is characterized by $q_{\boldsymbol{q}\alpha_2}(t_p) < 0$. Further, Fig. 3.6(c) shows a window resonance-shaped profile of $q_{\boldsymbol{q}\alpha_2}(t_p) \approx 0$ with $\mathrm{Im}\mathfrak{I}^{(C)}_{\boldsymbol{q}\beta_2\beta_2} = 0.70\pi$. The similar changes of the spectral profiles are also recognized in GaAs of Fig. 3.7(b), where the profile of Fig. 3.7(a) is the same as that of Fig. 3.3(e). The spectra of $q_{\boldsymbol{q}\alpha_2} \leq 0$ for $\mathrm{Im}\mathfrak{I}^{(C)}_{\boldsymbol{q}\beta_2\beta_2} < 0$ is also obtained, though not shown here. It is noted that in these calculations, we assume the non-adiabatic interaction at $t = t_C$ due to a crossing between the energetically adjacent quasiboson states, and treat it with given parameters. However after the completion of the laser irradiation, the effect of the non-adiabatic interaction would be actually small because the density matrices composing the non-adiabatic interaction are suppressed to some extent at $t = t_C$, and the energy curves vary slowly in time due to the rotating wave approximation.

Discussion from the viewpoint of the allocation of time constants

Prior to closing this section, we discuss the allocation of the time constants in Fig. 2.1 and Table 2.1 in order to deepen the understanding of the manifestation of the transient FR, particularly in Si. As shown in Fig. 3.3(b), we obtain the asymmetric spectral profile in the time region of $T_{\boldsymbol{q}12} \lesssim t_p < T_{12}$. Actually in the ETR of $t_p < T_{12}$, the photoexcited carriers are still populated around the energy region of $\omega_{\boldsymbol{q}}$, that is, $\mathcal{E}_{\boldsymbol{q}\beta} \approx \omega_{\boldsymbol{q}}$, leading to the coupling between the carriers and the LO phonon through $M_{\boldsymbol{q}\beta}$ to form the FR. Further, in the region of $T_{\boldsymbol{q}12} \lesssim t_p$, the contribution from $\tilde{\chi}_{\boldsymbol{q}}(t_p;\omega)$ decreases, and the spectral peak due to $\tilde{\chi}'_{\boldsymbol{q}}(t_p;\omega)$ comes into existence. In the case of the different allocation of the time constants, for instance, $T_{\boldsymbol{q}12}$ is close to T_{12}, that is, $T_{\boldsymbol{q}12} \sim T_{12}$, the FR profile is no longer discernible because this is covered with the structureless continuum due to $\tilde{\chi}_{\boldsymbol{q}}(t_p;\omega)$ even in the temporal region $t_p < T_{12}$. Moreover, in the region of $t_p \sim T_{12}$, the effect of $M_{\boldsymbol{q}\beta}$ is so small that the FR is not caused. Therefore, it is understood that the allocation of the time constants provided by Fig. 2.1 is a requirement for the manifestation of the FR of Si in $\bar{I}_{\boldsymbol{q}}(t_p;\omega)$, otherwise it is never realized.

3.2 Irregular Oscillatory-Patterns in the Early-Time Region

In the present section, we show the calculated results of the oscillatory patterns $Q_{\boldsymbol{q}}(\tau)$ of Eq. (2.109) and the power spectra $S_{\boldsymbol{q}}(\omega)$ of Eq. (2.111) for Si. We employ a Gaussian-shaped pulse laser with the pulse width $\tau_L = 10$ fs, and furthermore we assume $\xi_{\boldsymbol{q}}(\tau, 0) = 1$ of Eq. (2.113).

3.2.1 Rabi frequency dependence

In Figs. 3.8(a) and 3.8(b), we show the calculated results of $\Theta_{\boldsymbol{q}}(\tau)$ and $C_{\boldsymbol{q}}(\tau)$ at $\tau = 20$ fs in the ETR as a function of Ω_{0cv}, respectively, with $\Delta = 0$ meV and -136 meV. Both $\Theta_{\boldsymbol{q}}(\tau)$ and $C_{\boldsymbol{q}}(\tau)$ for $\Delta = 0$ meV represent irregular changes with cusp structures at $\Omega_{0cv} = \Omega^{(C1)}_{0cv} \equiv 82$ meV and $\Omega^{(C2)}_{0cv} \equiv 286$ meV. Further, the envelopes of both functions show steep changes around $\Omega_{0cv} = 350$ meV. In contrast, the behaviors of $\Theta_{\boldsymbol{q}}(\tau)$ and $C_{\boldsymbol{q}}(\tau)$ for $\Delta = -136$ meV are moderate over Ω_{0cv}.

For the more precise interpretation of the results, we evaluate the real parts of the adiabatic energy $E_{\boldsymbol{q}j}(\tau)$ at $\tau = 20$ fs as a function of Ω_{0cv}. Figure 3.8(c) shows the calculated
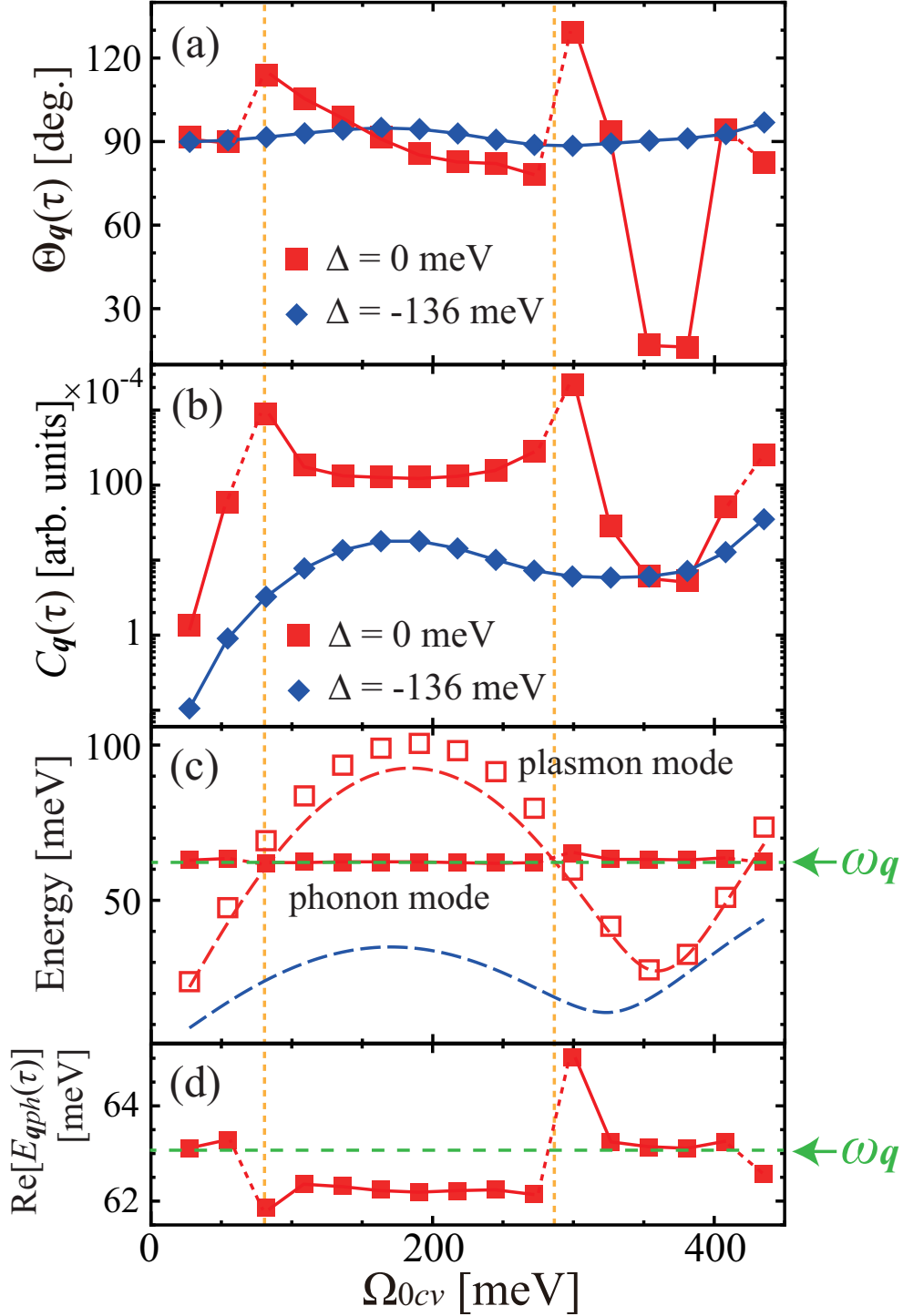
Figure 3.8: (a) $\Theta_q(\tau)$ and (b) $C_q(\tau)$ as a function of Ω_{0cv} (in the unit of meV) for $\Delta = 0$ meV (red square) and -136 meV (blue diamond). (c) The real parts of $E_{qph}(\tau)$ and $E_{qpl}(\tau)$ as a function of Ω_{0cv} (in the unit of meV); filled and open red squares represent the eigenvalues mainly governed by the phonon and plasmon modes, respectively. $\omega_{qpl}(\tau)$ for $\Delta = 0$ meV and -136 meV are represented by red and blue dash lines, respectively, and furthermore, the energy of the phonon $\omega_q = 63$ meV is represented by a green dash line. (d) The enlarged view of $\mathrm{Re}[E_{qph}(\tau)]$ around ω_q for $\Delta = 0$ meV in panel (c). In all panels, $\tau = 20$ fs, and the positions of $\Omega_{0cv}^{(C1)}$ and $\Omega_{0cv}^{(C2)}$ are shown by vertical brown dash lines. (From Ref. [71] with partial modification.)

45
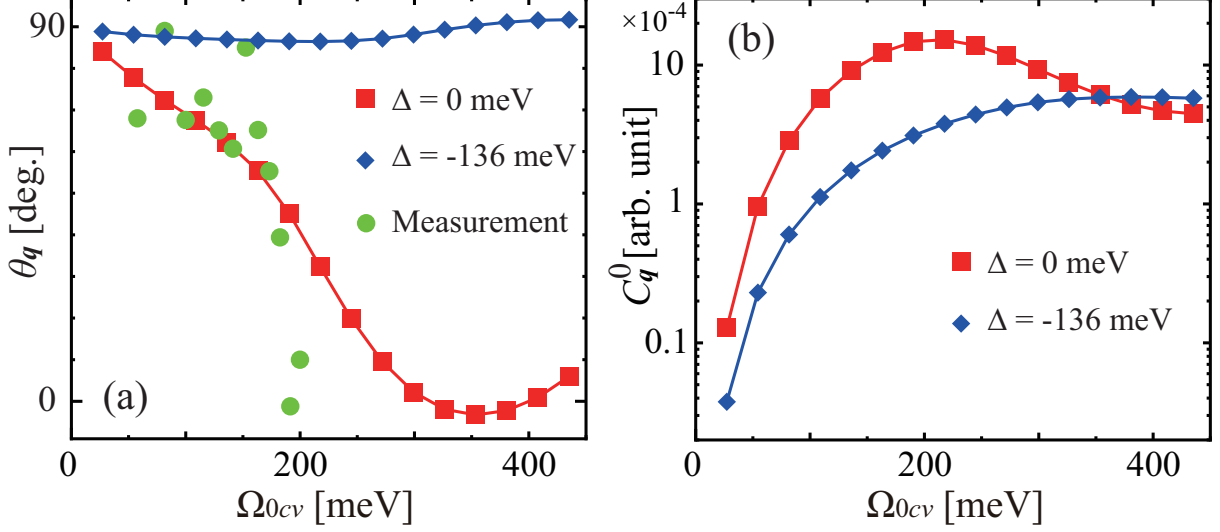
Figure 3.9: (a) $\theta_{\boldsymbol{q}}$ and (b) $C_{\boldsymbol{q}}^0$ as a function of Ω_{0cv} (in the unit of meV) for $\Delta = 0$ meV (red square) and -136 meV (blue diamond). Experimental data of $\theta_{\boldsymbol{q}}$ (green circle) [8] are also shown. (From Ref. [71] with partial modification.)

results for $\Delta = 0$ meV, where filled and open red squares represent the eigenvalues mainly governed by the phonon ($j = ph$) and the plasmon ($j = pl$), respectively. The plasma frequencies $\omega_{\boldsymbol{q}pl}(\tau)$ for $\Delta = 0$ meV and -136 meV are also shown by red and blue dash lines, respectively. $\omega_{\boldsymbol{q}pl}(\tau)$ for $\Delta = 0$ meV obviously coincides with $\omega_{\boldsymbol{q}}$ at $\Omega_{0cv} = \Omega_{0cv}^{(C1)}$ and $\Omega_{0cv}^{(C2)}$, and it leads to anticrossings between $\mathrm{Re}[E_{\boldsymbol{q}ph}(\tau)]$ and $\mathrm{Re}[E_{\boldsymbol{q}pl}(\tau)]$.

Figure 3.8(d) shows the enlarged view of $\mathrm{Re}[E_{\boldsymbol{q}ph}(\tau)]$ in Fig. 3.8(c). The difference between $\mathrm{Re}[E_{\boldsymbol{q}ph}(\tau)]$ and $\omega_{\boldsymbol{q}}$ shows the self-energy, which is attributed almost to the interaction between the phonon and the plasmon; the effects of the single-particle excitation modes would be much smaller. The self-energy for $\Delta = 0$ meV alters steeply at $\Omega_{0cv} = \Omega_{0cv}^{(C1)}$ and $\Omega_{0cv}^{(C2)}$, and these positions are in agreement with those of the manifestation of the cusp structures in Figs. 3.8(a) and 3.8(b). Therefore, it is concluded that the anomalies in $\Theta_{\boldsymbol{q}}(\tau)$ and $C_{\boldsymbol{q}}(\tau)$ are clearly ascribed to the anticrossings resulting from the energetically *resonant* interaction between the phonon and the plasmon of the photoexcited carriers. According to Fig. 3.8(d), the plasmon-phonon interaction remains effective in the range of $[\Omega_{0cv}^{(C1)}, \Omega_{0cv}^{(C2)}]$. As regards the case for $\Delta = -136$ meV, such anomalies are not obtained since $\omega_{\boldsymbol{q}} > \omega_{\boldsymbol{q}pl}(\tau)$ within the present range of Ω_{0cv}.

Moreover in Fig 3.8(c), $\omega_{\boldsymbol{q}pl}(\tau)$ denoted by a dash line oscillates with a period of approximately 350 meV. This is attributed to the interband Rabi flopping of the photoexcited carriers [41, 79], where it ends at $\tau \approx \tau_L/2$, because the approximate estimate of 2π-pulse is $\Omega_{0cv} = \Omega_{0cv}^{(2\pi)} \equiv 388$ meV for $\tau_L = 10$ fs except for the Coulomb correction; that of π-pulse is $\Omega_{0cv}^{(\pi)} = \Omega_{0cv}^{(2\pi)}/2$. Therefore, the evident alterations of $\Theta_{\boldsymbol{q}}(\tau)$ and $C_{\boldsymbol{q}}(\tau)$ around $\Omega_{0cv} = \Omega_{0cv}^{(2\pi)}$ for $\Delta = 0$ meV shown in Figs. 3.8(a) and 3.8(b) result from the Rabi oscillation.

The calculated results of the initial phase $\theta_{\boldsymbol{q}}$ and the asymptotic amplitude $C_{\boldsymbol{q}}^0$ as a function of Ω_{0cv} are shown in Figs. 3.9(a) and 3.9(b), respectively, and the two quantities are defined by Eqs. (2.114) and (2.115). It is seen that the Rabi-oscillatory patterns still

appear in both of θ_q and C_q^0 for $\Delta = 0$ meV around $\Omega_{0cv} = \Omega_{0cv}^{(2\pi)}$, whereas the cusp structures vanish because the plasmon-phonon coupling is suppressed due to the carrier relaxation. The experimental results of θ_q, which represent the dependence on the pump fluence for lightly n-doped Si [8], are also shown in Fig. 3.9(a). As the fluence increases, θ_q varies from $90°$ to the vicinity of $0°$. The result is in agreement with the calculated one for $\Delta = 0$ meV. We'll discuss the results of θ_q and C_q^0 later again.

Figures 3.10(a)-3.10(d) represent the calculated results of $Q_q(\tau)$ in the ETR as a function of τ for $\Delta = 0$ meV. Here, Ω_{0cv} is set to $\Omega_{0cv}^{(C1)'} \equiv 81.6$ meV, $\Omega_{0cv}^{(\pi)'} \equiv 190.4$ meV, $\Omega_{0cv}^{(C2)'} \equiv 299.2$ meV, and $\Omega_{0cv}^{(2\pi)'} \equiv 353.6$ meV, in the proximity to $\Omega_{0cv}^{(C1)}$, $\Omega_{0cv}^{(\pi)}$, $\Omega_{0cv}^{(C2)}$, and $\Omega_{0cv}^{(2\pi)}$, respectively. As shown in Fig 3.8(c), the number of excited carriers is maximized at $\Omega_{0cv} = \Omega_{0cv}^{(\pi)'}$, and minimized at $\Omega_{0cv} = \Omega_{0cv}^{(2\pi)'}$ of the four. At $\Omega_{0cv} = \Omega_{0cv}^{(C1)'}$ and $\Omega_{0cv}^{(C2)'}$, owing to the plasmon-phonon resonant coupling, $Q_q(\tau)$'s show irregular oscillatory patterns from a simple harmonics with a period of $2\pi/\omega_q = 66$ fs. The transitory amplitudes $C_q(\tau)$ at $\Omega_{0cv} = \Omega_{0cv}^{(C1)'}$ and $\Omega_{0cv}^{(C2)'}$ of the resonant conditions are approximately ten times larger than that at $\Omega_{0cv} = \Omega_{0cv}^{(\pi)'}$ of the π-pulse laser condition, whereas the asymptotic amplitudes C_q^0 of the resonant conditions are several times smaller than that of π-pulse laser condition [see Fig. 3.9(b)]. Moreover, it is seen that the renormalized phase $\Theta_q(\tau)$ changes anomalously, in particular at $\Omega_{0cv} = \Omega_{0cv}^{(C1)'}$; the phase varies rapidly over 2π around $\tau = 10$ fs attributed presumably to the appearance of the strong anticrossing. Besides, $Q_q(\tau)$ of $\Omega_{0cv} = \Omega_{0cv}^{(\pi)'}$ deviates from a simple harmonics due to the maximized carrier inversion. In contrast, $\Theta_q(\tau)$ and $C_q(\tau)$ of $\Omega_{0cv} = \Omega_{0cv}^{(2\pi)'}$ are almost unchanged, and gradually approaches the asymptotes; $Q_q(\tau)$ represents a damped harmonic oscillation in most of the time-region.

3.2.2 Detuning dependence

In Figs. 3.11(a)-3.11(d), we show the calculated results of $Q_q(\tau)$ as a function of τ and their power spectra $S_q(\omega)$. The detuning is set to $\Delta = -136, -54.4, -27.2,$ and 108.8 meV with $\Omega_{0cv} = 108.8$ meV. It is noted that in the calculations, we assume that the interaction between the phonon and the plasmon, namely, M_{qph} in Eq. (2.95) is suppressed owing to the phenomenological carrier relaxation time T_{12} which is set to 4000 a.u. ≈ 100 fs: $M_{qph} \rightarrow M_{qph}e^{-\tau/T_{12}}$ is considered. It is seen that in Fig. 3.11(a), $Q_q(\tau)$ represents almost sinusoidal, and the spectral profile of $S_q(\omega)$ is symmetric. In Figs. 3.11(b) and 3.11(c), $Q_q(\tau)$'s oscillate with much larger amplitudes in $\tau \lesssim 100$ fs of the ETR than those in $\tau \gtrsim 100$ fs. Further, both $Q_q(\tau)$'s in the ETR show irregular oscillatory patterns similar to those of Figs. 3.10(a)-3.10(c). It is remarked that asymmetric spectra are manifested, and the Fano's asymmetric q values [47] are negative. Here, it is noted that the asymmetric spectral profiles are not due to FR, and the detail is shown later. In contrast, in Fig. 3.11(d), the amplitudes in the ETR and the classical region are comparable, and a symmetric spectrum is manifested. The oscillations with enhanced amplitudes in the ETR in Figs 3.11(b) and 3.11(c) are attributed to the energetically resonant coupling between the phonon and the plasmon. Here, at $\tau = 20$ fs, the plasma frequency $\omega_{qpl}(\tau) = 59.6$ meV for $\Delta = -54.4$ meV, and $\omega_{qpl}(\tau) = 68.7$ meV for $\Delta = -27.2$ meV. As time passes, the plasmon-phonon interaction vanishes due to the carrier relaxation, and $Q_q(\tau)$ approaches the damped harmonic oscillation. It is readily shown that $S_q(\omega)$ attributed to the damped harmonic oscillation becomes symmetric, and therefore, it is concluded that asymmetric profiles of $S_q(\omega)$ are attributed to the anomalies of $Q_q(\tau)$ in the ETR.
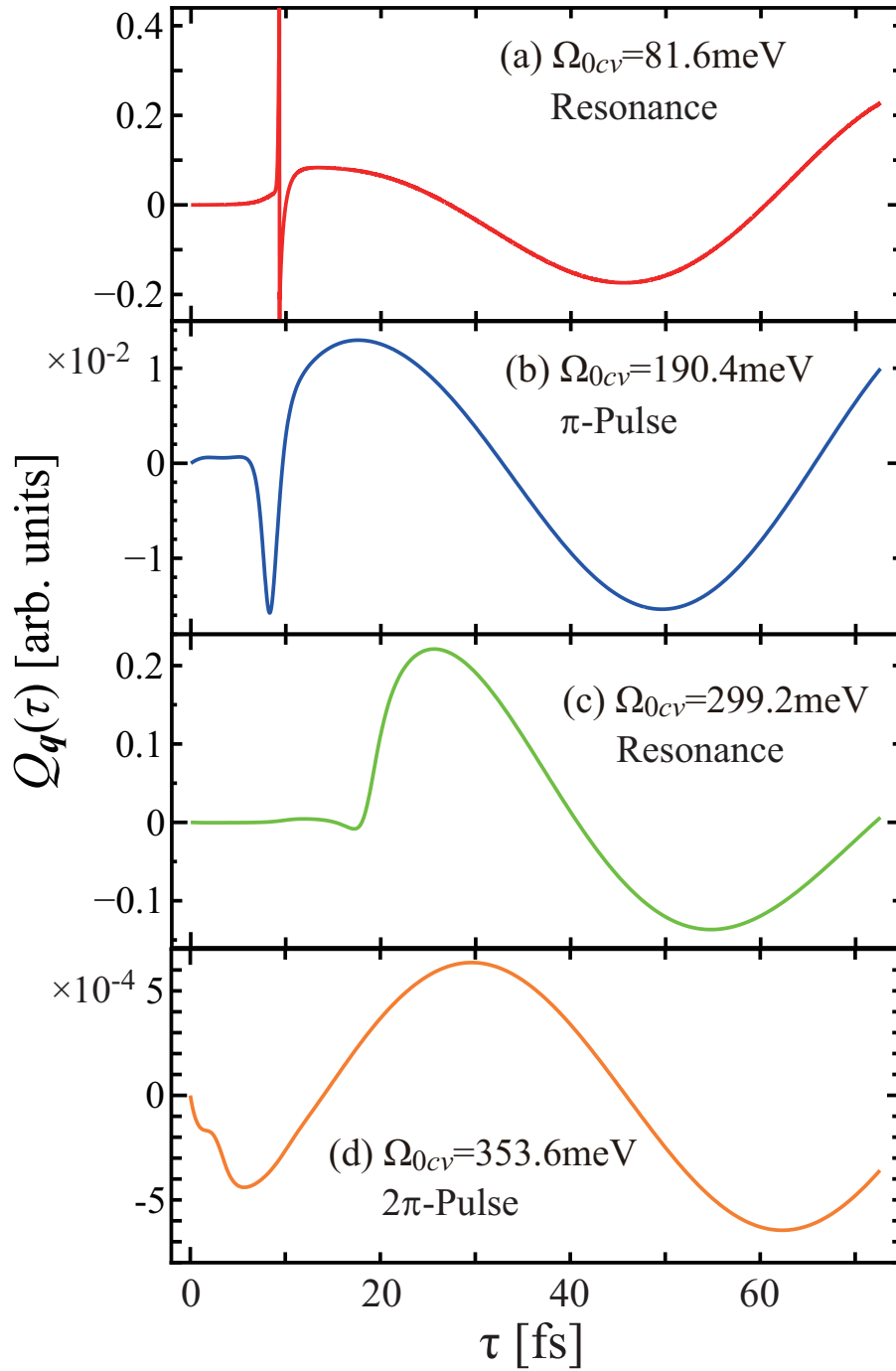
Figure 3.10: $Q_q(\tau)$ as a function of τ (in the unit of fs) in the ETR at four specific Ω_{0cv}'s provided in panels (a)-(d) with $\Delta = 0$ meV. (From Ref. [71].)
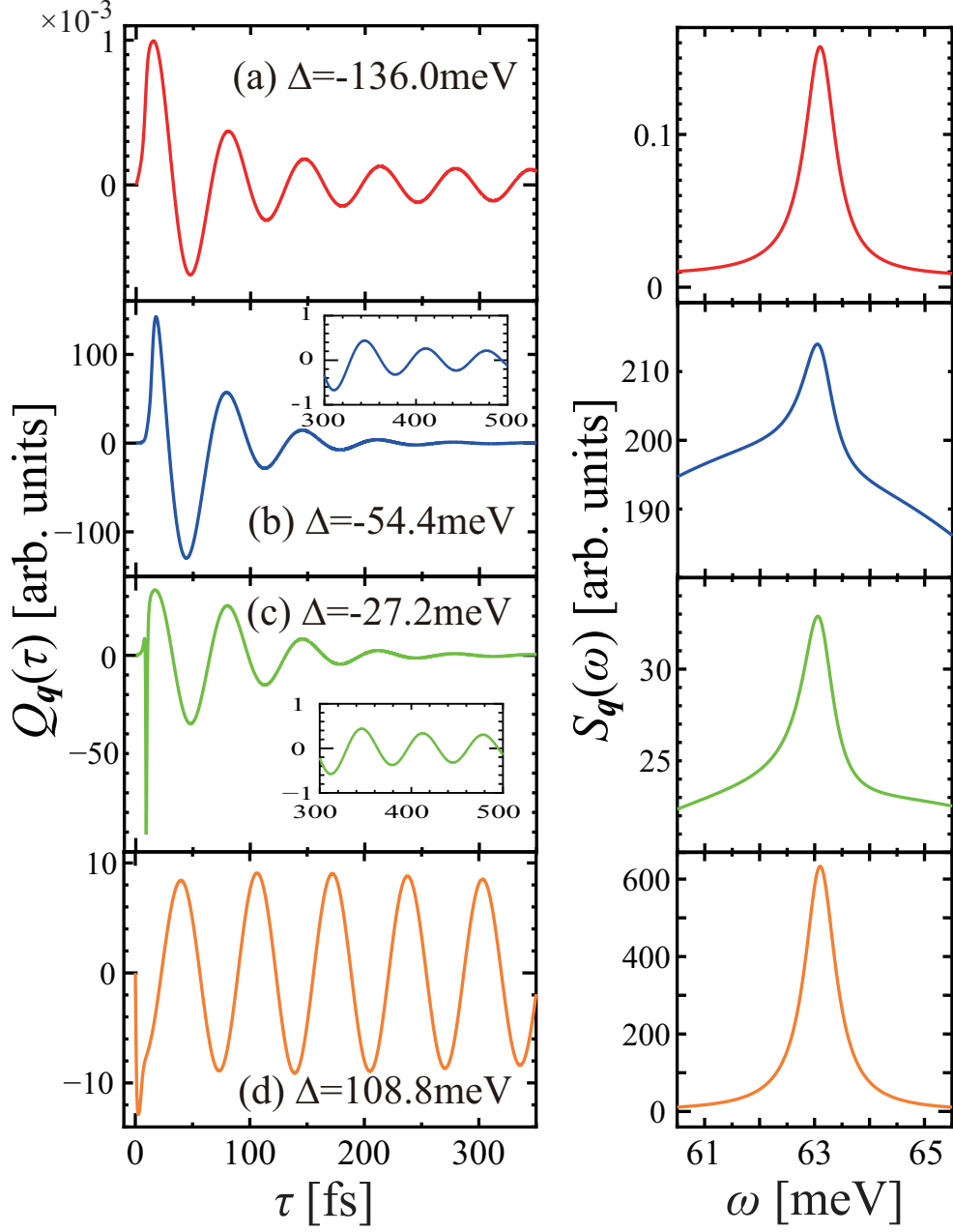
Figure 3.11: $Q_{\boldsymbol{q}}(\tau)$ as a function of τ (in the unit of fs) and $S_{\boldsymbol{q}}(\omega)$ as a function of ω (in the unit of meV) at four specific Δ's provided in panels (a)-(d) with $\Omega_{0cv} = 108.8$ meV. The insets of Figs. (b) and (c) emphasize $Q_{\boldsymbol{q}}(\tau)$ for 300 fs $\leq \tau \leq$ 500 fs. (From Ref. [72].)
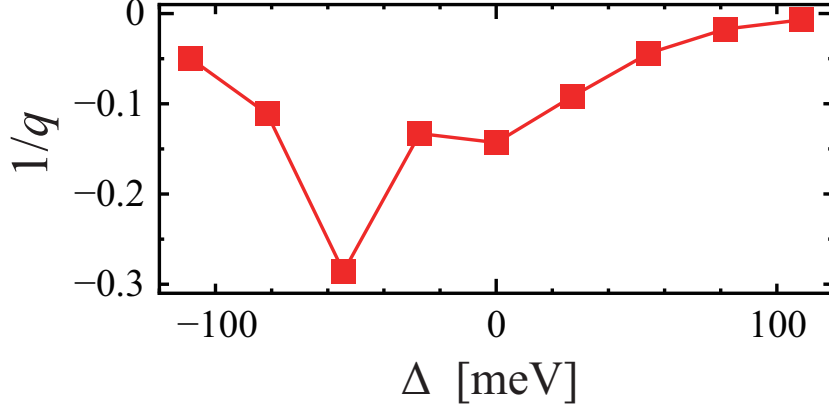
Figure 3.12: Asymmetry parameter $1/q$ of Fano profile for $S_{\boldsymbol{q}}(\omega)$ as a function of Δ (in the unit of meV) with $\Omega_{0cv} = 108.8$ meV. (From Ref. [72].)

In Fig. 3.12, we show the asymmetry parameter $1/q$ for $S_{\boldsymbol{q}}(\omega)$ as a function of Δ with $\Omega_{0cv} = 108.8$ meV. It is seen that $1/q$ are negative in the present Δ-region, and $1/q$ approaches zero at $\Delta \lesssim -100$ meV, that is, the spectral profile becomes symmetric. With the increase of Δ, the excited carrier density becomes large and $\omega_{\boldsymbol{q}pl}(\tau)$ approaches $\omega_{\boldsymbol{q}}$, and therefore the modulus of $1/q$ becomes large with its sign negative, since the resonant plasmon-phonon coupling becomes more effective, namely, the anomalies of $Q_{\boldsymbol{q}}(\tau)$ is manifested. At $\Delta = -54.4$ meV, $1/q = -0.286$ and the profile is the most asymmetric. As Δ increases further, $1/q$ approaches zero, namely, the profile becomes symmetric, since the resonant coupling vanishes with $\omega_{\boldsymbol{q}pl}(\tau)$ greater than $\omega_{\boldsymbol{q}}$. In other words, the contribution of the anomalies in the ETR becomes small, and the contribution of the damped harmonic oscillation out of the ETR becomes dominant. The asymmetric spectra of $S_{\boldsymbol{q}}(\omega)$ are reminiscent of FR. However, these asymmetric profiles are not always attributed to FR. The asymmetric spectra of $S_{\boldsymbol{q}}(\omega)$ obtained here are due to the coupling between the two discrete modes of the phonon and the plasmon.

Next, the abrupt behaviors of $Q_{\boldsymbol{q}}(\tau)$ at $\tau \sim 10$ fs shown in Figs. 3.11(b) and 3.11(c) are discussed in detail. These are attributed to time-dependent coupling between the plasmon and the phonon. In Fig. 3.13, we show $\mathrm{Re}[E_{\boldsymbol{q}pl}(\tau)]$'s for $\Delta = -54.4$ meV and -27.2 meV with $\Omega_{0cv} = 108.8$ meV. It is seen that these $E_{\boldsymbol{q}pl}(\tau)$'s deviate from the associated $\omega_{\boldsymbol{q}pl}(\tau)$'s particularly in the temporal region of $\tau \lesssim 10$ fs; at $\tau = 9$ fs, $\mathrm{Re}[E_{\boldsymbol{q}pl}(\tau)]$ is below $\omega_{\boldsymbol{q}pl}(\tau)$ by roughly 10 meV for $\Delta = -54.4$ meV, and 5 meV for $\Delta = -27.2$ meV. The difference from $\omega_{\boldsymbol{q}pl}(\tau)$ is attributed to the self-energy renormalization due to the electron-laser interaction, the electron-phonon interaction, and the Coulomb correction as shown in Eq. (2.100). As time passes, $E_{\boldsymbol{q}pl}(\tau)$ move toward $\omega_{\boldsymbol{q}pl}(\tau)$. As regards $\Delta = -54.4$ meV, $\mathrm{Re}[E_{\boldsymbol{q}pl}(\tau)]$ approaches $\omega_{\boldsymbol{q}}$ at $\tau \sim 10$ fs rapidly, while the associated $\omega_{\boldsymbol{q}pl}(\tau)$ remains almost unaltered. Thus, $\mathrm{Re}[E_{\boldsymbol{q}pl}(\tau)]$ becomes slightly below $\omega_{\boldsymbol{q}}$, and the resonant coupling between the phonon and the plasmon becomes dominant in the region $\tau \gtrsim 15$ fs. In other words, the resonance is manifested after the suppression of the laser irradiation, leading to the steep behavior of $Q_{\boldsymbol{q}}(\tau)$. On the other hand, $\mathrm{Re}[E_{\boldsymbol{q}pl}(\tau)]$ of $\Delta = -27.2$ meV surpasses $\omega_{\boldsymbol{q}}$ at $\tau \sim 9$ fs, and the resonance effect is maximized at this moment, causing the steep change of $Q_{\boldsymbol{q}}(\tau)$. In the region of $\tau \gtrsim 15$ fs, $\mathrm{Re}[E_{\boldsymbol{q}pl}(\tau)]$ is greater than $\omega_{\boldsymbol{q}}$ by approximately 10 meV, and the resonance effect is suppressed to a certain extent.
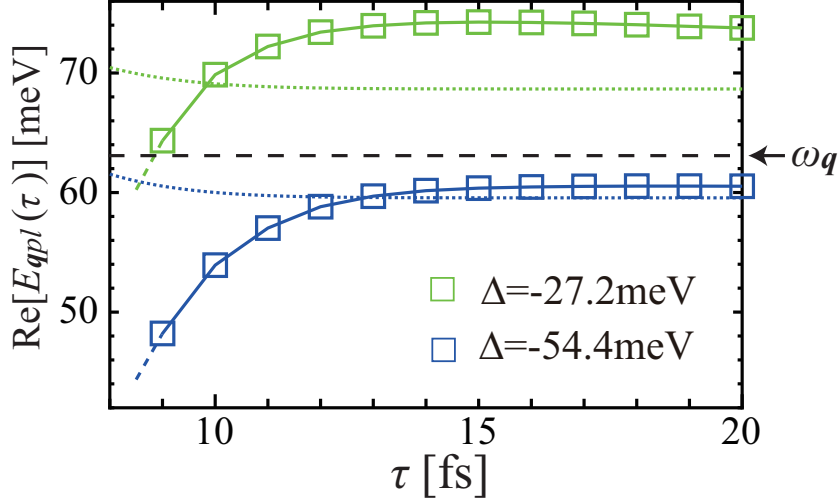
Figure 3.13: $\mathrm{Re}[E_{qpl}(\tau)]$ (in the unit of meV) as a function of τ (in the unit of fs) for $\Delta = -54.4$ meV (blue square) and -27.2 meV (green square). The associated plasma frequencies $\omega_{qpl}(\tau)$ are represented by the blue and green dot lines, respectively, and furthermore, the energy of the phonon ω_{q} is shown by the black dash line. (From Ref. [72].)

In Fig. 3.14(a) and 3.14(b), we show θ_{q} and C_{q}^{0} as a function of Δ, respectively. The Rabi frequency Ω_{0cv} is set to 54.4 meV, 108.8 meV, and 244.8 meV. It is seen that $\theta \approx 90°$ at $\Delta \sim -100$ meV for all Ω_{0cv}'s. With the increase of Δ, θ_{q} for $\Omega_{0cv} = 108.8$ meV and 244.8 meV change from 90°; at $\Delta = 108.8$ meV, $\theta_{q} = -45.9°$ and $-79.9°$ for $\Omega_{0cv} = 108.8$ meV and 244.8 meV, respectively. In contrast, θ_{q} for $\Omega_{0cv} = 54.4$ meV is almost unvaried. On the other hand, C_{q}^{0} for $\Omega_{0cv} = 54.4$ meV and 108.8 meV is enlarged with the increase of Δ, whereas that for $\Omega_{0cv} = 244.8$ meV is maximized at $\Delta \sim 0$.

The results of θ_{q} and C_{q}^{0} are understood in terms of the magnitudes of the interactions of electron with light and phonon. As shown in Eqs. (2.114) and (2.115), θ_{q} and C_{q}^{0} are determined in part by what happens in the ETR at $\tau = 0$. Actually, the eigenvectors appearing in Eqs. (2.114) and (2.115) are determined by the electron-light and electron-phonon interactions. For small Ω_{0cv} and negative Δ, the density of the photoexcited carriers is small, and thus the associated couplings are weak, and therefore $V_{qph,ph}^{L\dagger}(0) \to 1$ in Eqs. (2.114) and (2.115). Thus, θ_{q} approaches 90°, namely, a sine phase, and C_{q}^{0} becomes small. In contrast, in the case that Ω_{0cv} is large and Δ is positive, the density of the carriers is enhanced, and thus, θ_{q} changes from the sine phase, and C_{q}^{0} is enlarged. It is considered that the saturation of C_{q}^{0} for $\Omega_{0cv} = 244.8$ meV in the vicinity of $\Omega_{0cv}^{(\pi)}$ would be ascribed to the carrier inversion.

3.3   Comparison with Other Studies

In this section, we compare the calculated results shown in Secs. 3.1 and 3.2 with the results of other experimental and theoretical studies. We begin with a comparison with the experimental works for lightly n-doped Si of Refs. [6], [8], and [72], where a transient electro-optic reflectivity was measured as a function of time delay in $\Gamma_{25'}$ configuration. This would correspond to the symmetry $\Gamma_{25'} \downarrow C_{3v}$ given by Eq. (3.11), and the vibrational
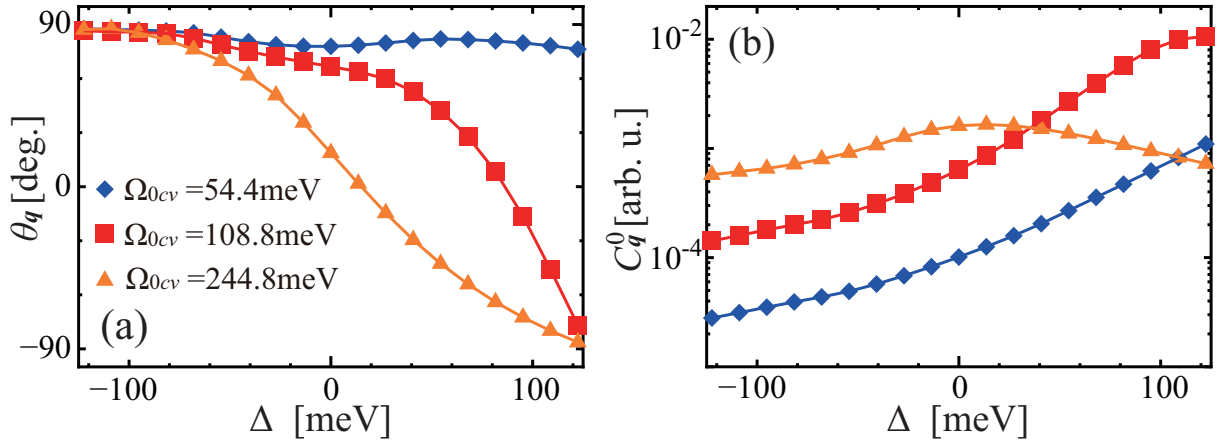
Figure 3.14: (a) θ_q and (b) C_q^0 as a function of Δ (in the unit of meV) for $\Omega_{0cv} = 54.4$ meV (blue diamond), 108.8 meV (red square), and 244.8 meV (orange triangle). (From Ref. [72] with partial modification.)
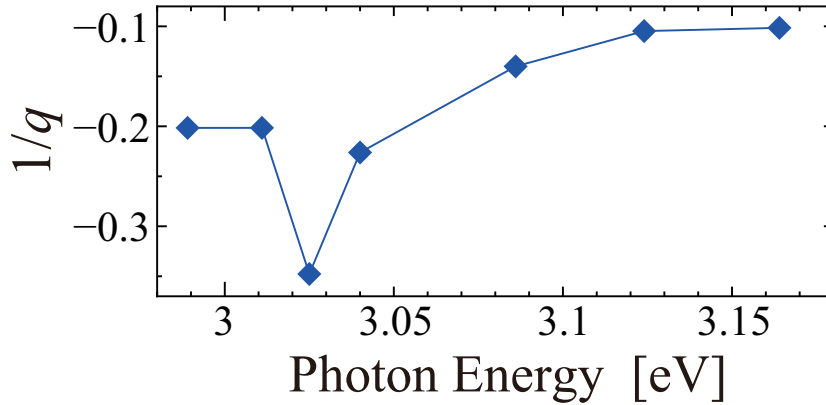
Figure 3.15: Asymmetry parameter $1/q$ of Fano profile obtained experimentally as a function of the photon energy (in the unit of eV). (From Ref. [72] with partial modification.)

state of the *dressed* crystal can be optically deexcited through an emission process induced by an infrared laser polarized in the [111] direction. As regards Ref. [6], the continuous-wavelet transform of the time signal was conducted, and asymmetric spectra were found around 50 fs immediately after the irradiation of the pump pulse. This conspicuous result suggested the transient manifestation of the quantum interference between the LO phonon and the excited carriers leading to FR. Moreover, the authors supposed the birth of a composite particle due to such a strong interaction, termed as PQ. The theoretical model presented here is based on this supposition, and as described in Sec. 3.1, the PQ picture succeeds in demonstrating the manifestation of the FR. The calculated result is in agreement with the experimental one to some extent. Nevertheless, this fact does not necessarily suggest that the PQ introduced here actually exists as a real entity. This is beyond the scope of this study, although it is quite challenging.

Further, the initial phase θ_q as a function of the pump fluence was also evaluated in Ref. [8], which is shown in Fig. 3.9(a). The calculated results of $\Delta = 0$ meV are qualitatively consistent with the experimental ones. Here, the excited carrier density is

$N_{ex} = 1.4 \times 10^{19}$ cm^{-3} in the calculation with $\Omega_{0cv} = 108.8$ meV, and $N_{ex} = 2.5 \times 10^{19}$ cm^{-3} is evaluated in the experiment with the pump fluence 2.5 J/cm^2 which corresponds to $\Omega_{0cv} = 100$ meV [8]. Moreover, FT spectra of the reflectivity signals, and the dependence of their asymmetric q values on the photon energy were investigated in Ref. [72]. Figure 3.15 shows the experimental results of $1/q$, and this is in agreement to a certain extent with the calculated ones shown in Fig. 3.12. Here, we refer to Δ and the photon energy as the pulse laser parameter in the present study and the experiment, respectively. In Si, the direct band gap energy at Γ point is $E_g \sim 3.3$ eV, and therefore the photon energy of the experiment correspond roughly to $-300 \lesssim \Delta \lesssim -100$ meV, whereas $-100 \lesssim \Delta \lesssim 100$ meV in the present calculation. This difference of Δ would be ascribed to bandgap renormalization via strong carrier excitation in the experiment [8]. Actually, as mentioned above, real carrier excitation occurs considerably even when $\Delta < 0$ in the experiment, and N_{ex} is a comparable order with the calculated results.

As regards theoretical approaches, there are two studies concerning the FR accompanied by the CP generation. One of them was reported by Lee *et al.* [43], where time-dependent Schrödinger equations were solved, and thus a phonon displacement function was calculated for the system of GaAs under the far above-gap excitation condition. Thus, the continuous-wavelet-transformed spectrum showed an asymmetric profile. Here, it is understood that the FR results from the interference between two of the one-phonon Raman processes with different time ordering. However, FR spectra have never been observed in the experiments for GaAs so far, and the FR of Ref. [6] was manifested under the resonant excitation condition with the real excited carriers. In the present study of $\bar{I}_q(t_p; \omega)$, the FR in Si does not originates from the interference between the Raman diagrams, and the FR is not manifested in GaAs except for the non-adiabatic correction.

The other was reported by Riffe [48], where a classical Fano oscillator model derived from the Fano-Anderson Hamiltonian [46] was proposed. The associated Hamiltonian is expressed in terms of the present PQ picture as

$$\hat{H}_{\boldsymbol{q}}^{(FA)} = \omega_{\boldsymbol{q}} c_{\boldsymbol{q}}^{\dagger} c_{\boldsymbol{q}} + \sum_{\beta} \mathcal{E}_{\boldsymbol{q}\beta} B_{\boldsymbol{q}\beta}^{\dagger} B_{\boldsymbol{q}\beta} + \sum_{\beta} (M_{\boldsymbol{q}\beta} c_{\boldsymbol{q}} B_{\boldsymbol{q}\beta}^{\dagger} + M_{\boldsymbol{q}\beta}^{*} c_{\boldsymbol{q}}^{\dagger} B_{\boldsymbol{q}\beta}), \qquad (3.13)$$

where the quasiboson is regarded as a real boson with real eigenenergy $\mathcal{E}_{\boldsymbol{q}\beta}$. Displacement functions related to the LO phonon and quasiboson operators are defined by

$$X_{\boldsymbol{q}}^{(+)}(t) = \langle c_{\boldsymbol{q}}(t) + c_{-\boldsymbol{q}}^{\dagger}(t) \rangle / 2 \qquad (3.14)$$

and

$$x_{\boldsymbol{q}\beta}^{(+)}(t) = \langle B_{\boldsymbol{q}\beta}(t) + B_{-\boldsymbol{q}\beta}^{\dagger}(t) \rangle / 2, \qquad (3.15)$$

respectively, and we obtain the associated equations of motion from Eq. (3.13). Further, in the equations of motion for $X_{\boldsymbol{q}}^{(+)}(t)$ and $x_{\boldsymbol{q}\beta}^{(+)}(t)$, a posteriori external forces are introduced, which are termed as $\mathcal{F}_{\boldsymbol{q}}(t)$ and $f_{\boldsymbol{q}\beta}(t)$, respectively. On the basis of the present PQ model, these forces are mainly attributed to the time derivative of quasiboson adiabatic energy $d\mathcal{E}_{\boldsymbol{q}\beta}(t)/dt$, the non-adiabatic coupling $W_{\boldsymbol{q}\beta\beta'}(t)$ of Eq. (2.42), and the time derivative of the effective coupling $dM_{\boldsymbol{q}\beta}(t)/dt$. Nevertheless in Riffe's work, it was assumed that $\mathcal{E}_{\boldsymbol{q}\beta}$ and $M_{\boldsymbol{q}\beta}$ were independent of time, and furthermore in $X_{\boldsymbol{q}}^{(+)}(t)$ and $x_{\boldsymbol{q}\beta}^{(+)}(t)$, expectation values with respect to a coherent state were considered. This assumption leads to the result that $d\mathcal{E}_{\boldsymbol{q}\beta}(t)/dt$, $dM_{\boldsymbol{q}\beta}(t)/dt$, and $W_{\boldsymbol{q}\beta\beta'}(t)$ vanish simultaneously. Eventually, $\mathcal{F}_{\boldsymbol{q}}(t)$

and $f_{q\beta}(t)$ are ascribed just to the residual frictional forces as follows:

$$\mathcal{F}_{\boldsymbol{q}}(t) \approx -\sum_{\beta\beta'} x_{\boldsymbol{q}\beta}^{(+)}(t)\text{Im}[\gamma_{\boldsymbol{q}\beta\beta'}^{(B)}(t)M_{\boldsymbol{q}\beta'}]/2 \tag{3.16}$$

and

$$f_{\boldsymbol{q}\beta}(t) \approx -\mathcal{E}_{\boldsymbol{q}\beta}\sum_{\beta'} x_{\boldsymbol{q}\beta'}^{(+)}(t)\text{Im}\gamma_{\boldsymbol{q}\beta'\beta}^{(B)}(t)/2, \tag{3.17}$$

respectively. In particular for Si, $M_{\boldsymbol{q}\beta}$ and $\gamma_{\boldsymbol{q}\beta'\beta}^{(B)}(t)$ are real. Therefore, both forces result in $\mathcal{F}_{\boldsymbol{q}}(t) \approx 0$ and $f_{\boldsymbol{q}\beta}(t) \approx 0$.

Finally, we compare the results of the initial phase $\theta_{\boldsymbol{q}}$ with those of two theoretical studies; one is the time-dependent density functional theory [44], and the other is the simplified two-level model based on a perturbation with respect to the electron-light interaction [49]. In the both results, $\theta_{\boldsymbol{q}} \sim 90°$, namely, the sine phase in the case that Δ is large negative. According to the former study, $\theta_{\boldsymbol{q}}$ changed from the sine phase with the increase of Δ, which is in agreement with the present results. The former also evaluated $\theta_{\boldsymbol{q}}$ for 0.5 eV $\lesssim \Delta \lesssim 2$ eV. However, such a large positive Δ of a non-resonant excitation condition is out of concern in the present analysis. As regards the latter study, $\theta_{\boldsymbol{q}}$ for $\Delta > 0$ was not examined.

3.4 Validity of the Present Model for the CP Generation

In this section, we discuss the validity of the model adopted in the present study for the CP generation from a viewpoint of the band structure. First, we assume a simple two-band parabolic energy dispersion, where c-band and v-band (heavy-hole band) are taken into consideration; the actual band structure is more complicated than that employed in the calculations. In fact, the joint-band energy dispersion of c-band with a light hole band referred to v'-band, and the dispersion of c-band with a spin-orbit split-off hole band referred to v''-band would also have contributions to the formation of the collective excitation (plasmon) and single-particle excitation modes to some extent. Hereafter, let us represent the joint-band energy dispersion of c-band with b_v-band as

$$\epsilon_{\boldsymbol{k}}^{(cb_v)} = \varepsilon_{c\boldsymbol{k}}^{(r)} - \varepsilon_{b_v\boldsymbol{k}}^{(r)} - E_g, \tag{3.18}$$

where $b_v = v$, v', and v'', and $\varepsilon_{b\boldsymbol{k}}^{(r)}$ is given in Eq. (2.13). An opaque interband transition forms real excited carriers, and the electron state with momentum $\boldsymbol{k}$ satisfying

$$\epsilon_{\boldsymbol{k}}^{(cb_v)} \lesssim 1/\tau_L, \tag{3.19}$$

contributes to this transition, where τ_L is the pulse width, and the case of $\Delta = 0$ is considered for the sake of simplicity. Thus, a hole band with greater effective mass plays a role for the real carrier excitation to a larger extent, because the electronic states up to larger $\boldsymbol{k}$ become effective. In fact, v-band mostly governs the carrier excitation, although v'- and v''-bands have limited contributions to it; for instance, values of the average effective mass of v-, v'-, and v''-bands are 0.54, 0.15, 0.23, respectively in Si, and 0.53, 0.08, and 0.15, respectively in GaAs [33]. Further, as regards v''-band, the

contribution of this would be smaller than that of the other bands since the spin-orbit splitting of the valence bands is of an order of tens to hundreds meV for semiconductors of concern [33], whereas v- and v'-bands are degenerate at Γ point. Therefore, it is remarked that the v-band electrons in the proximity to this critical point are dominant for the carrier formation.

Second, we take into account just the $\Gamma - \Gamma$ carrier transitions. Actually in the CP generation, a lot of carrier transitions along the Δ and Λ directions arise. In this paragraph, we discuss the band structure especially for Si. The energy dispersion of v-band along the Δ (X-valley) and Λ (L-valley) directions are almost parallel to the energy dispersion of c-band. Therefore, the joint-band energy dispersion of c-band with v-band becomes almost dispersionless, in other words, independent of $\boldsymbol{k}$ and $\epsilon_{\boldsymbol{k}}^{(cb_v)} \approx 0$. Thus, it is remarked that the $\boldsymbol{k}$-dispersive carrier distribution is produced by the interband transitions just near Γ point, leading to the collective excitation and single-particle excitation modes.

Third, as regards non-polar materials with the diamond crystal structure such as Si, the LO phonon mode and the transverse optical (TO) phonon mode are degenerate at $\Gamma_{25'}$ point. Therefore, the latter mode would partially contribute to the CP signal with the same asymptotic frequency as $\omega_{\boldsymbol{q}}$, and we consider the former mode exclusively in the present study. The TO phonon is coupled with the carriers through the deformation potential interaction, represented as a similar expression of Eqs. (2.53) and (2.95). However, unlike the LO phonon, the TO phonon does not interact with the plamon characteristic of a longitudinal wave [94, 95]. Therefore, it is stated that the irregular CP signals shown in Sec. 3.2 are governed mostly by the LO phonon. Incidentally, concerning the observation of TO phonon modes, this has been reported recently in a GaAs crystal, and the TO phonon is coherently excited by broadband terahertz pulses through direct coupling [96].

Chapter 4

Conclusion

The fully quantum mechanical model based on the PQ picture for the CP generation in semiconductors is constructed. In this model, the LO phonon, the plasmon of the collective excitation, and the electron-hole continua of the single-particle excitations are taken into consideration. The model is applied to the non-equilibrium and transient system induced by the opaque interband transition with the ultrashort pulse laser. Thereby, quantum mechanical effects inherent in the interactions among the above-mentioned modes are theoretically revealed, that is, the optically nonlinear and transient FR, the anomalous oscillatory pattern ascribed to the plasmon-phonon resonant interaction, and the Rabi flopping. It is found that these quantum effects enrich the underlying physics of the CP generation in the ETR.

The transient FR is manifested in the transient induced photoemission spectra; an asymmetric spectral profile appears in the temporal region of $T_{\boldsymbol{q}12} \lesssim t_p \lesssim T_{12}$ for Si, whereas the spectral profile of GaAs is always symmetric, apart from the non-adiabatic correction due to $I_{\boldsymbol{q}\beta\beta}(t)$. The difference between Si and GaAs is due to the effective coupling $M_{\boldsymbol{q}\beta}$ between the phonon and the quasiboson of the continuum state; by consulting Shore's model, the spectral profiles are strongly dependent on $\arg M_{\boldsymbol{q}\beta}$, and the asymmetry in spectra is due to the LO phonon deformation interaction rather than the Fröhlich interaction. After the ETR of $|M_{\boldsymbol{q}\beta}| \approx 0$, the profiles become symmetric in both Si and GaAs.

The transient plasmon-phonon resonance and the Rabi flopping also appear in the ETR. In the CP displacement function of Si, irregular oscillatory patterns due to the plasmon-phonon resonance are observed just in the ETR, and the associated power spectra become asymmetric, though this asymmetry is not attributed to FR. This resonance effect is expected to be verified in experiments by reducing the masking effect ascribed to coherent artifacts. To be concrete, for instance, orthogonal polarizations of the pump and probe beams with an attosecond pulse enable us to monitor dynamics in the ETR without coherent artifacts [97]. Further, the resonance effect would be enhanced in polar crystals such as GaAs because the Fröhlich interaction is much larger than the deformation potential interaction. On the other hand, the Rabi flopping is also manifested after the ETR, and discernible in experiments by measuring the initial phase and the asymptotic amplitude as a function of the Rabi frequency Ω_{0cv} up to more than $\Omega_{0cv}^{(2\pi)}$. As regards the initial phase, it shows the sine phase under the weak excitation conditions, and varies from the sine one as the excitation becomes stronger. The calculated results are in agreement with experimental and other theoretical ones to a certain extent.

The PQ model presented here is straightforward applicable to CP generation dynamics in heavily doped semiconductors and other attractive systems such as diamond [98] and SiC [99]. However, there is room to improve the means of the investigation. This model is not suitable for fully quantitative calculations because of the difficulty of evaluating the non-adiabatic coupling due to its spike-like behavior in the proximity of the crossing region between energetically adjacent adiabatic states, which can influence physical quantities. For instance, as shown in Figs. 3.6 and 3.7, the spectral profiles of $\bar{I}_{\boldsymbol{q}}(t_p; \omega)$ depend also on an imaginary part of $I_{\boldsymbol{q}\beta\beta}(t)$ in addition to $\arg M_{\boldsymbol{q}\beta}$, and the asymmetric profile is possibly manifested even in GaAs. Therefore, it is worth developing the theoretical framework so as to bear more quantitative investigation. As more sophisticated numerical recipes, for instance, a diabatic-by-sector method [100, 101] and a R-matrix propagation method [102, 103] are substituted for the adiabatic expansion, although a heavy numerical burden would be incurred.

Finally, it is remarked that the PQ model creates a byproduct of the plasmon-like mode, which is introduced as one of the quasiboson modes. The plasmon-like mode is affected not only by excited carrier density but also pump-laser field and Coulomb interaction. The energy of the plasmon $\mathcal{E}_{\boldsymbol{q}\alpha_1}$ or $E_{\boldsymbol{q}pl}$ differs from the plasma frequency under the laser irradiation, though the latter one is also renormalized by the plasmon-phonon interaction. Moreover, the energy-eigenvalue becomes of a complex number even with the transferred momentum $|\boldsymbol{q}| \to 0$; the imaginary part of the energy suggests an effect of Landau or anti-Landau damping. Therefore, the plasmon mode found in this study possibly has potential to enrich physics to be explored.

Acknowledgment

Appendix A

Derivation of Eq. (2.11): A Factrization Approximation

For the purpose of deriving Eq. (2.10), we apply the following commutation relation to $[\hat{H}_e + \hat{H}'(t), A_{\boldsymbol{q}}^\dagger(\boldsymbol{k}bb')]$ in a repeated manner:

$$
\begin{aligned}
\left[A_{\boldsymbol{q}_1}^\dagger(\boldsymbol{k}_1 b_1 b_1'), A_{\boldsymbol{q}_2}^\dagger(\boldsymbol{k}_2 b_2 b_2')\right] &= \left[a_{b_1,\boldsymbol{k}_1+\boldsymbol{q}_1}^\dagger a_{b_1'\boldsymbol{k}_1}, a_{b_2,\boldsymbol{k}_2+\boldsymbol{q}_2}^\dagger a_{b_2'\boldsymbol{k}_2}\right] \\
&= a_{b_1,\boldsymbol{k}_1+\boldsymbol{q}_1}^\dagger a_{b_2'\boldsymbol{k}_2} \delta_{b_1' b_2} \delta_{\boldsymbol{k}_1,\boldsymbol{k}_2+\boldsymbol{q}_2} \\
&\quad - a_{b_2,\boldsymbol{k}_2+\boldsymbol{q}_2}^\dagger a_{b_1'\boldsymbol{k}_1} \delta_{b_1 b_2'} \delta_{\boldsymbol{k}_1+\boldsymbol{q}_1,\boldsymbol{k}_2}.
\end{aligned} \tag{A.1}
$$

First, the commutator $[\hat{H}_e, A_{\boldsymbol{q}}^\dagger(\boldsymbol{k}bb')]$ is given by

$$
\begin{aligned}
\left[\hat{H}_e, A_{\boldsymbol{q}}^\dagger(\boldsymbol{k}bb')\right] &= (\varepsilon_{b\boldsymbol{k}+\boldsymbol{q}}' - \varepsilon_{b'\boldsymbol{k}}') A_{\boldsymbol{q}}^\dagger(\boldsymbol{k}bb') + \frac{1}{2} \sum_{\boldsymbol{q}'(\neq 0)\boldsymbol{k}'\tilde{b}} V_{\boldsymbol{q}'}^{(C)} \Big\{ A_{\boldsymbol{q}'}^\dagger(\boldsymbol{k}'\tilde{b}\tilde{b}) A_{\boldsymbol{q}-\boldsymbol{q}'}^\dagger(\boldsymbol{k}bb') \\
&\quad - A_{\boldsymbol{q}'}^\dagger(\boldsymbol{k}'\tilde{b}\tilde{b}) A_{\boldsymbol{q}-\boldsymbol{q}'}^\dagger(\boldsymbol{k}+\boldsymbol{q}'bb') + A_{\boldsymbol{q}+\boldsymbol{q}'}^\dagger(\boldsymbol{k}bb') A_{-\boldsymbol{q}'}^\dagger(\boldsymbol{k}'\tilde{b}\tilde{b}) \\
&\quad - A_{\boldsymbol{q}+\boldsymbol{q}'}^\dagger(\boldsymbol{k}-\boldsymbol{q}'bb') A_{-\boldsymbol{q}'}^\dagger(\boldsymbol{k}'\tilde{b}\tilde{b}) \Big\},
\end{aligned} \tag{A.2}
$$

where $\varepsilon_{b\boldsymbol{k}}' = \varepsilon_{b\boldsymbol{k}} - 1/2 \sum_{\boldsymbol{q}\neq 0} V_{\boldsymbol{q}}^{(C)}$. By means of the factorization approximation, the four-operator term of $A_{\boldsymbol{q}'}^\dagger(\boldsymbol{k}'\tilde{b}\tilde{b}) A_{\boldsymbol{q}-\boldsymbol{q}'}^\dagger(\boldsymbol{k}bb')$, which appears as the first term in the curl brackets of the right-hand side of Eq. (A.2), is rewritten as

$$
\begin{aligned}
A_{\boldsymbol{q}'}^\dagger(\boldsymbol{k}'\tilde{b}\tilde{b}) A_{\boldsymbol{q}-\boldsymbol{q}'}^\dagger(\boldsymbol{k}bb') &\approx \langle a_{\tilde{b},\boldsymbol{k}'+\boldsymbol{q}'}^\dagger a_{\tilde{b}\boldsymbol{k}'}\rangle A_{\boldsymbol{q}-\boldsymbol{q}'}^\dagger(\boldsymbol{k}bb') + A_{\boldsymbol{q}'}^\dagger(\boldsymbol{k}'\tilde{b}\tilde{b}) \langle a_{b,\boldsymbol{k}+\boldsymbol{q}-\boldsymbol{q}'}^\dagger a_{b'\boldsymbol{k}}\rangle \\
&\quad - \langle a_{\tilde{b},\boldsymbol{k}'+\boldsymbol{q}'}^\dagger a_{b'\boldsymbol{k}}\rangle a_{b,\boldsymbol{k}+\boldsymbol{q}-\boldsymbol{q}'}^\dagger a_{b'\boldsymbol{k}'} - a_{\tilde{b},\boldsymbol{k}'+\boldsymbol{q}'}^\dagger a_{b'\boldsymbol{k}} \langle a_{b,\boldsymbol{k}+\boldsymbol{q}-\boldsymbol{q}'}^\dagger a_{b'\boldsymbol{k}'}\rangle \\
&\approx \rho_{\tilde{b}\tilde{b}\boldsymbol{k}'} \delta_{\boldsymbol{q}'0} A_{\boldsymbol{q}}^\dagger(\boldsymbol{k}bb') + A_{\boldsymbol{q}}^\dagger(\boldsymbol{k}'\tilde{b}\tilde{b}) \rho_{bb'\boldsymbol{k}} \delta_{\boldsymbol{q}'\boldsymbol{q}} \\
&\quad - \rho_{\tilde{b}b'\boldsymbol{k}} \delta_{\boldsymbol{k}'+\boldsymbol{q}',\boldsymbol{k}} A_{\boldsymbol{q}}^\dagger(\boldsymbol{k}-\boldsymbol{q}'bb') - A_{\boldsymbol{q}}^\dagger(\boldsymbol{k}\tilde{b}b') \rho_{bb'\boldsymbol{k}'} \delta_{\boldsymbol{k}'+\boldsymbol{q}',\boldsymbol{k}+\boldsymbol{q}}. \tag{A.3}
\end{aligned}
$$

In the first equality, we make the factorization approximation to split the four-operator term into products of a two-operator term and a two-operator expectation value, where $\langle \hat{O} \rangle$ represents an expectation value of an operator $\hat{O}$ with respect to the ground state. Further, in the second equality, we make the random-phase approximation and replace the expectation value by a density matrix $\rho_{bb'\boldsymbol{k}} \equiv \langle a_{b,\boldsymbol{k}}^\dagger a_{b'\boldsymbol{k}}\rangle$. The similar reduction procedure is applied to the other four-operator terms in Eq. (A.2). As a result, the commutator of

$[\hat{H}_e, A_{\boldsymbol{q}}^\dagger(\boldsymbol{k}bb')]$ is expressed as the form which is linearized with respect to a single kind of operator of the form $A_{\boldsymbol{q}}^\dagger$.

Next, we evaluate the commutator $[\hat{H}'(t), A_{\boldsymbol{q}}^\dagger(\boldsymbol{k}bb')]$ by means of Eq. (A.1), leading to

$$
\begin{aligned}
{[\hat{H}'(t), A_{\boldsymbol{q}}^\dagger(\boldsymbol{k}bb')]} = & -\Omega_{cv}(t)\left[A_{\boldsymbol{q}}^\dagger(\boldsymbol{k}cb')\delta_{vb} - A_{\boldsymbol{q}}^\dagger(\boldsymbol{k}bv)\delta_{cb'}\right] \\
& -\Omega_{vc}(t)\left[A_{\boldsymbol{q}}^\dagger(\boldsymbol{k}vb')\delta_{cb} - A_{\boldsymbol{q}}^\dagger(\boldsymbol{k}bc)\delta_{vb'}\right].
\end{aligned} \tag{A.4}
$$

From the resulting expressions of Eqs. (A.2) and (A.4), we eventually obtain Eq. (2.10),

$$
[\hat{\mathcal{H}}_e(t), A_{\boldsymbol{q}}^\dagger(\boldsymbol{k}bb')] \approx \sum_{\tilde{\boldsymbol{k}}\tilde{b}\tilde{b}'} A_{\boldsymbol{q}}^\dagger(\tilde{\boldsymbol{k}}\tilde{b}\tilde{b}')Z_{\boldsymbol{q}}(\tilde{\boldsymbol{k}}\tilde{b}\tilde{b}', \boldsymbol{k}bb'). \tag{A.5}
$$

The expression of $Z_{\boldsymbol{q}}$ given in Eq. (2.11), and it is linearized with respect to the operator $A_{\boldsymbol{q}}^\dagger$.

Appendix B

Solutions of Eigenvalue Equations of Eqs. (2.33) and (2.34)

First, we solve the left eigenvalue equation of Eq. (2.33) in an analytic manner. Explicit expressions of the equations for respective components of the left eigenvector $U_{\boldsymbol{q}}^{L\dagger}$ are provided as follows:

$$U_{\boldsymbol{q}}^{L\dagger}(\boldsymbol{k}cc) = g_{cc\boldsymbol{k}\boldsymbol{q}}\left\{V_{\boldsymbol{q}}^{(C)}\Delta\bar{\rho}_{cc\boldsymbol{k}\boldsymbol{q}}\sum_{\boldsymbol{k}'}U_{\boldsymbol{q}}^{(+)}(\boldsymbol{k}') - \left[\bar{\Omega}_{vc\boldsymbol{k}}^{(R)}\,U_{\boldsymbol{q}}^{L\dagger}(\boldsymbol{k}vc) - \bar{\Omega}_{cv\boldsymbol{k}}^{(R)}\,U_{\boldsymbol{q}}^{L\dagger}(\boldsymbol{k}cv)\right]\right\},$$

(B.1)

$$U_{\boldsymbol{q}}^{L\dagger}(\boldsymbol{k}vv) = g_{vv\boldsymbol{k}\boldsymbol{q}}\left\{V_{\boldsymbol{q}}^{(C)}\Delta\bar{\rho}_{vv\boldsymbol{k}\boldsymbol{q}}\sum_{\boldsymbol{k}'}U_{\boldsymbol{q}}^{(+)}(\boldsymbol{k}') + \left[\bar{\Omega}_{vc\boldsymbol{k}}^{(R)}\,U_{\boldsymbol{q}}^{L\dagger}(\boldsymbol{k}vc) - \bar{\Omega}_{cv\boldsymbol{k}}^{(R)}\,U_{\boldsymbol{q}}^{L\dagger}(\boldsymbol{k}cv)\right]\right\},$$

(B.2)

$$U_{\boldsymbol{q}}^{L\dagger}(\boldsymbol{k}cv) = g_{cv\boldsymbol{k}\boldsymbol{q}}\left\{V_{\boldsymbol{q}}^{(C)}\Delta\bar{\rho}_{cv\boldsymbol{k}\boldsymbol{q}}\sum_{\boldsymbol{k}'}U_{\boldsymbol{q}}^{(+)}(\boldsymbol{k}') + \bar{\Omega}_{vc\boldsymbol{k}}^{(R)}\,U_{\boldsymbol{q}}^{(-)}(\boldsymbol{k})\right\},$$

(B.3)

and

$$U_{\boldsymbol{q}}^{L\dagger}(\boldsymbol{k}vc) = g_{vc\boldsymbol{k}\boldsymbol{q}}\left\{V_{\boldsymbol{q}}^{(C)}\Delta\bar{\rho}_{vc\boldsymbol{k}\boldsymbol{q}}\sum_{\boldsymbol{k}'}U_{\boldsymbol{q}}^{(+)}(\boldsymbol{k}') - \bar{\Omega}_{cv\boldsymbol{k}}^{(R)}\,U_{\boldsymbol{q}}^{(-)}(\boldsymbol{k})\right\},$$

(B.4)

where

$$g_{bb'\boldsymbol{k}\boldsymbol{q}} = [\mathcal{E}_{\boldsymbol{q}\alpha} - \bar{\omega}_{bb'\boldsymbol{q}}]^{-1}$$

(B.5)

with $\bar{\omega}_{bb'\boldsymbol{k}\boldsymbol{q}} \equiv \omega_{bb'\boldsymbol{k}\boldsymbol{q}} - \bar{\omega}_{bb'}$, and

$$U_{\boldsymbol{q}}^{(\pm)}(\boldsymbol{k}) = U_{\boldsymbol{q}}^{L\dagger}(\boldsymbol{k}cc) \pm U_{\boldsymbol{q}}^{L\dagger}(\boldsymbol{k}vv).$$

(B.6)

Besides, $\omega_{bb'\boldsymbol{q}}$, $\Delta\bar{\rho}_{bb'\boldsymbol{k}\boldsymbol{q}}$, and $\bar{\Omega}_{bb'\boldsymbol{k}}^{(R)}$ are provided in Eqs. (2.12), (2.15), and (2.19), respectively.

We eliminate $U_{\boldsymbol{q}}^{L\dagger}(\boldsymbol{k}cv)$ and $U_{\boldsymbol{q}}^{L\dagger}(\boldsymbol{k}vc)$ by putting Eqs. (B.3) and (B.4) into Eqs. (B.1) and (B.2). Further, employing Eq. (B.6), we obtain a set of equations for $U_{\boldsymbol{q}}^{(\pm)}(\boldsymbol{k})$:

$$U_{\boldsymbol{q}}^{(+)}(\boldsymbol{k}) = V_{\boldsymbol{q}}^{(C)}\mathcal{P}_{\boldsymbol{k}\boldsymbol{q}}^{(1)}\sum_{\boldsymbol{k}'}U_{\boldsymbol{q}}^{(+)}(\boldsymbol{k}') + [g_{cc\boldsymbol{k}\boldsymbol{q}} - g_{vv\boldsymbol{k}\boldsymbol{q}}]W_{\boldsymbol{k}\boldsymbol{q}}U_{\boldsymbol{q}}^{(-)}(\boldsymbol{k}),$$

(B.7)

and

$$U_{\boldsymbol{q}}^{(-)}(\boldsymbol{k}) = V_{\boldsymbol{q}}^{(C)}\mathcal{P}_{\boldsymbol{k}\boldsymbol{q}}^{(2)}\sum_{\boldsymbol{k}'}U_{\boldsymbol{q}}^{(+)}(\boldsymbol{k}'),$$

(B.8)

where $\mathcal{P}_{kq}^{(1)}$ and $\mathcal{P}_{kq}^{(2)}$ are provided by

$$\mathcal{P}_{kq}^{(1)} = g_{cckq}\Delta\bar{\rho}_{cckq} + g_{vvkq}\Delta\bar{\rho}_{vvkq} + (g_{cckq} - g_{vvkq})\Delta\Omega_{kq}, \tag{B.9}$$

and

$$\begin{aligned}
\mathcal{P}_{kq}^{(2)} &= [1 - (g_{cckq} + g_{vvkq})W_{kq}]^{-1} \\
&\times [g_{cckq}\Delta\bar{\rho}_{cckq} - g_{vvkq}\Delta\bar{\rho}_{vvkq} + (g_{cckq} + g_{vvkq})\Delta\Omega_{kq}],
\end{aligned} \tag{B.10}$$

respectively Further, $\Delta\Omega_{kq}$ and W_{kq} are given by

$$\Delta\Omega_{kq} = \bar{\Omega}_{cvk}^{(R)}g_{cvkq}\Delta\bar{\rho}_{cvkq} - \bar{\Omega}_{vck}^{(R)}g_{vckq}\Delta\bar{\rho}_{vckq}, \tag{B.11}$$

and

$$W_{kq} = \bar{\Omega}_{vck}^{(R)}g_{vckq}\bar{\Omega}_{cvk}^{(R)} + \bar{\Omega}_{cvk}^{(R)}g_{cvkq}\bar{\Omega}_{vck}^{(R)}, \tag{B.12}$$

respectively. We eliminate $U_q^{(-)}(\boldsymbol{k})$ by putting Eq. (B.8) into Eq. (B.7), leading to

$$U_q^{(+)}(\boldsymbol{k}) = V_q^{(C)}\mathcal{P}_{kq}\sum_{\boldsymbol{k}'} U_q^{(+)}(\boldsymbol{k}'), \tag{B.13}$$

where $\mathcal{P}_{kq}$ is given by

$$\mathcal{P}_{kq} = \mathcal{P}_{kq}^{(1)} + (g_{cckq} - g_{vvkq})W_{kq}\mathcal{P}_{kq}^{(2)}. \tag{B.14}$$

We take the summation of both sides of Eq. (B.13) over $\boldsymbol{k}$, expressed as

$$\sum_{\boldsymbol{k}} U_q^{(+)}(\boldsymbol{k}) = V_q^{(C)}\sum_{\boldsymbol{k}}\mathcal{P}_{kq}\sum_{\boldsymbol{k}'} U_q^{(+)}(\boldsymbol{k}'), \tag{B.15}$$

and obtain an identity relation:

$$1 = V_q^{(C)}\sum_{\boldsymbol{k}}\mathcal{P}_{kq}(\mathcal{E}_{q\alpha}), \tag{B.16}$$

where the energy-dependence of $\mathcal{P}_{kq}$ is explicitly shown. We solve the transcendental equation of Eq. (B.16), and determine a full set of eigenenergies denoted as $\{\mathcal{E}_{q\alpha}\}$. The αth solution of $U_{q\alpha}^{(+)}(\boldsymbol{k})$ is given by

$$U_{q\alpha}^{(+)}(\boldsymbol{k}) = N_{q\alpha}^L V_q^{(C)}\mathcal{P}_{kq}(\mathcal{E}_{q\alpha}), \tag{B.17}$$

where $N_{q\alpha}^L$ represents a proportional constant to be determined later. Further, in terms of the identity relation of Eq. (B.16), we obtain the following relation

$$\sum_{\boldsymbol{k}} U_{q\alpha}^{(+)}(\boldsymbol{k}) = N_{q\alpha}^L, \tag{B.18}$$

and thus, by use of Eq. (B.8), the αth solution of $U_{q\alpha}^{(-)}(\boldsymbol{k})$ is written as

$$U_{q\alpha}^{(-)}(\boldsymbol{k}) = N_{q\alpha}^L V_q^{(C)}\mathcal{P}_{kq}^{(2)}(\mathcal{E}_{q\alpha}). \tag{B.19}$$

Therefore, owing to the relation of Eq. (B.6), $U_{\boldsymbol{q}}^{L\dagger}(\boldsymbol{k}cc)$ and $U_{\boldsymbol{q}}^{L\dagger}(\boldsymbol{k}vv)$ are determined. Moreover, $U_{\boldsymbol{q}}^{L\dagger}(\boldsymbol{k}cv)$ and $U_{\boldsymbol{q}}^{L\dagger}(\boldsymbol{k}vc)$ are also determined by inserting the expressions of $U_{\boldsymbol{q}\alpha}^{(\pm)}(\boldsymbol{k})$ into Eqs. (B.3) and (B.4). In summary, $U_{\boldsymbol{q}}^{L\dagger}(\boldsymbol{k}bb')$ is expressed as

$$U_{\boldsymbol{q}\alpha}^{L\dagger}(\boldsymbol{k}bb') = N_{\boldsymbol{q}\alpha}^{L}V_{\boldsymbol{q}}^{(C)}u_{\boldsymbol{q}\alpha}^{L\dagger}(\boldsymbol{k}bb'), \tag{B.20}$$

where

$$u_{\boldsymbol{q}\alpha}^{L\dagger}(\boldsymbol{k}cc) = \frac{1}{2}\left[\mathcal{P}_{\boldsymbol{k}\boldsymbol{q}}(\mathcal{E}_{\boldsymbol{q}\alpha}) + \mathcal{P}_{\boldsymbol{k}\boldsymbol{q}}^{(2)}(\mathcal{E}_{\boldsymbol{q}\alpha})\right], \tag{B.21}$$

$$u_{\boldsymbol{q}\alpha}^{L\dagger}(\boldsymbol{k}vv) = \frac{1}{2}\left[\mathcal{P}_{\boldsymbol{k}\boldsymbol{q}}(\mathcal{E}_{\boldsymbol{q}\alpha}) - \mathcal{P}_{\boldsymbol{k}\boldsymbol{q}}^{(2)}(\mathcal{E}_{\boldsymbol{q}\alpha})\right], \tag{B.22}$$

$$u_{\boldsymbol{q}\alpha}^{L\dagger}(\boldsymbol{k}cv) = g_{cv\boldsymbol{k}\boldsymbol{q}}\left[\Delta\bar{\rho}_{cv\boldsymbol{k}\boldsymbol{q}} + \bar{\Omega}_{vc\boldsymbol{k}}^{(R)}\mathcal{P}_{\boldsymbol{k}\boldsymbol{q}}^{(2)}(\mathcal{E}_{\boldsymbol{q}\alpha})\right], \tag{B.23}$$

and

$$u_{\boldsymbol{q}\alpha}^{L\dagger}(\boldsymbol{k}vc) = g_{vc\boldsymbol{k}\boldsymbol{q}}\left[\Delta\bar{\rho}_{vc\boldsymbol{k}\boldsymbol{q}} - \bar{\Omega}_{cv\boldsymbol{k}}^{(R)}\mathcal{P}_{\boldsymbol{k}\boldsymbol{q}}^{(2)}(\mathcal{E}_{\boldsymbol{q}\alpha})\right]. \tag{B.24}$$

Next, we solve the right eigenvalue equation of Eq. (2.34) in an analytic manner. Explicit expressions of the equations for respective components of the right eigenvector $U_{\boldsymbol{q}}^{R}$ are provided as follows:

$$U_{\boldsymbol{q}}^{R}(\boldsymbol{k}cc) = g_{cc\boldsymbol{k}\boldsymbol{q}}\left\{V_{\boldsymbol{q}}^{(C)}\sum_{\boldsymbol{k}'}U_{\boldsymbol{q}}^{\prime(+)}(\boldsymbol{k}') + W_{\boldsymbol{k}\boldsymbol{q}}U_{\boldsymbol{q}}^{\prime(-)}(\boldsymbol{k}')\right\}, \tag{B.25}$$

$$U_{\boldsymbol{q}}^{R}(\boldsymbol{k}vv) = g_{vv\boldsymbol{k}\boldsymbol{q}}\left\{V_{\boldsymbol{q}}^{(C)}\sum_{\boldsymbol{k}'}U_{\boldsymbol{q}}^{\prime(+)}(\boldsymbol{k}') - W_{\boldsymbol{k}\boldsymbol{q}}U_{\boldsymbol{q}}^{\prime(-)}(\boldsymbol{k}')\right\}, \tag{B.26}$$

$$U_{\boldsymbol{q}}^{R}(\boldsymbol{k}cv) = g_{cv\boldsymbol{k}\boldsymbol{q}}\bar{\Omega}_{cv\boldsymbol{k}}^{(R)}U_{\boldsymbol{q}}^{\prime(-)}(\boldsymbol{k}'), \tag{B.27}$$

and

$$U_{\boldsymbol{q}}^{R}(\boldsymbol{k}vc) = -g_{vc\boldsymbol{k}\boldsymbol{q}}\bar{\Omega}_{vc\boldsymbol{k}}^{(R)}U_{\boldsymbol{q}}^{\prime(-)}(\boldsymbol{k}'), \tag{B.28}$$

where

$$U_{\boldsymbol{q}}^{\prime(+)}(\boldsymbol{k}) = \sum_{bb'}\Delta\bar{\rho}_{bb'\boldsymbol{k}\boldsymbol{q}}U_{\boldsymbol{q}}^{R}(\boldsymbol{k}bb'), \tag{B.29}$$

and

$$U_{\boldsymbol{q}}^{\prime(-)}(\boldsymbol{k}) = U_{\boldsymbol{q}}^{R}(\boldsymbol{k}cc) - U_{\boldsymbol{q}}^{R}(\boldsymbol{k}vv). \tag{B.30}$$

We define $U_{\boldsymbol{q}}^{\prime(d)}(\boldsymbol{k})$ as

$$U_{\boldsymbol{q}}^{\prime(d)}(\boldsymbol{k}) = \sum_{b}\Delta\bar{\rho}_{bb\boldsymbol{k}\boldsymbol{q}}U_{\boldsymbol{q}}^{R}(\boldsymbol{k}bb), \tag{B.31}$$

and thus, Eq. (B.29) is cast into

$$U_{\boldsymbol{q}}^{\prime(+)}(\boldsymbol{k}) = U_{\boldsymbol{q}}^{\prime(d)}(\boldsymbol{k}) + \Delta\Omega_{\boldsymbol{k}\boldsymbol{q}}U_{\boldsymbol{q}}^{\prime(-)}(\boldsymbol{k}). \tag{B.32}$$

We put Eqs. (B.25) and (B.26) into Eqs. (B.30) and (B.31), and thus, obtain

$$U_{\boldsymbol{q}}^{\prime(-)}(\boldsymbol{k}) = V_{\boldsymbol{q}}^{(C)}\mathcal{P}_{\boldsymbol{k}\boldsymbol{q}}^{\prime(2)}\sum_{\boldsymbol{k}'}U_{\boldsymbol{q}}^{\prime(+)}(\boldsymbol{k}') \tag{B.33}$$

and

$$U_q'^{(d)}(\boldsymbol{k}) = \left(\sum_b \Delta\bar{\rho}_{bb\boldsymbol{k}\boldsymbol{q}}\, g_{bb\boldsymbol{k}\boldsymbol{q}}\right) V_q^{(C)} U_q'^{(+)}(\boldsymbol{k}) + \mathcal{P}_{\boldsymbol{k}\boldsymbol{q}}'^{(3)} U_q'^{(-)}(\boldsymbol{k}), \tag{B.34}$$

where

$$\mathcal{P}_{\boldsymbol{k}\boldsymbol{q}}'^{(2)} = [1 - (g_{cc\boldsymbol{k}\boldsymbol{q}} + g_{vv\boldsymbol{k}\boldsymbol{q}})W_{\boldsymbol{k}\boldsymbol{q}}]^{-1}\,(g_{cc\boldsymbol{k}\boldsymbol{q}} - g_{vv\boldsymbol{k}\boldsymbol{q}})\,V_q^{(C)} \tag{B.35}$$

and

$$\mathcal{P}_{\boldsymbol{k}\boldsymbol{q}}'^{(3)} = (\Delta\bar{\rho}_{cc\boldsymbol{k}\boldsymbol{q}}\, g_{cc\boldsymbol{k}\boldsymbol{q}} - \Delta\bar{\rho}_{vv\boldsymbol{k}\boldsymbol{q}}\, g_{vv\boldsymbol{k}\boldsymbol{q}})\, W_{\boldsymbol{k}\boldsymbol{q}}. \tag{B.36}$$

We put Eqs. (B.33) and (B.34) into Eq. (B.32), leading to

$$U_q'^{(+)}(\boldsymbol{k}) = V_q^{(C)}\mathcal{P}_{\boldsymbol{k}\boldsymbol{q}} \sum_{\boldsymbol{k}'} U_q'^{(+)}(\boldsymbol{k}'), \tag{B.37}$$

which looks similar to Eq. (B.13).

By taking the summation of both sides of Eq. (B.37), the identity relation of Eq. (B.16) is obtained again, and the αth solution of $U_{q\alpha}'^{(+)}(\boldsymbol{k})$ is given by the form:

$$U_{q\alpha}'^{(+)}(\boldsymbol{k}) = N_{q\alpha}^R V_q^{(C)}\mathcal{P}_{\boldsymbol{k}\boldsymbol{q}}(\mathcal{E}_{q\alpha}) \tag{B.38}$$

with the normalization constant of $N_{q\alpha}^R$. Moreover, the following relation is straightforward derived

$$\sum_{\boldsymbol{k}} U_{q\alpha}'^{(+)}(\boldsymbol{k}) = N_{q\alpha}^R, \tag{B.39}$$

and thus, by use of Eq. (B.33), the αth solution of $U_{q\alpha}'^{(-)}(\boldsymbol{k})$ is given by

$$U_{q\alpha}'^{(-)}(\boldsymbol{k}) = N_{q\alpha}^R V_q^{(C)}\mathcal{P}_{\boldsymbol{k}\boldsymbol{q}}'^{(2)}(\mathcal{E}_{q\alpha}). \tag{B.40}$$

$U_q^R(\boldsymbol{k}bb')$ is expressed as

$$U_{q\alpha}^R(\boldsymbol{k}bb') = N_{q\alpha}^R V_q^{(C)} u_{q\alpha}^R(\boldsymbol{k}bb'), \tag{B.41}$$

and explicit expressions of $u_{q\alpha}^R(\boldsymbol{k}bb')$ are obtained by means of Eqs. (B.25)-(B.28), (B.38), and (B.40). In summary,

$$u_{q\alpha}^R(\boldsymbol{k}cc) = g_{cc\boldsymbol{k}\boldsymbol{q}}\left[1 + (g_{cc\boldsymbol{k}\boldsymbol{q}} - g_{vv\boldsymbol{k}\boldsymbol{q}})\mathcal{G}_{\boldsymbol{k}\boldsymbol{q}}W_{\boldsymbol{k}\boldsymbol{q}}\right], \tag{B.42}$$

$$u_{q\alpha}^R(\boldsymbol{k}vv) = g_{vv\boldsymbol{k}\boldsymbol{q}}\left[1 - (g_{cc\boldsymbol{k}\boldsymbol{q}} - g_{vv\boldsymbol{k}\boldsymbol{q}})\mathcal{G}_{\boldsymbol{k}\boldsymbol{q}}W_{\boldsymbol{k}\boldsymbol{q}}\right], \tag{B.43}$$

$$u_{q\alpha}^R(\boldsymbol{k}cv) = g_{cv\boldsymbol{k}\boldsymbol{q}}\bar{\Omega}_{\boldsymbol{k}cv}^{(R)}(g_{cc\boldsymbol{k}\boldsymbol{q}} - g_{vv\boldsymbol{k}\boldsymbol{q}})\mathcal{G}_{\boldsymbol{k}\boldsymbol{q}}, \tag{B.44}$$

and

$$u_{q\alpha}^R(\boldsymbol{k}vc) = -g_{vc\boldsymbol{k}\boldsymbol{q}}\bar{\Omega}_{\boldsymbol{k}vc}^{(R)}(g_{cc\boldsymbol{k}\boldsymbol{q}} - g_{vv\boldsymbol{k}\boldsymbol{q}})\mathcal{G}_{\boldsymbol{k}\boldsymbol{q}}, \tag{B.45}$$

where

$$\mathcal{G}_{\boldsymbol{k}\boldsymbol{q}} = [1 - (g_{cc\boldsymbol{k}\boldsymbol{q}} + g_{vv\boldsymbol{k}\boldsymbol{q}})W_{\boldsymbol{k}\boldsymbol{q}}]^{-1}. \tag{B.46}$$

Both of the left and right eigenvectors thus obtained evidently satisfy the biorthogonal relation

$$\sum_{\boldsymbol{k}bb'} U_{q\alpha}^{L\dagger}(\boldsymbol{k}bb')U_{q\alpha'}^R(\boldsymbol{k}bb') = \delta_{\alpha\alpha'}, \tag{B.47}$$

and the completeness

$$\sum_\alpha U^R_{q\alpha}(\boldsymbol{k}_1 b_1 b'_1) U^{L\dagger}_{q\alpha}(\boldsymbol{k}_2 b_2 b'_2) = \delta_{\boldsymbol{k}_1 \boldsymbol{k}_2} \delta_{b_1 b_2} \delta_{b'_1 b'_2}. \tag{B.48}$$

We determine the normalization constants $N^L_{q\alpha}$ and $N^R_{q\alpha}$ with the normalization condition

$$\sum_{\boldsymbol{k}bb'} U^{L\dagger}_{q\alpha}(\boldsymbol{k}bb') U^R_{q\alpha}(\boldsymbol{k}bb') = 1, \tag{B.49}$$

which is expressed in terms of Eqs. (B.20) and (B.41) as

$$\left[N^L_{q\alpha} N^R_{q\alpha} \left(V^{(C)}_q \right)^2 \right]^{-1} = \sum_{\boldsymbol{k}bb'} u^{L\dagger}_{q\alpha}(\boldsymbol{k}bb') u^R_{q\alpha}(\boldsymbol{k}bb'). \tag{B.50}$$

Finally, we derive the expressions of the eigenenergy-determining transcendental equation of Eq. (B.16) and the normalization condition of Eq. (B.50) in the small-$\boldsymbol{q}$ limit of our primary concern. In this limit, $\bar{\rho}_{bb'\boldsymbol{k}q}$, $g_{bb'\boldsymbol{k}q}$, and $\mathcal{G}_{\boldsymbol{k}q}$ are written as

$$\Delta \bar{\rho}_{bb'\boldsymbol{k}q} \simeq -|\boldsymbol{q}| \hat{\boldsymbol{q}} \cdot \boldsymbol{\nabla} \bar{\rho}_{bb'\boldsymbol{k}}, \tag{B.51}$$

$$g_{bb\boldsymbol{k}q} \simeq \frac{1}{\mathcal{E}_q} \left(1 + \frac{1}{\mathcal{E}_q} |\boldsymbol{q}| \hat{\boldsymbol{q}} \cdot \boldsymbol{\nabla} \varepsilon^{(r)}_{b\boldsymbol{k}} \right), \tag{B.52}$$

$$g_{b\bar{b}\boldsymbol{k}q} \simeq g_{b\bar{b}\boldsymbol{k},q=0} \equiv g_{b\bar{b}\boldsymbol{k}}, \tag{B.53}$$

and

$$\mathcal{G}_{\boldsymbol{k}q} = \left(1 - \frac{2W_{\boldsymbol{k}q}}{\mathcal{E}_q} \right)^{-1}, \tag{B.54}$$

where $\boldsymbol{\nabla}$ represents a gradient with respect to $\boldsymbol{k}$, in other words, $\partial/\partial \boldsymbol{k}$. $\varepsilon^{(r)}_{b\boldsymbol{k}}$ is provided in Eq. (2.13). $\hat{\boldsymbol{q}} = \boldsymbol{q}/|\boldsymbol{q}|$, and $\bar{b}$ represents $\bar{b} \neq b$. Equation (B.16) is cast into the form

$$K(\mathcal{E}_q) = 1, \tag{B.55}$$

where

$$
\begin{aligned}
K(\mathcal{E}_q) &= \frac{V^{(C)}_q \boldsymbol{q}^2}{\mathcal{E}^2_q} \sum_{\boldsymbol{k}} \Bigg\{ \bar{\rho}_{cc\boldsymbol{k}} (\hat{\boldsymbol{q}} \cdot \boldsymbol{\nabla}) \left[\left(\hat{\boldsymbol{q}} \cdot \boldsymbol{\nabla} \varepsilon^{(r)}_{c\boldsymbol{k}} \right) + \left(\hat{\boldsymbol{q}} \cdot \boldsymbol{\nabla} \Delta \varepsilon^{(r)}_{\boldsymbol{k}} \right) \frac{W_{\boldsymbol{k}q} \mathcal{G}_{\boldsymbol{k}q}}{\mathcal{E}_q} \right] \\
&\quad + \bar{\rho}'_{vv\boldsymbol{k}} (\hat{\boldsymbol{q}} \cdot \boldsymbol{\nabla}) \left[\left(\hat{\boldsymbol{q}} \cdot \boldsymbol{\nabla} \varepsilon^{(r)}_{v\boldsymbol{k}} \right) - \left(\hat{\boldsymbol{q}} \cdot \boldsymbol{\nabla} \Delta \varepsilon^{(r)}_{\boldsymbol{k}} \right) \frac{W_{\boldsymbol{k}q} \mathcal{G}_{\boldsymbol{k}q}}{\mathcal{E}_q} \right] \\
&\quad + \bar{\rho}_{cv\boldsymbol{k}} (\hat{\boldsymbol{q}} \cdot \boldsymbol{\nabla}) \left[\left(\hat{\boldsymbol{q}} \cdot \boldsymbol{\nabla} \Delta \varepsilon^{(r)}_{\boldsymbol{k}} \right) \bar{\Omega}^{(R)}_{\boldsymbol{k}cv} g_{\boldsymbol{k}cv} \left(1 + \frac{2W_{\boldsymbol{k}q} \mathcal{G}_{\boldsymbol{k}q}}{\mathcal{E}_q} \right) \right] \\
&\quad - \bar{\rho}_{vc\boldsymbol{k}} (\hat{\boldsymbol{q}} \cdot \boldsymbol{\nabla}) \left[\left(\hat{\boldsymbol{q}} \cdot \boldsymbol{\nabla} \Delta \varepsilon^{(r)}_{\boldsymbol{k}} \right) \bar{\Omega}^{(R)}_{\boldsymbol{k}vc} g_{\boldsymbol{k}vc} \left(1 + \frac{2W_{\boldsymbol{k}q} \mathcal{G}_{\boldsymbol{k}q}}{\mathcal{E}_q} \right) \right] \Bigg\}
\end{aligned} \tag{B.56}
$$

with

$$\Delta \varepsilon^{(r)}_{\boldsymbol{k}} = \varepsilon^{(r)}_{c\boldsymbol{k}} - \varepsilon^{(r)}_{v\boldsymbol{k}}. \tag{B.57}$$

Further,

$$\bar{\rho}'_{vv\boldsymbol{k}} = \bar{\rho}_{vv\boldsymbol{k}} - 1 \leq 0, \tag{B.58}$$

and $|\bar{\rho}'_{vvk}|$ represents a hole density, where the second term in $\nabla\bar{\rho}'_{vvk}$ becomes zero. Using Eqs. (B.5) and (B.12), and defining

$$D_{kq}(\mathcal{E}_q) = \mathcal{E}_q^2 - \bar{w}_{cvkq}^2 - |2\bar{\Omega}_{kcv}^{(R)}|^2, \tag{B.59}$$

Eq. (B.56) is expressed as

$$
\begin{aligned}
K(\mathcal{E}_q) =\ & \frac{1}{\mathcal{E}_q^2}\left(\omega_{qpl}^2 + \frac{4\pi}{\epsilon_\infty}\sum_k\left\{\frac{1}{2}\left(\bar{\rho}_{cck} - \bar{\rho}'_{vvk}\right)(\hat{q}\cdot\nabla)\left[\left(\hat{q}\cdot\nabla\Delta\varepsilon_k^{(r)}\right)\frac{|2\bar{\Omega}_{kcv}^{(R)}|^2}{D_{kq}(\mathcal{E}_q)}\right]\right.\right. \\
& +\bar{\rho}_{cvk}\left(\hat{q}\cdot\nabla\right)\left[\left(\hat{q}\cdot\nabla\Delta\varepsilon_k^{(r)}\right)\frac{\bar{\Omega}_{kcv}^{(R)}(\mathcal{E}_q + \bar{w}_{cvkq})}{D_{kq}(\mathcal{E}_q)}\right] \\
& \left.\left.-\bar{\rho}_{vck}\left(\hat{q}\cdot\nabla\right)\left[\left(\hat{q}\cdot\nabla\Delta\varepsilon_k^{(r)}\right)\frac{\bar{\Omega}_{kvc}^{(R)}(\mathcal{E}_q + \bar{w}_{vckq})}{D_{kq}(\mathcal{E}_q)}\right]\right\}\right).
\end{aligned}
\tag{B.60}
$$

Here, ω_{qpl} shows the plasma frequency, provided by

$$\omega_{qpl} = \left[V_q^{(C)}q^2\sum_{kb}\bar{\rho}_{bbk}\nabla_k^2\varepsilon_{bk}^{(r)}\right]^{\frac{1}{2}}. \tag{B.61}$$

In the case of the Rabi frequency terms, that is, $\bar{\Omega}_{kcv}^{(R)}$ and $\bar{\Omega}_{kvc}^{(R)}$ being negligibly small, Eq.(B.55) is straightforward solved to provide $\mathcal{E}_q^2$ equal to ω_{qpl}^2.

Next, Eq. (B.50) is cast into the form

$$\left[N_{q\alpha}^L N_{q\alpha}^R\left(V_q^{(C)}\right)^2\right]^{-1} = -\frac{q^2}{\mathcal{E}_{q\alpha}^2}\sum_{kbb'}(\hat{q}\cdot\nabla\bar{\rho}_{bb'k})\,f_{bb'k}, \tag{B.62}$$

where

$$f_{cck} = \frac{1}{\mathcal{E}_q}\left[(\hat{q}\cdot\nabla)\left(\varepsilon_{ck}^{(r)} + \varepsilon_{vk}^{(r)}\right) + \left(\hat{q}\cdot\nabla\Delta\varepsilon_k^{(r)}\right)\mathcal{G}_{kq}d_{kq}\right], \tag{B.63}$$

$$f_{vvk} = \frac{1}{\mathcal{E}_q}\left[(\hat{q}\cdot\nabla)\left(\varepsilon_{ck}^{(r)} + \varepsilon_{vk}^{(r)}\right) - \left(\hat{q}\cdot\nabla\Delta\varepsilon_k^{(r)}\right)\mathcal{G}_{kq}d_{kq}\right], \tag{B.64}$$

$$f_{cvk} = \left(\hat{q}\cdot\nabla\Delta\varepsilon_k^{(r)}\right)g_{cvk}\bar{\Omega}_{kcv}^{(R)}\mathcal{G}_{kq}\left(g_{cvk} + \frac{2d_{kq}}{\mathcal{E}_q}\right), \tag{B.65}$$

and

$$f_{vck} = -\left(\hat{q}\cdot\nabla\Delta\varepsilon_k^{(r)}\right)g_{vck}\bar{\Omega}_{kvc}^{(R)}\mathcal{G}_{kq}\left(g_{vck} + \frac{2d_{kq}}{\mathcal{E}_q}\right), \tag{B.66}$$

with

$$d_{kq} = 1 + \mathcal{G}_{kq}W_{kq}\left(\frac{1}{\mathcal{E}_q} + \frac{g_{cvk}^2 + g_{vck}^2}{g_{cvk} + g_{vck}}\right) \approx 1 + \frac{2}{\mathcal{E}_q}\mathcal{G}_{kq}W_{kq} \approx \mathcal{G}_{kq}. \tag{B.67}$$

It is noted that the normalization constants and both of $u_q^{L\dagger}$ and u_q^R are in proportion to $|q|$ in the small q-limit.

Moreover, replacing $\mathcal{E}_{q\alpha}$ by $-\mathcal{E}_{q\alpha}^*$ in Eq. (B.60) and taking a complex conjugate of both sides of the equation, we readily obtain a relation

$$K(\mathcal{E}_{q\alpha}) = \left[K(-\mathcal{E}_{q\alpha}^*)\right]^*. \tag{B.68}$$

66

This fact implies that a pair of $\mathcal{E}_{\boldsymbol{q}\alpha_+}$ and $\mathcal{E}_{\boldsymbol{q}\alpha_-}(\equiv -\mathcal{E}^*_{\boldsymbol{q}\alpha_+})$ are solutions of Eq. (B.55) simultaneously. We apply the same procedure to Eq. (B.62), and obtain a relation

$$N^L_{\boldsymbol{q}\alpha_+} N^R_{\boldsymbol{q}\alpha_+} = -\left[N^L_{\boldsymbol{q}\alpha_-} N^R_{\boldsymbol{q}\alpha_-} \right]^*. \tag{B.69}$$

According to an energy-phase of $\exp\left[i \int_{t'}^t \mathcal{E}_{\boldsymbol{q}\alpha}(\tau)d\tau \right]$, it is seen that $\mathcal{E}_{\boldsymbol{q}\alpha_+}$ plays a role of a complex energy of a quasiboson created by an operator of $B^\dagger_{\boldsymbol{q}\alpha_+}$. Thus, amplitude of this operator is temporally damps, following $\exp\left[-\int_{t'}^t \mathrm{Im}\mathcal{E}_{\boldsymbol{q}\alpha_+}(\tau)d\tau \right]$. Similarly, $\mathcal{E}_{\boldsymbol{q}\alpha_-}$ is readily interpreted as a complex energy of the quasiboson annihilated by an operator $B_{\boldsymbol{q}\alpha_-}$, where amplitude of it diminishes following $\exp\left[-\int_{t'}^t \mathrm{Im}\mathcal{E}_{\boldsymbol{q}\alpha_+}(\tau)d\tau \right]$ again.

Appendix C

Closed Analytic Forms of $F_{q\beta}^\dagger$ and $F_{q\beta}$ Derived by Solving Eq. (2.61)

C.1 Introduction of Operators of $F_{q\beta}^{0\dagger}$ and $F_{q\beta}^0$

Before solving Eq. (2.61), we consider an equation of motion of another PQ operator

$$F_{q\beta}^{0\dagger} = \sum_{\beta'} B_{q\beta'}^{0\dagger} V_{q\beta'\beta} + B_{q\alpha_1}^{0\dagger} V_{q\alpha_1\beta} + c_q^\dagger V_{q\alpha_2\beta}, \tag{C.1}$$

which is provided by

$$-i\frac{d}{dt}F_{q\beta}^{0\dagger} = F_{q\beta}^{0\dagger}\mathcal{E}_{q\beta}^0. \tag{C.2}$$

Eq. (C.1) resembles Eq. (2.59), but a quasiboson operator $B_q^{0\dagger}$ and an $[(N+2) \times N]$-rectangular matrix V_q are different from $B_q^\dagger$ and V_q^R, respectively. V_q satisfies an equation

$$h_q^0 V_q = V_q \mathcal{E}_q^0, \tag{C.3}$$

which differs from Eq. (2.58). h_q^0 represents a Hermitian matrix provided by

$$h_q^0 = \begin{bmatrix} \mathcal{E}_q^0 & M_q \\ M_q^\dagger & \omega_q \end{bmatrix}, \tag{C.4}$$

where, $\mathcal{E}_q^0$ is real, as defined below Eq. (C.12). Moreover, similarly to Eq. (2.60), we introduce an $[N \times (N+2)]$-rectangular matrix $\bar{V}_q$ to ensure the inverse relation of Eq. (C.1), that is,

$$B_{q\alpha}^{0\dagger} = \sum_{\beta} F_{q\beta}^{0\dagger} \bar{V}_{q\beta\alpha}, \quad c_q^\dagger = \sum_{\beta} F_{q\beta}^{0\dagger} \bar{V}_{q\beta\alpha_2}. \tag{C.5}$$

Therefore, we obtain $\bar{V}_q V_q = 1$ and $V_q \bar{V}_q = 1$ which correspond to the expressions provided below Eq. (2.60) for V_q^R and $V_q^{L\dagger}$. In addition, we introduce F_q^0 as a Hermitian-conjugate of $F_q^{0\dagger}$, namely,

$$F_{q\beta}^0 = \sum_{\beta'} V_{q\beta\beta'}^* B_{q\beta'}^0 + V_{q\beta\alpha_1}^* B_{q\alpha_1}^0 + V_{q\beta\alpha_2}^* c_q. \tag{C.6}$$

Here, both of $F_{q\beta}^0$ and $F_{q\beta}^{0\dagger}$ are required to satisfy the expectation values of equal-time commutation relations as follows:

$$\langle[F_{q\beta}^0, F_{q'\beta'}^{0\dagger}]\rangle = \delta_{qq'}\delta_{\beta\beta'}, \tag{C.7}$$

and

$$\langle[F_{q\beta}^0, F_{q'\beta'}^0]\rangle = \langle[F_{q\beta}^{0\dagger}, F_{q'\beta'}^{0\dagger}]\rangle = 0, \tag{C.8}$$

instead of the corresponding equal-time commutation relations where expectation values are not taken. Under these conditions, we can consider $F_{q\beta}^0$ and $F_{q\beta}^{0\dagger}$ as boson operators. In Eqs. (C.7) and (C.8), we omit the argument t of these operators just for the sake of simplicity. Applying Eqs. (C.1) and (C.6) to Eqs. (C.7) and (C.8), it is seen that the following conditions are imposed on $B_{q\alpha}^0$ and $B_{q\alpha}^{0\dagger}$ as:

$$\langle[B_{q\alpha}^0, B_{q'\alpha'}^{0\dagger}]\rangle = \delta_{qq'}\delta_{\alpha\alpha'}, \tag{C.9}$$

$$\langle[B_{q\alpha}^0, B_{q'\alpha'}^0]\rangle = \langle[B_{q\alpha}^{0\dagger}, B_{q'\alpha'}^{0\dagger}]\rangle = 0, \tag{C.10}$$

and

$$\bar{V}_q = V_q^\dagger. \tag{C.11}$$

In Sec. C.3, we examine the criteria of the validity of this bosonization scheme.

A set of solutions V_q of the Fano problem provided by the adiabatic coupled-equations of Eq. (C.3) is shown in Sec. C.4. On the other hand, a set of eigenvalues $\mathcal{E}_q^0$ follows the equation

$$K^0(\mathcal{E}_q^0) = 1, \tag{C.12}$$

where $K^0(\mathcal{E}_q^0)$ is expressed as

$$
\begin{aligned}
K^0(\mathcal{E}_q^0) &= \left(\frac{1}{\mathcal{E}_q^0}\right)^2 \left\{ \omega_{qpl}^2 + \frac{4\pi}{\epsilon_\infty} \sum_k \frac{1}{2}(\bar{\rho}_{cck} - \bar{\rho}'_{vvk})\,(\hat{q}\cdot\boldsymbol{\nabla}) \right. \\
&\quad \left. \times \left[\left(\hat{q}\cdot\boldsymbol{\nabla}\Delta\varepsilon_k^{(r)}\right) \frac{|2\bar{\Omega}_{kcv}^{(R)}|^2}{\left(\mathcal{E}_q^0\right)^2 - \bar{w}_{cvkq}^2 - |2\bar{\Omega}_{kcv}^{(R)}|^2} \right] \right\}.
\end{aligned}
\tag{C.13}
$$

Here, ω_{qpl} is the plasma frequency provided by Eq. (B.61), $\hat{q} = q/|q|$, and $\boldsymbol{\nabla} \equiv \partial/\partial k$. [Actually, $K^0(\mathcal{E}_q^0)$ is substituted for $K(\mathcal{E}_q)$ of Eq. (B.60) by employing the approximation for deriving Eq. (C.46) from Eq. (C.42). In other words, we adopt the equality of Eq. (C.51), and neglect interband density matrices.]

Below, we discuss a couple of properties of solutions of the transcendental equation of Eq. (C.12). In Fig. C.1, we show a trace of $K^0(\mathcal{E}_q^0)$ as a function of $\mathcal{E}_q^0$ for Si; we also obtain the similar trace for GaAs, though not shown here. Points of intersection of $K^0(\mathcal{E}_q^0)$ with unity represent *real* solutions of Eq. (C.12). [It should be noted that just a set of solutions, where the corresponding normalization constants satisfy Eq. (C.52), is suitable for the present bosonization scheme.] Hereafter, let the normalization constants for the αth state be expressed as

$$N_{q\alpha}^L = N_{q\alpha}^{R*} \equiv N_{q\alpha}^0, \tag{C.14}$$

where $N_{q\alpha}^0$ is real, unless otherwise stated. Existence of such a set of real eigenvalues, $\{\mathcal{E}_{q\alpha}^0\}$, is in agreement with the requirement that h_q^0 should be Hermitian.
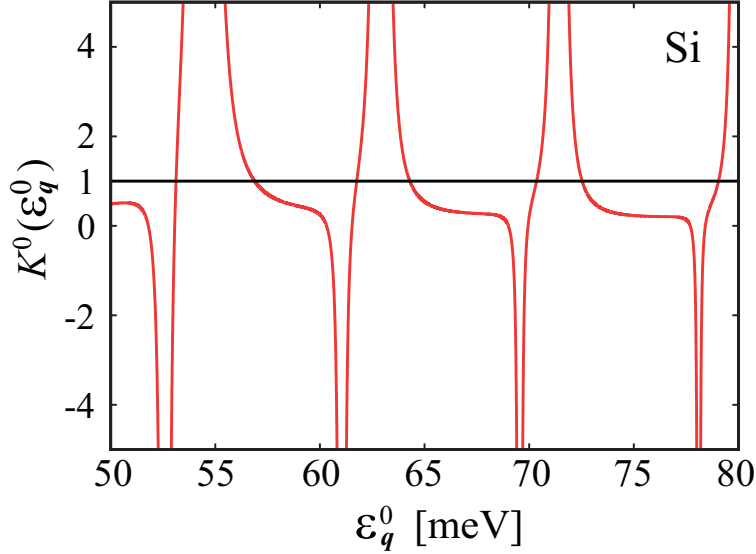
Figure C.1: A trace of $K^0(\mathcal{E}_{\boldsymbol{q}}^0)$ as a function of $\mathcal{E}_{\boldsymbol{q}}^0$ (in the unit of meV). $K^0(\mathcal{E}_{\boldsymbol{q}}^0) = 1$ is shown by a horizontal solid line.

Figure C.2 shows this set of eigenvalues as a function of time. It seems that these energy curves well reproduce those in Fig. 3.2 calculated without the bosonization scheme. This fact would demonstrate the validity of this scheme. Moreover, it is noted that even after the completion of the laser irradiation, $\bar{\Omega}_{\boldsymbol{k}cv}^{(R)}$ does not vanish because of the Coulomb correction. In the case of $\bar{\Omega}_{\boldsymbol{k}cv}^{(R)} = 0$, we obtain just solutions of $\mathcal{E}_{\boldsymbol{q}}^0 = \pm\omega_{\boldsymbol{q}pl}$ for Eq. (C.12), and the solutions of the electron-hole continua of Fig. C.2 vanish. Therefore, the Coulomb correction is essential so as to form the continuum states. The continuum states are coupled with the LO phonon, resulting in FR after the completion of the laser irradiation.

According to Fig. C.1, it is seen that the eigenvalues belonging to the continuum states β's are located in the vicinity of the poles attributed to the denominator in the square brackets of the right-hand side of Eq. (C.13), except for a solution of $\mathcal{E}_{\boldsymbol{q}\alpha_1}^0$ corresponding to the plasmon. Hence, the eigenvalue for the βth state is well approximated to be

$$\mathcal{E}_{\boldsymbol{q}\beta}^0 \approx \pm\sqrt{\bar{\omega}_{cv\boldsymbol{k}\boldsymbol{q}}^2 + |2\bar{\Omega}_{\boldsymbol{k}cv}^{(R)}|^2}, \tag{C.15}$$

and furthermore, we can consider the index β to be approximately equal to Bloch momentum $|\boldsymbol{k}|$: as regards plus and minus signs of Eq. (C.15), consult Eq.(B.68).

C.2 Approximate Solutions of $F_{\boldsymbol{q}\beta}^{\dagger}$ and $F_{\boldsymbol{q}\beta}$

We solve Eq. (2.61) in an approximate manner in terms of the PQ operators of $F_{\boldsymbol{q}\beta}^{0\dagger}$ introduced above. [Refer to Secs. 2.3.1 and 2.3.2 for the approximation employed.] To do this, firstly we define a new operator $\tilde{F}_{\boldsymbol{q}\beta}^{0\dagger}$ as

$$\tilde{F}_{\boldsymbol{q}\beta}^{0\dagger}(t) = F_{\boldsymbol{q}\beta}^{0\dagger}(t)\, e^{-3_{\boldsymbol{q}\beta}^{*}(t,t_0)}, \tag{C.16}$$

70
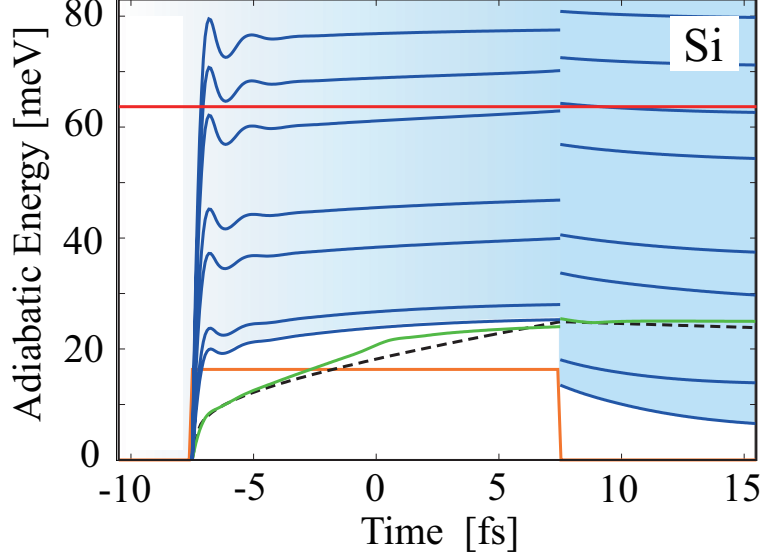
Figure C.2: Adiabatic energy curves of Si (in the unit of meV) as a function of time t (in the unit of fs). The curves are calculated on the basis of Eq. (C.12). A green solid line represents a plasmon-like mode, and blue solid lines represent a bundle of the electron-hole continua. Further, an orange line represents the alternation of bare Rabi frequency Ω_{0cv} of squared shape [see Eqs. (2.7) and (2.66)] as a function of t. In addition, a red solid line represents the LO phonon energy $\omega_{\boldsymbol{q}} = 63$ meV, and a broken line represents the plasma frequency $\omega_{\boldsymbol{q}pl}$ proportional to the total electron density, just for the purpose of comparison of the plasmon-like mode. The gradation of blue color shows the schematic change of the excited carrier density in t, where the lowest limit of the gradation means the threshold energy of a bundle of the electron-hole continua.

where t_0 represents initial time when an initial condition is imposed before the laser irradiation: $t_0 < -\tau_L/2$. Here, both effects of the non-adiabatic correction due to diagonal components and the phenomenological damping are incorporated in

$$\mathfrak{Z}_{\boldsymbol{q}\beta}(t, \tilde{t}) = \int_{\tilde{t}}^{t} dt' \left[\frac{\gamma_{\boldsymbol{q}\beta}^{(0)}(t')}{2} + I_{\boldsymbol{q}\beta\beta}^*(t') \right]. \tag{C.17}$$

For the sake of later convenience, we define $\mathfrak{I}_{\boldsymbol{q}\beta}(t, \tilde{t})$ as

$$\mathfrak{I}_{\boldsymbol{q}\beta}(t, \tilde{t}) = \int_{\tilde{t}}^{t} dt' I_{\boldsymbol{q}\beta\beta}^*(t'). \tag{C.18}$$

Consulting Eq. (C.2), it is seen that $\tilde{F}_{\boldsymbol{q}\beta}^{0\dagger}(t)$ fulfills the equation of motion provided by

$$-i \frac{d}{dt} \tilde{F}_{\boldsymbol{q}\beta}^{0\dagger}(t) = \tilde{F}_{\boldsymbol{q}\beta}^{0\dagger}(t) \left\{ \mathcal{E}_{\boldsymbol{q}\beta}^{0}(t) + i \left[\frac{\gamma_{\boldsymbol{q}\beta}^{(0)}(t)}{2} + I_{\boldsymbol{q}\beta\beta}(t) \right] \right\}. \tag{C.19}$$

Subtracting Eq. (C.19) from Eq. (2.61) side by side, and defining $\Delta F_{\boldsymbol{q}\beta}^{\dagger}$ as

$$\Delta F_{\boldsymbol{q}\beta}^{\dagger} = F_{\boldsymbol{q}\beta}^{\dagger} - \tilde{F}_{\boldsymbol{q}\beta}^{0\dagger}, \tag{C.20}$$

71

we obtain the following equation of motion as:

$$-i\frac{d}{dt}\Delta F_{\boldsymbol{q}\beta}^{\dagger}(t) = \Delta F_{\boldsymbol{q}\beta}^{\dagger}(t)\left\{\mathcal{E}_{\boldsymbol{q}\beta}(t) + i\left[\frac{\gamma_{\boldsymbol{q}\beta}^{(0)}(t)}{2} + I_{\boldsymbol{q}\beta\beta}(t)\right]\right\} + \tilde{F}_{\boldsymbol{q}\beta}^{0\dagger}(t)\left[\mathcal{E}_{\boldsymbol{q}\beta}(t) - \mathcal{E}_{\boldsymbol{q}\beta}^{0}(t)\right]$$

$$+i\sum_{\beta'(\neq\beta)}\left[\tilde{F}_{\boldsymbol{q}\beta'}^{0\dagger}(t) + \Delta F_{\boldsymbol{q}\beta'}^{\dagger}(t)\right]I_{\boldsymbol{q}\beta'\beta}(t). \tag{C.21}$$

The formal solution of this is given by

$$\Delta F_{\boldsymbol{q}\beta}^{\dagger}(t) = \Delta F_{\boldsymbol{q}\beta}^{\dagger}(t_0)e^{i\Theta_{\boldsymbol{q}\beta}^{*}(t,t_0)} + i\int_{t_0}^{t}dt'\,\tilde{F}_{\boldsymbol{q}\beta}^{0\dagger}(t')\left[\mathcal{E}_{\boldsymbol{q}\beta}(t') - \mathcal{E}_{\boldsymbol{q}\beta}^{0}(t')\right]e^{-i\left[\Theta_{\boldsymbol{q}\beta}^{*}(t',t_0) - \Theta_{\boldsymbol{q}\beta}^{*}(t,t_0)\right]}$$

$$-\sum_{\beta'(\neq\beta)}\int_{t_0}^{t}dt'\left[\tilde{F}_{\boldsymbol{q}\beta'}^{0\dagger}(t') + \Delta F_{\boldsymbol{q}\beta'}^{\dagger}(t')\right]I_{\boldsymbol{q}\beta'\beta}(t')e^{-i\left[\Theta_{\boldsymbol{q}\beta}^{*}(t',t_0) - \Theta_{\boldsymbol{q}\beta}^{*}(t,t_0)\right]}, \tag{C.22}$$

where $\Theta_{\boldsymbol{q}\beta}(t,t')$ represents an adiabatic energy phase provided by

$$\Theta_{\boldsymbol{q}\beta}(t,t') = \int_{t'}^{t}dt''\left\{\mathcal{E}_{\boldsymbol{q}\beta}^{*}(t'') - i\left[\frac{\gamma_{\boldsymbol{q}\beta}^{(0)}(t'')}{2} + I_{\boldsymbol{q}\beta\beta}^{*}(t'')\right]\right\}. \tag{C.23}$$

It is supposed that the initial condition of the above equation is provided by

$$\Delta F_{\boldsymbol{q}\beta}^{\dagger}(t_0) = 0, \tag{C.24}$$

that is, $F_{\boldsymbol{q}\beta}^{\dagger}(t_0) = F_{\boldsymbol{q}\beta}^{0\dagger}(t_0)$, with an additional approximation that $\mathcal{E}_{\boldsymbol{q}\beta}^{*}(t) \approx \mathcal{E}_{\boldsymbol{q}\beta}^{0}(t)$, leading to

$$\Theta_{\boldsymbol{q}\beta}(t,t') \approx \int_{t'}^{t}dt'\left\{\mathcal{E}_{\boldsymbol{q}\beta}^{0}(t'') - i\left[\frac{\gamma_{\boldsymbol{q}\beta}^{(0)}(t'')}{2} + I_{\boldsymbol{q}\beta\beta}^{*}(t'')\right]\right\}. \tag{C.25}$$

Therefore, Eq. (C.22) becomes

$$\Delta F_{\boldsymbol{q}\beta}^{\dagger}(t) \approx -\sum_{\beta'(\neq\beta)}\int_{t_0}^{t}dt'\left[\tilde{F}_{\boldsymbol{q}\beta'}^{0\dagger}(t') + \Delta F_{\boldsymbol{q}\beta'}^{\dagger}(t')\right]I_{\boldsymbol{q}\beta'\beta}(t')e^{-i\left[\Theta_{\boldsymbol{q}\beta}^{*}(t',t_0) - \Theta_{\boldsymbol{q}\beta}^{*}(t,t_0)\right]}. \tag{C.26}$$

By putting Eq. (2.67) into Eq. (C.26), we obtain

$$\Delta F_{\boldsymbol{q}\beta}^{\dagger}(t) \approx -\sum_{j}\sum_{\beta'(\neq\beta)}\left[\tilde{F}_{\boldsymbol{q}\beta'}^{0\dagger}(t_j) + \Delta F_{\boldsymbol{q}\beta'}^{\dagger}(t_j)\right]\mathfrak{I}_{\boldsymbol{q}\beta'\beta}^{(j)*}\theta(t - t_j)e^{-i\left[\Theta_{\boldsymbol{q}\beta}^{*}(t_j,t_0) - \Theta_{\boldsymbol{q}\beta}^{*}(t,t_0)\right]}. \tag{C.27}$$

As described in Sec. 2.3.1, from among a set of the off-diagonal elements of the non-adiabatic interaction, we retain just the single leading contribution at $t = t_D = \tau_L/2$. Thus, we obtain

$$\Delta F_{\boldsymbol{q}\beta}^{\dagger}(t_D) \approx -\sum_{\beta'}\tilde{F}_{\boldsymbol{q}\beta'}^{0\dagger}(t_D)\left[\phi_{\boldsymbol{q}}(t_D)\frac{1}{1 + \phi_{\boldsymbol{q}}(t_D)}\right]_{\beta'\beta}, \tag{C.28}$$

where

$$\phi_{\boldsymbol{q}\beta'\beta}(t) = \mathfrak{I}_{\boldsymbol{q}\beta'\beta}^{(D)*}\theta(t - t_D)\bar{\delta}_{\beta'\beta} \tag{C.29}$$

72

with $\bar{\delta}_{\beta'\beta} = 1 - \delta_{\beta'\beta}$. If we consider more than two contributions of $\{\mathfrak{I}_{\boldsymbol{q}\beta'\neq\beta}^{(j)}\}$, we obtain a set of $\Delta F_{\boldsymbol{q}\beta}^{\dagger}(t_j)$'s in a more complicated closed-form than Eq. (C.28). Hereafter, we simply take account of just $\mathfrak{I}_{\boldsymbol{q}\beta'\beta}^{(D)}$ since the present theoretical framework is described succinctly.

By putting Eq. (C.28) back into Eq. (C.27), we obtain $\Delta F_{\boldsymbol{q}\beta}^{\dagger}(t)$ as

$$\Delta F_{\boldsymbol{q}\beta}^{\dagger}(t) \approx -e^{i\Theta_{\boldsymbol{q}\beta}^{*}(t,t_0)} \sum_{\beta'} F_{\boldsymbol{q}\beta'}^{0\dagger}(t_0) \left[\frac{1}{1+\tilde{\phi}_{\boldsymbol{q}}(t_D)} \tilde{\phi}_{\boldsymbol{q}}(t) \right]_{\beta'\beta}, \qquad (C.30)$$

where $\tilde{\phi}_{\boldsymbol{q}}$ is defined as

$$\tilde{\phi}_{\boldsymbol{q}\beta'\beta}(t) = e^{i\Theta_{\beta'}^{*}(t_D,t_0)} \phi_{\boldsymbol{q}\beta'\beta}(t) e^{-i\Theta_{\beta}^{*}(t_D,t_0)}, \qquad (C.31)$$

and Eq. (C.16) is used. Therefore, in view of Eq. (C.20), $F_{\boldsymbol{q}\beta}^{\dagger}(t)$ is provided by

$$\begin{aligned} F_{\boldsymbol{q}\beta}^{\dagger}(t) &= e^{i\Theta_{\boldsymbol{q}\beta}^{*}(t,t_0)} \sum_{\beta'} F_{\boldsymbol{q}\beta'}^{0\dagger}(t_0) \left[\frac{1+\tilde{\phi}_{\boldsymbol{q}}(t_D) - \tilde{\phi}_{\boldsymbol{q}}(t)}{1+\tilde{\phi}_{\boldsymbol{q}}(t_D)} \right]_{\beta'\beta} \\ &= e^{i\Theta_{\boldsymbol{q}\beta}^{*}(t,t_D)} \sum_{\beta'} F_{\boldsymbol{q}\beta'}^{0\dagger}(t_D) \mathcal{T}_{\boldsymbol{q}\beta'\beta}'(t), \end{aligned} \qquad (C.32)$$

and by taking its Hermitian-conjugate, we obtain

$$F_{\boldsymbol{q}\beta}(t) = e^{-i\Theta_{\boldsymbol{q}\beta}(t,t_D)} \sum_{\beta'} \mathcal{T}_{\boldsymbol{q}\beta\beta'}'^{\dagger}(t) F_{\boldsymbol{q}\beta'}^{0}(t_D). \qquad (C.33)$$

Here, the off-diagonal components of the non-adiabatic interaction are incorporated to $\mathcal{T}_{\boldsymbol{q}}'(t)$ defined as

$$\mathcal{T}_{\boldsymbol{q}\beta'\beta}'(t) = \left[\frac{1+\tilde{\phi}_{\boldsymbol{q}}(t_D) - \tilde{\phi}_{\boldsymbol{q}}(t)}{1+\tilde{\phi}_{\boldsymbol{q}}(t_D)} \right]_{\beta'\beta} e^{-\mathfrak{I}_{\boldsymbol{q}\beta}^{*}(t_D,t_0)}. \qquad (C.34)$$

The retarded Green function is defined in terms of $F_{\boldsymbol{q}}$ and $F_{\boldsymbol{q}}^{\dagger}$ as [79, 80]

$$G_{\boldsymbol{q}\beta\beta'}^{R}(t,t') = -i\theta(t-t') \left\langle \left[F_{\boldsymbol{q}\beta}(t), F_{\boldsymbol{q}\beta'}^{\dagger}(t') \right] \right\rangle, \qquad (C.35)$$

and the concomitant advanced Green function is provided by

$$G_{\boldsymbol{q}\beta\beta'}^{A}(t,t') = \left[G_{\boldsymbol{q}\beta'\beta}^{R}(t',t) \right]^{*}. \qquad (C.36)$$

Putting Eqs. (C.32) and (C.33) into Eq. (C.35), the retarded Green function ends up with

$$G_{\boldsymbol{q}\beta\beta'}^{R}(t,t') = -i\theta(t-t') e^{-i\Theta_{\boldsymbol{q}\beta}(t,t_D)} \sum_{\gamma\gamma'} V_{\boldsymbol{q}\beta\gamma}^{R\dagger}(t_D) T_{\boldsymbol{q}\gamma\gamma'}(t,t') V_{\boldsymbol{q}\gamma'\beta'}^{R}(t_D) e^{i\Theta_{\boldsymbol{q}\beta'}^{*}(t',t_D)}, \quad (C.37)$$

where Eq. (C.7) is employed. Here, we introduce the matrix of $T_{\boldsymbol{q}}$ for the purpose of later convenience as

$$T_{\boldsymbol{q}}(t,t') = \mathcal{T}_{\boldsymbol{q}}^{\dagger}(t) \mathcal{T}_{\boldsymbol{q}}(t') \qquad (C.38)$$

with

$$\mathcal{T}_{\boldsymbol{q}}(t) = \mathcal{T}_{\boldsymbol{q}}'(t) \bar{V}_{\boldsymbol{q}}^{R}(t_D). \qquad (C.39)$$

73

Similarly to Eq. (C.37), we evaluate the expectation values of equal-time commutation relations for the PQ operators as

$$\langle[F_{\boldsymbol{q}\beta}(t), F^\dagger_{\boldsymbol{q}'\beta'}(t)]\rangle = e^{-i\Theta_{\boldsymbol{q}\beta}(t,t_D)} \sum_{\gamma\gamma'} V^{R\dagger}_{\boldsymbol{q}\beta\gamma}(t_D) T_{\boldsymbol{q}\gamma\gamma'}(t,t) V^R_{\boldsymbol{q}\gamma'\beta'}(t_D) e^{i\Theta^*_{\boldsymbol{q}\beta'}(t,t_D)}, \qquad (C.40)$$

and

$$\langle[F_{\boldsymbol{q}\beta}(t), F_{\boldsymbol{q}'\beta'}(t)]\rangle = \langle[F^\dagger_{\boldsymbol{q}\beta}(t), F^\dagger_{\boldsymbol{q}'\beta'}(t)]\rangle = 0, \qquad (C.41)$$

due to Eq. (C.8).

C.3 Bosonization Scheme and its Approximate Validity

First, we evaluate the expectation value of $\langle[B_{\boldsymbol{q}\alpha}, B^\dagger_{\boldsymbol{q}'\alpha'}]\rangle$, and it is reduced to

$$
\begin{aligned}
\langle[B_{\boldsymbol{q}\alpha}, B^\dagger_{\boldsymbol{q}'\alpha'}]\rangle &= \sum_{\boldsymbol{k}\boldsymbol{k}'b_1'b_1'b_2b_2'} U^{R\dagger}_{\boldsymbol{q}\alpha}(\boldsymbol{k}b_1b_1')\langle[\bar{A}_{\boldsymbol{q}}(\boldsymbol{k}b_1b_1'), \bar{A}^\dagger_{\boldsymbol{q}'}(\boldsymbol{k}'b_2b_2')]\rangle U^R_{\boldsymbol{q}'\alpha'}(\boldsymbol{k}'b_2b_2') \\
&= \delta_{\boldsymbol{q}\boldsymbol{q}'} \sum_{\boldsymbol{k}b_2b_3} \left\{ \sum_{\boldsymbol{k}b_1} \left[U^{R\dagger}_{\boldsymbol{q}\alpha}(\boldsymbol{k}b_1b_2)\bar{\rho}_{b_1b_3\boldsymbol{k}} - U^{R\dagger}_{\boldsymbol{q}\alpha}(\boldsymbol{k}b_3b_1)\bar{\rho}_{b_2b_1\boldsymbol{k}+\boldsymbol{q}} \right] \right\} \\
&\quad \times U^R_{\boldsymbol{q}\alpha'}(\boldsymbol{k}b_2b_3), \qquad (C.42)
\end{aligned}
$$

where Eqs. (2.38) and (2.39) are employed in the first equality. Here, we define $\bar{U}^{L\dagger}_{\boldsymbol{q}\alpha}$ as the term in the curl brackets of the second equality of the right-hand side of Eq. (C.42), that is,

$$\bar{U}^{L\dagger}_{\boldsymbol{q}\alpha}(\boldsymbol{k}b_2b_3) = N^{R*}_{\boldsymbol{q}\alpha} V^{(C)}_{\boldsymbol{q}} \bar{u}^{L\dagger}_{\boldsymbol{q}\alpha}(\boldsymbol{k}b_2b_3), \qquad (C.43)$$

where

$$\bar{u}^{L\dagger}_{\boldsymbol{q}\alpha}(\boldsymbol{k}b_2b_3) = \sum_{b_1} \left[u^{R\dagger}_{\boldsymbol{q}\alpha}(\boldsymbol{k}b_1b_2)\bar{\rho}_{b_1b_3\boldsymbol{k}} - u^{R\dagger}_{\boldsymbol{q}\alpha}(\boldsymbol{k}b_3b_1)\bar{\rho}_{b_2b_1\boldsymbol{k}+\boldsymbol{q}} \right]. \qquad (C.44)$$

Thus, Eq. (C.42) is cast into the form

$$\langle[B_{\boldsymbol{q}\alpha}, B^\dagger_{\boldsymbol{q}'\alpha'}]\rangle = \delta_{\boldsymbol{q}\boldsymbol{q}'} \sum_{\boldsymbol{k}b_2b_3} \bar{U}^{L\dagger}_{\boldsymbol{q}\alpha}(\boldsymbol{k}b_2b_3) U^R_{\boldsymbol{q}\alpha'}(\boldsymbol{k}b_2b_3). \qquad (C.45)$$

If $\bar{U}^{L\dagger}_{\boldsymbol{q}\alpha}(\boldsymbol{k}b_2b_3)$ were exactly in agreement with $U^{L\dagger}_{\boldsymbol{q}\alpha}(\boldsymbol{k}b_2b_3)$, the expectation value of present concern would satisfy a desirable relation of

$$\langle[B_{\boldsymbol{q}\alpha}, B^\dagger_{\boldsymbol{q}'\alpha'}]\rangle = \delta_{\boldsymbol{q}\boldsymbol{q}'}\delta_{\alpha\alpha'} \qquad (C.46)$$

due to $U^{L\dagger}_{\boldsymbol{q}} U^R_{\boldsymbol{q}} = 1$.

Below, we evaluate the following quantity:

$$
\begin{aligned}
x_{\alpha\alpha'} &= \left| \delta_{\alpha\alpha'} - \langle[B_{\boldsymbol{q}\alpha}, B^\dagger_{\boldsymbol{q}'\alpha'}]\rangle \right| \\
&= \left| \sum_{\boldsymbol{k}bb'} \left[U^{L\dagger}_{\boldsymbol{q}\alpha}(\boldsymbol{k}bb') - \bar{U}^{L\dagger}_{\boldsymbol{q}\alpha}(\boldsymbol{k}bb') \right] U^R_{\boldsymbol{q}\alpha'}(\boldsymbol{k}bb') \right| \\
&= \left| N^L_{\boldsymbol{q}\alpha} N^R_{\boldsymbol{q}\alpha'} (V^{(C)}_{\boldsymbol{q}})^2 \sum_{\boldsymbol{k}bb'} \left[u^{L\dagger}_{\boldsymbol{q}\alpha}(\boldsymbol{k}bb') - \frac{N^{R*}_{\boldsymbol{q}\alpha'}}{N^L_{\boldsymbol{q}\alpha}} \bar{u}^{L\dagger}_{\boldsymbol{q}\alpha}(\boldsymbol{k}bb') \right] u^R_{\boldsymbol{q}\alpha'}(\boldsymbol{k}bb') \right|, \quad (C.47)
\end{aligned}
$$

where Eqs. (B.21)-(B.24) and (B.42)-(B.45) are used in the last equality. $x_{\alpha\alpha'}$ plays a role for an estimate of the criterion of the validity of concern.

We evaluate this expression in the small-$|\boldsymbol{q}|$ limit. In terms of the power series with respect to the ratio of the Rabi frequency $\bar{\Omega}_{\boldsymbol{k}cv}^{(R)}$ of Eq. (2.19) to adiabatic energy $\mathcal{E}_{\boldsymbol{q}\alpha}$, namely,

$$r_{\boldsymbol{k}\boldsymbol{q}\alpha} \equiv \frac{\bar{\Omega}_{\boldsymbol{k}cv}^{(R)}}{\mathcal{E}_{\boldsymbol{q}\alpha}}, \tag{C.48}$$

the summation in the last equality of Eq. (C.47) is expressed as

$$\sum_{\boldsymbol{k}bb'} \left[u_{\boldsymbol{q}\alpha}^{L\dagger}(\boldsymbol{k}bb') - \frac{N_{\boldsymbol{q}\alpha'}^{R*}}{N_{\boldsymbol{q}\alpha}^{L}} \bar{u}_{\boldsymbol{q}\alpha}^{L\dagger}(\boldsymbol{k}bb') \right] u_{\boldsymbol{q}\alpha'}^{R}(\boldsymbol{k}bb')$$

$$= -\frac{\boldsymbol{q}^2}{\mathcal{E}_{\boldsymbol{q}\alpha}\mathcal{E}_{\boldsymbol{q}\alpha'}} \left[\left(\frac{1}{\mathcal{E}_{\boldsymbol{q}\alpha}} + \frac{1}{\mathcal{E}_{\boldsymbol{q}\alpha'}} \right) - \frac{N_{\boldsymbol{q}\alpha'}^{R*}}{N_{\boldsymbol{q}\alpha}^{L}} \left(\frac{1}{\mathcal{E}_{\boldsymbol{q}\alpha}^{*}} + \frac{1}{\mathcal{E}_{\boldsymbol{q}\alpha'}} \right) \right] \sum_{\boldsymbol{k}b} (\hat{\boldsymbol{q}} \cdot \nabla \bar{\rho}_{bb\boldsymbol{k}})(\hat{\boldsymbol{q}} \cdot \nabla \varepsilon_{\boldsymbol{k}b}^{(r)})$$

$$+ \sideset{}{'}\sum_{n,n'} \sum_{\boldsymbol{k}} (\text{terms factorized by } r_{\boldsymbol{k}\boldsymbol{q}\alpha}^{n} r_{\boldsymbol{k}\boldsymbol{q}\alpha'}^{n'}) \tag{C.49}$$

Here, $\sum'$ means that the summation over n and n' are taken except for the term with $n = n' = 0$.

As is stated in Sec. 2.3.2, we are concerned particularly with the temporal region after the completion of the laser irradiation. In this region, Eq. (C.48) is described by the ratio of the Coulomb correction to adiabatic energy, that is,

$$r_{\boldsymbol{k}\boldsymbol{q}\alpha} = \frac{\sum_{\boldsymbol{q}} V_{\boldsymbol{q}}^{(C)} \bar{\rho}_{cv\boldsymbol{k}+\boldsymbol{q}}}{\mathcal{E}_{\boldsymbol{q}\alpha}}. \tag{C.50}$$

The adiabatic energy of concern is around the LO phonon energy $\omega_{\boldsymbol{q}}$, and $\omega_{\boldsymbol{q}} = 63$ meV for Si and 35 meV for GaAs. On the other hand, according to our calculation, the magnitude of the Coulomb correction is of the order of several meV at most. Therefore, the second term in the right-hand side of Eq. (C.49) is negligibly small compared with the first term.

Further, additional conditions are imposed on Eq. (C.49) so as to satisfy that $x_{\alpha\alpha'}$ almost vanishes as follows: the first is that the limited set of $\{\alpha\}$ with $\mathcal{E}_{\boldsymbol{q}\alpha}$ of real is retained out of the solutions of Eqs. (2.33) and (2.34), and the second is that

$$N_{\boldsymbol{q}\alpha}^{R*} = N_{\boldsymbol{q}\alpha}^{L}. \tag{C.51}$$

Most of the solutions of Eq. (C.13), namely, $\mathcal{E}_{\boldsymbol{q}\alpha}^{0}$ are real or satisfy $|\text{Re}\mathcal{E}_{\boldsymbol{q}\alpha}^{0}| \gg |\text{Im}\mathcal{E}_{\boldsymbol{q}\alpha}^{0}|$, which ensures the first condition. Further, the corresponding normalization constants with

$$N_{\boldsymbol{q}\alpha}^{L} N_{\boldsymbol{q}\alpha}^{R} = |N_{\boldsymbol{q}\alpha}^{L}|^2 > 0 \tag{C.52}$$

provide $N_{\boldsymbol{q}\alpha}^{L} = N_{\boldsymbol{q}\alpha}^{R} = N_{\boldsymbol{q}\alpha}^{0}$ of real c-numbers. Eventually, Eq. (C.9) proves to be approximately correct. Moreover as a result of the approximation made here, the relation of Eq. (C.10) can be assumed, and thus, the effective coupling constants of $M_{-\boldsymbol{q}\alpha}''$ and $M_{\boldsymbol{q}\alpha}'^{*}$ are reduced to $M_{-\boldsymbol{q}\alpha}'' = 0$ and $M_{\boldsymbol{q}\alpha}'^{*} = M_{\boldsymbol{q}\alpha}^{*}$, respectively.

C.4 Solutions of the Fano Problem given by Adiabatic Coupled-Equations of Eq. (C.3)

In this section, we seek solutions of the Fano Problem provided by Eq. (C.3). Hereafter, just for the sake of typographical simplicity, we omit a superscript "0" of $h_{\boldsymbol{q}}^0$, $N_{\boldsymbol{q}}^0$, $E_{\boldsymbol{q}}^0$, and $\mathcal{E}_{\boldsymbol{q}}^0$, and replace these notations with non-superscript counterparts of $h_{\boldsymbol{q}}$, $N_{\boldsymbol{q}}$, $E_{\boldsymbol{q}}$, and $\mathcal{E}_{\boldsymbol{q}}$, respectively, as far as it is not likely to cause unnecessary confusion between them. Therefore, Eq. (C.3) is read as

$$h_{\boldsymbol{q}} V_{\boldsymbol{q}} = V_{\boldsymbol{q}} \mathcal{E}_{\boldsymbol{q}}, \tag{C.53}$$

where the Hermitian matrix $h_{\boldsymbol{q}}$ is provided by

$$h_{\boldsymbol{q}} = \begin{bmatrix} \mathcal{E}_{\boldsymbol{q}} & 0 & M_{\boldsymbol{q}} \\ 0 & \omega_{\boldsymbol{q}\alpha_1} & M_{\boldsymbol{q}\alpha_1} \\ M_{\boldsymbol{q}}^\dagger & M_{\boldsymbol{q}\alpha_1}^* & \omega_{\boldsymbol{q}\alpha_2} \end{bmatrix} \equiv \begin{bmatrix} \mathcal{E}_{\boldsymbol{q}} & z_{\boldsymbol{q}} \\ z_{\boldsymbol{q}}^\dagger & h_{\boldsymbol{q}}^{(d)} \end{bmatrix}. \tag{C.54}$$

Recalling the notations employed right below Eq. (2.58), N means the number of discretized continua. Here, $\mathcal{E}_{\boldsymbol{q}} = \{\mathcal{E}_{\boldsymbol{q}\beta}\delta_{\beta\beta'}\}$ represents a $(N \times N)$-diagonal matrix, $M_{\boldsymbol{q}} = \{M_{\boldsymbol{q}\beta}\}$ is a $(N \times 1)$-matrix, $\omega_{\boldsymbol{q}\alpha_1} \equiv \mathcal{E}_{\boldsymbol{q}\alpha_1}$, and $\omega_{\boldsymbol{q}\alpha_2} \equiv \omega_{\boldsymbol{q}}$. Moreover, $z_{\boldsymbol{q}}$ is a $(N \times 2)$-matrix and $h_{\boldsymbol{q}}^{(d)}$ is a (2×2)-matrix, provided by

$$z_{\boldsymbol{q}} = \begin{bmatrix} 0 & M_{\boldsymbol{q}} \end{bmatrix} \tag{C.55}$$

and

$$h_{\boldsymbol{q}}^{(d)} = \begin{bmatrix} \omega_{\boldsymbol{q}\alpha_1} & M_{\boldsymbol{q}\alpha_1} \\ M_{\boldsymbol{q}\alpha_1}^* & \omega_{\boldsymbol{q}\alpha_2} \end{bmatrix}, \tag{C.56}$$

respectively.

The Fano problem of concern is a scattering problem with a given energy $\mathcal{E}_{\boldsymbol{q}\beta}$ with one open-channel and two closed channels [47]. Hence, Eq. (C.53) is of the form of

$$h_{\boldsymbol{q}} \begin{bmatrix} \eta_{\boldsymbol{q}} \\ \nu_{\boldsymbol{q}} \end{bmatrix} = \begin{bmatrix} \eta_{\boldsymbol{q}} \\ \nu_{\boldsymbol{q}} \end{bmatrix} \mathcal{E}_{\boldsymbol{q}}, \tag{C.57}$$

where $\eta_{\boldsymbol{q}} = \{\eta_{\boldsymbol{q}\beta\beta}\}$ and $\nu_{\boldsymbol{q}} = \{\nu_{\boldsymbol{q}\mu\beta}\}$ $(\mu = \{\alpha_1, \alpha_2\})$ represent block matrices with size of $(N \times N)$ and $(2 \times N)$, respectively, and $V_{\boldsymbol{q}}$ is replaced by $V_{\boldsymbol{q}} = {}^t[\eta_{\boldsymbol{q}}, \nu_{\boldsymbol{q}}]$. We obtain explicit expressions of Eq. (C.57) as:

$$\mathcal{E}_{\boldsymbol{q}\beta'}\eta_{\boldsymbol{q}\beta'\beta} + \sum_{\mu} z_{\boldsymbol{q}\beta'\mu}\nu_{\boldsymbol{q}\mu\beta} = \eta_{\boldsymbol{q}\beta'\beta}\mathcal{E}_{\boldsymbol{q}\beta}, \tag{C.58}$$

and

$$\sum_{\beta'} z_{\boldsymbol{q}\beta'\mu}^*\eta_{\boldsymbol{q}\beta'\beta} + \sum_{\mu'} h_{\boldsymbol{q}\mu\mu'}^{(d)}\nu_{\boldsymbol{q}\mu'\beta} = \nu_{\boldsymbol{q}\mu\beta}\mathcal{E}_{\boldsymbol{q}\beta}. \tag{C.59}$$

Equation (C.58) is rewritten as

$$\eta_{\boldsymbol{q}\beta'\beta} = \left(\mathbb{P}\frac{1}{\mathcal{E}_{\boldsymbol{q}\beta} - \mathcal{E}_{\boldsymbol{q}\beta'}} + \Delta_{\boldsymbol{q}\beta}\delta_{\beta'\beta}\right)\sum_{\mu} z_{\boldsymbol{q}\beta'\mu}\nu_{\boldsymbol{q}\mu\beta}, \tag{C.60}$$

where $\mathbb{P}[1/(\mathcal{E}_{q\beta} - \mathcal{E}_{q\beta'})]$ means that a Cauchy's principle value of $[1/(\mathcal{E}_{q\beta} - \mathcal{E}_{q\beta'})]$ is taken, and $\Delta_{q\beta}$ is a constant to be determined later. By putting this expression back into Eq. (C.59), we obtain

$$\sum_{\mu'} \left[h^{(d)}_{q\mu\mu'} + \sigma_{q\mu\mu'}(\mathcal{E}_{q\beta}) \right] \nu_{q\mu'\beta} + \Delta_{q\beta} z^*_{q\beta\mu} \sum_{\mu'} z_{q\beta\mu'} \nu_{q\mu'\beta} = \nu_{q\mu\beta} \mathcal{E}_{q\beta}, \tag{C.61}$$

where $\sigma_{q\mu\mu'}(\mathcal{E}_{q\beta})$ is provided by

$$\sigma_{q\mu\mu'}(\mathcal{E}_{q\beta}) = \sum_{\beta'} \mathbb{P} \frac{z^*_{q\beta'\mu} z_{q\beta'\mu'}}{\mathcal{E}_{q\beta} - \mathcal{E}_{q\beta'}}. \tag{C.62}$$

We make the matrix elements in square brackets of the first term of the left-hand side of Eq. (C.61) diagonal in terms of a diagonalization matrix $A^{(r)}$ as follows:

$$\left[h^{(d)}_q + \sigma_q(\mathcal{E}_{q\beta}) \right]_{\mu\mu'} = \sum_{\mu''} A^{(r)}_{\mu'\mu''} \omega_{q\mu''} A^{(r)\dagger}_{\mu''\mu}, \tag{C.63}$$

with an eigenvalue as $\omega_{q\mu}$. Therefore, defining $\tilde{\nu}_q$ and $\tilde{z}_q$ as

$$\tilde{\nu}_{q\mu\beta} = \sum_{\nu'} A^{(r)\dagger}_{\mu\mu'} \nu_{q\mu'\beta}, \tag{C.64}$$

and

$$\tilde{z}_{q\beta\mu} = \sum_{\nu'} z_{q\beta\mu'} A^{(r)}_{\mu'\mu}, \tag{C.65}$$

Eq. (C.61) is cast into the form:

$$\tilde{\nu}_{q\mu\beta} = \Delta_{q\beta} \frac{\tilde{z}^*_{q\beta\mu}}{\mathcal{E}_{q\beta} - \omega_{q\mu}} \sum_{\mu'} \tilde{z}_{q\beta\mu'} \tilde{\nu}_{q\mu'\beta}, \tag{C.66}$$

where $\Delta_{q\beta}$ is determined by

$$\Delta^{-1}_{q\beta} = \sum_\mu \frac{|\tilde{z}_{q\beta\mu}|^2}{\mathcal{E}_{q\beta} - \omega_{q\mu}}. \tag{C.67}$$

According to the commutation relations of Eqs. (C.7) and (C.9), we obtain the following relations:

$$\sum_\beta \tilde{\nu}_{q\mu\beta} \tilde{\nu}^*_{q\mu'\beta} = \delta_{\mu\mu'}, \tag{C.68}$$

$$\sum_\beta \tilde{\nu}_{q\mu\beta} \eta^*_{q\beta'\beta} = 0, \quad \sum_\beta \eta_{q\beta'\beta} \tilde{\nu}^*_{q\mu\beta} = 0, \tag{C.69}$$

and

$$\sum_{\beta''} \eta_{q\beta\beta''} \eta^*_{q\beta'\beta''} = \delta_{\beta\beta'}, \tag{C.70}$$

where Eq. (C.5) is employed in view of Eq. (C.11). By putting Eq. (C.60) into the two equations of Eq. (C.69), and subtracting the resulting equations side by side, we obtain

$$\sum_{\beta''} \tilde{z}_{q\beta\beta''} \left(\mathbb{P} \frac{1}{\mathcal{E}_{q\beta''} - \mathcal{E}_{q\beta}} - \mathbb{P} \frac{1}{\mathcal{E}_{q\beta''} - \mathcal{E}_{q\beta'}} \right) \tilde{z}^\dagger_{q\beta''\beta'} = \tilde{z}_{q\beta\beta'} \Delta_{q\beta'} \tilde{z}^\dagger_{q\beta'\beta'} - \tilde{z}_{q\beta\beta} \Delta_{q\beta} \tilde{z}^\dagger_{q\beta\beta'}, \tag{C.71}$$

where

$$\tilde{\mathcal{Z}}_{\boldsymbol{q}\beta\beta'} = \sum_{\mu} \tilde{z}_{\boldsymbol{q}\beta\mu}\tilde{\nu}_{\boldsymbol{q}\mu\beta'}. \tag{C.72}$$

Moreover, applying Eq. (C.60) to Eq. (C.70) again yields

$$
\begin{aligned}
\delta_{\beta\beta'} &= \sum_{\beta''} \tilde{\mathcal{Z}}_{\boldsymbol{q}\beta\beta''}\mathbb{P}\left(\frac{1}{\mathcal{E}_{\boldsymbol{q}\beta''} - \mathcal{E}_{\boldsymbol{q}\beta}}\frac{1}{\mathcal{E}_{\boldsymbol{q}\beta''} - \mathcal{E}_{\boldsymbol{q}\beta'}}\right)\tilde{\mathcal{Z}}_{\boldsymbol{q}\beta''\beta'}^{\dagger} + \tilde{\mathcal{Z}}_{\boldsymbol{q}\beta\beta}\Delta_{\boldsymbol{q}\beta}\mathbb{P}\frac{1}{\mathcal{E}_{\boldsymbol{q}\beta} - \mathcal{E}_{\boldsymbol{q}\beta'}}\tilde{\mathcal{Z}}_{\boldsymbol{q}\beta\beta'} \\
&\quad - \tilde{\mathcal{Z}}_{\boldsymbol{q}\beta\beta'}\Delta_{\boldsymbol{q}\beta'}\mathbb{P}\frac{1}{\mathcal{E}_{\boldsymbol{q}\beta} - \mathcal{E}_{\boldsymbol{q}\beta'}}\tilde{\mathcal{Z}}_{\boldsymbol{q}\beta'\beta'} + \delta_{\beta\beta'}\Delta_{\boldsymbol{q}\beta}^{2}|\tilde{\mathcal{Z}}_{\boldsymbol{q}\beta\beta}|^{2} \\
&= \delta_{\beta\beta'}\left[(\pi\rho_{\boldsymbol{q}\beta})^{2} + \Delta_{\boldsymbol{q}\beta}^{2}\right]|\tilde{\mathcal{Z}}_{\boldsymbol{q}\beta\beta}|^{2},
\end{aligned}
\tag{C.73}
$$

where in the first equality, Eq. (C.72) is employed. Further, in the second equality, Poincaré's theorem is applied, that is,

$$
\begin{aligned}
\mathbb{P}\left(\frac{1}{\mathcal{E}_{\boldsymbol{q}\beta''} - \mathcal{E}_{\boldsymbol{q}\beta}}\frac{1}{\mathcal{E}_{\boldsymbol{q}\beta''} - \mathcal{E}_{\boldsymbol{q}\beta'}}\right) &= \frac{1}{\mathcal{E}_{\boldsymbol{q}\beta} - \mathcal{E}_{\boldsymbol{q}\beta'}}\left(\mathbb{P}\frac{1}{\mathcal{E}_{\boldsymbol{q}\beta''} - \mathcal{E}_{\boldsymbol{q}\beta}} - \mathbb{P}\frac{1}{\mathcal{E}_{\boldsymbol{q}\beta''} - \mathcal{E}_{\boldsymbol{q}\beta'}}\right) \\
&\quad + \pi^{2}\delta(\mathcal{E}_{\boldsymbol{q}\beta''} - \mathcal{E}_{\boldsymbol{q}\beta})\delta(\mathcal{E}_{\boldsymbol{q}\beta''} - \mathcal{E}_{\boldsymbol{q}\beta'}),
\end{aligned}
\tag{C.74}
$$

where a density of state $\rho_{\boldsymbol{q}\beta}$ of state β is defined as

$$\rho_{\boldsymbol{q}\beta} = \frac{d\beta}{d\mathcal{E}_{\boldsymbol{q}\beta}}. \tag{C.75}$$

Here, by substituting $\mathcal{Z}_{\boldsymbol{q}\beta}$ for $\Delta_{\boldsymbol{q}\beta}\tilde{\mathcal{Z}}_{\boldsymbol{q}\beta\beta}$ just for the sake of simplicity, we obtain

$$\mathcal{Z}_{\boldsymbol{q}\beta} = \Delta_{\boldsymbol{q}\beta}\tilde{\mathcal{Z}}_{\boldsymbol{q}\beta\beta} = \left[1 + \left(\pi\rho_{\boldsymbol{q}\beta}\sum_{\mu}\frac{|\tilde{z}_{\boldsymbol{q}\beta\mu}|^{2}}{\mathcal{E}_{\boldsymbol{q}\beta} - \omega_{\boldsymbol{q}\mu}}\right)^{2}\right]^{-1/2} \tag{C.76}$$

from Eq. (C.73) in view of Eq. (C.67).

Therefore, from Eq. (C.66), we readily obtain

$$\tilde{\nu}_{\boldsymbol{q}\mu\beta} = \frac{\tilde{z}_{\boldsymbol{q}\beta\mu}^{*}}{\mathcal{E}_{\boldsymbol{q}\beta} - \omega_{\boldsymbol{q}\mu}}\mathcal{Z}_{\boldsymbol{q}\beta}, \tag{C.77}$$

and eventually, $\nu_{\boldsymbol{q}\mu\beta}$ is given by means of Eq. (C.64). Further, by putting Eq. (C.77) into Eq. (C.72), we obtain the expression of $\tilde{\mathcal{Z}}_{\boldsymbol{q}\beta\beta'}$. Accordingly, from Eq. (C.60), $\eta_{\boldsymbol{q}\beta'\beta}$ is provided by

$$\eta_{\boldsymbol{q}\beta'\beta} = \left[\sum_{\mu}\left(\mathbb{P}\frac{\tilde{z}_{\boldsymbol{q}\beta'\mu}\tilde{z}_{\boldsymbol{q}\beta\mu}^{*}}{\mathcal{E}_{\boldsymbol{q}\beta} - \mathcal{E}_{\boldsymbol{q}\beta'}}\frac{1}{\mathcal{E}_{\boldsymbol{q}\beta} - \omega_{\boldsymbol{q}\mu}}\right) + \delta_{\beta'\beta}\right]\mathcal{Z}_{\boldsymbol{q}\beta}. \tag{C.78}$$

Appendix D

Derivation of an Expression of Total Retarded Longitudinal Susceptibility within the Framework of the Bosonization Scheme

D.1 Derivation of a Redatderd Susceptibility due to Electron-Induced Interaction $\chi_{\boldsymbol{q}}(t, t')$

Using Eqs. (2.70) and (2.80), the retarded susceptibility $\chi_{\boldsymbol{q}}(t, t')$ of Eq. (2.23) is read as

$$i\chi_{-\boldsymbol{q}}(t, t') = \frac{4\pi}{V} \sum_{\alpha\alpha'\gamma\gamma'} N_{\boldsymbol{q}\alpha}^{L*}(t) \left\{ R_{\boldsymbol{q}\alpha\gamma}(t, t_D) T_{\boldsymbol{q}\gamma\gamma'}(t, t') \left[R_{\boldsymbol{q}}(t', t_D) \right]_{\gamma'\alpha'}^{\dagger} \right\} N_{\boldsymbol{q}\alpha'}^{L}(t'), \quad \text{(D.1)}$$

where $R_{\boldsymbol{q}\gamma\gamma'}(t, t_D)$ is defined as

$$R_{\boldsymbol{q}\gamma\gamma'}(t, t_D) = \sum_{\beta} V_{\boldsymbol{q}\gamma\beta}^{L}(t) e^{-i\Theta_{\boldsymbol{q}\beta}(t)} V_{\boldsymbol{q}\beta\gamma'}^{R\dagger}(t_D). \quad \text{(D.2)}$$

Hereafter, it is understood that $\Theta_{\boldsymbol{q}\beta}(t, t_D)$ provided in Eq. (C.25) is replaced by $\Theta_{\boldsymbol{q}\beta}(t)$, that is,

$$\Theta_{\boldsymbol{q}\beta}(t) = \Theta_{\boldsymbol{q}\beta}(t, t_D) \quad \text{(D.3)}$$

just for the sake of simplicity.

Unfortunately, without approximation, we would tackle a formidable task to solve the non-Hermitian Fano problem of Eq. (2.58), and hence to obtain $V_{\boldsymbol{q}}^{R}$ and $V_{\boldsymbol{q}}^{L}$ for evaluating Eq. (D.2). Therefore, it would be preferable to approximately substitute a Hermitian Fano problem for Eq. (2.58), that is, Eq. (C.3) is solved. Such an approximation would be correct within the criterion of the validity of the bosonization scheme described in Sec. C.3. Hereafter, just for the sake of typographical simplicity, we omit a superscript "0" of $h_{\boldsymbol{q}}^{0}$, $N_{\boldsymbol{q}}^{0}$, $E_{\boldsymbol{q}}^{0}$, and $\mathcal{E}_{\boldsymbol{q}}^{0}$, and replace these notations with non-superscript counterparts of $h_{\boldsymbol{q}}$, $N_{\boldsymbol{q}}$, $E_{\boldsymbol{q}}$, and $\mathcal{E}_{\boldsymbol{q}}$, respectively, as far as it is not likely to cause unnecessary confusion between them. Thus, Eq. (2.58) is read as Eq. (C.53).

Accordingly, we substitute $V_{\boldsymbol{q}}$, $V_{\boldsymbol{q}}^{\dagger}$, and $N_{\boldsymbol{q}}$ for $V_{\boldsymbol{q}}^{R}$, $V_{\boldsymbol{q}}^{L\dagger}$, and $N_{\boldsymbol{q}}^{L}$, respectively [see Eqs. (C.11) and (C.14)], and thus, Eq. (D.2) becomes of the approximated form:

$$R_{\boldsymbol{q}\gamma\gamma'}(t,t_D) \approx \sum_{\beta} V_{\boldsymbol{q}\gamma\beta}(t)e^{-i\Theta_{\boldsymbol{q}\beta}(t)}V_{\boldsymbol{q}\beta\gamma'}^{\dagger}(t_D). \tag{D.4}$$

For the convenience of practical calculations, we evaluate

$$\tilde{R}_{\boldsymbol{q}\gamma\gamma'}(t,t_D) = \sum_{\beta} \tilde{V}_{\boldsymbol{q}\gamma\beta}(t)e^{-i\Theta_{\boldsymbol{q}\beta}(t)}\tilde{V}_{\boldsymbol{q}\beta\gamma'}^{\dagger}(t_D), \tag{D.5}$$

rather than $R_{\boldsymbol{q}}(t,t_D)$, where $\tilde{V}_{\boldsymbol{q}}(t)$ is defined as

$$\tilde{V}_{\boldsymbol{q}\gamma\beta}(t) = \sum_{\gamma'} \mathcal{A}_{\boldsymbol{q}\gamma\gamma'}^{(r)}(t)V_{\boldsymbol{q}\gamma'\beta}(t). \tag{D.6}$$

Here, a $[(N+2) \times (N+2)]$-matrix $\mathcal{A}^{(r)}$ is introduced as follows:

$$\mathcal{A}_{\boldsymbol{q}}^{(r)} = \begin{bmatrix} 1 & 0 \\ 0 & A_{\boldsymbol{q}}^{(r)} \end{bmatrix}, \tag{D.7}$$

where $\mathcal{A}^{(r)}$ is composed of two diagonal block matrices of a $[N \times N]$-unit block matrix with γ, $\gamma' = 1 \sim N$, and a (2×2)-block-matrix just equal to $A_{\boldsymbol{q}}^{(r)}$ related to $h_{\boldsymbol{q}}^{(d)}$ in Eq. (C.54) with γ, $\gamma' = (N+1) \sim (N+2)$. $A_{\boldsymbol{q}}^{(r)}$ is defined in Eq. (C.63), which indicates the degree of mixing between the two discrete levels of α_1 and α_2. The rest of off-diagonal block matrices is nothing but rectangular matrices with null components. Thus, Eq. (D.4) is provided by

$$R_{\boldsymbol{q}\gamma\gamma'}(t,t_D) = \sum_{\gamma''\gamma'''} \mathcal{A}_{\boldsymbol{q}\gamma\gamma''}^{(r)\dagger}(t)\tilde{R}_{\boldsymbol{q}\gamma''\gamma'''}(t,t_D)\mathcal{A}_{\boldsymbol{q}\gamma'''\gamma'}^{(r)}(t_D). \tag{D.8}$$

An explicit expression of $\tilde{R}_{\boldsymbol{q}\gamma\gamma'}(t,t_D)$ with $\gamma = \alpha$, which is derived in Sec. D.4, is provided by

$$\begin{aligned} R_{\boldsymbol{q}\alpha\gamma'}(t,t_D) &= \sum_{\beta} \mathcal{A}_{\boldsymbol{q}\alpha\beta}^{(r)\dagger}(t)\exp\left[-i\int_{t_D}^{t}\mathcal{E}_{\boldsymbol{q}\beta}(t'')dt''\right]e^{-3_{\boldsymbol{q}\beta}(t,t_D)}\mathcal{A}_{\boldsymbol{q}\beta\gamma'}^{(r)}(t_D) \\ &+ \sum_{p=1,2} \mathcal{A}_{\boldsymbol{q}\alpha\alpha_p}^{(r)\dagger}(t)\exp\left[-i\int_{t_D}^{t}\mathcal{E}_{\boldsymbol{q}\alpha_p}^{(r)}(t'')dt''\right]\exp\left[-\int_{t_D}^{t}\frac{\Gamma_{\boldsymbol{q}\alpha_p}(t'')}{2}dt''\right] \\ &\times e^{-3_{\boldsymbol{q}\beta_p}(t,t_D)}\mathcal{D}_{\boldsymbol{q}\alpha_p}(t,t_D)\mathcal{A}_{\boldsymbol{q}\alpha_p\gamma'}^{(r)}(t_D). \end{aligned} \tag{D.9}$$

Here, $\mathcal{E}_{\boldsymbol{q}\alpha_p}^{(r)}$ represents resonance energy of state α_p ($\alpha_p = \alpha_1, \alpha_2$), provided by

$$\mathcal{E}_{\boldsymbol{q}\alpha_p}^{(r)}(t) = \mathcal{E}_{\boldsymbol{q}\beta_p}(t), \tag{D.10}$$

and $\Gamma_{\boldsymbol{q}\alpha_p}$ represents natural resonance width (full width at half maximum) of state α_p, provided by

$$\Gamma_{\boldsymbol{q}\alpha_p}(t) = 2\pi\rho_{\boldsymbol{q}\beta_p}(t)|\tilde{z}_{\boldsymbol{q}\beta_p\alpha_p}(t)|^2, \tag{D.11}$$

where

$$\tilde{z}_{\boldsymbol{q}\beta\mu} = \sum_{\mu'} z_{\boldsymbol{q}\beta\mu'}A_{\boldsymbol{q}\mu'\mu}^{(r)} = M_{\boldsymbol{q}\beta}A_{\boldsymbol{q}\alpha_2\mu}^{(r)}. \tag{D.12}$$

80

Further, we introduce a new index β_p, which implies the index of continuum β with $\mathcal{E}_{q\beta} \approx \mathcal{E}_{q\alpha_p}$. By solving Eq. (C.12), we obtain the adiabatic energy $\mathcal{E}_{q\alpha_2}^{(r)}(t)$ of Si, and Fig. D.1 shows its energy curve as a function time. It is seen that the adiabatic energy varies within a couple of meV. We obtain the similar result for GaAs, though not shown here.
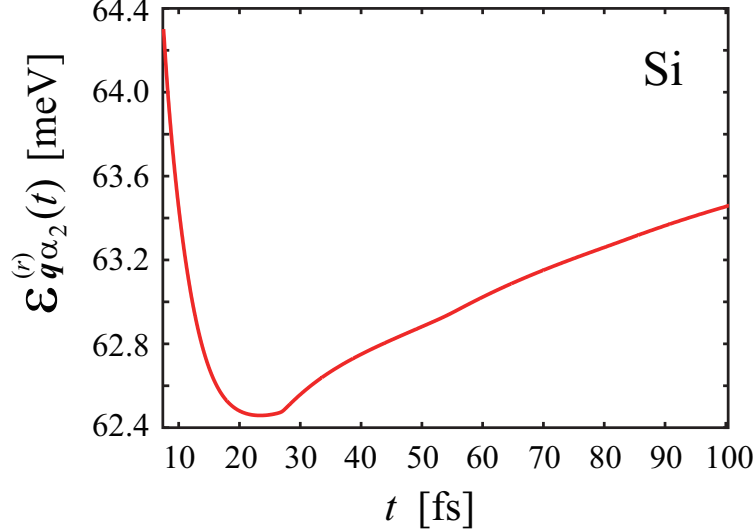

Figure D.1: A trace of adiabatic energy $\mathcal{E}_{q\alpha_2}^{(r)}(t)$ (in the unit of meV) as a function of time t (in the unit of fs).

In Eq. (D.11), $\rho_{q\beta_p}(t)$ represents a density of state of β_p at time t, and we obtain an approximate expression of $\rho_{q\beta_p}(t)$ in terms of Eq. (C.15). It is noted that the contribution of the non-adiabatic correction is incorporated in $\mathfrak{Z}_{q\beta}(t, t_D)$ of Eq. (C.17), that is, $\mathfrak{Z}_{q\beta}(t, t_D)$ of Eq. (C.18). This is a complex number in general, and is approximately provided by

$$\mathfrak{Z}_{q\beta}(t, t_D) \approx \sum_j \mathfrak{Z}_{q\beta\beta}^{(j)} \theta(t - t_j)\theta(t_j - t_D), \tag{D.13}$$

due to Eq. (2.67). In particular, the imaginary part of it as $\sum_j \mathrm{Im}\mathfrak{Z}_{q\beta\beta}^{(j)} \theta(t - t_j)\theta(t_j - t_D)$ plays a significant role of determining the spectral profiles attributed to the transient FR, as shown in Sec. 3.1.2. In addition, $\gamma_{q\beta_2}^{(0)}(t')$ in $\mathfrak{Z}_{q\beta_2}(t, t_D)$ is considered as negligibly small, that is,

$$\gamma_{q\beta_2}^{(0)}(t') \approx 0, \tag{D.14}$$

since $V_{q\alpha\beta_2} \approx 0$ because of $\alpha \neq \alpha_2$; a discrete-like FR-feature is mostly determined by the component $V_{q\alpha_2\beta_2} \approx 1$.

Moreover, in Eq.(D.9), $\mathcal{D}_{q\alpha_p}(t, t_D)$ is provided by

$$
\begin{aligned}
\mathcal{D}_{q\alpha_p}(t, t_D) \;=\; & \frac{\pi\rho_{q\beta_p}^0}{\overline{\Gamma}_{q\alpha_p}(t, t_D)/2} \left\{ \left[\Delta\Gamma_{q\alpha_p}(t; t) - i\tilde{z}_{q\beta_p\alpha_p}(t)\right] \left[\Delta\Gamma_{q\alpha_p}(t; t_D) + i\tilde{z}_{q\beta_p\alpha_p}^*(t_D)\right] \right. \\
& - \left[\Delta\Gamma_{q\alpha_p}(t; t) - \pi\rho_{q\beta_p}^0|\tilde{z}_{q\beta_p\alpha_p}(t)|^2\right] \left[\Delta\Gamma_{q\alpha_p}(t; t_D) - \pi\rho_{q\beta_p}^0|\tilde{z}_{q\beta_p\alpha_p}(t_D)|^2\right] \\
& \left. + (\pi\rho_{q\beta_p}^0)^2|\tilde{z}_{q\beta_p\alpha_p}(t)|^2|\tilde{z}_{q\beta_p\alpha_p}(t_D)|^2 \right\},
\end{aligned}
\tag{D.15}
$$

81

where

$$\Delta\Gamma_{\boldsymbol{q}\alpha_p}(t;t') = \frac{1}{2}\bar{\Gamma}_{\boldsymbol{q}\alpha_p}(t,t_D) - \pi\rho^0_{\boldsymbol{q}\beta_p}|\tilde{z}_{\boldsymbol{q}\beta_p\alpha_p}(t')|^2, \tag{D.16}$$

$$\bar{\Gamma}_{\boldsymbol{q}\alpha_p}(t,t_D) = \frac{1}{2}\left[\Gamma_{\boldsymbol{q}\alpha_p}(t) + \Gamma_{\boldsymbol{q}\alpha_p}(t_D)\right], \tag{D.17}$$

and $\rho^0_{\boldsymbol{q}\beta_p} = \rho_{\boldsymbol{q}\beta_p}(t_D)$ [see also Eqs. (D.51) and (D.57)]. It is remarked that the first and second terms of the right-hand side of Eq. (D.9) represent the contributions from a background continuum and a resonance state α_p, respectively. Furthermore, it is noted that $\Delta\Gamma_{\boldsymbol{q}\alpha_p}(t_D;t_D) = 0$ at equal time, and thus, $\mathcal{D}_{\boldsymbol{q}\alpha_p}(t_D,t_D) = 1$ and $R_{\boldsymbol{q}\alpha\gamma}(t_D,t_D) = \delta_{\alpha\gamma}$, as it should be.

As discussed in Sec. 3.1, in particular, the function $\mathcal{D}_{\boldsymbol{q}\alpha_2}(t;t_D)$ plays an essential role of determining the spectral profiles of the transient FR of concern. $R_{\boldsymbol{q}\gamma\gamma'}(t,t_D)$ consists of $\mathcal{D}_{\boldsymbol{q}\alpha_2}(t;t_D)$ as shown in Eq. (D.9), and $R_{\boldsymbol{q}\gamma\gamma'}(t,t_D)$ contains a meaning of time-evolution of PQ from state γ' at t_D to state γ at t, as is shown in Eq. (D.4).

Owing to the presence of the adiabatic energy phase in Eq. (D.9), $i\chi_{-\boldsymbol{q}}$ of Eq. (D.1) includes the following form of expression as

$$S_{\alpha\alpha'}(t,t') = \exp\left[-i\int_{t_D}^t \mathcal{E}_\alpha(t'')dt''\right]X_{\alpha\alpha'}(t,t')\exp\left[i\int_{t_D}^{t'}\mathcal{E}^*_{\alpha'}(t'')dt''\right], \tag{D.18}$$

where $\mathcal{E}_\alpha(t)$ represents a complex energy, if necessary, with a negative imaginary part ascribed to natural resonance width, and $X_{\alpha\alpha'}(t,t')$ represents an arbitrary matrix element; specific forms of $\mathcal{E}_\alpha(t)$ and $X_{\alpha\alpha'}(t,t')$ will be provided later in Eqs. (D.25) and (D.26). We set $\tau \equiv t - t' \geq 0$, and obtain

$$S_{\alpha\alpha'}(t,t') = e^{-i\mathcal{E}_{\alpha'}(t_D)\tau}\Xi_{\alpha\alpha'}(t'+\tau,t'), \tag{D.19}$$

where

$$\begin{aligned}\Xi_{\alpha\alpha'}(t'+\tau,t') &= X_{\alpha\alpha'}(t'+\tau,t')\exp\left\{-i\int_{t'}^{t'+\tau}\left[\mathcal{E}^*_{\alpha'}(t'') - \mathcal{E}_{\alpha'}(t_D)\right]dt''\right\}\\ &\times\exp\left\{-i\int_{t_D}^{t'+\tau}\left[\mathcal{E}_\alpha(t'') - \mathcal{E}^*_{\alpha'}(t'')\right]dt''\right\}.\end{aligned} \tag{D.20}$$

Further, $\Xi_{\alpha\alpha'}(t'+\tau,t')$ is approximated as

$$\Xi_{\alpha\alpha'}(t'+\tau,t') \approx \delta_{\alpha\alpha'}\Xi_\alpha(t'+\tau,t'), \tag{D.21}$$

where

$$\begin{aligned}\Xi_\alpha(t'+\tau,t') &= X_{\alpha\alpha}(t'+\tau,t')\exp\left\{-i\int_{t'}^{t'+\tau}\left[\mathcal{E}^*_\alpha(t'') - \mathcal{E}_\alpha(t_D)\right]dt''\right\}\\ &\times\exp\left\{-2\int_{t_D}^{t'+\tau}\mathrm{Im}\mathcal{E}_\alpha(t'')dt''\right\}.\end{aligned} \tag{D.22}$$

This approximation would be verified for relatively large t satisfying the condition that

$$\left|\int_{t_D}^{t'+\tau}\mathrm{Re}\left[\mathcal{E}_\alpha(t'') - \mathcal{E}^*_{\alpha'}(t'')\right]dt''\right| \gg 2\pi, \tag{D.23}$$

82

because the last exponential function in the right-hand side of Eq. (D.20) oscillates rapidly with the increase of t, and a dominant contribution originates just from $\mathrm{Re}\mathcal{E}_\alpha(t'') = \mathrm{Re}\mathcal{E}_{\alpha'}(t'')$.

Applying Eqs. (D.9) and (D.19) to Eq. (D.1), Eq. (2.80) ends up with

$$
\begin{aligned}
i\chi_{-\boldsymbol{q}}(t'+\tau,t') &= \frac{4\pi}{V}\theta(\tau)\Bigg[\sum_\beta e^{-i\mathcal{E}_{\boldsymbol{q}\beta}\tau}\Xi_{\boldsymbol{q}\beta}^{(c)}(t'+\tau,t') \\
&\quad + \sum_{p=1,2} e^{-i[\mathcal{E}_{\boldsymbol{q}\alpha_p}^{(r)}-i\Gamma_{\boldsymbol{q}\alpha_p}/2]\tau}\Xi_{\boldsymbol{q}\beta_p}^{(r)}(t'+\tau,t')\Bigg].
\end{aligned}
\tag{D.24}
$$

Hereafter, we omit the argument of t_D in $\mathcal{E}_{\boldsymbol{q}\beta}(t_D)$, $\mathcal{E}_{\boldsymbol{q}\alpha_p}^{(r)}(t_D)$, and $\Gamma_{\boldsymbol{q}\alpha_p}(t_D)$ just for the sake of simplicity, unless otherwise stated. $\Xi_{\boldsymbol{q}\beta}^{(c)}(t'+\tau,t')$ and $\Xi_{\boldsymbol{q}\alpha_p}^{(r)}(t'+\tau,t')$ correspond to Eq. (D.22), where $X_{\alpha\alpha}(t'+\tau,t')$ is replaced by $X_{\boldsymbol{q}\beta\beta}^{(c)}(t'+\tau,t')$ and $X_{\boldsymbol{q}\alpha_p\alpha_p}^{(r)}(t'+\tau,t')$, respectively. Further, $\mathcal{E}_\alpha$ is replaced by $\mathcal{E}_{\boldsymbol{q}\beta}$ and $\mathcal{E}_{\boldsymbol{q}\alpha_p}^{(r)}-i\Gamma_{\boldsymbol{q}\alpha_p}/2$, respectively. $X_{\boldsymbol{q}\alpha\beta}^{(c)}(t'+\tau,t')$ and $X_{\boldsymbol{q}\alpha_p\alpha_p}^{(r)}(t'+\tau,t')$ are provided by

$$
X_{\boldsymbol{q}\beta\beta}^{(c)}(t'+\tau,t') = N_{\boldsymbol{q}\beta}(t'+\tau)T_{\boldsymbol{q}\beta\beta}(t'+\tau,t')N_{\boldsymbol{q}\beta}(t')e^{-\mathfrak{Z}_{\boldsymbol{q}\beta}(t'+\tau,t')}e^{-2\mathrm{Re}\mathfrak{Z}_{\boldsymbol{q}\beta}(t',t_D)},
\tag{D.25}
$$

and

$$
\begin{aligned}
X_{\boldsymbol{q}\alpha_p\alpha_p}^{(r)}(t'+\tau,t') &= \tilde{N}_{\boldsymbol{q}\alpha_p}^{(r)}(t'+\tau)\mathcal{D}_{\boldsymbol{q}\alpha_p}(t'+\tau,t_D)\tilde{T}_{\boldsymbol{q}\alpha_p\alpha_p}^{(r)}(t'+\tau,t') \\
&\quad \times \mathcal{D}_{\boldsymbol{q}\alpha_p}^*(t',t_D)\tilde{N}_{\boldsymbol{q}\alpha_p}^{(r)\dagger}(t')e^{-\mathfrak{Z}_{\boldsymbol{q}\beta_p}(t'+\tau,t')}e^{-2\mathrm{Re}\mathfrak{Z}_{\boldsymbol{q}\beta_p}(t',t_D)},
\end{aligned}
\tag{D.26}
$$

respectively. Here

$$
\tilde{N}_{\boldsymbol{q}\alpha_p}^{(r)}(t) = [N_{\boldsymbol{q}}(t)\mathcal{A}_{\boldsymbol{q}}^{(r)\dagger}(t)]_{\alpha_p},
\tag{D.27}
$$

and

$$
\tilde{T}_{\boldsymbol{q}}^{(r)} = \mathcal{A}_{\boldsymbol{q}}^{(r)}(t_D)T_{\boldsymbol{q}}\mathcal{A}_{\boldsymbol{q}}^{(r)\dagger}(t_D).
\tag{D.28}
$$

It is remarked that in the first term in the squared brackets of the right-hand side of Eq. (D.24), the summation over β contains not only terms with positive energy $\mathcal{E}_{\boldsymbol{q}\beta} > 0$, but also terms with negative energy $\mathcal{E}_{\boldsymbol{q}\beta} < 0$.

D.2 Derivation of a Retarded Susceptibility due to LO-Phonon-Induced Interaction $\chi'_{\boldsymbol{q}}(t,t')$

On the other hand, as regards the retarded susceptibility of $\chi'_{\boldsymbol{q}}(t'+\tau,t')$ of Eq. (2.28), the associated retarded phonon Green function $\bar{D}_{\boldsymbol{q}}'^R(t,t')$ in Eq. (2.32) is rewritten as

$$
\begin{aligned}
i\bar{D}_{\boldsymbol{q}}'^R(t,t') &= \sum_{\beta\beta'} V_{\boldsymbol{q}\alpha_2\beta}(t)\Big\langle\Big[F_{\boldsymbol{q}\beta}(t),F_{\boldsymbol{q}\beta'}^\dagger(t')\Big]\Big\rangle V_{\boldsymbol{q}\beta'\alpha_2}^\dagger(t'), \\
&= i\sum_{\beta\beta'} V_{\boldsymbol{q}\alpha_2\beta}(t)G_{\boldsymbol{q}\beta\beta'}^R(t,t')V_{\boldsymbol{q}\beta'\alpha_2}^\dagger(t') \\
&= \sum_{\gamma\gamma'} R_{\boldsymbol{q}\alpha_2\gamma}(t,t_D)T_{\boldsymbol{q}\gamma\gamma'}(t,t')\left[R_{\boldsymbol{q}}(t',t_D)\right]_{\gamma'\alpha_2}^\dagger,
\end{aligned}
\tag{D.29}
$$

where Eqs. (2.59), (2.60), and (C.35) are employed. Further, in the third equality, Eqs. (2.70) and (D.4) are used. Similarly to Eq. (D.9), $R_{\boldsymbol{q}\alpha_2\gamma}(t, t_D)$ is expressed as

$$
\begin{aligned}
R_{\boldsymbol{q}\alpha_2\gamma}(t, t_D) &= \sum_{p=1,2} \mathcal{A}^{(r)\dagger}_{\boldsymbol{q}\alpha_2\alpha_p}(t) \exp\left[-i \int_{t_D}^{t} \mathcal{E}^{(r)}_{\boldsymbol{q}\alpha_p}(t'')dt''\right] \exp\left[-\int_{t_D}^{t} \frac{\Gamma_{\boldsymbol{q}\alpha_p}(t'')}{2}dt''\right] \\
&\times e^{-\mathfrak{Z}_{\boldsymbol{q}\beta_p}(t, t_D)} \mathcal{D}_{\boldsymbol{q}\alpha_p}(t, t_D) \mathcal{A}^{(r)}_{\boldsymbol{q}\alpha_p\gamma}(t_D).
\end{aligned}
\tag{D.30}
$$

Therefore, $\chi'_{\boldsymbol{q}}(t' + \tau, t')$ of Eq. (2.28) becomes

$$
\begin{aligned}
i\chi'_{\boldsymbol{q}}(t' + \tau, t') &= \frac{4\pi}{V} \sum_{p=1,2} \left\{ e^{-i[\mathcal{E}^{(r)}_{\boldsymbol{q}\alpha_p} - i\Gamma_{\boldsymbol{q}\alpha_p}/2]\tau} \Pi^{(r)}_{\boldsymbol{q}\alpha_p}(t' + \tau, t') \right. \\
&\left. - e^{i[\mathcal{E}^{(r)}_{-\boldsymbol{q}\alpha_p} + i\Gamma_{-\boldsymbol{q}\alpha_p}/2]\tau} \Pi^{(r)*}_{-\boldsymbol{q}\alpha_p}(t' + \tau, t') \right\},
\end{aligned}
\tag{D.31}
$$

where

$$
\begin{aligned}
\Pi^{(r)}_{\boldsymbol{q}\alpha_p}(t' + \tau, t') &= P^{(r)}_{\boldsymbol{q}\alpha_p\alpha_p}(t' + \tau, t') \exp\left\{ -i \int_{t'}^{t'+\tau} \left[\mathcal{E}^*_{\boldsymbol{q}\beta_p}(t'') - \mathcal{E}^{(r)}_{\boldsymbol{q}\alpha_p} \right] dt'' \right\} \\
&\times \exp\left\{ \int_{t_D}^{t'+\tau} \Gamma_{\boldsymbol{q}\beta_p}(t'')dt'' \right\},
\end{aligned}
\tag{D.32}
$$

and

$$
\begin{aligned}
P^{(r)}_{\boldsymbol{q}\alpha_p\alpha_p}(t' + \tau, t') &= |g'_{\boldsymbol{q}}|^2 A^{(r)\dagger}_{\boldsymbol{q}\alpha_2\alpha_p}(t' + \tau) \mathcal{D}_{\boldsymbol{q}\alpha_p}(t' + \tau, t_D) \tilde{T}^{(r)}_{\boldsymbol{q}\alpha_p\alpha_p}(t' + \tau, t') \\
&\times \mathcal{D}^*_{\boldsymbol{q}\alpha_p}(t', t_D) A^{(r)}_{\boldsymbol{q}\alpha_p\alpha_2}(t') e^{-\mathfrak{Z}_{\boldsymbol{q}\beta_p}(t'+\tau, t')} e^{-2\mathrm{Re}\mathfrak{Z}_{\boldsymbol{q}\beta_p}(t', t_D)}.
\end{aligned}
\tag{D.33}
$$

D.3 Expression of $\chi^{(t)}_{\boldsymbol{q}}(t' + \tau, t')$

According to Eqs. (D.24) and (D.31), we eventually obtain the explicit expression of the total retarded susceptibility $\chi^{(t)}_{\boldsymbol{q}}(t' + \tau, t')$ of Eq. (2.22) as

$$
\begin{aligned}
-i\chi^{(t)}_{\boldsymbol{q}}(t' + \tau, t') &= \frac{4\pi}{V} \left\{ \sum_{\beta=\beta_\pm} e^{i\mathcal{E}_{\boldsymbol{q}\beta}\tau} \Xi^{(c)*}_{\boldsymbol{q}\beta}(t' + \tau, t') \right. \\
&+ \sum_{p=1,2} e^{i[\mathcal{E}^{(r)}_{\boldsymbol{q}\alpha_p} + i\Gamma_{\boldsymbol{q}\alpha_p}/2]\tau} \left[\Xi^{(r)*}_{\boldsymbol{q}\alpha_p}(t' + \tau, t') + \Pi^{(r)*}_{\boldsymbol{q}\alpha_p}(t' + \tau, t') \right] \\
&\left. - \sum_{p=1,2} e^{-i[\mathcal{E}^{(r)}_{\boldsymbol{q}\alpha_p} - i\Gamma_{\boldsymbol{q}\alpha_p}/2]\tau} \Pi^{(r)}_{\boldsymbol{q}\alpha_p}(t' + \tau, t') \right\}.
\end{aligned}
\tag{D.34}
$$

Further, we take into account the following relations as: $\mathcal{E}_{\boldsymbol{q}\beta} = \mathcal{E}_{-\boldsymbol{q}\beta}$, $\mathcal{E}^{(r)}_{\boldsymbol{q}\alpha_p} = \mathcal{E}^{(r)}_{-\boldsymbol{q}\alpha_p}$, $\Gamma_{\boldsymbol{q}\alpha_p} = \Gamma_{-\boldsymbol{q}\alpha_p}$, and $\Xi^{(r)}_{\boldsymbol{q}\alpha_p}(t'+\tau, t') = \Xi^{(r)}_{-\boldsymbol{q}\alpha_p}(t'+\tau, t')$, which are readily verified by consulting Appendix B within the framework of the bosonization scheme provided in Sec. C.3 and the small-$\boldsymbol{q}$ limit.

D.4 Calculation of $\tilde{R}_{\boldsymbol{q}\gamma\gamma'}(t, t_D)$ of Eq. (D.5)

For the calculation of $\tilde{R}_{\boldsymbol{q}\gamma\gamma'}(t, t_D)$ of Eq. (D.5), we take into account the following four cases:

$$\tilde{R}_{\boldsymbol{q}\alpha_p\alpha_{p'}}(t, t_D) = \sum_{\beta} \tilde{\nu}_{\boldsymbol{q}\alpha_p\beta}(t)e^{-i\Theta_{\boldsymbol{q}\beta}(t)}\tilde{\nu}^*_{\boldsymbol{q}\alpha_{p'}\beta}(t_D), \tag{D.35}$$

$$\tilde{R}_{\boldsymbol{q}\alpha_p\beta'}(t, t_D) = \sum_{\beta} \tilde{\nu}_{\boldsymbol{q}\alpha_p\beta}(t)e^{-i\Theta_{\boldsymbol{q}\beta}(t)}\eta^*_{\boldsymbol{q}\beta'\beta}(t_D), \tag{D.36}$$

$$\tilde{R}_{\boldsymbol{q}\beta'\alpha_p}(t, t_D) = \sum_{\beta} \eta_{\boldsymbol{q}\beta'\beta}(t)e^{-i\Theta_{\boldsymbol{q}\beta}(t)}\tilde{\nu}^*_{\boldsymbol{q}\alpha_p\beta}(t_D), \tag{D.37}$$

and

$$\tilde{R}_{\boldsymbol{q}\beta'\beta''}(t, t_D) = \sum_{\beta} \eta_{\boldsymbol{q}\beta'\beta}(t)e^{-i\Theta_{\boldsymbol{q}\beta}(t)}\eta^*_{\boldsymbol{q}\beta''\beta}(t_D), \tag{D.38}$$

where the matrix components of $\tilde{\nu}_{\boldsymbol{q}\alpha_p\beta}(t)$ and $\eta_{\boldsymbol{q}\beta'\beta}(t)$ in $\tilde{V}_{\boldsymbol{q}\gamma\beta}$ are provided by Eqs. (C.77) and (C.78), respectively. Further, time-dependence of every term is explicitly shown, and $\alpha_p, \alpha_{p'} = \alpha_1, \alpha_2$.

All of the expressions of $\tilde{R}_{\boldsymbol{q}\gamma\gamma'}(t, t_D)$ given above contain a common factor of $\mathcal{Z}_{\boldsymbol{q}\beta}(t)\mathcal{Z}^*_{\boldsymbol{q}\beta}(t_D)$. According to Eq. (C.76), $[\mathcal{Z}_{\boldsymbol{q}\beta}(t)]^{-2}$ is written as

$$[\mathcal{Z}_{\boldsymbol{q}\beta}(t)]^{-2} = \{[\mathcal{E}_{\boldsymbol{q}\beta}(t) - \omega_{\boldsymbol{q}\alpha_1}(t)][\mathcal{E}_{\boldsymbol{q}\beta}(t) - \omega_{\boldsymbol{q}\alpha_2}(t)]\}^{-2} L_{\boldsymbol{q}\beta}(t), \tag{D.39}$$

where

$$
\begin{aligned}
L_{\boldsymbol{q}\beta}(t) &= \{[\mathcal{E}_{\boldsymbol{q}\beta}(t) - \omega_{\boldsymbol{q}\alpha_1}(t)][\mathcal{E}_{\boldsymbol{q}\beta}(t) - \omega_{\boldsymbol{q}\alpha_2}(t)]\}^2 + [\gamma_{\boldsymbol{q}\beta\alpha_2}(t)/2]^2[\mathcal{E}_{\boldsymbol{q}\beta}(t) - \omega_{\boldsymbol{q}\alpha_1}(t)]^2 \\
&\quad + [\gamma_{\boldsymbol{q}\beta\alpha_1}(t)/2]^2[\mathcal{E}_{\boldsymbol{q}\beta}(t) - \omega_{\boldsymbol{q}\alpha_2}(t)]^2 + 2[\gamma_{\boldsymbol{q}\beta\alpha_1}(t)/2]^2[\gamma_{\boldsymbol{q}\beta\alpha_2}(t)/2]^2 \\
&\quad \times [\mathcal{E}_{\boldsymbol{q}\beta}(t) - \omega_{\boldsymbol{q}\alpha_1}(t)]^2[\mathcal{E}_{\boldsymbol{q}\beta}(t) - \omega_{\boldsymbol{q}\alpha_2}(t)],
\end{aligned} \tag{D.40}
$$

with

$$\gamma_{\boldsymbol{q}\beta\alpha_p}(t) = 2\pi\rho_{\boldsymbol{q}\beta}(t)|\tilde{z}_{\boldsymbol{q}\beta\alpha_p}(t)|^2 \tag{D.41}$$

[for $\rho_{\boldsymbol{q}\beta}(t)$, refer to Eq. (C.75)]. Obviously, we have four solutions, provided by $\mathcal{E}_{\boldsymbol{q}\beta}(t) = \mathcal{E}^{(\pm)}_{\boldsymbol{q}\beta_p}(t)$, ensuring an algebraic equation of $L_{\boldsymbol{q}\beta}(t) = 0$ with $p = 1, 2$. By assuming that an order of $[\gamma_{\boldsymbol{q}\beta\alpha_p}(t)/2]/[\omega_{\boldsymbol{q}\alpha_{p'}}(t) - \omega_{\boldsymbol{q}\alpha_p}(t)]$ for $p \neq p'$ is negligibly small, namely,

$$\frac{\gamma_{\boldsymbol{q}\beta\alpha_p}(t)/2}{|\omega_{\boldsymbol{q}\alpha_{p'}}(t) - \omega_{\boldsymbol{q}\alpha_p}(t)|} \approx \frac{\Gamma_{\boldsymbol{q}\alpha_p}(t)/2}{|\omega_{\boldsymbol{q}\alpha_{p'}}(t) - \omega_{\boldsymbol{q}\alpha_p}(t)|} \ll 1, \tag{D.42}$$

the solutions of $\mathcal{E}^{(\pm)}_{\boldsymbol{q}\beta_p}(t)$ are given in an approximate manner as

$$\mathcal{E}^{(\pm)}_{\boldsymbol{q}\beta_p}(t) \approx \omega_{\boldsymbol{q}\alpha_p}(t) \pm i\gamma_{\boldsymbol{q}\beta\alpha_p}(t)/2 \approx \omega_{\boldsymbol{q}\alpha_p}(t) \pm i\Gamma_{\boldsymbol{q}\alpha_p}(t)/2. \tag{D.43}$$

Here, in both of the first equality of Eq. (D.42) and the second equality of Eq. (D.43), $\gamma_{\boldsymbol{q}\beta\alpha_p}(t)$ is evaluated in the proximity of $\mathcal{E}_{\boldsymbol{q}\beta}(t) \approx \omega_{\boldsymbol{q}\alpha_p}(t)$, and $\Gamma_{\boldsymbol{q}\alpha_p}(t)$ is substituted for $\gamma_{\boldsymbol{q}\beta\alpha_p}(t)$, namely,

$$\Gamma_{\boldsymbol{q}\alpha_p}(t) = 2\pi\rho_{\boldsymbol{q}\beta_p}(t)|\tilde{z}_{\boldsymbol{q}\beta_p\alpha_p}(t)|^2 \tag{D.44}$$

[for β_p, see below Eq. (D.12)]. Therefore, Eq. (D.40) is rewritten as

$$L_{\boldsymbol{q}\beta}(t) \approx \prod_{p=1,2} \left[\mathcal{E}_{\boldsymbol{q}\beta}(t) - \mathcal{E}_{\boldsymbol{q}\beta_p}^{(+)}(t) \right] \left[\mathcal{E}_{\boldsymbol{q}\beta}(t) - \mathcal{E}_{\boldsymbol{q}\beta_p}^{(-)}(t) \right]. \tag{D.45}$$

Thus, in terms of $L_{\boldsymbol{q}\beta}^0(t)$ defined as

$$L_{\boldsymbol{q}\beta}^0(t) = \prod_{p=1,2} \left[\mathcal{E}_{\boldsymbol{q}\beta}(t) - \omega_{\boldsymbol{q}\alpha_p}(t) \right], \tag{D.46}$$

$\mathcal{Z}_{\boldsymbol{q}\beta}(t)\mathcal{Z}_{\boldsymbol{q}\beta}^*(t_D)$ is cast into

$$\mathcal{Z}_{\boldsymbol{q}\beta}(t)\mathcal{Z}_{\boldsymbol{q}\beta}^*(t_D) = \frac{L_{\boldsymbol{q}\beta}^0(t)L_{\boldsymbol{q}\beta}^0(t_D)}{[L_{\boldsymbol{q}\beta}(t)L_{\boldsymbol{q}\beta}(t_D)]^{1/2}}. \tag{D.47}$$

The factor of $L_{\boldsymbol{q}\beta}(t)L_{\boldsymbol{q}\beta}(t_D)$ in the denominator of Eq. (D.47) is rewritten as products of a term

$$\mathcal{L}_{\boldsymbol{q}\beta}^{(p,\pm)}(t,t_D) = \left[\mathcal{E}_{\boldsymbol{q}\beta}(t) - \mathcal{E}_{\boldsymbol{q}\beta_p}^{(\pm)}(t) \right] \left[\mathcal{E}_{\boldsymbol{q}\beta}(t_D) - \mathcal{E}_{\boldsymbol{q}\beta_p}^{(\pm)}(t_D) \right], \tag{D.48}$$

that is,

$$L_{\boldsymbol{q}\beta}(t)L_{\boldsymbol{q}\beta}(t_D) = \prod_{p,\sigma=\pm} \mathcal{L}_{\boldsymbol{q}\beta}^{(p,\sigma)}(t,t_D), \tag{D.49}$$

where a plus or minus sign corresponds to the signs in Eq. (D.48). In fact, $\mathcal{L}_{\boldsymbol{q}\beta}^{(p,\pm)}(t,t_D)$ is reduced to the approximate form:

$$\mathcal{L}_{\boldsymbol{q}\beta}^{(p,\pm)}(t,t_D) \approx \left\{ \mathcal{E}_{\boldsymbol{q}\beta}(t_D) - \omega_{\boldsymbol{q}\alpha_p}(t_D) \mp \frac{i}{2}\bar{\Gamma}_{\boldsymbol{q}\alpha_p}(t,t_D) \right\}^2, \tag{D.50}$$

and

$$\bar{\Gamma}_{\boldsymbol{q}\alpha_p}(t,t_D) = \frac{1}{2} \left[\Gamma_{\boldsymbol{q}\alpha_p}(t) + \Gamma_{\boldsymbol{q}\alpha_p}(t_D) \right]. \tag{D.51}$$

For deriving Eqs. (D.49) and (D.50), the approximations of

$$\mathcal{E}_{\boldsymbol{q}\beta}(t) - \omega_{\boldsymbol{q}\alpha_p}(t) \approx \mathcal{E}_{\boldsymbol{q}\beta}(t_D) - \omega_{\boldsymbol{q}\alpha_p}(t_D), \tag{D.52}$$

and

$$\Gamma_{\boldsymbol{q}\alpha_p}(t) \approx \Gamma_{\boldsymbol{q}\alpha_p}(t_D) \tag{D.53}$$

are partially employed, respectively. It is noted that these approximations would be verified in the case of $\mathcal{E}_{\boldsymbol{q}\beta} \approx \omega_{\boldsymbol{q}\alpha_p}$, that is, in the resonant condition of $\beta \approx \beta_p$. Using Eq. (D.50), the denominator of Eq. (D.47) becomes

$$[L_{\boldsymbol{q}\beta}(t)L_{\boldsymbol{q}\beta}(t_D)]^{1/2} = \prod_{p} \left\{ \left[\mathcal{E}_{\boldsymbol{q}\beta}(t_D) - \omega_{\boldsymbol{q}\alpha_p}(t_D) \right]^2 + \left[\bar{\Gamma}_{\boldsymbol{q}\alpha_p}(t,t_D)/2 \right]^2 \right\}. \tag{D.54}$$

This indicates that an integrand of $\tilde{R}_{\boldsymbol{q}\gamma\gamma'}(t,t_D)$ in Eqs. (D.35)-(D.38) as a function of $\mathcal{E}_{\boldsymbol{q}\beta}(t_D)$ contains two first-order poles at

$$\mathcal{E}_{\boldsymbol{q}\beta}(t_D) = \omega_{\boldsymbol{q}\alpha_p}(t_D) - \frac{i}{2}\bar{\Gamma}_{\boldsymbol{q}\alpha_p}(t,t_D) \tag{D.55}$$

86

in the lower-half complex-$\mathcal{E}_{\boldsymbol{q}\beta}(t_D)$-plane with $p = 1, 2$.

To begin with an evaluation of Eq. (D.35), by using Eq. (C.77), $\tilde{R}_{\boldsymbol{q}\alpha_p\alpha_{p'}}(t, t_D)$ is recast into

$$
\begin{aligned}
\tilde{R}_{\boldsymbol{q}\alpha_p\alpha_{p'}}(t, t_D) &= \sum_\beta \frac{\tilde{z}^*_{\boldsymbol{q}\beta\alpha_p}(t)\tilde{z}_{\boldsymbol{q}\beta\alpha_{p'}}(t_D)e^{-i\Theta_{\boldsymbol{q}\beta}(t)}\mathcal{Z}_{\boldsymbol{q}\beta}(t)\mathcal{Z}^*_{\boldsymbol{q}\beta}(t_D)}{\left[\mathcal{E}_{\boldsymbol{q}\beta}(t) - \omega_{\boldsymbol{q}\alpha_p}(t)\right]\left[\mathcal{E}_{\boldsymbol{q}\beta}(t_D) - \omega_{\boldsymbol{q}\alpha_{p'}}(t_D)\right]} \\
&= \oint_{\text{lower}} d\mathcal{E}_{\boldsymbol{q}\beta}(t_D)\rho^0_{\boldsymbol{q}\beta} \\
&\quad \times \frac{\tilde{z}^*_{\boldsymbol{q}\beta\alpha_p}(t)\tilde{z}_{\boldsymbol{q}\beta\alpha_{p'}}(t_D)e^{-i\Theta_{\boldsymbol{q}\beta}(t)}\mathcal{Z}_{\boldsymbol{q}\beta}(t)\mathcal{Z}^*_{\boldsymbol{q}\beta}(t_D)}{\left[\mathcal{E}_{\boldsymbol{q}\beta}(t) - \omega_{\boldsymbol{q}\alpha_p}(t)\right]\left[\mathcal{E}_{\boldsymbol{q}\beta}(t_D) - \omega_{\boldsymbol{q}\alpha_{p'}}(t_D)\right]}.
\end{aligned}
\tag{D.56}
$$

Here, in the second equality, we replace the summation over β with an integral over $\mathcal{E}_{\boldsymbol{q}\beta}(t_D)$ in view of Eq. (C.75). Further, a density of state, $\rho^0_{\boldsymbol{q}\beta}$, at time t_D is represented as

$$
\rho^0_{\boldsymbol{q}\beta} = \rho_{\boldsymbol{q}\beta}(t_D).
\tag{D.57}
$$

Moreover, this is rewritten as a contour integral with respect to a complex variable of $\mathcal{E}_{\boldsymbol{q}\beta}(t_D)$. The contour is along a semicircle with an infinite radius in a lower-half plane including a real axis, and this choice of the path is ensured by existence of a vanishing exponential function of $\exp[-i\Theta_{\boldsymbol{q}\beta}(t)]$ along the lower-half plane. This would be verified by rewriting the adiabatic energy phase $\Theta_{\boldsymbol{q}\beta}(t)$ of Eqs. (C.25) and (D.3) as

$$
\Theta_{\boldsymbol{q}\beta}(t) \approx \mathcal{E}_{\boldsymbol{q}\beta}(t_D)(t - t_D) + \int_{t_D}^t dt' \left[\mathcal{E}_{\boldsymbol{q}\beta_p}(t') - \mathcal{E}_{\boldsymbol{q}\beta_p}(t_D)\right] - i\mathfrak{Z}_{\boldsymbol{q}\beta_p}(t, t_D),
\tag{D.58}
$$

where $\mathfrak{Z}_{\boldsymbol{q}\beta}(t, t_D)$ is provided by Eq. (C.17), and β is approximately replaced by β_p in the second and third terms of Eq. (D.58). Therefore, the evaluation of Eq. (D.56) results in calculus of residues at the poles provided by Eq. (D.55); it is noted that spurious poles emerging in a denominator of the integrand of Eq. (D.56) are exactly canceled with a factor of $L^0_{\boldsymbol{q}\beta}(t)L^0_{\boldsymbol{q}\beta}(t_D)$ in $\mathcal{Z}_{\boldsymbol{q}\beta}(t)\mathcal{Z}^*_{\boldsymbol{q}\beta}(t_D)$, as shown in Eq. (D.47). The resulting expression is represented as follows:

$$
\begin{aligned}
\tilde{R}_{\boldsymbol{q}\alpha_p\alpha_{p'}}(t, t_D) &\approx \delta_{\alpha_p\alpha_{p'}}\exp\left\{-i\int_{t_D}^t \left[\mathcal{E}^{(r)}_{\boldsymbol{q}\alpha_p}(t'') - i\frac{\Gamma_{\boldsymbol{q}\alpha_p}(t'')}{2}\right]dt''\right\} \\
&\quad \times e^{-\mathfrak{Z}_{\boldsymbol{q}\beta_p}(t, t_D)}\frac{\pi\rho^0_{\boldsymbol{q}\beta_p}}{\bar{\bar{\Gamma}}_{\boldsymbol{q}\alpha_p}(t, t_D)/2}\tilde{z}_{\boldsymbol{q}\beta_p\alpha_p}(t)\tilde{z}^\dagger_{\boldsymbol{q}\beta_p\alpha_p}(t_D),
\end{aligned}
\tag{D.59}
$$

where $\mathcal{E}^{(r)}_{\boldsymbol{q}\alpha_p}(t'')$ is substituted for $\mathcal{E}_{\boldsymbol{q}\beta_p}(t'')$. It is evident that this expression is just consistent with the identity relation provided by

$$
\tilde{R}_{\boldsymbol{q}\alpha_p\alpha_{p'}}(t_D, t_D) = \delta_{\alpha_p\alpha_{p'}}
\tag{D.60}
$$

owing to $\mathfrak{Z}_{\boldsymbol{q}\beta_p}(t_D, t_D) = 1$, where this arises from an equal-time commutation relation of Eq. (C.68). In fact, such compatibility is realized by virtue of neglecting additional terms emerging on the way of reduction of Eq. (D.56), on the basis of the approximations made in Eqs. (D.42) and Eq. (D.50).

We employ the similar reduction procedures to that of Eq. (D.35) in order to evaluate Eqs. (D.36)-(D.38). Thus, below, we remark just the points of difference between the ways

of calculations of the former equation and the latter three ones without describing details of derivations. As regards Eq. (D.36), $\eta_{\boldsymbol{q}\beta'\beta}$ is composed of two terms including $\delta_{\beta'\beta}$ and a Cauchy's principle value, as seen in Eq. (C.78). For the reason to be mentioned right below, we evaluate an expression of the form, $\sum_{\beta'} \tilde{R}_{\boldsymbol{q}\alpha_p\beta'}(t,t_D)C_{\beta'}$, rather than Eq. (D.36), where $C_{\beta'}$ represents an auxiliary regular-function of $\mathcal{E}_{\boldsymbol{q}\beta'}$. One part of this expression with $\delta_{\beta'\beta}$ is straightforward evaluated in the similar way as done for Eq. (D.35). On the other hand, the other part of it contains the Cauchy's principle value of an integral over $\mathcal{E}_{\boldsymbol{q}\beta}$. For evaluating this contour integral, the path of integral is to be modified from that taken in Eq. (D.35) so as to avoid a singular point of $\mathcal{E}_{\boldsymbol{q}\beta} = \mathcal{E}_{\boldsymbol{q}\beta'}$. The equation resulting from this integration is cast into the form of another integral over $\mathcal{E}_{\boldsymbol{q}\beta'}$. That is the reason why the auxiliary function $C_{\beta'}$ is introduced in advance. We implement the integration by means of calculus of residues, and obtain the expression as follows:

$$
\begin{aligned}
\tilde{R}_{\boldsymbol{q}\alpha_p\beta'}(t,t_D) \;\approx\; & \delta_{\beta_p\beta'}\exp\left\{-i\int_{t_D}^t\left[\mathcal{E}_{\boldsymbol{q}\alpha_p}^{(r)}(t'')-i\frac{\Gamma_{\boldsymbol{q}\alpha_p}(t'')}{2}\right]dt''\right\} \\
& \times(-i)e^{-\Im_{\boldsymbol{q}\beta_p}(t,t_D)}\pi\rho_{\boldsymbol{q}\beta_p}^0\left[1-\frac{\pi\rho_{\boldsymbol{q}\beta_p}^0|\tilde{z}_{\boldsymbol{q}\beta_p\alpha_p}(t_D)|^2}{\bar{\Gamma}_{\boldsymbol{q}\alpha_p}(t,t_D)/2}\right]\tilde{z}_{\boldsymbol{q}\beta_p\alpha_p}(t). \text{ (D.61)}
\end{aligned}
$$

Similarly, Eq. (D.37) becomes

$$
\begin{aligned}
\tilde{R}_{\boldsymbol{q}\beta'\alpha_p}(t,t_D) \;\approx\; & \delta_{\beta'\beta_p}\exp\left\{-i\int_{t_D}^t\left[\mathcal{E}_{\boldsymbol{q}\alpha_p}^{(r)}(t'')-i\frac{\Gamma_{\boldsymbol{q}\alpha_p}(t'')}{2}\right]dt''\right\} \\
& \times(+i)e^{-\Im_{\boldsymbol{q}\beta_p}(t,t_D)}\pi\rho_{\boldsymbol{q}\beta_p}^0\left[1-\frac{\pi\rho_{\boldsymbol{q}\beta_p}^0|\tilde{z}_{\boldsymbol{q}\beta_p\alpha_p}(t)|^2}{\bar{\Gamma}_{\boldsymbol{q}\alpha_p}(t,t_D)/2}\right]\tilde{z}_{\boldsymbol{q}\beta_p\alpha_p}^*(t_D). \text{ (D.62)}
\end{aligned}
$$

It is evident that this expression is just consistent with the identity relation provided by

$$
\tilde{R}_{\boldsymbol{q}\alpha_p\beta}(t_D,t_D)=0, \quad \tilde{R}_{\boldsymbol{q}\beta\alpha_p}(t_D,t_D)=0, \tag{D.63}
$$

where these are attributed to equal-time commutation relations of Eq. (C.69).

Finally, for evaluation of Eq. (D.38), this is more complicated than the others of Eqs. (D.35)-(D.37), since a dual integral of Cauchy's principle values is included ascribed to the presence of the first term in parentheses of Eq. (C.78). For the same reason as the introduction of an auxiliary function to $\tilde{R}_{\boldsymbol{q}\beta\alpha_p}(t,t_D)$ in advance, we introduce auxiliary regular-functions of $\mathcal{E}_{\boldsymbol{q}\beta'}$ and $\mathcal{E}_{\boldsymbol{q}\beta''}$, namely, $C_{\beta'}$ and $C'_{\beta''}$, respectively, and calculate $\sum_{\beta'\beta''} C_{\beta'}\tilde{R}_{\boldsymbol{q}\beta'\beta''}(t,t_D)C'_{\beta''}$ in place of Eq. (D.38). Because of Poincaré's theorem of Eq. (C.74), the product of Cauchy's principle values is split into a sum of two Cauchy's principle values and delta-functions, which makes the resulting contour integrals feasible. We conduct lengthy but elementary calculations, and obtain the following final expression of Eq. (D.38) as:

$$
\begin{aligned}
\tilde{R}_{\boldsymbol{q}\beta'\beta''}(t,t_D) \;\approx\; & \delta_{\beta'\beta''}\exp\left\{-i\int_{t_D}^t\mathcal{E}_{\boldsymbol{q}\beta'}(t'')dt''\right\}e^{-\Im_{\boldsymbol{q}\beta'}(t,t_D)} \\
& +\sum_p\delta_{\beta'\beta_p}\delta_{\beta''\beta_p}\exp\left\{-i\int_{t_D}^t\left[\mathcal{E}_{\boldsymbol{q}\alpha_p}^{(r)}(t'')-i\frac{\Gamma_{\boldsymbol{q}\alpha_p}(t'')}{2}\right]dt''\right\} \\
& \times e^{-\Im_{\boldsymbol{q}\beta_p}(t,t_D)}(\pi\rho_{\boldsymbol{q}\beta_p}^0)^2\left[|\tilde{z}_{\boldsymbol{q}\beta_p\alpha_p}(t)|^2+|\tilde{z}_{\boldsymbol{q}\beta_p\alpha_p}(t_D)|^2\right. \\
& \left. -\frac{2\pi\rho_{\boldsymbol{q}\beta_p}^0|\tilde{z}_{\boldsymbol{q}\beta_p\alpha_p}(t)|^2|\tilde{z}_{\boldsymbol{q}\beta_p\alpha_p}(t_D)|^2}{\bar{\Gamma}_{\boldsymbol{q}\alpha_p}(t,t_D)/2}\right].
\end{aligned}
\tag{D.64}
$$

It is evident that this expression is just consistent with the identity relation provided by

$$\tilde{R}_{\boldsymbol{q}\beta'\beta''}(t_D, t_D) = \delta_{\beta'\beta''}, \tag{D.65}$$

where this is attributed to equal-time commutation relation of Eq. (C.70).

Appendix E

The Phase-Transformation Invariance of the Present Study

In a biorthogonal set of eigenvectors $\{U_{\boldsymbol{q}\alpha}^{L}(t), U_{\boldsymbol{q}\alpha}^{R}(t)\}$ provided in Eqs. (2.33) and (2.34), the normalization constants $N_{\boldsymbol{q}\alpha}^{L}(t)$ and $N_{\boldsymbol{q}\alpha}^{R}(t)$ are not determined up to overall phase factors. Here, owing to such arbitrariness, the set of $\{\tilde{U}_{\boldsymbol{q}\alpha}^{L}(t), \tilde{U}_{\boldsymbol{q}\alpha}^{R}(t)\}$ are also solutions, given as

$$\tilde{U}_{\boldsymbol{q}\alpha}^{L\dagger}(t) = e^{-i\eta_{\boldsymbol{q}\alpha}(t)} U_{\boldsymbol{q}\alpha}^{L\dagger}(t) \tag{E.1}$$

and

$$\tilde{U}_{\boldsymbol{q}\alpha}^{R}(t) = e^{i\eta_{\boldsymbol{q}\alpha}(t)} U_{\boldsymbol{q}\alpha}^{R}(t) \tag{E.2}$$

under the normalization condition that $\tilde{U}_{\boldsymbol{q}\alpha}^{L\dagger}(t)\tilde{U}_{\boldsymbol{q}\alpha}^{R}(t) = U_{\boldsymbol{q}\alpha}^{L\dagger}(t)U_{\boldsymbol{q}\alpha}^{R}(t) = 1$. Here, $\eta_{\boldsymbol{q}\alpha}(t)$ represents an arbitrary real function of time. Because the operators $B_{\boldsymbol{q}\alpha}^{\dagger}$ and $B_{\boldsymbol{q}\alpha}$ are defined as $B_{\boldsymbol{q}\alpha}^{\dagger} = \bar{A}_{\boldsymbol{q}}^{\dagger}U_{\boldsymbol{q}\alpha}^{R}$ and $B_{\boldsymbol{q}\alpha} = U_{\boldsymbol{q}\alpha}^{R\dagger}\bar{A}_{\boldsymbol{q}}$, respectively, as shown in Eqs. (2.38) and (2.39), these are transformed as

$$B_{\boldsymbol{q}\alpha}^{\dagger}(t) \to \tilde{B}_{\boldsymbol{q}\alpha}^{\dagger}(t) = B_{\boldsymbol{q}\alpha}^{\dagger}(t)e^{i\eta_{\boldsymbol{q}\alpha}(t)} \tag{E.3}$$

and

$$B_{\boldsymbol{q}\alpha}(t) \to \tilde{B}_{\boldsymbol{q}\alpha}(t) = B_{\boldsymbol{q}\alpha}(t)e^{-i\eta_{\boldsymbol{q}\alpha}(t)}, \tag{E.4}$$

respectively. It is understood that such a transformation corresponds to the (temporally local) gauge transformation with respect to the operators $B_{\boldsymbol{q}\alpha}^{\dagger}$ and $B_{\boldsymbol{q}\alpha}$.

It is readily confirmed that a set of equations of motion provided by Eqs. (2.54) and (2.55) remains unchanged under the transformation of Eqs. (E.3) and (E.4), since $M_{\boldsymbol{q}\alpha}$, $M_{-\boldsymbol{q}\alpha}''$, $M_{\boldsymbol{q}\alpha}'^{*}$, and $\mathcal{W}_{\boldsymbol{q}\alpha'\alpha}$ given by Eqs. (2.46), (2.49), (2.50), and (2.41), respectively are transformed as follows:

$$M_{\boldsymbol{q}\alpha}(t) \to \tilde{M}_{\boldsymbol{q}\alpha}(t) = e^{-i\eta_{\boldsymbol{q}\alpha}(t)} M_{\boldsymbol{q}\alpha}(t), \tag{E.5}$$

$$M_{-\boldsymbol{q}\alpha}''(t) \to \tilde{M}_{-\boldsymbol{q}\alpha}''(t) = e^{i\eta_{\boldsymbol{q}\alpha}(t)} M_{-\boldsymbol{q}\alpha}''(t), \tag{E.6}$$

$$M_{\boldsymbol{q}\alpha}'^{*}(t) \to \tilde{M}_{\boldsymbol{q}\alpha}'^{*}(t) = e^{i\eta_{\boldsymbol{q}\alpha}(t)} M_{\boldsymbol{q}\alpha}'^{*}(t), \tag{E.7}$$

and

$$\mathcal{W}_{\boldsymbol{q}\alpha'\alpha} \to \tilde{\mathcal{W}}_{\boldsymbol{q}\alpha'\alpha} = e^{-i[\eta_{\boldsymbol{q}\alpha'}(t)-\eta_{\boldsymbol{q}\alpha}(t)]}\mathcal{W}_{\boldsymbol{q}\alpha'\alpha} - i\frac{d\eta_{\boldsymbol{q}\alpha}(t)}{dt}\delta_{\alpha'\alpha}, \tag{E.8}$$

respectively.

On the other hand, the matrix $h_{\boldsymbol{q}} = \{h_{\boldsymbol{q}\gamma\gamma'}\}$ provided by Eq. (2.57) with $\{\gamma\} = (\{\alpha\}, \alpha_2)$ and $\{\gamma'\} = (\{\alpha'\}, \alpha'_2)$ is transformed into

$$
\begin{aligned}
h_{\boldsymbol{q}}(t) \to \tilde{h}_{\boldsymbol{q}}(t) &\equiv \mathcal{P}_{\boldsymbol{q}}(t) h_{\boldsymbol{q}}(t) \mathcal{P}_{\boldsymbol{q}}^{\dagger}(t) \\
&= \begin{bmatrix} \mathcal{E}_{\boldsymbol{q}}(t) & \tilde{M}_{\boldsymbol{q}} \\ \tilde{M}_{\boldsymbol{q}}'^{\dagger} & \omega_{\boldsymbol{q}} \end{bmatrix},
\end{aligned}
\tag{E.9}
$$

where $\mathcal{P}_{\boldsymbol{q}}$ represents a diagonal matrix defined as

$$
\mathcal{P}_{\boldsymbol{q}\gamma\gamma'}(t) = e^{-i[\eta_{\boldsymbol{q}\alpha}(t) + \eta_{\boldsymbol{q}\alpha_2}(t)]} \delta_{\gamma\gamma'} \delta_{\gamma\alpha} + e^{-i\eta_{\boldsymbol{q}\alpha_2}} \delta_{\gamma\gamma'} \delta_{\gamma\alpha_2}.
\tag{E.10}
$$

$\eta_{\boldsymbol{q}\alpha_2}(t)$ is an arbitrary real function of t. The matrix equation provided by Eq. (2.58) is transformed into

$$
\sum_{\gamma'} \tilde{h}_{\boldsymbol{q}\gamma\gamma'} \tilde{V}_{\boldsymbol{q}\gamma'\beta}^{R} = \tilde{V}_{\boldsymbol{q}\gamma\beta}^{R} \mathcal{E}_{\boldsymbol{q}\beta},
\tag{E.11}
$$

and thus, we obtain the relations of

$$
\tilde{V}_{\boldsymbol{q}}^{R}(t) = \mathcal{P}_{\boldsymbol{q}}(t) V_{\boldsymbol{q}}^{R}(t), \; \tilde{V}_{\boldsymbol{q}}^{L\dagger}(t) = V_{\boldsymbol{q}}^{L\dagger}(t) \mathcal{P}_{\boldsymbol{q}}^{\dagger}(t).
\tag{E.12}
$$

Here, $V_{\boldsymbol{q}}^{L\dagger}$ and $\tilde{V}_{\boldsymbol{q}}^{L\dagger}$ represent the left vectors associated with the right vectors $V_{\boldsymbol{q}}^{R}$ and $\tilde{V}_{\boldsymbol{q}}^{R}$, respectively, ensuring the normalization conditions $V_{\boldsymbol{q}}^{L\dagger} V_{\boldsymbol{q}}^{R} = \tilde{V}_{\boldsymbol{q}}^{L\dagger} \tilde{V}_{\boldsymbol{q}}^{R} = 1$. Given Eqs. (E.3) and (E.12), the PQ operators are simply transformed into

$$
F_{\boldsymbol{q}\beta}^{\dagger}(t) \to \tilde{F}_{\boldsymbol{q}\beta}^{\dagger}(t) = F_{\boldsymbol{q}\beta}^{\dagger}(t) e^{-i\eta_{\boldsymbol{q}\alpha_2}(t)}
\tag{E.13}
$$

and

$$
F_{\boldsymbol{q}\beta}(t) \to \tilde{F}_{\boldsymbol{q}\beta}(t) = F_{\boldsymbol{q}\beta}(t) e^{i\eta_{\boldsymbol{q}\alpha_2}(t)}.
\tag{E.14}
$$

Thus, the retarded Green function provided by Eq. (2.69) is transformed such that

$$
G_{\boldsymbol{q}\beta\beta'}^{R}(t,t') \to \tilde{G}_{\boldsymbol{q}\beta\beta'}^{R}(t,t') = G_{\boldsymbol{q}\beta\beta'}^{R}(t,t') e^{i[\eta_{\boldsymbol{q}\alpha_2}(t) - \eta_{\boldsymbol{q}\alpha_2}(t')]}.
\tag{E.15}
$$

Below, we show that the total retarded longitudinal susceptibility $\chi_{\boldsymbol{q}}^{(t)}(t,t')$ provided by Eq. (2.22) is unaltered under the phase transformation of concern. This is given by a sum of the retarded susceptibility attributed to the electron-induced interaction $\chi_{\boldsymbol{q}}(t,t')$ and that of the LO phonon-induced interaction $\chi_{\boldsymbol{q}}'(t,t')$. Further, these are composed of the correlation functions $D_{\boldsymbol{q}}^{R}(t,t')$ and $\bar{D}_{\boldsymbol{q}}'^{R}(t,t')$ provided by Eqs. (2.80) and (2.81), respectively. Therefore, in view of Eq. (E.1), (E.2), (E.12), and (E.15), it is readily verified that these are unchanged under the phase transformation.

In conclusion, the theory developed in the dissertation remains invariant under the phase transformation, as it should be, and physical quantities related to $\chi_{\boldsymbol{q}}^{(t)}(t,t')$ are independent of the selection of the phases of $\eta_{\boldsymbol{q}\alpha}(t)$ and $\eta_{\boldsymbol{q}\alpha_2}(t)$.

Appendix F

Eigenvalue Problem of $\bar{\mathscr{Z}}_{\boldsymbol{q}}$ in Eq. (2.100)

Owing to a relatively sparse form of the matrix $\bar{\mathscr{Z}}_{\boldsymbol{q}}$ of Eq. (2.100), we obtain analytical expressions of transcendental equation for determining the eigenvalues and the associated eigenvectors. The transcendental equation to be solved for the eigenvalues is expressed as follows:

$$(\tilde{\omega}_{\boldsymbol{q}pl} - E_{\boldsymbol{q}}) \prod_{j \neq pl} (\tilde{\omega}_{\boldsymbol{q}j} - E_{\boldsymbol{q}}) - \sum_{j \neq pl} M_{\boldsymbol{q}j} M'_{\boldsymbol{q}j} \prod_{j' \neq j, pl} (\tilde{\omega}_{\boldsymbol{q}j'} - E_{\boldsymbol{q}}) = 0, \qquad (F.1)$$

where $\tilde{\omega}_{\boldsymbol{q}j}$ is provided by $\tilde{\omega}_{\boldsymbol{q}pl} = \omega_{\boldsymbol{q}pl} - iW_{\boldsymbol{q}pl} + i\gamma_{\boldsymbol{q}pl}$, $\tilde{\omega}_{\boldsymbol{q}ph} = \omega_{\boldsymbol{q}} + i\gamma_{\boldsymbol{q}ph}$, and $\tilde{\omega}_{\boldsymbol{q}(\boldsymbol{k}b\bar{b})} = \bar{\omega}_{b\bar{b}\boldsymbol{k}\boldsymbol{q}} + i\gamma_{b\bar{b}\boldsymbol{k}\boldsymbol{q}}$, respectively. Further, $M'_{\boldsymbol{q}ph} = M^*_{\boldsymbol{q}ph}$ and $M^{(\prime)}_{\boldsymbol{q}(\boldsymbol{k}b\bar{b})} = M^{(\prime)}_{\boldsymbol{q}}(\boldsymbol{k}b\bar{b})$. Equation (F.1) is cast into the form of

$$E_{\boldsymbol{q}j} = \tilde{\omega}_{\boldsymbol{q}j} - \frac{\tilde{\omega}_{\boldsymbol{q}j} - E_{\boldsymbol{q}j}}{\tilde{\omega}_{\boldsymbol{q}pl} - E_{\boldsymbol{q}j}} \sum_{j' \neq pl} \frac{M_{\boldsymbol{q}j'} M'_{\boldsymbol{q}j'}}{\tilde{\omega}_{\boldsymbol{q}j'} - E_{\boldsymbol{q}j}}. \qquad (F.2)$$

Here, $M_{\boldsymbol{q}}(\boldsymbol{k}b\bar{b})$ of Eq. (2.92) and $M'_{\boldsymbol{q}}(\boldsymbol{k}b\bar{b})$ of Eq. (2.93) are expressed in the small $\boldsymbol{q}$-limit as

$$M_{\boldsymbol{q}}(\boldsymbol{k}b\bar{b}) = -|\boldsymbol{q}| \mathcal{N}^L_{\boldsymbol{q}} V^{(C)}_{\boldsymbol{q}} \left[\frac{\bar{\Omega}^{(R)}_{\bar{b}b\boldsymbol{k}}(t)}{\omega_{\boldsymbol{q}pl}} (\hat{\boldsymbol{q}} \cdot \boldsymbol{\nabla}) (\bar{\rho}_{bb\boldsymbol{k}} - \bar{\rho}_{\bar{b}b\boldsymbol{k}}) + (\hat{\boldsymbol{q}} \cdot \boldsymbol{\nabla}) \bar{\rho}_{b\bar{b}\boldsymbol{k}} \right] \qquad (F.3)$$

and

$$M'_{\boldsymbol{q}}(\boldsymbol{k}b\bar{b}) = |\boldsymbol{q}| \mathcal{N}^R_{\boldsymbol{q}} V^{(C)}_{\boldsymbol{q}} \frac{\bar{\Omega}^{(R)}_{b\bar{b}\boldsymbol{k}}(t)}{\omega^2_{\boldsymbol{q}pl}} (\hat{\boldsymbol{q}} \cdot \boldsymbol{\nabla} \Delta \varepsilon^{(r)}_{\boldsymbol{k}}), \qquad (F.4)$$

respectively. $\Delta\varepsilon_{\boldsymbol{k}}^{(r)}$ is provided by Eq. (B.57). Further, the summation with respect to $j' = \{(\boldsymbol{k}b\bar{b})\}$ in the second term of the right-hand side of Eq. (F.2) is expressed as

$$
\sum_{\boldsymbol{k}b} \frac{M_{\boldsymbol{q}}(\boldsymbol{k}b\bar{b})M'_{\boldsymbol{q}}(\boldsymbol{k}b\bar{b})}{\tilde{\omega}_{b\bar{b}\boldsymbol{k}\boldsymbol{q}} - E_{\boldsymbol{q}j}} = -\boldsymbol{q}^2 \frac{\mathcal{N}_{\boldsymbol{q}}^L \mathcal{N}_{\boldsymbol{q}}^R V_{\boldsymbol{q}}^{(C)2}}{\omega_{\boldsymbol{q}pl}^2} \sum_{\boldsymbol{k}}
$$

$$
\times \left[(\hat{\boldsymbol{q}} \cdot \boldsymbol{\nabla}\bar{\rho}_{cc\boldsymbol{k}})(\hat{\boldsymbol{q}} \cdot \boldsymbol{\nabla}\Delta\varepsilon_{\boldsymbol{k}}^{(r)}) \frac{|\bar{\Omega}_{cv\boldsymbol{k}}^{(R)}(t)|^2}{\omega_{\boldsymbol{q}pl}} \left(\frac{1}{\tilde{\omega}_{cv\boldsymbol{k}\boldsymbol{q}} - E_{\boldsymbol{q}j}} + \frac{1}{\tilde{\omega}_{vc\boldsymbol{k}\boldsymbol{q}} - E_{\boldsymbol{q}j}} \right) \right.
$$

$$
- (\hat{\boldsymbol{q}} \cdot \boldsymbol{\nabla}\bar{\rho}_{vv\boldsymbol{k}})(\hat{\boldsymbol{q}} \cdot \boldsymbol{\nabla}\Delta\varepsilon_{\boldsymbol{k}}^{(r)}) \frac{|\bar{\Omega}_{cv\boldsymbol{k}}^{(R)}(t)|^2}{\omega_{\boldsymbol{q}pl}} \left(\frac{1}{\tilde{\omega}_{cv\boldsymbol{k}\boldsymbol{q}} - E_{\boldsymbol{q}j}} + \frac{1}{\tilde{\omega}_{vc\boldsymbol{k}\boldsymbol{q}} - E_{\boldsymbol{q}j}} \right)
$$

$$
+ (\hat{\boldsymbol{q}} \cdot \boldsymbol{\nabla}\bar{\rho}_{cv\boldsymbol{k}})(\hat{\boldsymbol{q}} \cdot \boldsymbol{\nabla}\Delta\varepsilon_{\boldsymbol{k}}^{(r)}) \frac{\bar{\Omega}_{cv\boldsymbol{k}}^{(R)}(t)}{\tilde{\omega}_{cv\boldsymbol{k}\boldsymbol{q}} - E_{\boldsymbol{q}j}}
$$

$$
\left. - (\hat{\boldsymbol{q}} \cdot \boldsymbol{\nabla}\bar{\rho}_{vc\boldsymbol{k}})(\hat{\boldsymbol{q}} \cdot \boldsymbol{\nabla}\Delta\varepsilon_{\boldsymbol{k}}^{(r)}) \frac{\bar{\Omega}_{vc\boldsymbol{k}}^{(R)}(t)}{\tilde{\omega}_{vc\boldsymbol{k}\boldsymbol{q}} - E_{\boldsymbol{q}j}} \right]. \tag{F.5}
$$

The left and right eigenvectors are provided by

$$
\mathcal{V}_{\boldsymbol{q}j}^{L\dagger} = \bar{\mathcal{N}}_{\boldsymbol{q}j}^L v_{\boldsymbol{q}j}^{L\dagger}, \quad \mathcal{V}_{\boldsymbol{q}j}^R = \bar{\mathcal{N}}_{\boldsymbol{q}j}^R v_{\boldsymbol{q}j}^R. \tag{F.6}
$$

$\bar{\mathcal{N}}_{\boldsymbol{q}j}^L$ and $\bar{\mathcal{N}}_{\boldsymbol{q}j}^R$ are normalization constants of the left and right eigenvectors, respectively. Hereafter, a matrix index $l = \{ph, (\boldsymbol{k}b\bar{b})\}$ is employed, and thus, $v_{\boldsymbol{q}j}^{L\dagger}$ is determined by the following equations as

$$
(\tilde{\omega}_{\boldsymbol{q}l} - E_{\boldsymbol{q}j})v_{\boldsymbol{q}l,j}^{L\dagger} + M_{\boldsymbol{q}l}v_{\boldsymbol{q}pl,j}^{L\dagger} = 0 \tag{F.7}
$$

and

$$
\sum_l M'_{\boldsymbol{q}l}v_{\boldsymbol{q}l,j}^{L\dagger} + (\tilde{\omega}_{\boldsymbol{q}pl} - E_{\boldsymbol{q}j})v_{\boldsymbol{q}plj}^{L\dagger} = 0. \tag{F.8}
$$

On the other hand, $v_{\boldsymbol{q}j}^R$ are determined by the following equations as

$$
(\tilde{\omega}_{\boldsymbol{q}l} - E_{\boldsymbol{q}j})v_{\boldsymbol{q}l,j}^R + M'_{\boldsymbol{q}l}v_{\boldsymbol{q}pl,j}^R = 0 \tag{F.9}
$$

and

$$
\sum_l M_{\boldsymbol{q}l}v_{\boldsymbol{q}l,j}^R + (\tilde{\omega}_{\boldsymbol{q}pl} - E_{\boldsymbol{q}j})v_{\boldsymbol{q}pl,j}^R = 0. \tag{F.10}
$$

In particular, for the analysis of the initial phase of an undoped semiconductor, we are concerned with the normalization constants just for $j = ph$. In the case that $v_{\boldsymbol{q}ph,ph}^{L\dagger}$ and $v_{\boldsymbol{q}ph,ph}^R$ are set to 1, other components of the eigenvectors are provided by

$$
v_{\boldsymbol{q}pl,ph}^{L\dagger} = \frac{E_{\boldsymbol{q}ph} - \tilde{\omega}_{\boldsymbol{q}ph}}{M_{\boldsymbol{q}ph}}, \quad v_{\boldsymbol{q}l,ph}^{L\dagger} = \frac{M_{\boldsymbol{q}l}(E_{\boldsymbol{q}ph} - \tilde{\omega}_{\boldsymbol{q}ph})}{M_{\boldsymbol{q}ph}(E_{\boldsymbol{q}ph} - \tilde{\omega}_{\boldsymbol{q}l})} \tag{F.11}
$$

and

$$
v_{\boldsymbol{q}pl,ph}^R = \frac{E_{\boldsymbol{q}ph} - \tilde{\omega}_{\boldsymbol{q}ph}}{M'_{\boldsymbol{q}ph}}, \quad v_{\boldsymbol{q}l,ph}^R = \frac{M'_{\boldsymbol{q}l}(E_{\boldsymbol{q}ph} - \tilde{\omega}_{\boldsymbol{q}ph})}{M_{\boldsymbol{q}ph}(E_{\boldsymbol{q}ph} - \tilde{\omega}_{\boldsymbol{q}l})}. \tag{F.12}
$$

The normalization constants are determined by the normalization condition of $\mathcal{V}_{\boldsymbol{q}ph}^{L\dagger}\mathcal{V}_{\boldsymbol{q}ph}^R = 1$, which is cast into the form of

$$
\left(\bar{N}_{\boldsymbol{q}ph}^L \bar{N}_{\boldsymbol{q}ph}^R\right)^{-1} = 1 + \frac{(E_{\boldsymbol{q}ph} - \tilde{\omega}_{\boldsymbol{q}ph})^2}{|M_{\boldsymbol{q}ph}|^2} + \frac{(E_{\boldsymbol{q}ph} - \tilde{\omega}_{\boldsymbol{q}ph})^2}{|M_{\boldsymbol{q}ph}|^2} \sum_{\boldsymbol{k}b} \frac{M_{\boldsymbol{q}}(\boldsymbol{k}b\bar{b})M'_{\boldsymbol{q}}(\boldsymbol{k}b\bar{b})}{(E_{\boldsymbol{q}ph} - \tilde{\omega}_{b\bar{b}\boldsymbol{k}\boldsymbol{q}})^2}, \tag{F.13}
$$

where the summation in the third term of the right hand side of Eq. (F.13) becomes the similar expression to Eq. (F.5).

Bibliography

[1] K. Yamanouchi, S. Cundiff, R. de Vivie-Riedle, M. Kuwata-Gonokami, and L. Di-Mauro (Editors), *Ultrafast Phenomena XIX: Proceedings of the 19th International Conference*, Springer Proceedings in Physics **162**, (Springer-Verlag, Berlin, 2015).

[2] T. Dekorsy, G. C. Cho, and H. Kurz, "Coherent phonons in condensed media," in *Light Scattering in Solids VIII: Fullerens, Semiconductor Surfaces, Coherent Phonons*, Topics in Applied Physics Vol. 76, edited by M. Cardona and G. Güntherodt (Springer-Verlag, Berlin, 2000) Chap. 4.

[3] A. V. Kuznetsov and C. J. Stanton, "Theory of coherent phonon oscillations in bulk GaAs," in *Ultrafast Phenomena in Semiconductors*, edited by K. T. Tsen (Springer-Verlag, Berlin, 2001) Chap. 7.

[4] G. C. Cho, W. Kütt, and H. Kurz, "Subpicosecond time-resolved coherent-phonon oscillations in GaAs," Phys. Rev. Lett. **65**, 764 (1990).

[5] T. Pfeifer, W. Kütt, H. Kurz, and R. Scholz, "Generation and detection of coherent optical phonons in germanium," Phys. Rev. Lett. **69**, 3248 (1992).

[6] M. Hase, M. Kitajima, A. M. Constantinescu, and H. Petek, "The birth of a quasiparticle in silicon observed in time-frequency space," Nature (London) **426**, 51 (2003).

[7] K. Kato, A. Ishizawa, K. Oguri, K. Tateno, T. Tawara, H. Gotoh, M. Kitajima, and H. Nakano, "Anisotropy in ultrafast carrier and phonon dynamics in p-type heavily doped Si," Jpn. J. Appl. Phys. **48**, 100205 (2009).

[8] M. Hase, M. Katsuragawa, A. M. Constantinescu, and H. Petek, "Frequency comb generation at terahertz frequencies by coherent phonon excitation in silicon," Nature Photon. **6**, 243 (2012).

[9] A. K. Basak, H. Petek, K. Ishioka, E. M. Thatcher, and C. J. Stanton, "Ultrafast coupling of coherent phonons with a nonequilibrium electron-hole plasma in GaAs," Phys. Rev. B **91**, 125201 (2015).

[10] S. Yoshino, G. Oohata, and K. Mizoguchi, "Dynamical Fano-like interference between Rabi oscillations and coherent phonons in a semiconductor microcavity system," Phys. Rev. Lett. **115**, 157402 (2015).

[11] M. Hase, K. Mizoguchi, H. Harima, S. Nakashima, M. Tani, K. Sakai, and M. Hangyo, "Optical control of coherent phonons in bismuth films," Appl. Phys. Lett. **69**, 2474 (1996).

[12] K. Ishioka, M. Kitajima, and O. V. Misochko, "Temperature dependence of coherent A_{1g} and E_g phonons in bismuth," J. Appl. Phys. **100**, 093501 (2006).

[13] M. Hase, J. Demsar, and M. Kitajima, "Photoinduced Fano resonance of coherent phonons in zinc," Phys. Rev. B **74**, 212301 (2006).

[14] O. V. Misochko, K. Ishioka, M. Hase, and M. Kitajima, "Fano interference for large-amplitude coherent phonons in bismuth," J. Phys.: Condens. Matter **19**, 156227 (2007).

[15] K. Ishioka, M. Kitajima, and O. V. Misochko, "Coherent A_{1g} and E_g phonons of antimony," J. Appl. Phys. **103**, 123505 (2008).

[16] J. J. Li, J. Chen, D. A. Reis, S. Fahy, and R. Merlin, "Optical probing of ultrafast electronic decay in Bi and Sb with slow phonons," Phys. Rev. Lett. **110**, 047401 (2013).

[17] O. V. Misochko and M. V. Lebedeva, "Fano interference at the excitation of coherent phonons: Relation between the asymmetry parameter and the initial phase of coherent oscillations," J. Exp. Theor. Phys. **120**, 651 (2015).

[18] J. M. Chwalek, C. Uher, J. F. Whitaker, G. A. Mourou, J. Agostinelli, and M. Lelental, "Femtosecond optical absorption studies of nonequilibrium electronic processes in high T_c superconductors," Appl. Phys. Lett. **57**, 1696 (1990).

[19] W. Albrecht, Th. Kruse, and H. Kurz, "Time-resolved observation of coherent phonons in superconducting $YBa_2Cu_3O_{7-\delta}$ thin films," Phys. Rev. Lett. **69**, 1451 (1992).

[20] O. V. Misochko, K. Kisoda, K. Sakai, and S. Nakashima, "Dynamics of low-frequency phonons in the $YBa_2Cu_3O_{7-x}$ superconductor studies by time- and frequency-domain spectroscopies," Phys. Rev. B **61**, 4305 (2000).

[21] I. Bozovic, M. Schneider, Y. Xu, R. Sobolewski, Y. H. Ren, G. Lüpke, J. Demsar, A. J. Taylor, and M. Onellion, "Long-lived coherent acoustic waves generated by femtosecond light pulses," Phys. Rev. B **69**, 132503 (2004).

[22] H. J. Bakker, S. Hunsche, and H. Kurz, "Observation of THz phonon-polariton beats in $LiTaO_3$," Phys. Rev. Lett. **69**, 2823 (1992).

[23] H. J. Bakker, S. Hunsche, and H. Kurz, "Coherent phonon palaritons as probes of anharmonic phonons in ferroelectrics," Rev. Mod. Phys. **70**, 523 (1998).

[24] K. Norimatsu, J. Hu, A. Goto, K. Igarashi, T. Sasagawa, and K. G. Nakamura, "Coherent optical phonons in a Bi_2Se_3 single crystal measured via transient anisotropic reflectivity," Solid State Commun. **157**, 58 (2013).

[25] Y. D. Glinka, S. Bakakiray, T. A. Johnson, A. D. Bristow, M. B. Holcomb, and D. Lederman, "Ultrafast carrier dynamics in thin-films of the topological insulator Bi_2Se_3," Appl. Phys. Lett. **103**, 151903 (2013).

[26] O. V. Misochko, J. Flock, and T. Dekorsy, "Polarization dependence of coherent phonon generation and detection in the three-dimensional topological insulator Bi_2Te_3," Phys. Rev. B **91**, 174303 (2015).

[27] Y. -X. Yan, E. B. Gamble, and K. A. Nelson, "Impulsive stimulated scattering: General importance in femtosecond laser pulse interactions with matter, and spectroscopic applications," J. Chem. Phys. **83**, 5391 (1985).

[28] Y. -X. Yan and K. A. Nelson, "Impulsive stimulated light scattering. I. General theory," J. Chem. Phys. **87**, 6240 (1987).

[29] H. J. Zeiger, J. Vidal, T. K. Cheng, E. P. Ippen, G. Dresselhaus, and M. S. Dresselhaus, "Theory for displacive excitation of coherent phonons," Phys. Rev. B **45**, 768 (1992).

[30] A. V. Kuznetsov and C. J. Stanton, "Theory of coherent phonon oscillations in semiconductor," Phys. Rev. Lett. **73**, 3243 (1994).

[31] T. Pfeifer, T. Dekorsy, W. Kütt, and H. Kurz, "Generation mechanism for coherent LO phonons in surface-space-charge fields of III-V-compounds," Appl. Phys. A: Solids Surf. **55**, 482 (1992).

[32] T. Dekorsy, T. Pfeifer, W. Kütt, and H. Kurz, "Subpicosecond carrier transport in GaAs surface-space-charge fields," Phys. Rev. B **47**, 3842 (1993).

[33] P. Y. Yu and M. Cardona, *Fundamentals of Semiconductors, fourth ed.,* (Springer-Verlarg, Berlin, 2010) Chaps. 2 and 3.

[34] K. Ishioka, A. K. Basak, and H. Petek, "Allowed and forbidden Raman scattering mechanisms for detection of coherent LO phonon and plasmon-coupled modes in GaAs," Phys. Rev. B **84**, 235202 (2011).

[35] R. Merlin, "Generating coherent THz phonons with light pulses," Solid State Commun. **102**, 207 (1997).

[36] G. A. Garrett, T. F. Albrecht, J. F. Whitaker, and R. Merlin, "Coherent THz phonons driven by light pulses and the Sb problem: What is the mechanism?," Phys. Rev. Lett. **77**, 3661 (1996).

[37] A. I. Lobad and A. J. Taylor, "Coherent phonon generation mechanism in solids," Phys. Rev. B **64**, 180301(R) (2001).

[38] T. E. Stevens, J. Kuhl, and R. Merlin, "Coherent phonon generation and the two stimulated Raman tensors," Phys. Rev. B **65**, 144304 (2002).

[39] A. V. Bragas, C. Aku-Leh, S. Costantino, A. Ingale, J. Zhao, and R. Merlin, "Ultrafast optical generation of coherent phonons in $CdTe_{1-x}Se_x$ quantum dots," Phys. Rev. B **69**, 205306 (2004).

[40] D. M. Riffe and A. J. Sabbah, "Coherent excitation of the optic phonon in Si: Transiently stimulated Raman scattering with a finite-lifetime electronic excitation," Phys. Rev. B **76**, 085207 (2007).

[41] H. Haug and S. W. Koch, *Quantum Theory of the Optical and Electronic Properties of Semiconductors, fifth ed.*, (World Scientific, Singapore, 2009).

[42] R. Scholz, T. Pfeifer, and H. Kurz, "Density-matrix theory of coherent phonon oscillations in germanium," Phys. Rev. B **47**, 16229 (1993).

[43] J. D. Lee, J. Inoue, and M. Hase, "Ultrafast Fano resonance between optical phonons and electron-hole pairs at the onset of quasiparticle generation in a semiconductor," Phys. Rev. Lett. **97**, 157405 (2006).

[44] Y. Shinohara, K. Yabana, Y. Kawashita, J.-I. Iwata, T. Otobe, and G. F. Bertsch, "Coherent phonon generation in time-dependent density functional theory," Phys. Rev. B **82**, 155110 (2010).

[45] Y. Shinohara, S. A. Sato, K. Yabana, J.-I. Iwata, T. Otobe, and G. F. Bertsch, "Nonadiabatic generation of coherent phonons," J. Chem. Phys. **137**, 22A527 (2012).

[46] G. D. Mahan, *Many-Particle Physics* (Plenum, New York, 1981), Chaps. 4 and 5.

[47] U. Fano, "Effects of configuration interaction on intensities and phase shifts," Phys. Rev. **124**, 1866 (1961).

[48] D. M. Riffe, "Classical Fano oscillator," Phys. Rev. B **84**, 064308 (2011).

[49] K. G. Nakamura, Y. Shikano, and Y. Kayanuma, "Influence of pulse width and detuning on coherent phonon generation," Phys. Rev. B **92**, 144304 (2015).

[50] Y. Kayanuma and K. G. Nakamura, "Dynamic Jahn-Teller viewpoint for generation mechanism of asymmetric modes of coherent phonons," Phys. Rev. B **95**, 104302 (2017).

[51] Z. Vardeny and J. Tauc, "Picosecond coherence coupling in the pump and probe technique," Optics Comm., **39**, 396 (1981).

[52] P. Borri, F. Romstad, W. Langbein, A. E. Kelly, J. Mork, and J. M. Hvam, "Separation of coherent and incoherent nonlinearities in a heterodyne pump-probe experiment," Opt. Express **7**, 107 (2000).

[53] M. V. Lebedev, O. V. Misochko, T. Dekorsy, and N. Georgiev, "On the nature of "coherent artifact"," J. Exp. Theor. Phys., **100**, 272 (2005).

[54] P. Gaal, W. Kuehn, K. Reimann, M. Woerner, T. Elsaesser, and R. Hey, "Internal motions of a quasiparticle governing its ultrafast nonlinear response," Nature (London) **450**, 1210 (2007).

[55] A. E. Miroshnichenko, S. Flach, and Y. S. Kivshar, "Fano resonances in nanoscale structures," Rev. Mod. Phys. **82**, 2257 (2010).

[56] F. Cerdeira, T. A. Fjeldy, and M. Cardona, "Interaction between electronic and vibrational Raman scattering in heavily doped silicon," Solid State Commum. **13**, 325 (1973).

[57] F. Cerdeira, T. A. Fjeldy, and M. Cardona, "Effect of free carriers on zone-center vibrational modes in heavily doped p-type Si. II. Optical modes," Phys. Rev. B **8**, 4734 (1973).

[58] F. Cerdeira, T. A. Fjeldy, and M. Cardona, "Raman study of the interaction between localized vibrations and electronic excitations in boron-doped silicon," Phys. Rev. B **9**, 4344 (1974).

[59] M. Balkanski, K. P. Jain, R. Beserman, and M. Jouanne, "Theory of interference distortion of Raman scattering line shapes in semiconductors," Phys. Rev. B **12**, 4328 (1975).

[60] M. Chandrasekhar, J. B. Renucci, and M. Cardona, "Effects of interband excitations on Raman phonons in heavily doped n-Si," Phys. Rev. B **17**, 1623 (1978).

[61] M. Chandrasekhar, H. R. Chandrasekhar, M. Grimsditch, and M. Cardona, "Study of the vibrations of boron in heavily doped Si," Phys. Rev. B **22**, 4825 (1980).

[62] M. V. Klein, "Electronic Raman scattering," in *Light Scattering in Solids I: Introductory Concepts*, Topics in Applied Physics Vol. 8, edited by M. Cardona (Springer-Verlag, Berlin, 1983) Chap. 4.

[63] L. A. O. Nunes, L. Ioriatti, L. T. Florez, and J. P. Harbison, "Fano-like resonant interference in Raman spectra of electronic and LO-vibronic excitations in periodically δ-doped GaAs," Phys. Rev. B **47**, R13011 (1993).

[64] Yu. A. Pusep, M. T. O. Silva, J. C. Galzerani, S. W. da Silva, L. M. R. Scolfaro, R. Enderlein, A. A. Quivy, A. P. Lima, and J. R. Leite, "Raman study of Fano-like electron-phonon coupling in δ-doping GaAs superlattices," Phys. Rev. B **54**, 13927 (1996).

[65] K. -J. Jin, J. Zhang, Z. -H. Chen, G. -Z. Yang, Z. H. Chen, X. H. Shi, and S. C. Shen, "Phonon-induced photoconductive response in doped semiconductors," Phys. Rev. B **64**, 205203 (2001).

[66] U. Siegner, M.-A. Mycek, S. Glutsch, and D. S. Chemla, "Ultrafast coherent dynamics of Fano resonances in semiconductors," Phys. Rev. Lett. **74**, 470 (1995).

[67] U. Siegner, M.-A. Mycek, S. Glutsch, and D. S. Chemla, "Quantum interference in the system of Lorentzian and Fano magnetoexciton resonances in GaAs," Phys. Rev. B **51**, 4953 (1995).

[68] K.-i. Hino, K. Goto, and N. Toshima, "Asymmetric Autler-Townes-like doublets in laser-driven excitonic Fano resonance in biased superlattices: Role of many-body Coulomb exchange," Phys. Rev. B **69**, 035322 (2004).

[69] Y. Watanabe, K. Hino, M. Hase and N. Maeshima, "Polaronic quasiparticle picture for generation dynamics of coherent phonons in semiconductors: Transient and nonlinear Fano resonance," Phys. Rev. B **95**, 014301 (2017).

[70] Y. Watanabe, K. Hino, M. Hase and N. Maeshima, "Laser-induced Fano resonance in condensed matter," in *Resonance*, edited by J. Awrejcewicz (InTech Open, 2017) Chap. 11.

[71] Y. Watanabe, K. Hino, M. Hase and N. Maeshima, "Irregular oscillatory patterns in the early-time region of coherent phonon generation in silicon," Phys. Rev. B **96**, 125204 (2017).

[72] Y. Watanabe, K. Hino, M. Hase and N. Maeshima (unpublished work).

[73] B. B. Varga, "Coupling of plasmons to polar phonons in degenerate semiconductors," Phys. Rev. **137**, A1896 (1965).

[74] A. Mooradian and A. L. McWhorter, "Polarization and intensity of Raman scattering from plasmons and phonons in gallium arsenide," Phys. Rev. Lett. **19**, 849 (1967).

[75] M. Hase, S. -I. Nakashima, K. Mizogichi, H. Harima, and K. Sakai, "Ultrafast decay of coherent plasmon-phonon coupled modes in highly doped GaAs," Phys. Rev. B **60**, 16526 (1999).

[76] R. Huber, F. Tauser, A. Brodschelm, M. Bichler, G. Abstreiter, and A. Leitenstorfer, "How many-particle interactions develop after ultrafast excitation of an electron-hole plasma," Nature **414**, 286 (2001).

[77] R. Huber, C. Kübler, S. Tübel, A. Leitenstorfer, Q. T. Vu, H. Haug, F. Köhler, and M.-C. Amann, "Femtosecond formation of coupled phonon-plasmon modes in InP: Ultrabroadband THz experiment and quantum kinetic theory," Phys. Rev. Lett. **94**, 027401 (2005).

[78] Y. -M. Chang, "Formation of coherent longitudinal optical phonon and plasmon coupling modes in semiconductors," in *Conference on Lasers and Electro-Optics/Quantum Electronics and Laser Science Conference 2010 Technical Digest* (Optical Society of America, Washington, DC, 2010), QThF1.

[79] W. Schäfer and M. Wegener, *Semiconductor Optics and Transport Phenomena* (Springer-Verleg, Berlin, 2002) Chaps. 2, 10 and 11.

[80] A. L. Fetter and J. D. Walecka, *Quantum Theory of Many-Particle Systems*, (McGraw-Hill, Inc., New York, 1971) Chaps. 3-5.

[81] N. Moiseyev, *Non-Hermitian Quantum Mechanics*, (Cambridge, New York, 2011) Chaps. 7-9.

[82] F. J. Dyson, "General theory of spin-wave interactions," Phys. Rev. **102**, 1217 (1956).

[83] F. J. Dyson, "Thermodynamic behavior of an ideal ferromagnet," Phys. Rev. **102**, 1230 (1956).

[84] E. E. Nikitin and S. Ya. Umanskii, *Theory of Slow Atomic Collisions*, Springer Series in Chemical Physics Vol. 30, (Springer-Verlag, Berlin, 1984) Chaps. 7.

[85] A. J. Sabbah and D. M. Riffe, "Femtosecond pump-probe reflectivity study of silicon carrier dynamics," Phys. Rev. B **66**, 165217 (2002).

[86] R. Binder, D. Scott, A. E. Paul, M. Lindberg, K. Henneberger, and S. W. Koch, "Carrier-carrier scattering and optical dephasing in highly excited semiconductors," Phys. Rev. B **45**, 1107 (1992).

[87] T. R. Hart, R. L. Aggarwal, and B. Lax, "Temperature dependence of Raman scattering in silicon," Phys. Rev. B **1**, 638 (1970).

[88] J. Menéndez and M. Cardona, "Temperature dependence of the first-order Raman scattering by phonons in Si, Ge, and α-Sn: Anharmonic effects," Phys. Rev. B **29**, 2051 (1984).

[89] W. Pötz and P. Vogl, "Theory of optical-phonon deformation potentials in tetrahedral semiconductors," Phys, Rev. B **24**, 2025 (1981).

[90] B. W. Shore, "Scattering theory of absorption-line profiles and refractivity," Rev. Mod. Phys. **39**, 439 (1967).

[91] T. Inui, Y. Tanabe, and Y. Onodera, *Group Theory and Its Applications in Physics*, Springer Series in Solid-State Sciences **78**, (Springer-Verlag, Berlin, 1990) Chaps. 11 and 12.

[92] H. W. K. Tom, T .F. Heinz, and Y. R. Shen, "Second-harmonic reflection from silicon surfaces and its relation to structural symmetry," Phys. Rev. Lett. **51**, 1983 (1983).

[93] P. Stampfli and K. H. Bennemann, "Time dependence of the laser-induced femtosecond lattice instability of Si and GaAs: Role of longitudinal optical distortions," Phys. Rev. B **49**, 7299 (1994).

[94] S. J. Sheih, K. T. Tsen, D. K. Ferry, A. Botchkarev, B. Sverdlov, A. Salvador, and H. Morkoc, "Electron-phonon interactions in the wide band-gap semiconductor GaN," Appl. Phys. Lett. **67**, 1757 (1995).

[95] K. J. Yee, K. G. Lee, E. Oh, D. S. Kim, and Y. S. Lim, "Coherent optical phonon oscillations in bulk GaN excited by far below the band gap photons," Phys. Rev. Lett. **88**, 105501 (2002).

[96] Z. Fu and M. Yamaguchi, "Coherent excitation of optical phonons in GaAs by broadband terahertz pulses," Sci. Rep. **6**, 38264 (2016).

[97] M. Schultze, K. Ramasesha, C. D. Pemmaraju, S. A. Sato, D. Whitmore, A. Gandman, J. S. Prell, L. J. Borja, D. Prendergast, K. Yabana, D. M. Neumark, and S. R. Leone, "Attosecond band-gap dynamics in silicon," Science **346**, 1348 (2014).

[98] K. Ishioka, M. Hase, K. Kitajima, and H. Petek, "Coherent optical phonons in diamond," Appl. Phys. Lett. **89**, 231916 (2006); **92**, 019903 (2008).

[99] K. Kato, K. Oguri, A. Ishizawa, H. Nakano, and T. Sogawa, "Ultrafast carrier and coherent phonon dynamics in semi-insulated and n-type 4H-SiC," J. Appl. Phys. **111**, 113520 (2012).

[100] J. Z. Tang, S. Watanabe, and M. Matsuzawa, "General computational method for two-electron-system," Phys. Rev. A **46**, 2437 (1992).

[101] K. Hino, A. Igarashi, and J. H. Macek, "Criteria for the validity of the diabatic-by-sector expansion in the hyperspherical coordinate method," Phys. Rev. A **56**, 1038 (1997).

[102] K. Hino, "Conspicuous influence of hole-subband mixing on Fano-resonance profiles of excitons in a wide quantum well," Phys. Rev. B **62**, R10626 (2000).

[103] P. G. Burke, *R-Matrix Theory of Atomic Collisions: Application to Atomic, Molecular and Optical Processes* (Springer-Verlag, Berlin, 2011) Chap. 9.